

INVESTIGATIONS ON LASER INDUCED FLUORESCENCE  
AND RELATED ASPECTS OF BARIUM SULPHIDE PHOSPHOR  
DOPED WITH COPPER AND RARE-EARTH ELEMENTS

**REETHAMMA THOMAS**

THESIS SUBMITTED TO  
COCHIN UNIVERSITY OF SCIENCE AND TECHNOLOGY  
FOR THE AWARD OF THE DEGREE OF  
**DOCTOR OF PHILOSOPHY**

LASER DIVISION, DEPARTMENT OF PHYSICS  
COCHIN UNIVERSITY OF SCIENCE AND TECHNOLOGY  
COCHIN - 682022

**1991.**

## CERTIFICATE

Certified that this thesis is the report of the original work carried out by Ms. Reethamma Thomas in the Department of Physics, Cochin University of Science and Technology, under my guidance and supervision and that no part thereof has been included in any other thesis submitted previously for the award of any degree.

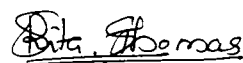


Dr.V.P.N. Nampoori  
Professor of Physics  
Cochin University of  
Science & Technology  
(Supervising Teacher)

Cochin-682 022  
March 7th, 1991.

## DECLARATION

Certified that the work presented in this thesis is based on the original work done by me under the guidance of Dr. V.P.N. Nampoori, Professor, Department of Physics, Cochin University of Science and Technology and has not been included in any other thesis submitted previously for the award of any degree.



**Reethamma Thomas**

Cochin -682 022  
March 7th, 1991.

## PREFACE

Luminescence is one of the phenomena which has been investigated extensively by scientists resulting in valuable contributions to the field of pure and applied sciences. Understanding of luminescence and related properties exhibited by certain class of materials influenced the advancement in such diverse fields as display devices, laser systems, light-matter interactions, lattice dynamics etc. Any study on luminescence addresses the key questions such as

1. What is the molecular and atomic nature of the origin of luminescence ?
2. What are the detailed paths of molecular excitations and de-activations ?
3. What are the structures of excited states ?
4. Can one design devices using specific and useful properties of luminescent materials ?

Luminescence is the emission of UV, visible, IR radiations from materials under various types of excitations and arises from a radiative transition between the excited state and a lower state. The classification of luminescence depends on how the excited states are derived. Photoluminescence arises following excitation of luminescence centres by the absorption of a photon of light. Short lived emissions (within a life-time  $\sim 10^{-8}$  sec) have been considered as fluorescence while long-lived emissions the phosphorescence. Thermoluminescence (TL) is the luminescence that arises on warming up of the material.

The phosphors are the materials capable of emitting radiation when subjected to UV or some other form of excitations. The fluorescence emission of these phosphors depends on incorporated impurities. Research on these phosphor systems has shown a well understanding of the characteristic luminescence since the properties of these phosphors can be studied on simple model compounds. In these materials the emission occurs in the luminescence centres as a result of an electron transition that, in principle, could also be possible if the centre is situated in free-space instead of in a crystal lattice. In the case of rare-earth (RE) activated phosphors, the characteristic properties of rare-earth ions are attributable to the presence of ion of a deep-lying 4f shell, which gives rise to a number of discrete energy levels.

The alkaline earth sulphide (AES) phosphors produce emission from UV to near IR region in the presence of various activators and co-activators. They possess simple face centered cubic crystal structure with wide band gap (3.8eV to 5.2eV) and offer themselves as good host materials in the preparation of phosphors for various applications and uses. From the earlier reports it has been found that the amount of work on Barium Sulphide (BaS) phosphors is not of that magnitude as compared to the work on other members of the AES group. Rare-earth dopants along with certain metallic impurities like Cu are found to alter the characteristics of these phosphors by exhibiting interesting features like sensitized luminescence

and energy transfer between the two luminescence centres. Such phenomena will enhance the overall efficiency of the phosphor too.

The investigations presented in this thesis are centered on the fluorescence emission characteristics and related aspects of Barium Sulphide phosphor doped with copper and rare-earth impurities. The RE acts as the best co-activator due to its characteristic emission in the visible region. In addition, the crystal field splitting of  $RE^{3+}$  ions introduce localized levels within the forbidden gap of BaS. By exciting with suitable radiation, the transitions between these levels can be achieved which in turn enhances the quantum yield of fluorescence emission. The TL and the emission decay of the phosphors are used as a means to investigate the mechanism of luminescence. The decay analysis is helpful to understand the kinetics involved in the process. Nature and distribution of trapping states in the lattice are also studied by emission decay and TL analysis.

The thesis is organised into seven chapters and an appendix.

The first chapter of the thesis is a general introduction to the luminescence phenomena and related aspects. The necessary theoretical background used for the analysis of the results obtained are discussed in this chapter.

A brief overview of the present status of the work on fluorescence related properties of AES phosphors are reported in chapter II with a special reference to BaS.

Chapter III presents a concise description of the method of sample preparation and experimental techniques used. This involves the design and fabrication of the sample cell, the experimental set up and the data acquisition techniques employed for recording the fluorescence, phosphorescence and thermoluminescence spectra.

The absorption spectra of various phosphors under consideration, and their fluorescence emission under Nitrogen laser excitation are discussed in chapter IV. It has been observed that a good number of RE ions in crystal lattice absorb UV radiation to emit fluorescence in the visible region. A pulsed  $N_2$  laser radiation of 337.1 nm wavelength (10 ns pulse width, 25 pps, 300 KW) was used as the source of excitation.  $N_2$  laser induced fluorescence spectra of singly and doubly doped BaS phosphors such as BaS:Cu, BaS:RE, BaS:Cu:RE, BaS:RE<sub>1</sub>:RE<sub>2</sub> systems (where RE stands for the rare-earth - La, Pr, Nd, Sm, Gd, Dy etc.) are presented in this chapter. A detailed spectral analysis and the energy levels involved in the emission processes are also discussed at length. Results obtained are used to characterise the possible sites of dopants in BaS lattice.

The subject matter of chapter V forms the emission characteristics of BaS:Ce, BaS:Cu, BaS:Ce:Cu phosphor systems under UV (365 line of mercury lamp) excitation and their TL properties.

In chapter VI, the phosphorescence decay analysis of the phosphor systems are discussed in detail.

The last chapter gives the general conclusions drawn from the present investigations.

The studies on the photoluminescence of Y-Ba-Cu-O superconducting samples are given as an appendix.

The reference to literature are made at the end of the respective chapters.

Based on the present investigations, the following research papers have been published/communicated to standard journals/presented in International/national symposia

**(a). Standard refereed journals.**

1. "On the luminescence characteristics of Cerium and Copper doped Barium Sulphide phosphor"  
Reethamma Thomas and V.P. N. Nampoori,  
Solid State Communications; Vol., 68, No. 9 (1988) p.821.
2. "Laser induced fluorescence of BaS:Sm phosphor and energy level splitting of Sm<sup>3+</sup> ion"  
Reethamma Thomas and V.P. N. Nampoori,  
Solid State Communications; Vol., 73, No. 12 (1990) p.802.
3. "Energy transfer and fluorescence spectra of BaS:RE phosphor system under N<sub>2</sub> laser excitation"  
Reethamma Thomas and V.P. N. Nampoori,  
Communicated to the journal - Lanthanide and Actinide Research
4. "Laser induced fluorescence emission from BaS:Pr phosphor"  
Reethamma Thomas and V.P.N. Nampoori,  
Communicated to the journal - Pramana Journal of Physics
5. "Sensitization of Cu<sup>+</sup> centres in BaS:RE phosphors under N<sub>2</sub> laser excitation"  
Reethamma Thomas and V.P.N. Nampoori,  
Communicated to the journal - Physica Status Solidi.
6. "Phosphorescence decay studies on BaS:RE phosphors"  
Reethamma Thomas and V.P.N. Nampoori,  
To be Communicated.

(b) **National/International symposia**

1. "Phosphorescence and thermoluminescence of BaS:Ce:Cu phosphors"  
Reethamma Thomas and V.P.N. Nampoori,  
Proceedings of Nuclear and Solid State Symposium (DAE), Mysore, Dec. 22-27, (1983),  
Vol 26C, Solid state Phys. p. 202.
2. "Fluorescence emission from SrS:Ce and BaS:Ce phosphors under N<sub>2</sub> laser excitation",  
Thomas Baby, Reethamma Thomas and V.P.N. Nampoori,  
Proceedings of DAE Symposium on Quantum Electronics, BARC, Bombay, Jan.14-16,  
(1985).
- ☆3. Sensitization of SrS:Sn by Cu",  
Reethamma Thomas, Regi Augustine and V P N Nampoori,  
19th National Seminar on Crystallography, Changanacherry, Dec. 18-20, (1987)  
abstract No.71C p. 27.
4. "Luminescence study of BaS:RE system"  
Reethamma Thomas and V.P.N. Nampoori,  
National Symposium on Current trends in Pure and Applied Physics, Cochin,  
Oct.24-25,(1988), Abstract No: M30 p. 54.
5. "Photoluminescence study of YBa<sub>2</sub>Cu<sub>3</sub>O<sub>7</sub>,"  
Reethamma Thomas and V.P.N. Nampoori,  
Proceedings of International Symposium on High T<sub>c</sub> Superconductivity, Jaipur,  
July 6-8 (1988),p.241.
6. "Effect of Cu<sup>+</sup> on the luminescence emission from BaS:RE phosphors"  
Reethamma Thomas and V.P.N. Nampoori,  
Proceedings of the IInd IPA/DST Symposium on Lasers and Applications,  
BHU,Varanasi, Dec.11-15, (1989), Abstract No:LA19 p. 158.
7. "Fluorescence emission from BaS:(Sm,Pr) phosphor system under N<sub>2</sub> laser excitation"  
Reethamma Thomas and V.P.N. Nampoori,  
Proceedings of International Symposium on Luminescence,C.E.C.R.I., Karaikudi,  
Jan.8-11,(1990). Published in the book "*LUMINESCENCE AND APLICATIONS*" Nova  
publishers edited by R.P. Rao.
- ☆ **Not included in this thesis.**

# CONTENTS

	Page No.
PREFACE	
CHAPTER I A GENERAL INTRODUCTION TO LUMINESCENCE PHENOMENA	
1.1 Introduction	.. 1
1.2 Some Basic Concepts	.. 2
1.2.1 Radiative and non-radiative processes	.. 4
(a) Fluorescence and phosphorescence	.. 4
(b) Radiationless transitions	.. 6
1.2.2 Quantum yield	.. 6
1.3 Role of Activators and Co-activators in Luminescence process	.. 7
1.4 Representations of Luminescence Spectra- Models of luminescence	.. 7
1.4.1 Configuration Co-ordinate model	.. 8
1.4.2 Energy band model	.. 12
1.5 Effect of Crystal Field on the Spectra of ions	.. 15
1.5.1 Crystal field splitting of $Cu^+$ energy levels	.. 15
1.5.2 Effect of crystal field on $RE^{3+}$ energy levels	.. 17
1.6 Transfer of Energy in Luminescence processes	.. 25
1.6.1 Resonant energy transfer	.. 28
1.6.2 Quenching	.. 29
1.7 Luminescence as a Function of Time	.. 29
1.7.1 Kinetics of luminescence	.. 29
1.7.2 Life time of a level	.. 31
1.7.3 Decay law	.. 32
1.7.4 Different decay mechanisms	.. 34
(a) Temperature - independent decay	.. 34
(b) Temperature - sensitive decay - Power law decay	.. 37
1.8 Thermoluminescence and Glow Curves	.. 40
1.8.1 Trapping parameters in TL process	.. 43
1.8.2 Methods to calculate trapping parameters	.. 43
References	.. 48
CHAPTER II REVIEW OF PREVIOUS WORK	.. 50
References	.. 54

CHAPTER III	PHOSPHOR SYNTHESIS AND EXPERIMENTATION	
3.1	Introduction	..56
3.2	Vacuum furnace	..56
3.3.	Sample preparation	..57
3.4	Experimental cell	..59
3.5	Excitation sources	..69
3.5.1	Mercury lamp	..69
3.5.2	Nitrogen laser system	..69
3.6	Experimental Details	..73
3.7	Data Acquisition Techniques	..78
3.7.1	Scanning Spectrometer	..78
3.7.2	Photomultiplier tube	..78
3.7.3	Pre-amplifier	..80
3.7.4	Recorder	..80
	References	..84
CHAPTER IV	LASER INDUCED FLUORESCENCE FROM BaS:RE PHOSPHORS	
4.1	Introduction	..85
4.2	The absorption Spectra	..85
4.3	N <sub>2</sub> laser induced fluorescence	..86
4.3.1	Spectral features and analysis	..86
	(a) Self - activated BaS	..86
	(b) Rare - earth doped BaS phosphors	..98
	(c) Copper doped BaS phosphors	..105
	(d) Rare - earth and copper doped BaS phosphors	..116
4.4	Fluorescence of BaS:Sm and BaS:Pr phosphors-	
	Fine structure analysis	..120
	(a) BaS:Sm phosphor	..120
	(b) BaS:Pr phosphor	..127
	References	..132
CHAPTER V	FLUORESCENCE AND THERMOLUMINESCENCE STUDIES USING ULTRA - VIOLET LAMP EXCITATION	
5.1	Fluorescence Emission studies	..133
5.1.1	Spectral features	..133
5.1.2	Emission model	..138
5.2	Thermoluminescence studies	..140
	References	..146



CHAPTER VI	ANALYSIS OF PHOSPHORESCENCE DECAY CHARACTERISTICS	
6.1	Introduction	..147
6.2	Nature of Phosphorescence decay	..147
6.3	Evaluation of Trap depth - E (ev)	..173
6.4	Population distribution of trapping levels	..177
6.5	Evaluation of Decay constant	..181
	References	..183
CHAPTER VII	GENERAL CONCLUSIONS	..184
APPENDIX	<i>PHOTOLUMINESCENCE STUDY OF <math>YBa_2Cu_3O_7</math> SUPERCONDUCTING SAMPLES</i>	
A.1	Introduction	I
A.2	Experimental	I
A.3	Results and discussion	II
	References	IV

-----

## **CHAPTER I**

# A GENERAL INTRODUCTION TO LUMINESCENCE PHENOMENA

## 1.1 Introduction

Luminescence is one of the phenomena which has attracted many research workers due to its applications in both fundamental and applied sciences. Range of applications of luminescence studies varies from the basic understanding of different types of energy processes in materials to the development of display devices. In this chapter various aspects of luminescence phenomena along with the necessary theoretical framework are outlined.

Luminescence is the emission of UV, visible or IR radiations from materials under various types of excitations and arises due to a radiative transition between the excited state and a lower state. Time scales involved in luminescence phenomena range from  $10^{-8}$  to  $10^{-1}$  sec which is very much large as compared to those involved in fast processes ( $\sim 10^{-14}$  sec) like Raman scattering, Compton Scattering, Rayleigh scattering, Cerenkov effect etc. At ordinary densities of excitation, the spontaneous transition probability predominates so that the luminescence radiation is incoherent; whereas when excited with high densities in special configuration, the induced transition probability may predominate which results in laser action and in that case the emission radiations will be coherent.

Excitation of the luminescent substance is a pre-requisite for luminescence emission. The general phenomenon of luminescence has been sub-divided according to the source of excitation energy. Since a given substance can frequently be made to luminesce by a number of different external exciting agents and the atomic and the electronic phenomena that cause luminescence are basically the same regardless of the mode of excitation, this sub-division of luminescence phenomena is only a matter of convenience and not of fundamental distinction. The following are the different types of luminescence phenomena which are usually encountered.

Photoluminescence-refers to the luminescence excited by the photons,

Cathodoluminescence or electronoluminescence - involves excitations by cathode rays, or energetic electrons impinging on a phosphor,

Radioluminescence or roentgenoluminescence - if the excitation energy comes from x-rays or from  $\gamma$ -rays.

Electroluminescence - involves the luminescence as a result of excitation with an applied electric

field in a phosphor,

Triboluminescence - is due to the mechanical excitation such as grinding,

Chemiluminescence - is the conversion of energy of a chemical reaction into luminescence emission,

Bioluminescence - excitation luminescence by biological process.

In all the above cases the luminescent material may be considered as a transformer of energy. The quality and quantity of luminescent radiations are strongly dependent on the nature of the emitting material [1]. The ability to luminesce is not confined to any particular state of matter. Even though the luminescence is observed in all forms of matter, the main applications involved are in solid luminescent materials.

A luminescent material is often referred to as a phosphor. The word '*phosphor*' comes from a Greek word meaning 'bearer of light'. Phosphors are the materials that absorb radiant energy of a given wavelength and re-radiate at longer wavelengths. Comparatively few pure solids like silicates, sulphides, selenides and oxides of Ca, Hg, Zn, and Ba luminesce efficiently at room temperature. The luminescence emissions of these phosphors can be modified by incorporating certain impurities known as activators.

The alkaline earth sulphides (AES) like CaS, BaS, SrS belong to a class of efficient phosphors which emit radiations from UV to near IR regions in the presence of suitable activators [2]. AES possess simple face centered cubic crystal structure with wide band gap (3.8 eV to 5.2 eV) and offer themselves as good host materials in the preparation of phosphors for various applications [3].

## 1.2 Some Basic Concepts

### (a) Absorption spectra

Absorption spectra are useful in identifying various energy levels involved in excitation and de-excitation processes in materials. Optical spectrum will reveal absorption bands when the material is illuminated with continuous source of electromagnetic radiation (Fig. 1.1 (a).)

### (b) Luminescence spectra

Ions in a luminescent material that are excited to an upper level will return to the ground state either by radiationless transitions or by radiative transitions. Emission transition is

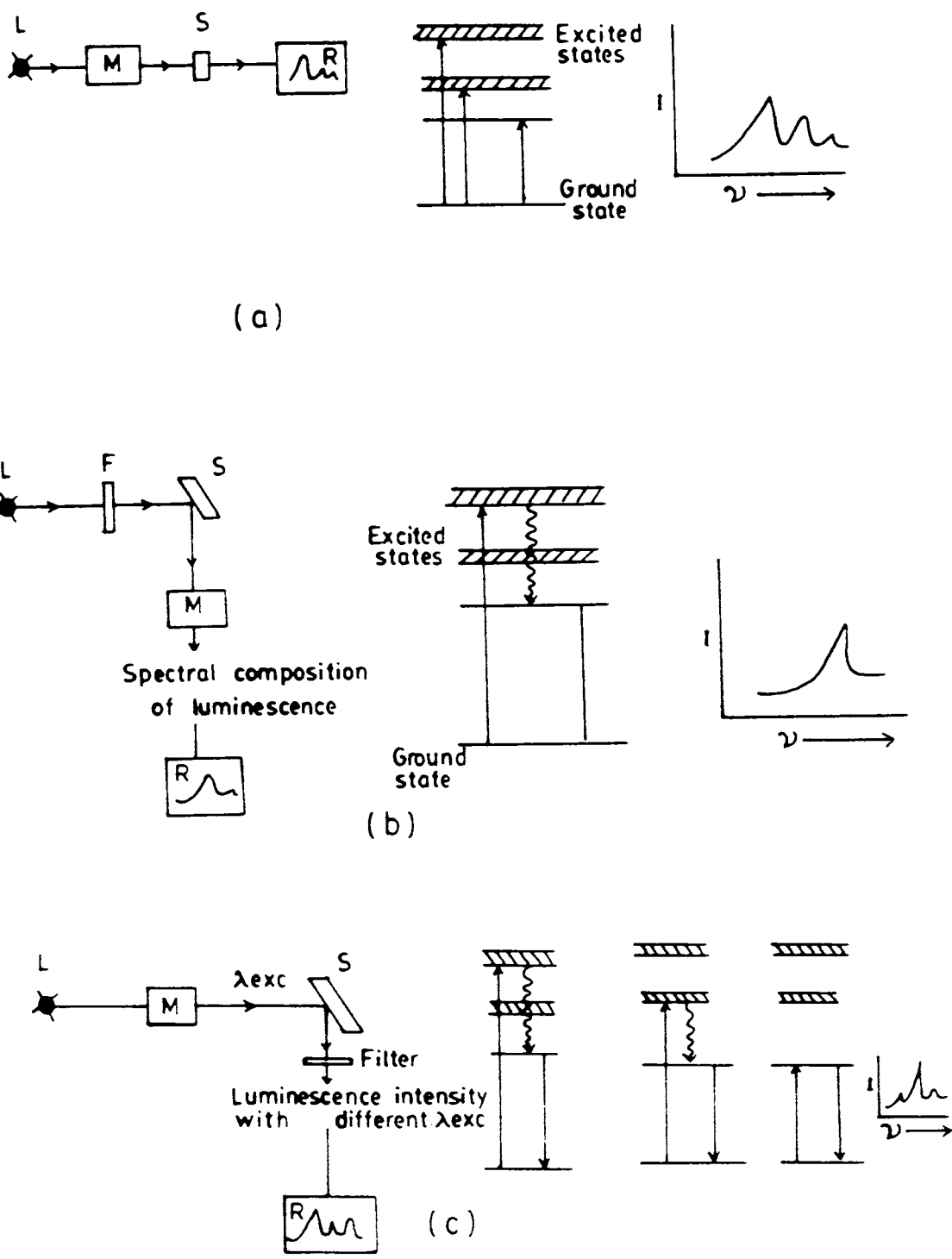


Fig. 1.1 Schematic Representations of (a) Absorption spectra, (b) Luminescence spectra and (c) Excitation spectra

L - light source, M - monochromator, S - sample  
 R - registration of spectra F - filter

registered in the form of a band in the luminescence spectrum does not depend on the method of excitation and is determined only by inter-level spacing. But certain bands may be present or absent in the spectrum depending on the mode of excitation. In fig.1.1(b) a single emission band is shown. In energy level diagram, however, there will be several levels and the transition from each one of them can be not only to the ground state but also to the intermediate levels. Moreover, the ground state can be splitted into sub-levels and then, transition from each emission level will be into these ground state sub-levels. This can result in the appearance of complex luminescence spectra consisting of many bands. Such complex spectra are characteristics of lanthanides and actinides [4].

### (c) Excitation spectra

A particular band or line in the luminescence spectrum can be excited by one or more wavelengths of excitation radiation. By maintaining the intensity of luminescence emission at a particular wavelength with respect to the wavelength of excitation radiation, one can get what is usually referred to as excitation spectrum. In general, different bands of luminescence spectrum will have different excitation spectrum. The excitation spectra, therefore, do not coincide with the absorption spectra. An example of excitation spectrum is shown in fig.1.1(c).

### 1.2.1 Radiative and non-radiative processes

An excited system can come to the ground state either by emitting photon (ie radiative processes) or by way of emitting phonons (ie. non-radiative processes).

#### (a) Fluorescence and phosphorescence

These are the cases of radiative emission transitions. It is a classification based on the persistence of emission after the source of exciting energy is removed. Many substances continue to luminesce for extended periods even after the exciting energy is cut off. The delayed emission is generally called phosphorescence and the emission during the time of excitation is called fluorescence. More clearly, the emission with a life time of  $10^{-8}$  sec to  $10^{-3}$  sec is indisputably fluorescence or to say, the short lived emissions are fluorescence where as long lived emissions are phosphorescence. [5]. Fig.1.2 shows the processes involved in fluorescence and phosphorescence. If the emitting ion is raised by excitation from the ground state 'G' to the excited state 'E', it will return to the ground state with the emission of light. The fluorescence emission occurs at a time ' $\tau$ ' after the excitation, which is the life time of the excited state and is usually of the order of  $10^{-8}$  sec for atomic dipole emission. But if, on the contrary, there exists a metastable level or a trapping centre 'M' then the excited species can make a transition to this state, which does not allow a further transition  $M \rightarrow G$ . If by some means the system receives an energy 'E' - the energy difference between M and E - it is lifted again

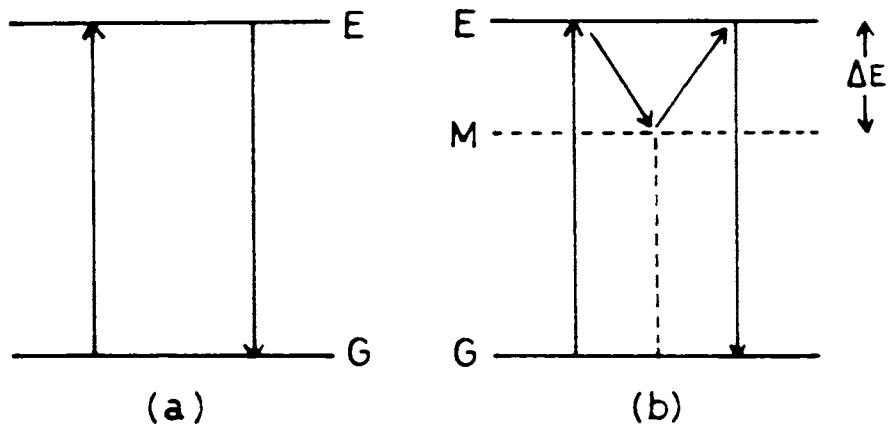


**Fig. 1.2** Simplified Model for the description of fluorescence and phosphorescence

to the state E and then the emission  $E \rightarrow G$  occurs. This is the case of phosphorescence, which is delayed by a time ' $\tau$ ' (seconds to even hours) equal to the time taken by trapped species to get released from the level 'M'. The energy 'E' (eV) (called the trap depth) may be so small which can be provided by the thermal agitation of the environment. It can also be provided by the absorption of an incident photon of appropriate energy.

**(b) Radiationless transitions**

The phonon assisted transitions are known as radiationless transitions. The larger the proportion of excitation energy transformed into phonons, the less will be the luminescence efficiency. Radiation loss of excitation energy also takes place by collapse of excitation states by small increments corresponding to phonon energies or by interaction of atoms or ions with each other.

**1.2.2 Quantum yield**

An important parameter of a phosphor material is the quantum yield which may be defined as the ratio of the number of photons emitted from a given level to the number of photons used to excite the atoms or ions. If ' $P_r$ ' represents the probability per sec for an excited species to return to the ground state with photon emission and ' $P_h$ ' is the probability for energy dissipation in the form of heat, then the quantum yield or luminescence efficiency ' $\eta$ ' can be defined as,

$$\eta = \frac{P_r}{P_r + P_h} \quad 1.(1)$$

Here  $P_r$  is assumed to be the temperature independent part, while  $P_h$  is a temperature dependent quantity. In the case of radiative transition,  $P_h$  is determined by the probability to find the excited state in a vibrational level corresponding to a frequency of emission  $\nu$ , then,

$$P_h = \nu \exp(-E/KT) \quad 1.(2)$$

When temperature, increases  $P_h$  also increases, so that luminescence efficiency will decrease with increase in temperature.



### 1.3. Role Of Activators And Co-activators In Luminescence Process

The development of a large number of inorganic phosphors is due to the discovery that certain impurities called activators, when present in amounts ranging from a few parts per million to several percent, can confer luminescent properties on compounds in which they are incorporated. The activators can be introduced mainly in two ways:

- (i) they may be impurity atoms occurring in relatively small concentrations in the host material
- (ii) they may be stoichiometric excess of one of the constituent of the host material itself. This is called self-activation.

For certain activators to function properly, it is necessary to incorporate an additional donor impurity, usually referred to as co-activator. For example, in ZnS type phosphors, along with the activators such as Cu, Ag, Au etc., incorporation of a trivalent impurity (donor; eg. Al) gives high quantum yield of luminescence emission [6]. Some activators are found to evoke or intensify the latent emission line or band of the host material. These types of activators are known as intensifiers. There is another class of activators known as originative activators which produce new emission lines or bands at the expense of the original emission bands of the host material. Two or more activators in suitable proportions in a given phosphor may sometimes be used to produce different emission bands. In certain cases the addition of impurity atoms may inhibit the luminescence efficiency and are referred to as killers [7]. In the preparation of good luminescent materials, the presence of killers should be avoided.

The incorporation of an activator in a phosphor normally gives rise to certain localized energy levels in the forbidden gap. Localized states are the extended states in the forbidden gap [8]. Depending upon the energy levels involved we can distinguish characteristic and non-characteristic luminescence. For characteristic luminescence, the energy levels involved are those of activator atoms themselves which may be get modified by the host lattice. Here the incident quantum of energy is absorbed by the activator atom. When the excited atom returns to its ground state, it loses a part of the energy due to lattice interaction and hence emits a photon of less energy. In this case the trapping does not occur at the same site at which the light emission occurs. In non-characteristic luminescence, number of electrons have to be excited into conduction band before light emission can occur. Here a charge transfer through the lattice is taking place. The energy levels of the host lattice may be modified due to the presence of activator atoms.

### 1.4. Representations Of Luminescence Spectra — Models of luminescence

Most of the luminescent solids exhibit broad, bell-shaped absorption bands near the fundamental absorption edge and emission bands corresponding to lower transition energies. The excitation and emission bands depend on the characteristics of activator system. In order

to explain the luminescence phenomenon, different models are suggested.

#### 1.4.1 Configuration co-ordinate model

Considering the luminescence of solid materials, two major observations need explanation, (a) The emission band appears on the longer wavelength side of the absorption band (b) The emission and absorption are often found as broad bands - hundreds of angstroms wide instead of narrow lines found in atomic luminescence. Both these effects can be explained by using the concept of configuration co-ordinate curves [1]. This can be suitably illustrated with the help of the fig. 1.3 and 1.4. In this model the ordinate is the total energy of system for ground and excited states of the luminescence centre including both ionic and electronic terms. In these curves this energy is shown to vary parabolically as some configuration co-ordinate, usually the distance from the luminescent centre, is changed. There is a value of the co-ordinate for which energy is a minimum. Value of the configuration co-ordinate at which energy is minimum is different for the ground and excited states because of different interactions of luminescence centre with its neighbours. Fig. 1.4 shows the generalised and simplified energy - level diagrams for interpreting many of the luminescence phenomena in solids based on this model. These diagrams which should be used together, are intended to portray the elemental energy transformations in a typical phosphor centre, that is, in the perturbed region produced by a substitutional or interstitial impurity atoms.

Fig. 1.3 shows the variation of potential energy of a phosphor centre ( in only two states) as a function of generalised configurational co-ordinate  $x$  which represents three dimensional changes in the geometrical arrangement of the atoms in the centre. A novel feature of this diagram is the near approach of the ground state and excited state curves at 'f'. When the centre is in energy level 'f', it is assumed to be in a configuration where there is high probability that any excitation energy stored in the centre or delivered to the centre will be dissipated quickly as heat to the surrounding region. An excited centre in equilibrium at, say room temperature, may be in the ground state vibrational level " $E_a$ " from which it can be raised to excited level  $E_b'' - E_a$ . The excited centre gives up some of this energy  $E_b'' - E_c'$  as heat in about  $10^{-12}$ sec and comes to equilibrium in the excited level  $E_c'$ . When the selection rules are favourable the centre may make a spontaneous radiative transition by emitting the energy  $E_c' - E_d'$  as a luminescence photon. At this point the centre still has an excess of vibrational energy above the initial equilibrium level and so it returns to the original ground level by giving up the energy  $E_d' - E_a$  as further heat to the surroundings. When the selection rules for a radiative transition from  $E_c'$  are unfavourable, so that  $E_c'$  is a metastable state, additional energy may have to be provided to raise the centre into a higher excited state from which a radiative transition is permitted. Under these circumstances, the centre in state  $E_c'$  functions as a trap. Excitations and de-excitations of centres take place according to Frank-Condon principle.

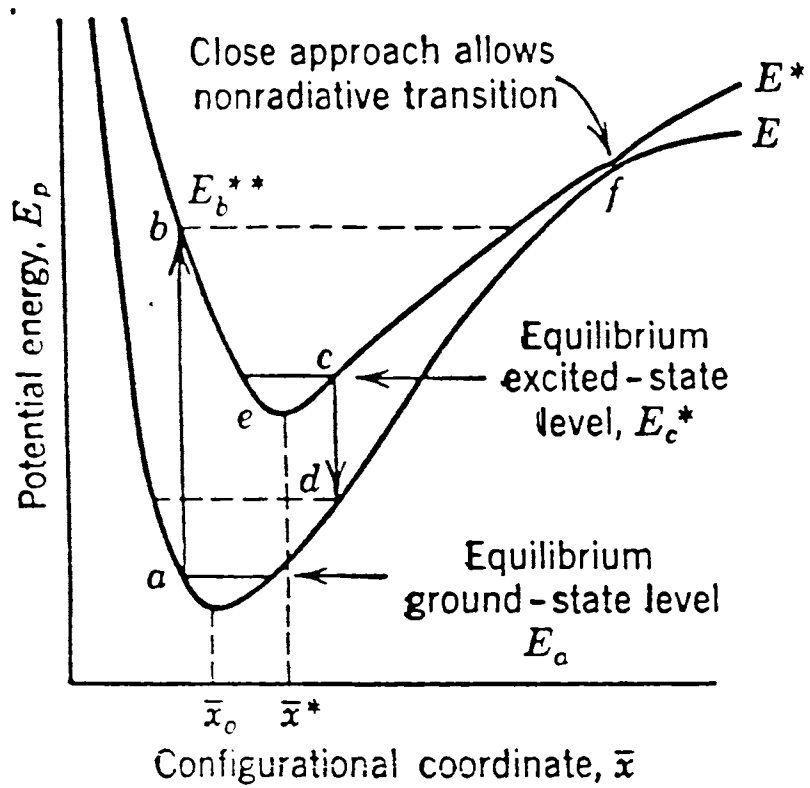


Fig. 1.3 Illustration of configuration co-ordinate model

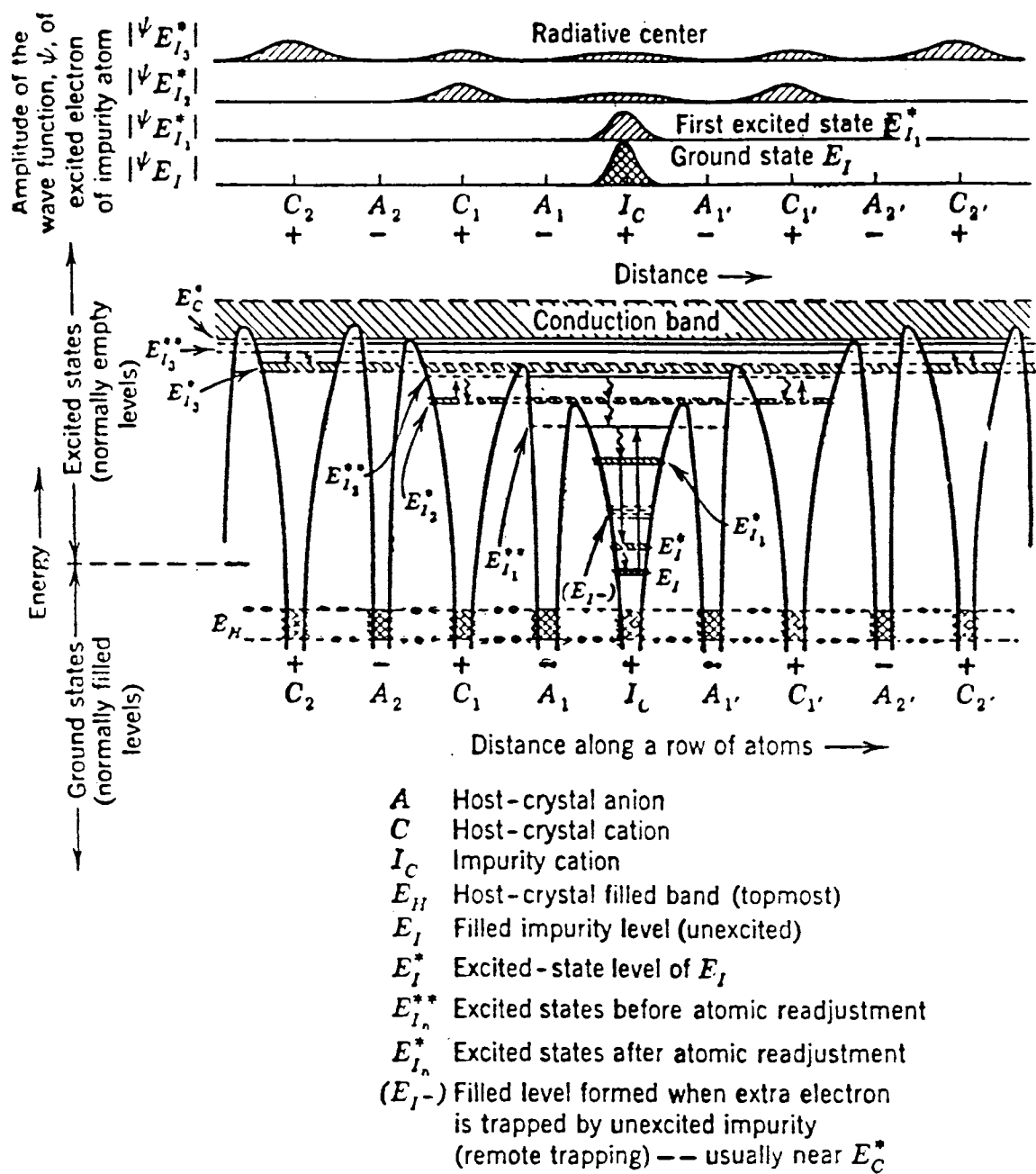


Fig. 1.4 Detailed description of energy level diagrams for interpreting the luminescence processes in solids based on configuration co-ordinate model [1].

When the temperature of the solid is raised, the equilibrium levels  $E_a$  and  $E_c^*$  rise in proportion to the additional vibrational and rotational energy in the centre. when the centre is in the indicated excited state, the probability of being raised thermally into the crossover level

at 'f' is equal to  $\nu_a \exp\left(\frac{-E^*}{KT}\right)$  where  $\nu_a$  is the frequency of vibration of the system

( $\sim 10^{12} \text{ sec}^{-1}$ ) and  $\Delta E^* = E_f^* - E_c^*$  is known as the activation energy. Fig.1.3 indicates how a phosphor centre may function as (1) an activator, by providing a highly probable radiative transition from an excited level well below 'f' (2) a trap, by receiving an additional activation energy to raise the excited centre into a state from which a radiative transition is probable and (3) a killer, by having the excited state equilibrium level sufficiently near or above 'f' so that radiationless transitions predominate. According to the diagram, a centre may operate predominantly as an activator and/or a trap at low temperatures and become increasingly a poison centre as the operating temperatures of the solid is raised to increase the probability of radiationless crossover. The diagram emphasizes, also, that the average inter nuclear spacing and atomic configurations in a centre change during the luminescence process.

Fig.1.4 shows some of the higher energy levels of both the surrounding host crystal and the impurity centre as a function of distance along a chain of atoms passing through the impurity atom. The diagram is drawn for a specific configurational co-ordinate x and so one must imagine that the potential barriers and energy levels change after electronic transitions in the centre. The impurity atom  $I_c$  is shown as introducing an additional occupied ground level (group of levels)  $E_i$  and excited levels  $E_{i1}^{**}$  (before inter nuclear readjustment) and  $E_{i1}^*$  (after inter nuclear readjustment) extending up into the conduction band. As the energy of the excited state increases, the wavefunction  $\Psi$  of the excited electron extends further into the region around the impurity atom. This is indicated by the plots of absolute value of  $\Psi$  at the top of the figure. The excitation transition  $E_i \rightarrow E_{i1}^{**}$  corresponds to  $E_a \rightarrow E_b^{**}$  in the fig.1.3 and the spontaneous radiative return  $E_{i1}^{**} \rightarrow E_i^*$  corresponds to  $E_c^* \rightarrow E_d$ . In this case the luminescence process is highly localized, and is determined mainly by the nature of the activator atom  $I_c$  which is modified by the influence of the host crystal. When the excitation proceeds to much higher energy levels, the activator atom loses control over the luminescence process to the extent that the excited electron wanders away from  $I_c$  and may get trapped at trapping centres so that it requires additional energy for liberation to make a radiative return. If the trapping is done within a parent centre as in  $E_{i2}^*$ , then the activator atom itself helps to provide the trap(s) and determines, in conjunction with the host crystal, the activation energy such as  $E_{i2}^{**} \rightarrow E_{i2}^*$  to release the trapped electron. If, on the other hand, the excited electron is given enough energy to escape from its parent centre, then it travels through the host crystal (in the conduction band levels) until it may be captured in another imperfection or centre. Some

impurities can capture an additional electron (or two) even in the unexcited state to form one or more new occupied levels such as ( $E_i$ ) in fig.1.4. A new set of excited levels is then allowed although these new sets of excited levels may overlap with  $E_c^*$  in those cases where  $E_i$  is near to  $E_c^*$  (shallow remote trap). This type of trapping is most probable when the activator atom is multivalent. When a remote, trapped electron is freed, it may return to its own or another ionized centre (positive hole) to make a radiative transition after entering to one or more of the relatively discrete excited levels associated with the centre. Accordingly, an excited free electron which belongs to the host crystal must become bound to the localized centre before it can make a radiative transition. This mechanism is much more probable than the direct radiative transition of free electrons from the conduction band.

There is another distinctive process whereby an excited electron trapped at  $E_i$  might make a radiative transition. In this process, a positive hole may come to the trapping centre through the filled band  $E_v$  and approach  $I_c$  where an electron may drop from  $E_i$  into the positive hole. The trap then becomes a normal excited centre with a positive hole localized at  $E_i^*$  and an excited electron (formerly trapped) at  $E_{i1}^*$  or at some higher level. By radiative transition of the excited electron to  $E_i^*$  the system returns to the ground state level  $E_i$ . By an extension of this process, it may be possible under certain conditions, to transfer excitation energy in the form of a localized positive hole, from one centre to another. If there are two different centres; one with a positive hole  $E_i^*$  (1), the other in the ground state  $E_i$  (2), then an electron might be raised thermally from  $E_v$  into  $E_i^*$  (1) and the positive hole in  $E_v$  could wander through the normally filled band to the other centre where an electron could drop from  $E_i^*$  (2) to provide a new localized positive hole  $E_i^*$  (2). This process tends to transfer positive hole from energy levels near  $E_v$  to higher levels.

For a given phosphor centre, energy level diagrams are determined by the nature of chemical species, charge, bonding characteristics and crystallographic location of the activator, coupled with the chemical and structural nature of the host material.

### 1.4.2 Energy band model

The usual method of explaining luminescence mechanism in phosphors is by the use of an energy level diagram. When atoms are arranged in an orderly way, the energy state for the electron in atoms are distributed by mutual interaction. As a result, the discrete electronic states are broadened into bands of allowed energy separated by the forbidden gap. The lowest energy band called the valence band, is completely filled with electrons, while the upper energy band corresponding to unoccupied higher levels is called the conduction band. The energy region between the valence band and conduction band is called the forbidden energy gap. Fig.1.5 (a) depicts simplified energy band model showing the mechanism of luminescence. Excitation (step 1) with a photon of sufficient energy across the band gap creates an electron - hole pair.

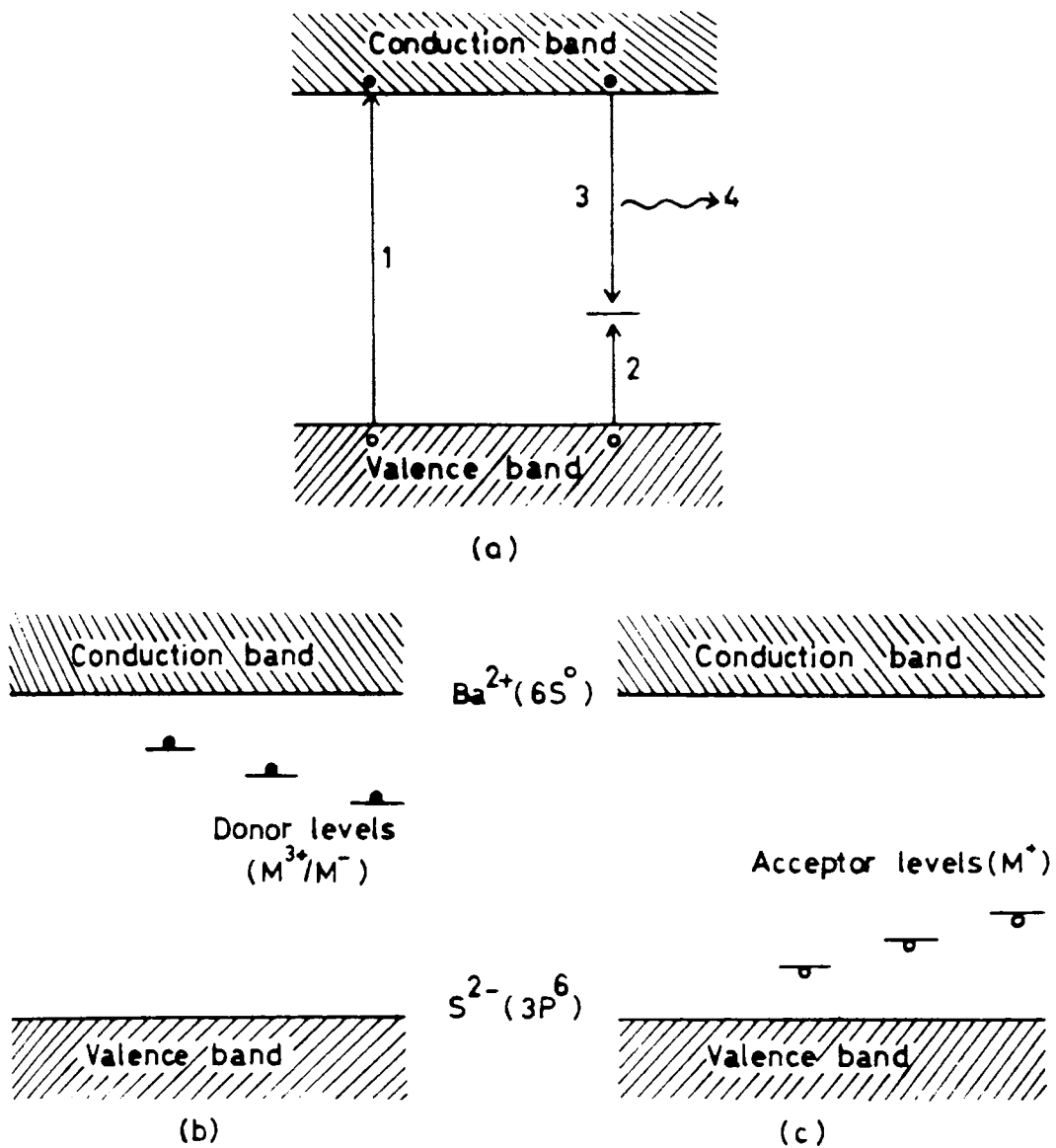
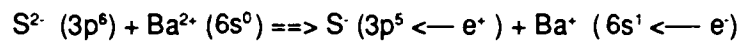


Fig. 1.5 (a) Simplified Energy band model showing mechanism of luminescence; and (b) and (c) show positions of donor and acceptor levels in BaS band gap according to this model

The hole diffuses to the level A, induced by the activator impurity or a defect as shown by step 2. The electron in the conduction band recombines with hole at A, (step 3) thereby releasing a photon (step 4).

The spectral emission of luminescence from phosphors will be a function of the band gap energy, the type of activator and the conditions of excitation. It is seen that as the band gap decreases the spectral distribution of emission shifts to longer wavelengths. In the case of BaS, for example, the conduction band is comprised largely of 6s orbitals of  $Ba^{2+}$  ( $6s^0$ ) cations. At the same time, the valence band of BaS consists of  $S^{2-}$  anions represented by the filled  $3p^6$  orbitals of  $S^{2-}$ . Due to an excitation by radiation with sufficient energy, the ionization states of ions get altered. This causes the detachment of electrons from them and transportation from valence band to conduction band. This can be schematically represented as



Here the sulphide shell remains with a missing electron which is designated as  $e^{\cdot}$  (hole). This hole transforms  $S^{2-} (3p^6)$  to  $S^{\cdot-} (3p^5)$ , with the formation of a hole centre  $S^{\cdot-}$  and it is distributed all over the sulphur atoms of BaS yielding an electron and capturing a hole. In the same manner, an electron transported into the conduction band causes the formation of an electron centre, due to the process  $Ba^{2+} (6s^0) + e^{\cdot} \longrightarrow Ba^{\cdot+} (6s^1)$  and is distributed among all atoms of Ba in BaS by the capture of electrons.

In addition to the usual lattice defects like cation and anion vacancies, the number of additional energy levels can be produced in the forbidden gap by the introduction of suitable impurities. Considering the position in the forbidden band region, the energy levels are divided into two groups [4] as,

- (i) Donor levels which arise due to the substitution of a trivalent ion ( $M^{3+}$ ) in BaS lattice. Two electrons contribute to the formation of a normal chemical bond and the third excess one enters the conduction band. Donor levels can also arise due to the substitution of a monovalent anion ( $M^-$ ) in BaS lattice, which also causes the formation of an excess positive charge. The position of donor level is near the conduction band. In the process of luminescence they act as electron traps and in normal case they are empty. With the capture of an electron, the valency of the donor impurity decreases and it accepts a new position in the band scheme. Here we have to deal with a localized electron. (fig. 1.5(b)).
- (ii) Acceptor levels which arise due to substituting a monovalent cation impurity ( $M^+$ ) in BaS lattice. Its position in the band scheme is near to the valence band. In luminescence process they act as hole traps and in normal state they are filled. When it traps a hole, its valency increases and here we have to deal with a localized hole (fig. 1.5 (b)).



As regards to the electron-hole centres a capture of an electron or hole in the excitation of luminescence by donor and acceptor defects gives rise to the formation of electron-hole centre which is referred to as a photosensitive centre.

Knowing the origin of levels in the forbidden gap, we can now trace out a sequence of events leading to luminescence phenomena. Different schemes suggested in this model are the following :

(a) Lambe-Klick scheme [9]

This is the formation of an electron centre. Here the luminescence appears in course of an electron centre re-combination with a hole in valence band, i.e. a localized electron combine with a free hole (fig. 1.6 (a) ).

(b) Schon-Klassen's scheme [10]

In this scheme the luminescence occurs due to the re-combination of a hole centre with an electron from conduction band or an electron combining with localized hole due to transition from conduction band to impurity or vacancy level (fig.1.6. (b) ).

(c) Donor - Acceptor model [11]

Here the donor level captures an electron from the conduction band and the acceptor level captures a hole from the valence band. After the capture, the emission occurs due to transition from acceptor level to donor level (fig.1.6 (c) ).

## 1.5. Effect Of Crystal field on the spectra of ion .

In fact the mechanism of luminescence process, is a complicated one due to the effect of crystal field or ligand field on the spectra of ions. When an ion or atom is located in the crystal, it is subjected to various inhomogeneous fields produced by the ligands. This causes either splitting up of ionic energy levels or modification of energy levels due to the interaction between the ligands and the impurity ions. Hence, for the complete description of the process, we have to take these effects also into account.

In general, the state of ion activators is described by the levels splitted by the ligand field [12]. The levels of electron-hole centres that originate from ion activators during their ionization are the levels of new ions, which are also splitted by ligand field.

### 1.5.1 Crystal field splitting of $\text{Cu}^+$ energy levels

As an example, let us consider the effect of crystal field on the energy levels of  $\text{Cu}^+$  ion in BaS lattice. For BaS, the crystal field has got a cubical symmetry. In cubical symmetry there

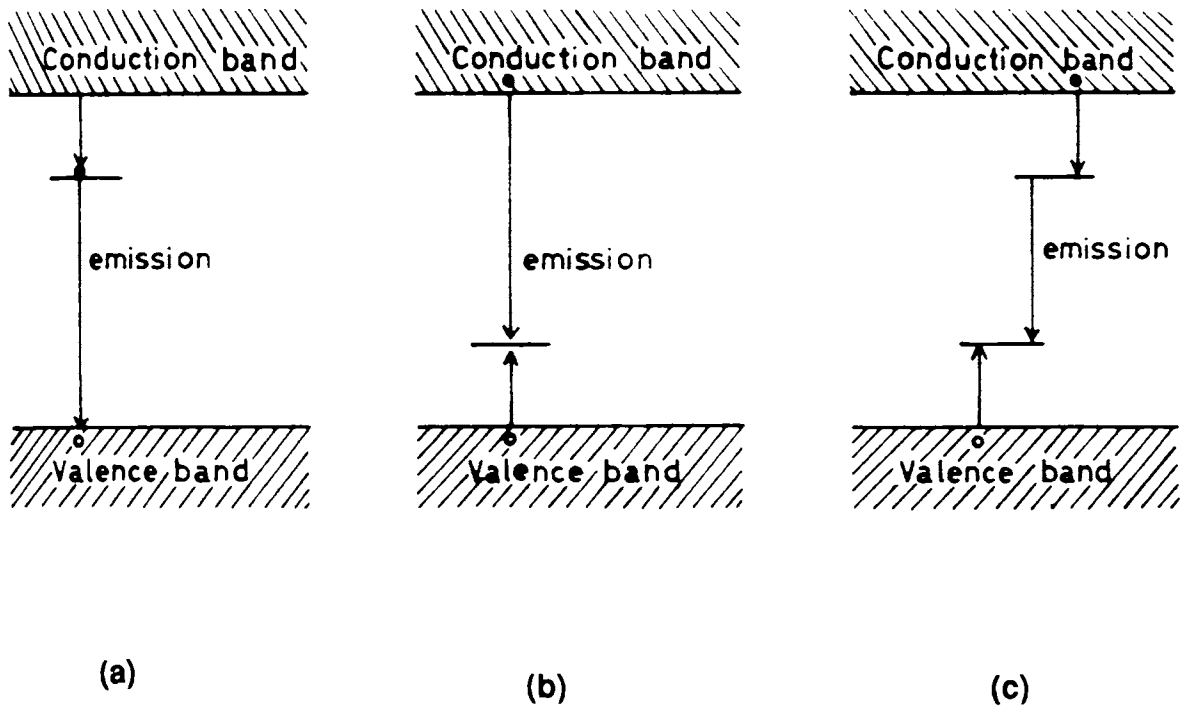


**Fig. 1.6 Different models suggested for the luminescence emission in solids. (a) Lambe-Klick Scheme (b) Schon-Klassen's Scheme and (c) donor-Acceptor model.**

will not be any splitting observed for s and p states of free ions. Usually the splitting is observed for levels for the states with  $l > 2$ . The electron configuration of Cu is Cu (—)  $3d^{10} 4s^1$ . When it is introduced in the lattice as  $Cu^{+}$  the free electronic state corresponds to the configuration Cu (—)  $3d^{10} 4s^0$ . The introduction of  $Cu^{+}$  causes the perturbation of  $O_h$  symmetry of BaS. Its free electronic states and modification in cubic crystal field is as shown in fig. 1.7.

### 1.5.2 Effect of crystal field on $RE^{3+}$ energy levels.

As far as the effect of crystal field on rare-earth (RE) ions is considered the difference lies in the fact that, rare-earth ions have unfilled f-orbitals, which are screened by the completely filled S and P electrons and can be written as.

$$(1s^2 2s^2 2p^6 3s^2 3p^6 3d^{10} 4s^0 4p^6 4d^{10}) 4f^n (5s^2 5p^6) (5d^1) 6s^2$$

Usually the splitting of the  $RE^{3+}$  energy levels by crystal field reaches a magnitude of the order of  $10^2 \text{ cm}^{-1}$  while spin-orbital interaction is of the order of  $10^3 \text{ cm}^{-1}$  [4]. The splitting of each one of the multiplet levels by the crystal field is determined by the quantum number  $l$  and the symmetry of the crystal field. Fig. 1.8 shows the multiplet  $RE^{3+}$  (lanthanides) energy levels owing to the principal transitions leading to luminescence emission [13]. The fine structures of  $RE^{3+}$  spectra depend on the characteristics of the host material, the presence of co-activators, local or non-local compensation of charge, the manner of ion's incorporation, concentration of the activator etc.

The multiplicities of various degenerate levels of  $RE^{3+}$  in the host crystal can be predicted theoretically by a method suggested by Lea et. al [14] and Zhong and Bryant [15] in conjunction with point charge crystal field model.

According to Lea et. al, for the 4f states of RE ions within a manifold of angular momentum composed of f electron wave functions, the most general operator equivalent potential with cubic point symmetry may be written as

$$H = B_4 (O_4^0 + 5 O_4^4) + B_6 (O_6^0 - 21 O_6^4) \quad 1.(3)$$

where  $O_l^m$  the spherical harmonic functions are given by

$$O_4^0 = 35 J_z^4 - [30 J(J+1) - 25] J_z^2 - 6 J(J+1) + 3 J^2(J+1)^2$$

$$O_4^4 = 1/2 (J_+^4 + J_-^4)$$

$$O_6^0 = 231 J_z^6 - 105 (3 J(J+1) - 7) J_z^4 + [105 J^2 (J+1)^2 - 525 J(J+1) + 294] J_z^2 - 5 J^3 (J+1)^3 + 40 J^2 (J+1)^2 - 60 J(J+1)$$

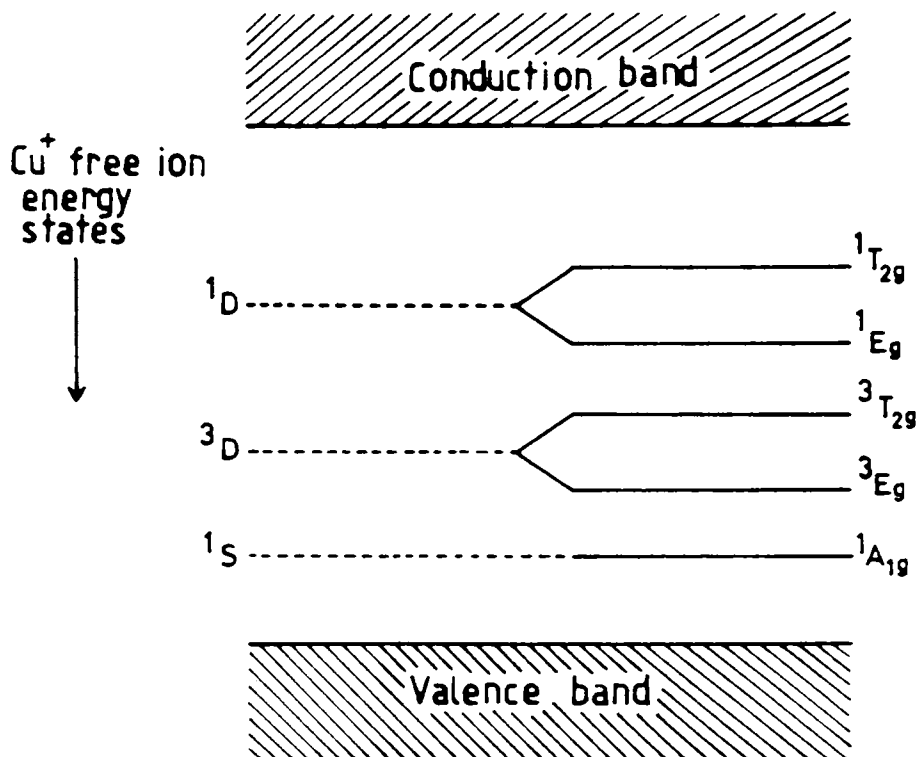


Fig. 1.7 Energy level diagram of  $\text{Cu}^+$  due to crystal field splitting

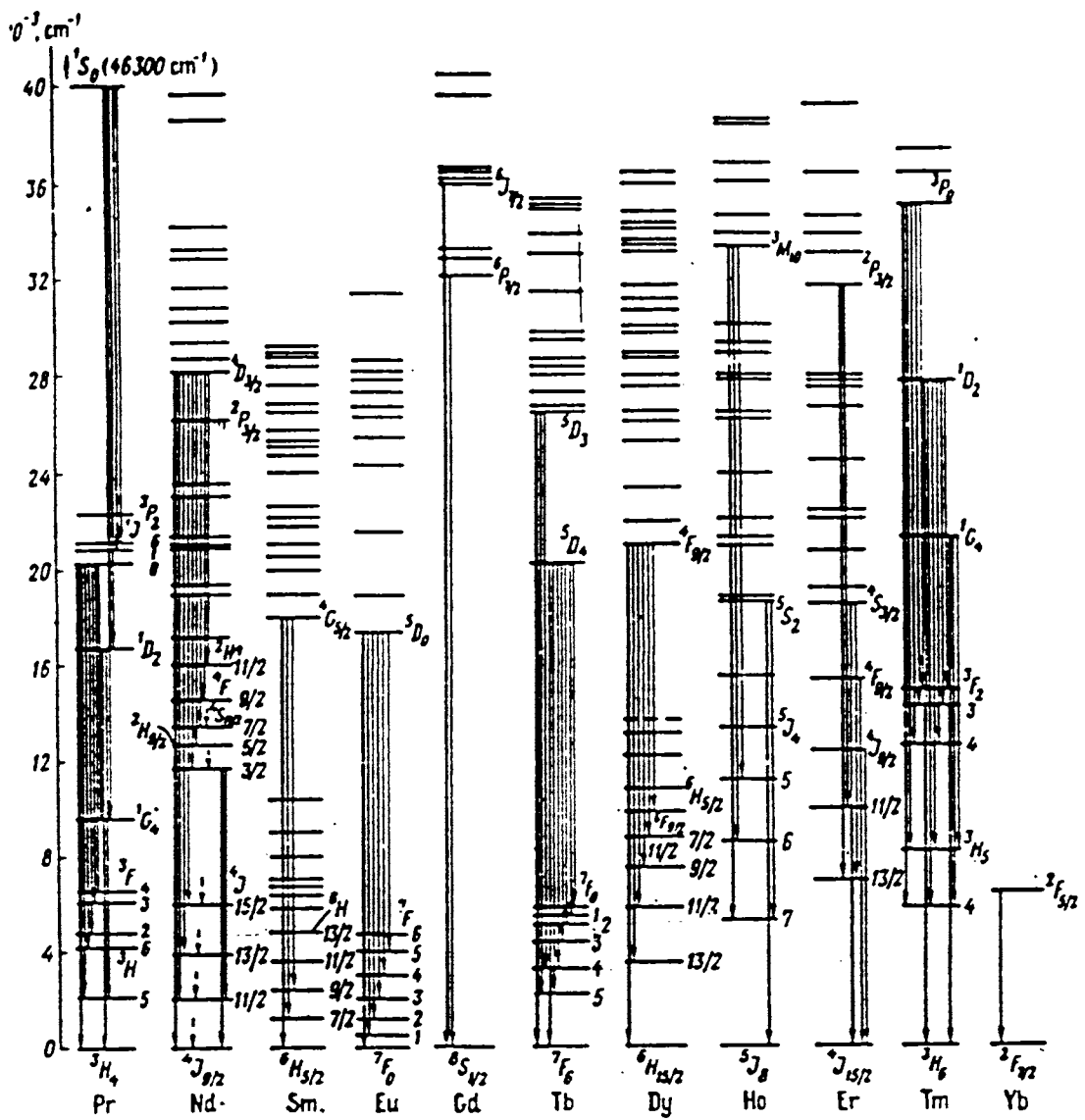


Fig. 1.8 Diagram showing energy terms of RE<sup>3+</sup> owing to principal transitions leading to luminescence emissions [13].

$$O_6^4 = 1/4 [11 J_z^2 - J(J+1) - 38] (J_z^4 + J_z^4) + 1/4 (J_z^4 + J_z^4) [11 J_z^2 - J(J+1) - 38]$$

with x,y,z axes chosen along the <100>, <010>, and <001> directions. The coefficients  $B_4$  and  $B_6$  are factors which determine the scale of the crystal field splittings. They are linear functions of  $\langle r^4 \rangle$  and  $\langle r^6 \rangle$ , the mean fourth and sixth powers of radii of the magnetic ion wave functions. Since these are very difficult to calculate quantitatively, it is customary to regard the coefficients  $B_4$  and  $B_6$  as parameters to be determined empirically.

For the numerical calculation of the eigen values for each J manifold, the  $(2J+1) \times (2J+1)$  matrix is written down using the operator equivalent matrix element as tabulated by Stevens and Elliot [16]. These contain factors common to all the matrix elements  $F(4)$  and  $F(6)$  and these are separated out in calculation, in order to keep the eigen values in the same numerical range for all ratios of the fourth and sixth degree terms. Then the Hamiltonian can be written as

$$H = B_4 F(4) \frac{O_4}{F(4)} + B_6 F(6) \frac{O_6}{F(6)} \quad 1.(4)$$

where  $O_4$  and  $O_6$  are given by

$$O_4 = O_4^0 + 5 O_4^4 \text{ and } O_6 = O_6^0 - 21 O_6^4$$

In order to cover all possible value of the ratio between the fourth and sixth degree terms, take

$$B_4 F(4) = Wx \quad 1.(5)$$

$$B_6 F(6) = W(1 - |x|) \quad 1.(6)$$

where x is a dimensionless parameter which can have values between -1 and +1. It follows that

$$\frac{B_4}{B_6} = \frac{x}{(1 - |x|)} \frac{F(6)}{F(4)} \quad 1.(7)$$

so that

$$\frac{B_4}{B_6} = 0 \text{ for } x = 0 \text{ while } \frac{B_4}{B_6} = +\infty \text{ for } x = \pm 1$$

Re-writing equation 1.(4)

$$H = W \left[ x \frac{O_4}{F(4)} + (1 - |x|) \frac{O_6}{F(6)} \right] \quad 1.(8)$$

The term expressed in the square bracket represents a matrix whose eigen vectors correspond to the most general combination of fourth and sixth degree crystal fields and where eigen values are related to the crystal field energy levels by a scale factor  $W$  defined by the eq. 1.(5) and 1.(6). The diagonalization of this matrix yields the eigen values and has been represented diagrammatically for various  $J$  values [14]. This will correspond to energy levels splitting pattern of  $RE^{3+}$  in a crystal field. Such pattern for the splitting of  $J$  manifold for  $J = 7/2$ ,  $J = 9/2$  and  $J = 4$  are shown in 1.9(a) and (b) and 1.9(c).

One can find the sign of the scale factor  $W$  and that of the parameter  $x$  directly from the signs of  $B_4$  and  $B_6$  as follows; (i) from eq. 1.(6), from which the sign of  $W$  is determined by the sign of  $B_6$ , since  $(1 - |x|)$  is always positive for  $-1 < x < +1$  and (ii) from eq. 1.(5) which shows the sign of  $x$  is determined by the sign of  $B_4/B_6$  since  $F(6)$  &  $F(4)$  both positive for all  $J$ 's. Sign of  $B_4$  and  $B_6$  can be found out from the point charge crystal field model for the geometrical co-ordination factors  $A_4$  and  $A_6$ . There are three types of cubic co-ordination corresponding to 4, 6 or 8 equidistant charges  $Ze$ . For each of these, the point charge model gives the following results (Table 1.1).

Table 1.1 Point charge model parameters [14]		
Type of co-ordination	$B_4 = A_4 \langle r^4 \rangle$	$B_6 = A_6 \langle r^6 \rangle$
Tetrahedral - (4)	$-\frac{7}{36} \frac{Ze^2 \langle r^4 \rangle}{R^5} \beta$	$+\frac{1}{18} \frac{Ze^2 \langle r^6 \rangle}{R^7} \gamma$
Octahedral - (6)	$+\frac{7}{36} \frac{Ze^2 \langle r^4 \rangle}{R^5} \beta$	$+\frac{3}{64} \frac{Ze^2 \langle r^6 \rangle}{R^7} \gamma$
Cubic - (8)	$-\frac{7}{18} \frac{Ze^2 \langle r^4 \rangle}{R^5} \beta$	$+\frac{1}{9} \frac{Ze^2 \langle r^6 \rangle}{R^7} \gamma$

Here  $R$  is the distance of the co-ordinating charges  $Ze$  from the magnetic ions, ' $e$ ' is the charge of the electron, ' $r$ ' is the radius of the ion,  $\beta$  and  $\gamma$  are the Stevens multiplicative constants [17]. The numerical values of  $\beta$  and  $\gamma$  for all  $RE^{3+}$  are given by Elliot and Stevens as given in Table 1.2.

<b>Table 1.2.</b>				
<b>Values of multiplicative factors <math>\beta</math> and <math>\gamma</math> (Stevens and Elliot [16])</b>				
Rare- Earth ion	Ground term	$\beta \times 10^4$	$\gamma \times 10^6$	$\beta/\gamma$
Ce <sup>3+</sup>	F <sub>5/2</sub>	63.4920	0	$\infty$
Pr <sup>3+</sup>	H <sub>4</sub>	-7.3462	60.9940	-12.0440
Nd <sup>3+</sup>	I <sub>9/2</sub>	-2.9111	-37.9880	7.6632
Pm <sup>3+</sup>	I <sub>4</sub>	4.0755	60.7810	6.7052
Sm <sup>3+</sup>	H <sub>5/2</sub>	25.0120	0	$\infty$
Tb <sup>3+</sup>	F <sub>6</sub>	1.2244	-1.1212	109.2000
Dy <sup>3+</sup>	H <sub>15/2</sub>	-0.5920	1.0350	57.2000
Ho <sup>3+</sup>	I <sub>8</sub>	-0.3330	-1.2937	25.7400
Er <sup>3+</sup>	I <sub>15/2</sub>	0.4440	2.0699	21.4500
Tm <sup>3+</sup>	H <sub>6</sub>	1.6325	-5.6081	-29.1200
Yb <sup>3+</sup>	F <sub>7/2</sub>	17.3160	148.0000	-11.7000



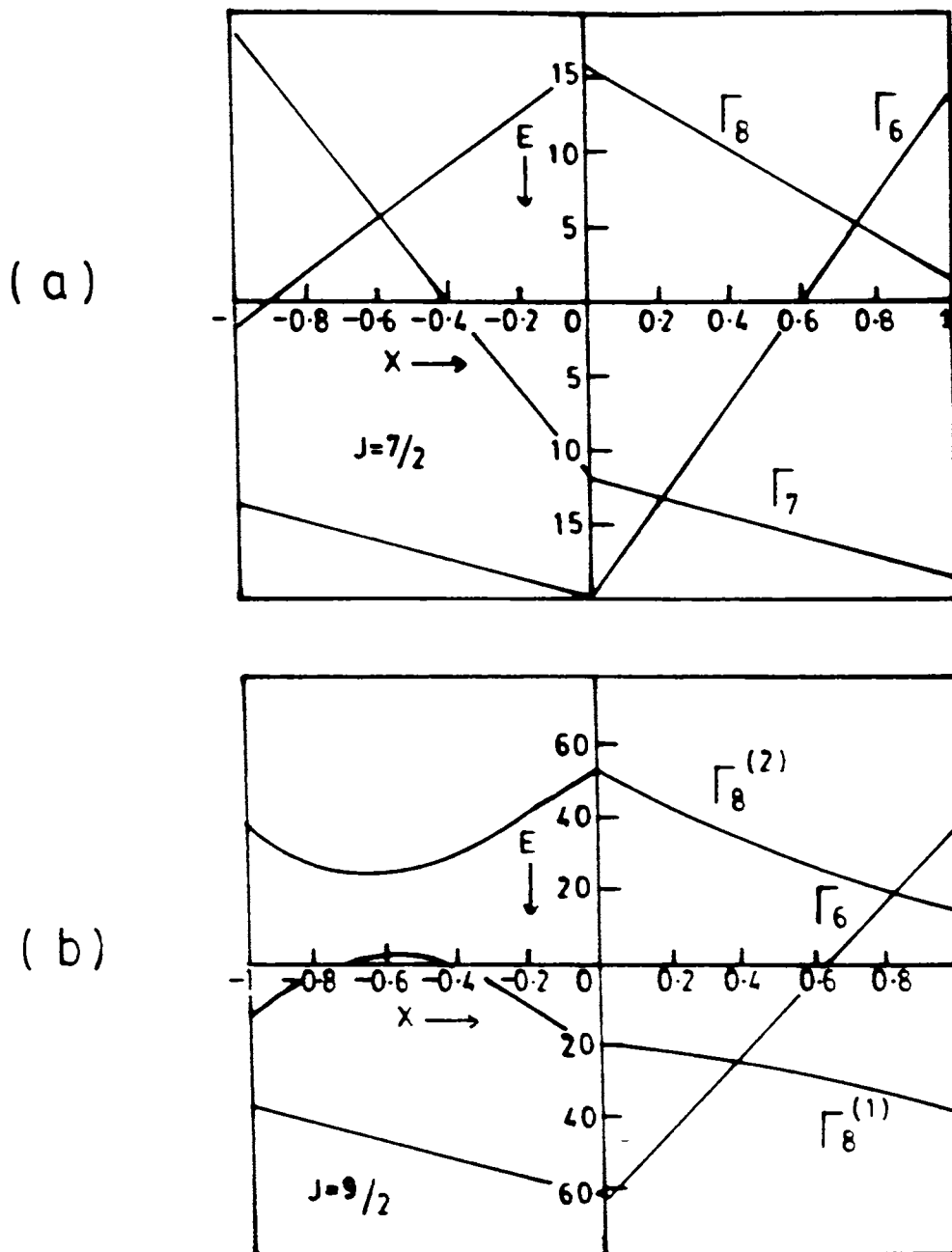


Fig. 1.9 Energy level splitting patterns of J manifold in cubic crystal field [14] for (a)  $J = 7/2$  (b)  $J = 9/2$  terms.

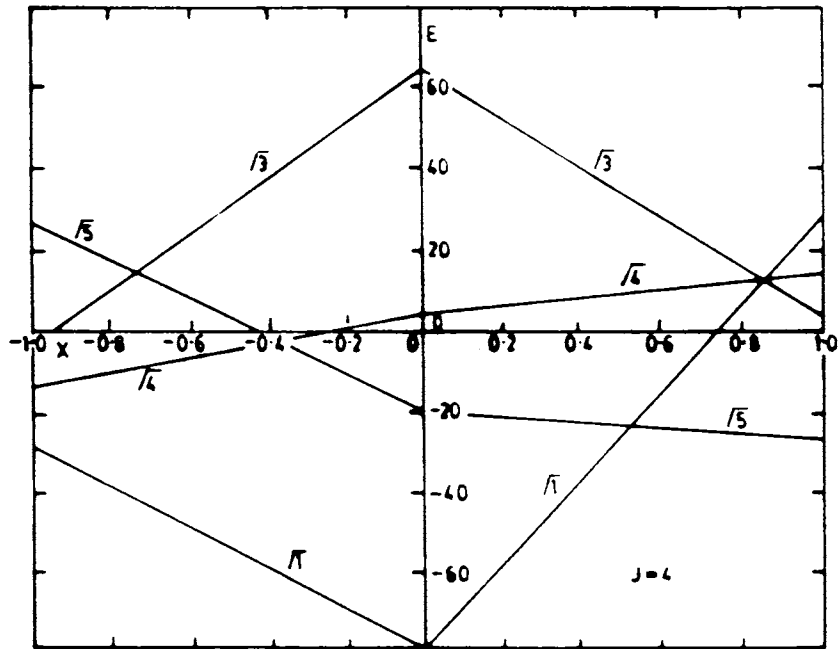


Fig. 1.9(c) Energy level splitting pattern of  $J$  manifold in cubic crystal field [14] for  $J = 4$  term.

Freeman and Watson[18] gave the values of  $\langle r^n \rangle$  for the 4f electrons of RE<sup>3+</sup> in terms of  $a_0$ - the Bohr radius ( given in Table 1.3).

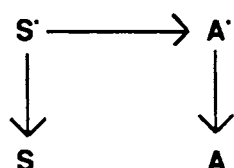
<b>Table 1.3</b> <b>Values of <math>\langle r^n \rangle</math> in units of Bohr Radii using 4f wave function</b> <b>(Freeman and Watson [18])</b>			
Rare-Earth ion	$\langle r^2 \rangle$	$\langle r^4 \rangle$	$\langle r^6 \rangle$
Ce <sup>3+</sup>	1.200	3.455	21.226
Pr <sup>3+</sup>	1.086	2.822	15.726
Nd <sup>3+</sup>	1.001	2.401	12.396
Sm <sup>3+</sup>	0.883	1.897	8.775
Eu <sup>3+</sup>	0.938	2.273	11.670
Gd <sup>3+</sup>	0.785	1.515	6.281
Dy <sup>3+</sup>	0.726	1.322	5.102
Er <sup>3+</sup>	0.666	1.126	3.978
Yb <sup>3+</sup>	0.613	0.960	3.104

### 1.6. Transfer Of Energy In Luminescence Processes.

Energy transfer occurring in luminescence processes during absorption and emission is not confined to same centre. Energy transfer plays an important role in luminescence phenomena. When there are two activators in a crystal, though the emission lines may not change due to the presence of the second activator, the following changes are possible. (i) the intensity of the luminescence spectrum of one ion can gain in strength at the expense of the other (ii) an ion not luminescent at a given concentration in a given crystal becomes luminescent in the

presence of another ion in the same crystal (iii) luminescence of an ion can be observed under conditions of excitation in which it is not luminescent without the presence of another ion (iv) with complete quenching of one centre, intensified luminescence can be observed from the other centre.

The above changes in luminescence of one ion in the presence of the other is due to transfer of excitation energy from one to the other. Luminescence of ions excited as a result of the energy transfer from one to the other excited ion is termed as sensitized luminescence and proceeds conformable to the scheme [19].



Here 'S' is the sensitizer (energy donor) and A is the activator (energy acceptor). Asterisks denote their excited states.

In sensitized luminescence, the energy absorbed in the absorption band of one ion (sensitizer) can be re-emitted in the emission band of the other ion (activator). Sensitization can be accomplished in two ways:

(i) Impurity sensitization -ie. with the help of admixture of different ions and (ii) lattice sensitization -ie. with aid of ions entering the composition of the host itself.

In these cases, the transfer of energy does not involve the motion of electrons; it is accomplished mainly due to following three schemes.

**(a) Emission re-absorption type**

This implies the emission of light by a single ion and its absorption (re-absorption) and emission by the other ion (fig.1.10(a)). In this case even though both the ions behave like independent systems, for this type of energy transfer to manifest, the essential requirement is the closeness of the emission energy of one ion to the absorption energy of the other. Both ions should be activators and have sufficiently intense absorption bands, while the luminescence emission band of one of them must be overlapped by the absorption band of the other.

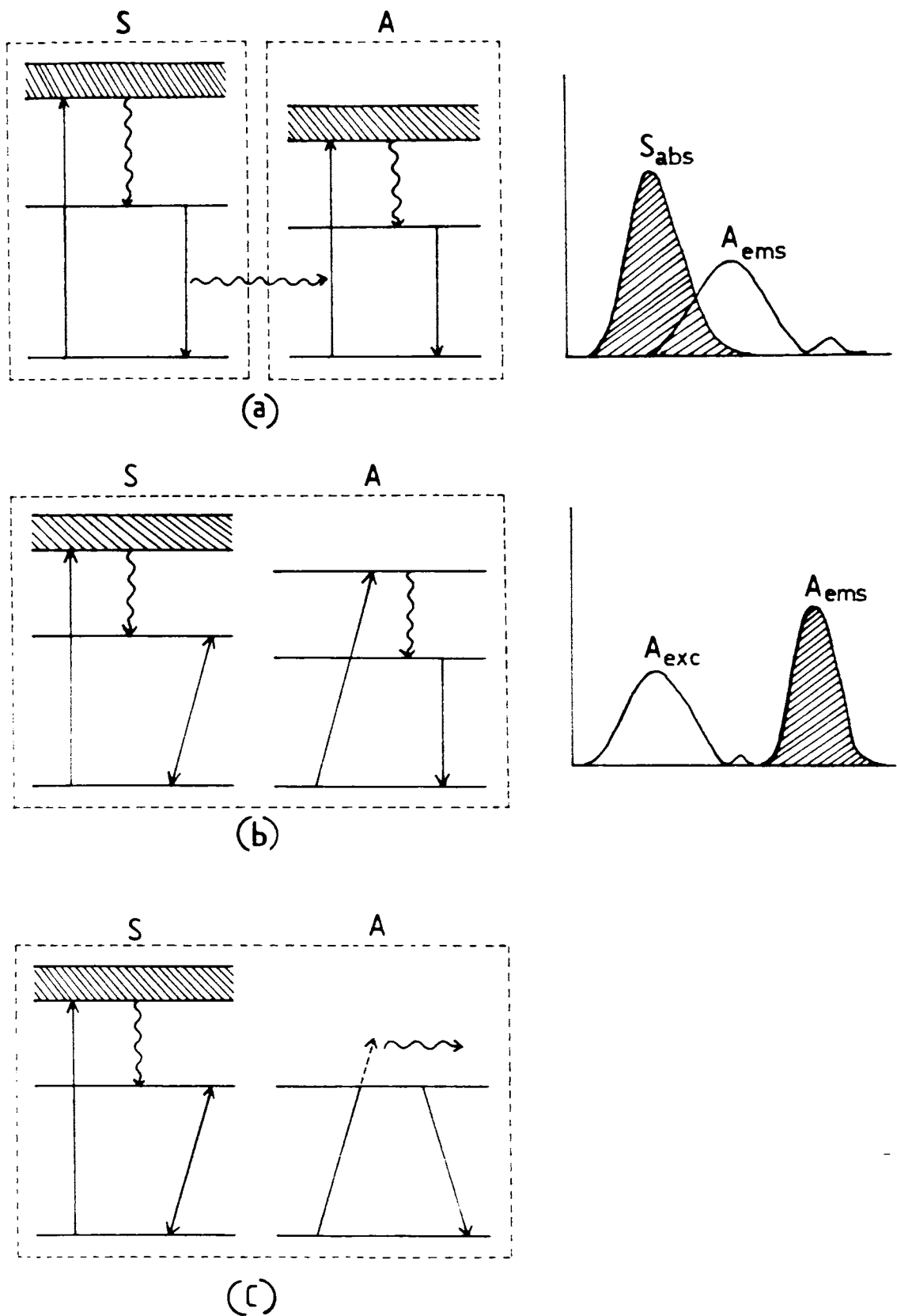


Fig. 1.10 Different energy transfer mechanisms (a) emission - reabsorption type (b) resonance - radiationless type (c) non-resonance - radiationless type

S - Sensitizer; A - Activator

**(b) Resonant - radiationless type**

This is the energy transfer effected between interacting systems behaving like a single system (fig 1.10(b)). In this case also the mechanism of energy transfer is effected due to the coincidence or the closeness of energy level pairs of the ion sensitizer and the ion activator. But the essential difference is that the transition between the levels of the sensitizer is not necessarily emissive, whereas the activator's absorption corresponding to the pair of levels close to the first one may be of low intensity. Then the emission of the activator does not necessarily occur as a result of transition between the pair of levels to which the energy of the sensitizer is transmitted. The ion sensitizer (energy donor) cannot by itself be an effective activator of luminescence; while the ion activator (energy acceptor) may not have sufficiently intense absorption bands suitable for inducing luminescence. However the broad absorption bands of the sensitizer and emission transitions of the activator comprise together a system capable of effective luminescence.

**(c) Non-resonant radiationless type**

In this case the mechanism leads to the transfer of energy, when the distance between the levels of an ion transferring energy is not coincident with that of ion receiving it. (fig.1.10(c)). The energy difference between these levels goes either to the lattice in the form of phonon or to a third ion which has a pair of levels corresponding to this difference.

This mechanism of energy transfer involves an exchange interaction between ions and comes into play over very short distances (upto 7-8 Å°).

**1.6.1. Resonant energy transfer**

The transfer of energy has been treated theoretically using quantum mechanics by assuming a model of resonance between coupled systems [20]. The sensitizer has an allowed transition only if it absorbs the exciting light appreciably. The probability of energy transfer P varies according to

$$P = \frac{1}{R^6 n^4} \int F_s F_A ds \tag{1.9}$$

where R - is the distance between sensitizer and activator

n - the index of refraction of the host material

$F_s$  - A function describing the emission band of the sensitizer as a function of energy and is

normalized so that the area under the curve is unity.

$F_A$  - is a function describing the absorption band of the activator and also normalized to unity.

The integral of the above expression measures the overlap of these bands and determines the resonant transfer. In typical cases, the sensitizer will transfer energy to an activator if the activator occupies only one of 1000-10,000 nearest available sites around the sensitizer [21].

### 1.6.2. Quenching

Another phenomenon related to the resonant transfer of energy is the quenching [22]. There are different types of quenching like temperature quenching, concentration quenching, impurity quenching etc. The main function of the quenchers are to reduce the life time of the excited state.

If the phosphors are prepared with increasing concentrations of activators, the brightness will first increase but will be quenched at higher concentrations. Change of brightness with growing activator's concentration is different for different activators. It is believed that at high concentrations the absorbed energy is able to get transferred from one activator to a nearby one by resonant transfer and this migrates through the solid. If there are quenching sites distributed in the material the migrating energy may reach one and be dissipated without luminescence. As the concentration is increased the speed of migration is increased and the quenching process becomes increasingly important.

## 1.7. Luminescence As A Function Of Time.

There are three obvious time components in an individual one-quantum luminescence process; (i) energy - absorption or excitation - transition time (ii) the life time of the excited state (iii) the energy - emission or radiative - transition time. These three components are experimentally inseparable and so they are treated as a single life time (of the excited state). This approximation is valid since magnitude of (i) and (iii) phenomena is very small as compared to (ii). The luminescence emission which occur at times greater than the natural fluorescence life times are called phosphorescence. It denotes a constrained, partially forbidden or unnatural decay in the radiative return of an excited system to the ground state. The decay phenomenon is usually associated with the existence of metastable states.

### 1.7.1 Kinetics of luminescence

We usually distinguish two kinds of luminescence processes viz., kinetics of first order

(monomolecular mechanism) and kinetics of second order (bimolecular mechanism)

(a) First - order kinetics

The number of excited electrons 'N' decreases according to a constant probability law,

$$\frac{dN}{N} = - \alpha dt \quad 1.(10)$$

which gives solution  $N = N_0 e^{-\alpha t}$  1.(11)

The luminescence intensity is given as

$$I \propto \frac{dN}{dt} ; \text{ then } I = I_0 e^{-\alpha t} \quad 1.(12)$$

The major characteristics is the life-time which is the average stay of ion in a given excited state.

(b) Second order kinetics

In this case if the probability for recombination is proportional to the number of centres; then

$$\frac{dN}{N^2} = - \alpha N dt \quad 1.(13)$$

$$N = \frac{N_0}{1 + N_0 \alpha t} \quad 1.(14)$$

This shows that N decreases hyperbolically with time

Since

$$I \propto \frac{dN}{dt} = \alpha N^2 \quad 1.(15)$$

$$I = \frac{I_0}{(1 + at)^2} \quad \text{where } a = \sqrt{I_0 \alpha} \quad 1.(16)$$

Here the decay become more rapid as the excitation intensity is increased.

The above kinetics can be applied only if the optical transition is associated with dipole radiation or to say if  $\tau \sim 10^{-8}$  sec. In the case of phosphorescence, the kinetics involved in the process depends on the spatial relation between luminescence centres and on the motion of conduction



electrons. The glow of activators resulting from the heat release at a constant temperature of electrons and holes captured by shallow traps is phosphorescence. The afterglow is longer at lower temperature and shorter at higher temperature showing the strong dependence of phosphorescence on temperature.

### 1.7.2. Life time of a level

The life of a level  $\tau_m$  is related to the probability  $A_{mn}$  of transition between levels  $m$  and  $n$  and also to the oscillation strength for the absorption band  $f_{nm}$ . In a free ion, life time  $\tau_m$  of an excited state 'm' is inversely proportional to the transition probability,  $A_{mn}$  from this level

$$\text{ie.} \quad \tau_m = \frac{1}{A_{mn}} \quad 1.(17)$$

This transition probability is related to oscillator strength  $f_{nm}$  through the relation

$$A_{mn} = \frac{8\pi^2 e^2 \nu^2}{3m_e c^3} f_{nm} \quad 1.(18)$$

$$\text{i.e.} \quad f_{nm} = \frac{3m_e c^3}{8\pi^2 e^2 \nu^2} A_{mn} \quad 1.(19)$$

substituting the values of atomic constants the charge and mass of e, 'e' 'm<sub>e</sub>',

$$A_{mn} = 0.22 \frac{\nu^2}{c^3} f_{nm} \quad 1.(20)$$

or

$$f_{nm} = 4.5 \frac{c^3}{\nu^2} A_{mn} \quad 1.(21)$$

From the above relations one can obtain the values for the transition probabilities  $A_{mn}$  and life time  $\tau_m$  in seconds. Relations among  $\tau$ ,  $A$  and  $f$  in the case of free ion and also for an ion in a crystal are as shown in fig 1.11.

If the transition from a given level 'm' occurs over several adjacent levels the life time  $\tau_m$  is given as

$$\tau_m = \frac{1}{\sum A_{mn}} \quad 1.(22)$$

The ion in a crystal interacts with the surrounding ions resulting in radiationless transition. The probability of radiationless transition is the probability of luminescence decay. The life time of the energy levels of an ion in a crystal is then reduced due to radiationless transition

$$\tau_m = \frac{1}{\Sigma A_{mn} + \Sigma C_{mn}} \quad 1.(23)$$

where  $C_{mn}$  is the probability of radiationless transition. This value of  $\tau_m$  determines the experimentally measured value of duration of glow.

### 1.7.3 Decay Law

The luminescence decay law determines the diminution of the number of emitted photons with time and is designated as  $N_i(t)$

$$N_i(t) = - \frac{dN}{dt} = - N_m A_{mn} = - \frac{N_m}{\tau_m} \quad 1.(24)$$

This decay law can be re-written as

$$N_i(t) = N_m e^{-A_{mn}t} \quad 1.(25)$$

$$\text{or } N_i(t) = N_m e^{-t/\tau} \quad 1.(26)$$

The decay thus proceeds exponentially.

The radiation power  $P$  is associated with the probability of transition  $A_{mn}$

$$P = h\nu_{mn} A_{mn} \quad 1.(27)$$

Hence the emission intensity can be written as

$$I_{\text{emission}} = N_m h\nu_{mn} A_{mn} \quad 1.(28)$$

The intensity of emission is thus determined by the probability of transition  $A_{mn}$  and the oscillator strength  $f_{nm}$  of a given transition. In the event of transition with great oscillator strength, interaction with the lattice can lead to a reduced emission intensity due to radiationless transition.

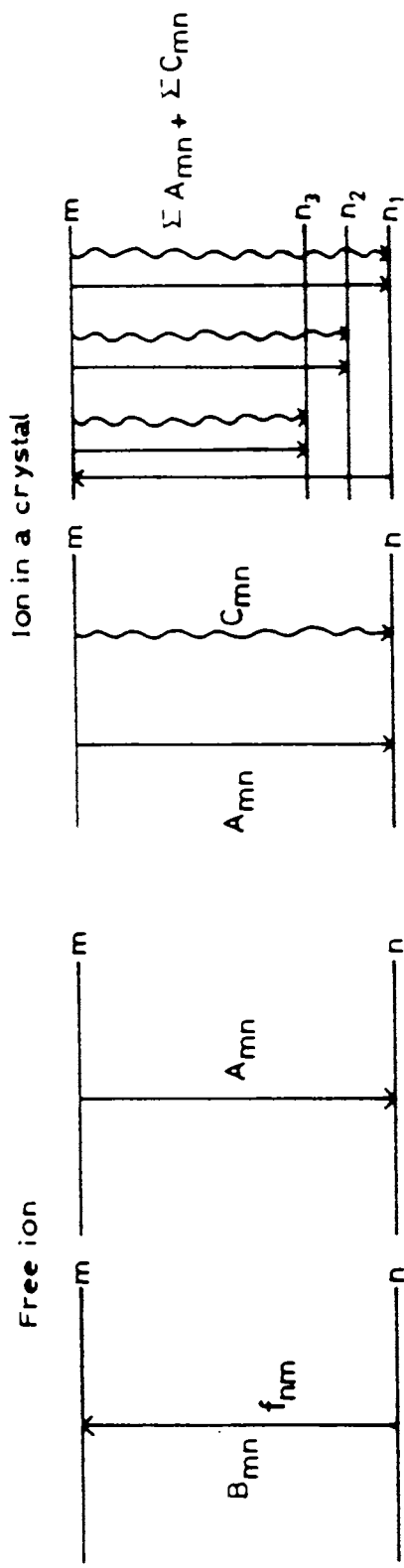


Fig. 1.11 Relations among  $\tau$ , A and f in the case of free ion and for the ion in a crystal

$B_{mn}$  - Probability of transition with  $n \rightarrow m$  absorption

$f_{nm}$  - Oscillator strength for absorption band  $n \rightarrow m$

$A_{mn}$  - Probability of emission transition  $m \rightarrow n$

$C_{mn}$  - Probability of radiationless transition  $m \rightarrow n$

$\Sigma A_{mn}$  - Sum total of probabilities for emission transitions  
 $m \rightarrow n_1, m \rightarrow n_2, m \rightarrow n_3$

$\Sigma C_{mn}$  - Sum total of probabilities for radiationless transitions  
 $m \rightarrow n_1, m \rightarrow n_2, m \rightarrow n_3$

**1.7.4 Different Decay mechanisms [1]**

The process of phosphorescence arises due to a number of complicated terms such as transitions between bands, activators with transfer of the electron and hole involving temporary capture by traps, by the presence of traps with different depths, by possible repeated trapping etc. In order to explain the mechanism of decay different methods are suggested.

**(a) Temperature - independent decay:**

**(i) Simple exponential decay**

As an elementary example of this type of decay consider the fig. 1.12(a) which represents an optical absorption 'E<sub>a</sub>' and resonance emission 'E<sub>e</sub>' transition of an isolated atom. If there be N excited atoms at time 't' then the luminescence intensity (radiance) I from N atoms will be given by

$$I \propto - \frac{dN}{dt} = \alpha N \tag{1.29}$$

ie. the number of photons emitted or atoms de-excited at time 't' is equal to a rate constant α times the number 'N' of the excited atoms existing at time 't'. Integration of eq.1.(29) yields

$$- \log I \propto - \log N = \alpha t \tag{1.30}$$

where the rate constant α is equal the reciprocal of the life time τ of the excited state

$$\alpha = \frac{1}{\tau} = S \exp (- E/KT) \tag{1.31}$$

(where 'S' the frequency factor)

and τ is the time taken by the system to decay to e<sup>-1</sup> I<sub>0</sub> (= 0.36788 I<sub>0</sub>)

where I<sub>0</sub> is the luminescence emission intensity at t = 0

(ie. at the instant of cessation of excitation).

Hence 
$$I = I_0 e^{-\alpha t} \tag{1.32}$$

A plot of log I vs 't' is a straight line for an exponential decay. There are no external constraints on the free atoms assumed in this example and so τ is about 10<sup>-8</sup> sec. The life time of the excited state decreases with increasing energy of the emitted photon E<sub>e</sub> and the line width

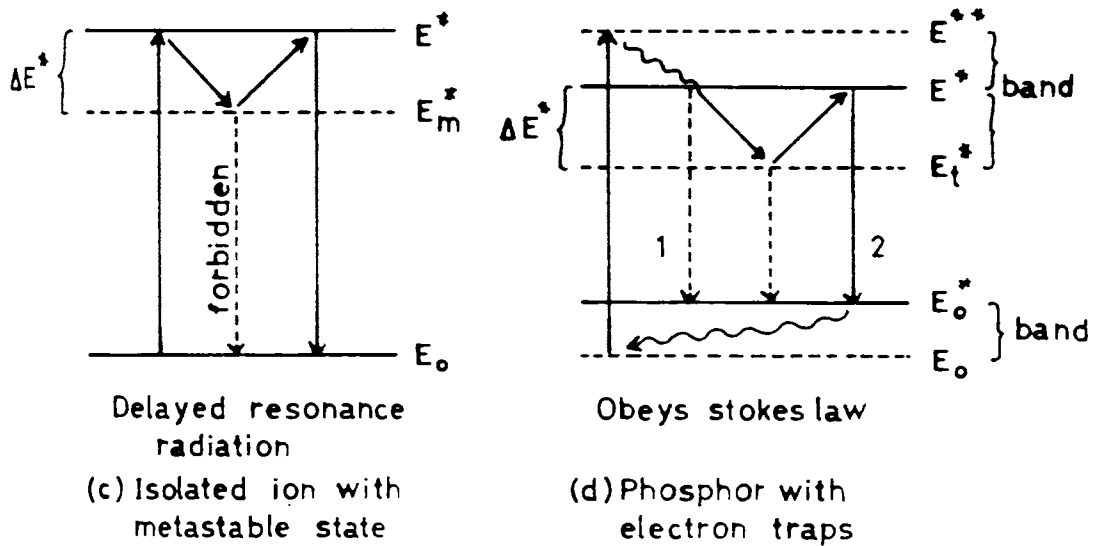
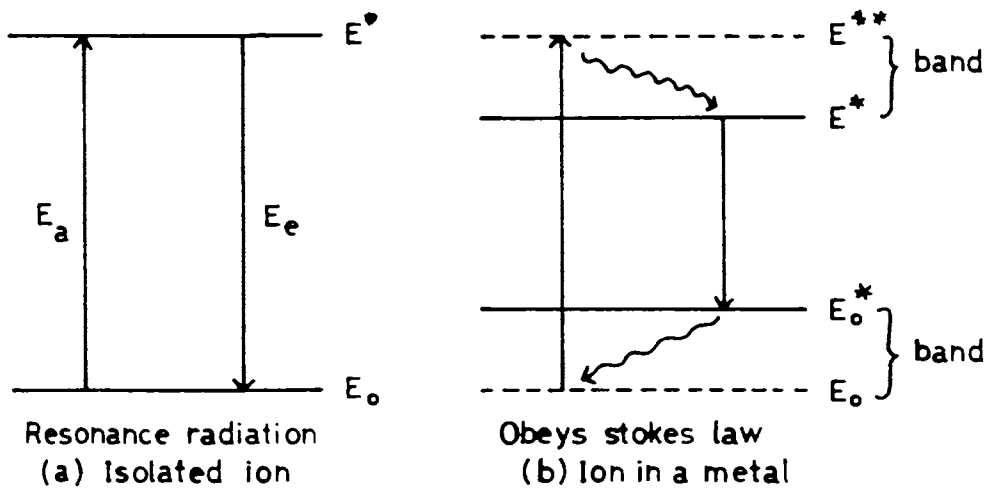


Fig. 1.12 Simplified energy level diagrams illustrating electronic transitions involved in two major decay processes - (a) and (b) illustrate the temperature independent decay ; (c) and (d) the temperature dependent decay

$\overline{\Delta E}$  increases with increasing  $E_0' = E' - E_0$ . Now consider the optical luminescence of an atom bound in a solid according to fig. 1.12(b). The energy of the photon used for excitation ( $E_0 = E'' - E_0$ ) is greater than that of the photon emitted ( $E_0 = E' - E_0'$ ) because some energy is transferred from the atom (centre) to the surrounding solid as heat.

Referring to eq. 1.(29) which is the general equation for simple temperature independent exponential decay, the decay of phosphorescence emission is

$$I \propto f(t) \propto \frac{dN}{dt} \quad \text{and the rate of decay is}$$

$$\frac{dI}{dt} \propto \frac{d^2N}{dt^2} \quad 1.(33)$$

A decay curve is a plot of  $I$  vs  $t$  during phosphorescence, and the rate of decay at time ' $t$ ' is the slope of the tangent of the decay curve at time ' $t$ '. When the decay of a phosphor follows the eq. 1.(32) it is found that the growth (during excitation) is also exponential and the shape of the growth curve is relatively uninfluenced by the changes in the temperature of the luminescing phosphor.

#### (ii) Hyperbolic Decay

This type of decay takes place in a system where on irradiation, shallow traps are also produced along with deeper traps. The decay of phosphorescence occurs generally in two or three groups depending upon the nature and concentration of traps. In such cases the observed intensity will be due to the superposition of all the exponentials corresponding to different traps and represented generally as [23]

$$I_t = I_0 t^{-b} \quad 1.(34)$$

where 'b' the decay constant. Also, in this case logarithm of intensity ( $I$ ) versus time ( $t$ ) plots are non-linear indicating the non-exponential form of decay. However the plots  $\log I$  vs  $\log t$  show linearity and the decay is said to be a hyperbolic one.

$$\text{Again, } I = I_0 t^{-b} = \sum_m I_{om} \exp(-P_m t) \quad 1.(35)$$

where  $I_{om}$  is the phosphorescence intensity due to electrons in traps of energy  $E_m$ .  
 $P_m = S \exp(-E_m/KT)$  is the probability of an electron escaping from a trap.

Here, the analysis of the decay curves will be usually done by adopting the "Peeling off" [24] procedure where each stage of decay will be associated with an exponential law. The trap depth corresponding to each exponential was calculated from the slopes of straight lines on the semi log plot using the relation

$$E = \log(S/\alpha) / KT \quad 1.(36)$$

where  $\alpha$  is the slope of each linear portion of the curve. The number of discontinuities in  $\log I - \log t$  plot corresponds to number of straight lines into which the semi-log plot can be splitted.

The value of 'b' is indicative of the decay rate and also provides information about relative population of trapping states at various depths. The relative population of trapping levels  $N_n$  at  $t = 0$  can be obtained by extrapolation of the plot  $\log I-t$  using the relation [25]

$$N_n(t)_{t=0} = I_n(t)_{t=0} \tau_n \quad 1.(37)$$

where  $\tau_n = 1/P_n$  is the life time of the electron trapped in the trap of depth  $E_n$ . So the ratio  $N_n(t)_{t=0} / N_n(t)_{t=5}$  for the 'peeled-off' components of the graph indicate the idea about distribution of trapping levels.

**(b) Temperature - sensitive decay - Power law decay**

At very long decay times, however the phosphorescence decay curve of the phosphor tends to depart from

$$I_n \propto \exp(-\alpha t) \quad \text{and can be written as}$$

$$I \propto t^{-n} \quad 1.(38)$$

so called power law-decay.

Power law-decays are quite sensitive to changes in temperature, excitation density and the kind of excitant. The interpretation of the so called power law-decays which is offered here is based simply on the evidence for electron traps in  $t^{-n}$  decay phosphors. A simple example of an electron trap is found in the occurrence of a metastable state in an isolated atom in a gas. When an atom is excited into a metastable state, for example  $E_m^*$  in fig. 1.12(c), it must absorb an amount  $\Delta E^*$  of activation energy to be raised into the radiative state  $E^*$ . If the radiative transition  $E_m^* \rightarrow E_0$  were not completely forbidden, this transition would occur as a slow temperature-independent exponential decay according to eq.1.(32). The transition to  $E_0$  from  $E_m^*$  via  $E^*$ , however is strongly temperature dependent following a relation of the type

$$I = -\frac{dN}{dt} = NS \exp(-\Delta E^*/KT) \quad 1.(39)$$

where N is the number of excited atoms in metastable states,  $\Delta E^*$  is the thermal activation energy required to raise an electron out of the 'trap'  $E_m^*$  into  $E^*$ , and S is the attempt-to-escape frequency for the transition from  $E_m^*$  to  $E^*$ . Under these conditions 'S' is the frequency of molecular collisions ( $S \propto T^{1/2}$ ). By integration eq. 1.(39), the phosphorescence output becomes (in the absence of retrapping),

$$I = I_0 e_m^{-St \exp(-\Delta E^*/KT)} \quad 1.(40)$$

where  $I_0$  is the output at  $t=0$ , and T is the temperature ( $^{\circ}K$ ). Here the eq 1.(40) assumes a single discrete trapping (metastable) level, whereas there may be one or more bands of trapping levels ( $E_c^*$  in fig.1.12(d)) in solids. Hence for a solid, equation 1.(40) can be expanded as

$$I = I_{10} e^{-S_1 t \exp(-\Delta E_1^*/KT)} + I_{20} e^{-S_2 t \exp(-\Delta E_2^*/KT)} + \dots + I_{N0} e^{-S_N t \exp(-\Delta E_N^*/KT)} \quad 1.(41)$$

where the subscripts 1,2.....N denote traps of different depths  $\Delta E_1^*$ ,  $\Delta E_2^*$  ...  $\Delta E_N^*$  and attempt frequencies  $S_1, S_2, \dots, S_N$  which may make different contributions  $I_{10}, I_{20}, \dots, I_{N0}$  to the output at time  $t = 0$ . Randall and Wilkins [26] have shown that for a hypothetical uniform trap distribution, that is, an equal number  $N_E$  of traps of all depths,

$$I = N_E \cdot KT (1 - e^{-St}) / t \quad 1.(42)$$

which reduces to the hyperbolic relationship

$$I = N_E \cdot KT / t \quad 1.(43)$$

where  $St \gg 1$  (ie after a microsec.  $e^{-St}$  is negligible).

The decay of many phosphors approximates to this law. In simple terms the reciprocal relation may be derived as follows. The intensity of phosphorescence emission due to the release of electrons from traps of certain depth is proportional to the rate of release of electron from those traps. The rate of release of an electron from a trap is inversely proportional to the mean life time of an electron in the trap. When there is a continuous distribution of trap depths, at a time 't' during phosphorescence, most of the light emission is due to the traps in which electrons spend a mean time 't', since the shallower traps are mostly emptied by that time and the deeper traps release electrons too slowly to contribute much to the phosphorescence. If there is an equal number of traps at all depth, the phosphorescence is at all times proportional to  $1/t$ .



If the trap distribution were exponential with trap depth

$$N_{E^*} = A e^{-\alpha E^*} dE^* \quad 1.(44)$$

where A is a constant then,

$$I \sim (S, KT) B t^{-(\alpha KT + 1)} \quad 1.(45)$$

which reduces to eq. 1.(44) when  $\alpha = 0$  (ie. uniform distribution of traps) and expresses an ideal bimolecular decay ( $I \propto t^{-2}$ ) when  $\alpha KT = 1$ .

An ideal bimolecular decay  $I = 1/b (I_0 b^{-1/2} + t)^2 \quad 1.(46)$

would obtain if there were two equally abundant remote recombination partners, that is free excited electrons and positive holes, which require no activation energy to become sufficiently mobile to seek each other out. In practice, the temperature sensitive phosphorescence mechanism comprises of an activated release of trapped excited electrons or positive holes followed by a bimolecular type recombination of those electrons and positive holes which have sufficient mobility to reach their opposite recombination partners without being retrapped and concluded by a monomolecular type of radiative transition. If it is assumed, for simplicity, that there are equal numbers of trapped electrons and holes and that the holes remain trapped, then the phosphorescence decay will prove to be largely according to eq. 1.(41), if the rate of release of electrons from traps is very slow relative to the rate of radiative recombination of the released free electrons with holes. This appears to be generally true and so thermal release is usually the rate-determining step. On the other hand, the influence of eq. 1.(46) should become larger when the rate of release of electrons from traps is very fast relative to the rate of radiative recombination of the free electrons and holes. In general, at the instant of cessation of excitation, there will be certain proportions of (i) free electrons with various velocities and various distances from suitable positive holes (ii) trapped electrons in traps of various depths and at various distances from holes (iii) mobile holes with various velocities and (iv) trapped positive holes. Phosphorescence decay during the first instants after cessation of excitation arises largely from the radiative recombination of nearby mobile excited electrons and positive holes; then the phosphorescence output comes mainly from the release of electrons from the shallowest traps and during the later stages of decay the phosphorescence contributions come from successively deeper traps. On this basis, it is understandable that the phosphorescence decay curves of  $t^{-n}$  are usually quite complex even neglecting (a) retrapping (b) non-uniformities in the degree of excitation within a volume of the phosphor and (c) optical complexities due to scattering and absorption. Also the brief initial non-exponential decay of some predominantly  $e^{-\alpha t}$  - decay phosphors is probably due to the radiative returns of free excited electrons which

happen to be in very shallow traps or the conduction band at the instant of cessation of excitation (Fig 1.4) [electrons in  $E_c^*$  and  $E_{13}^*$  (where  $E_{13}^* - E_{11}^* \ll KT$ ) first drop to  $E_{11}^*$  and then make a radiative transition from  $E_{11}^*$  to  $E_1^*$  ]

## 1.8 Thermoluminescence (TL) And Glow Curves.

Thermoluminescence does not refer to thermal excitation but rather to thermal stimulation of luminescence. This phenomenon is essentially phosphorescence measured during conditions of increasing temperature.

The production of TL in a sample by exposure to ionizing radiation may be divided into two stages; (i) electron and/or hole trapping and (ii) electron and hole recombination with photon emission. The energy band configuration for each stage explained below is shown in fig. 1.13. Ionizing radiation is absorbed in the material and free electrons are produced. This is equivalent to transferring electrons from the valence band to the conduction band (A). These electrons are free to move through the crystal (B), but if trapping levels such as (T) are present the electron may get trapped (C). The production of free holes which may also migrate via the valence band (b) and may be get trapped (c). Many hole centres are thermally unstable and may decay rapidly at room temperature (d). The trapped electrons will remain in the traps provided they do not acquire sufficient energy to escape. This will be determined by the trap depth and temperature of a particular material. If the temperature of the material is raised, trapped electrons may acquire sufficient thermal energy to escape (D). Released electrons may recombine with the holes at the luminescence centre (L). and emit visible or UV photons ( $E_p$ ). With electron capture at delayed recombination with a hole at the centre (L) is the mechanism of TL.

In thermoluminescence, heating imparts activation energy to an electron centre which releases an electron and then it migrates to the hole centre. This recombination delivers energy which induces luminescence. In a similar manner heating can liberate a hole from the hole centre. In this respect thermoluminescence means annihilation of electron hole centre registered by the luminescence of activator excited by these centre or by the luminescence of the centre themselves. The inter-relations of the trapping and emission centre can be understood if one proceeds from the existence of simultaneous presence of two capture centres (fig. 1(14) a to c) [27].

As the phosphor is heated the probability of releasing any particular electron is increased and at some temperature there is virtual certainty of its release. The emission (TL) will thus start to increase, go through a maximum and then decrease again to zero. The intensity of emitted light with temperature is known as a glow curve.

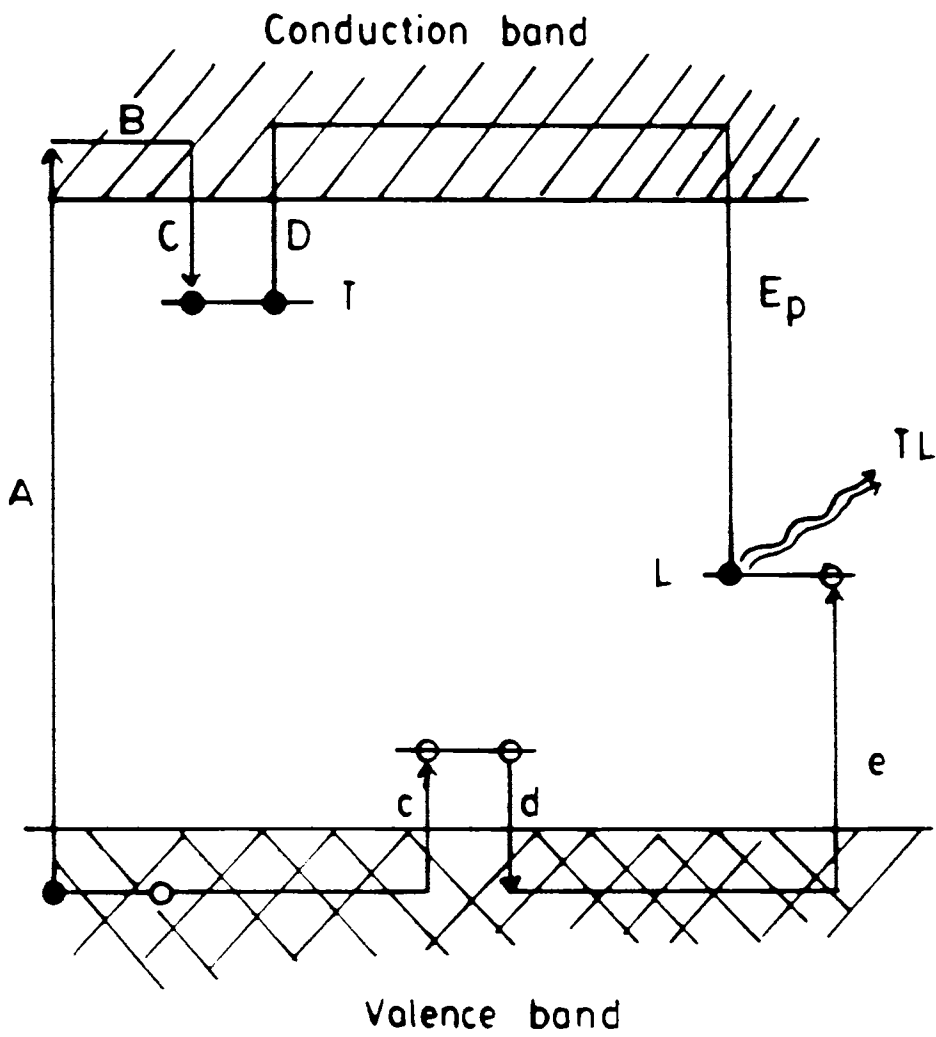
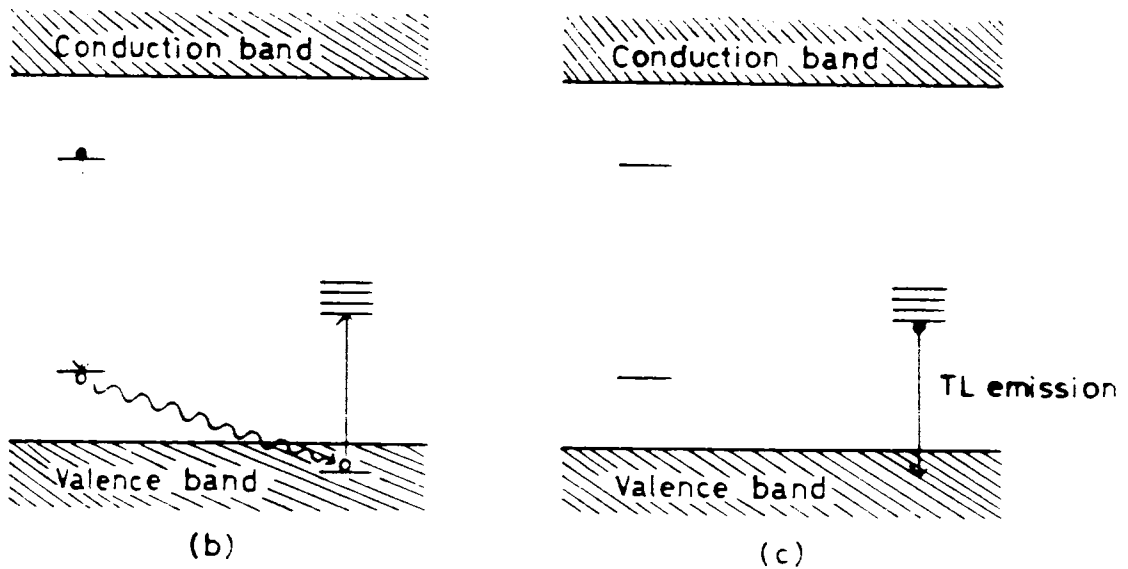
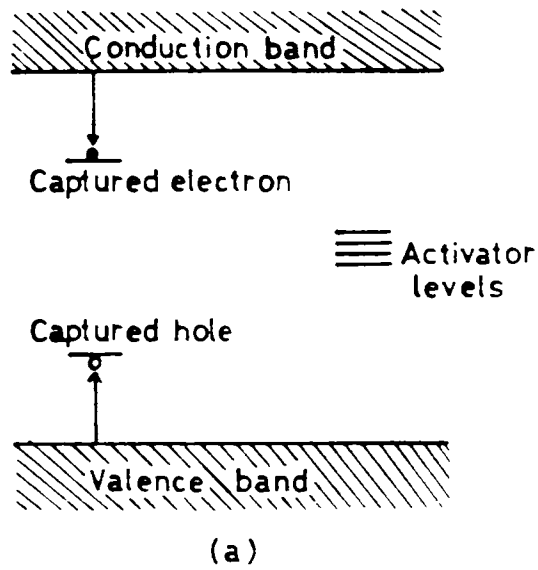


Fig. 1.13 A general model explaining TL process



**Fig. 1.14** (a), (b) and (c) Diagrams of levels representing the TL process involving the simultaneous presence of two capture centres.

### 1.8.1 Trapping parameters in TL process [28, 29]

The thermal energy spent in ionizing the electron centre is the trap depth 'E'. It is the distance (in eV) between the position of the electron centre level in the forbidden band and the conduction band. To calculate this value one has to know the position of the last occupied molecular orbital of the centre in the band scheme and its displacement caused by the thermal energy of the centre. Another parameter in connection with thermoluminescence is 'S' - which is a factor that characterises the capture centre from the stand point of thermal vibration releasing the electron from the trapping centre.

The nature of trapping states as well as the kinetics involved in the recombination phenomenon can be understood from the TL results. Utilising the information, the trapping parameters namely trap depth (E) and frequency factor (S) can be calculated by using different techniques.

### 1.8.2 Methods to calculate trapping parameters

There are several methods for calculating 'E' and 'S' from TL curves. The root of these calculations stems from the expression.

$$P = S \exp(-E/KT) \quad 1.(47)$$

where P - the probability of electron to escape from the trap - is related to  $\tau$ , the mean life time of electrons in the capture centre and is given as  $1/\tau = P$ . The intensity of glow which is proportional to a change in number of electrons 'N' during the time 't' expressed as

$$I \propto - \frac{dN}{dt} = -NP = -NS \exp(-E/KT) \quad 1.(48)$$

if the kinetics is of first order

and 
$$I = N^2 P \quad 1.(49)$$

for second order kinetics

Integrations of these kinetic equations render formulae for determining concentration of electrons in the trapping centres and for estimating glow intensity at temperature T, through the medium of parameters trap depth E, frequency factor S and the heating rate  $\beta^\circ/\text{sec}$ .

(a) Randall and Wilkins Method

Randall and Wilkins were the first to investigate thermoluminescence theoretically [23]. Their theory considered that (i) glow peaks corresponding to different trapping levels do not overlap (ii) no retrapping occurs in the process and (iii) the life time  $\tau$  for recombination is so small that  $dN/dt \ll N/\tau$  where  $N$  is the concentration of electrons in the conduction band. By using first order kinetics and assuming a uniform rate of heating, they obtained an expression for the variation of thermoluminescence with temperature as

$$I(t) = N_0 S \cdot \exp(-E/KT) \exp\left(-\int_{T_i}^T S \exp(-E/KT) dT/\beta\right) \quad 1.(50)$$

where  $N_0$  - the initial concentration of the trapped electrons,  $T$  - is the absolute temperature.  $K$  - the Boltzmann's constant, and  $E$  the trap depth at temperature  $T_m$  of the maximum glow intensity, can be obtained by setting  $(dI/dT)_{T_m} = 0$  as

$$\begin{aligned} E &= K T_m \log S (1 + f(S, \beta)) \\ &\sim K T_m \log S \end{aligned} \quad 1.(51)$$

Instead of first order, if the second order kinetics is considered then

$$\begin{aligned} N &= \frac{N_0}{1 + \int_{T_i}^T S \exp(-E/KT) dT/\beta} \\ \therefore I(t) &= \frac{N_0 S \cdot \exp(-E/KT)}{[1 + S \exp(-E/KT) dT/\beta]^2} \end{aligned} \quad 1.(52)$$

By setting  $dI/dT = 0$  (for  $T_m$ )

$$b \ E/KT_m - 1/2 [1 + S \exp(-E/KT) dT/\beta] S \exp(-E/KT_m) = 0 \quad 1.(53)$$

This differs from eq. 1.(50) by a factor  $1/2 [1 + \int_{T_i}^T S \exp(-E/KT) dT/\beta] = N_0/2n$

where  $n$  is number of electrons left in traps at  $T_m$ .

The thermoluminescence curve is not symmetrical and the change from  $T$  to  $T_m$  does not correspond exactly to the relation  $n = N_0 / 2$ . However this difference is not large and  $T_m$  is only changed by a percent or so by the above factor.

So the application of monomolecular formula to  $T_m$  gives approximately correct values for maximum trap distribution but if the whole curve is plotted then the bimolecular formula gives

a wider apparent distribution than really exist.

(b) Curie's Method

According to D.Curie [30] the trap depth

$$E(\text{eV}) = \frac{T_m (\text{°K}) - T_0 (\beta/S)}{K (\beta/S)} \quad 1.(54)$$

where  $\beta/S = \theta$ ,  $T_0$  and  $K$  are called Curie parameters, being obtained graphically as given in below :

Table 1.4 Values of $T_0$ and $K$ for various $\beta/s$ . ( D.Curie [30] )		
$\theta=(\beta/S)$ (°K)	$K$ (°K/eV)	$T_0$ (°K)
$10^{-4}$	833	35
$10^{-5}$	725	28
$10^{-6}$	642	22
$10^{-7}$	577	17
$10^{-8}$	524	13
$10^{-9}$	480	10
$10^{-10}$	441	7
$10^{-11}$	408	6
$10^{-12}$	379	6
$10^{-13}$	353	5
$10^{-14}$	331	5
$10^{-15}$	312	4

(c) Urbach's Method

The approximate formula given by Urbach [3] for the calculation of trap depth is

$$E = T_m / 500 \quad 1.(55)$$

Which also give the right order of values.

(d) Booth, Bohun And Hooganstraafen's Method [32 , 35]

By using different rates of heating  $\beta_1$  and  $\beta_2$  the trap depth E is given as

$$E = \frac{K T_{m1} T_{m2}}{T_{m1} - T_{m2}} \log \left( \beta_1 T_{m2}^2 / \beta_2 T_{m1}^2 \right) \quad 1.(56)$$

where  $T_{m1}$  and  $T_{m2}$  are the temperatures corresponding to the glow maxima for the heating rates  $\beta_1$  and  $\beta_2$  respectively and,

$$\log \left( T_m^2 / \beta \right) = E/KT_m + \log (SK/E) \quad 1.(57)$$

In this equation the plot between  $\log (T_m^2 / \beta)$  and  $T_m$  will be linear having slope (E/K) and gives an intercept equal to  $\log (SK/E)$  from which 'E' and 'S' can be calculated.

(e) Halperin and Braner's Method

Here the symmetry of the peak is considered, from which the activator energy is calculated using a simple formula [36,37]

$$E = (q/\delta) K T_m^2 \quad 1.(58)$$

where  $T_m$  - the peak temperature ; K - Boltzmann's constant ;  $\delta$  - the half-width towards the fall of temperature of the glow peak ; q - a factor which can be computed from the shape of the glow peak

If the value of  $q < 1$  - monomolecular kinetics

$1 < q < 2$  - bimolecular kinetics.



(f) Grosswiener's Method

Using first order kinetics Grosswiener [38] formulated the expression for activation energy for TL process as

$$E = \frac{1.51 K T_m T_1}{T_m - T_1} \quad 1.(59)$$


where  $T_1$  - the temperature corresponding to half intensity peak width on the low temperature side of the glow peak. Chen [39] has modified this formula by replacing 1.51 with 1.41 for better accuracy in the cases where  $S/\beta > 10^7 \text{ deg}^{-1}$  and  $E/KT_m > 20$

(g) Louchtchik's Method

Louchtchik [40] has obtained the expression for activation energy by approximating area under the glow curve to a triangle as

$$E = K T_m^2 / (T_2 - T_m) \text{ for first order kinetics}$$

and  $E = 2 K T_m^2 / (T_2 - T_m)$  for second order kinetics.



1.(60)

in this case Chen has suggested the multiplying constants as 0.978 and 0.853 respectively for better accuracy.

(h) Chen's Method

Chen [41] analysed the glow curve by applying first order kinetics. According to him the trap depth 'E' and the frequency factor 'S' are given by

$$E = 2.29 K T_m^2 / \omega \quad 1.(61)$$

$$\text{and } S = 2.67 (b/\omega) 10^{T_m/\omega} \quad 1.(62)$$

where  $\beta$  - the heating rate ;  $T_m$  - the maximum glow temperature ;  $\omega$  - the half-width

The above described methods are applicable only for well isolated single glow peaks. In the case of complex TL patterns, before applying the methods described above, the overlapping glow peaks are to be separated and attempts have thus to be made to resolve the TL patterns.

## REFERENCES :

- [1] Leverenz H.W., *"AN INTRODUCTION TO LUMINESCENCE OF SOLIDS"*, John Wiley & Sons Inc. London (1950)
- [2] Lenard, P., Schmidt F., and Tomaschek, R., *"HAND BOOK ON EXPERIMENTAL PHYSICS"*, Vol.23, Leipzig: Springer Verlag (1928)
- [3] Kato, K. and Okamoto F., *Jpn. J. Appl. Phys.* 22 (1983) p.76
- [4] Marfunin A.S., *"SPECTROSCOPY, LUMINESCENCE AND RADIATION CENTERS IN MINERALS"*, Springer Verlag, New York (1979)
- [5] Perrin F., "Fluorescence des solutions, Induction photochimie" *Ann de Phys.*, 12, 169, These, facult des sciences, Paris (1929)
- [6] Lehmann W., *J Electrochem. Soc.* 118 (1979) p.1389
- [7] Bube R.H., Larach S., and Sharader, *Phys. Rev.* 92 (1953) p.435
- [8] Mott N.F. and Davis E.A., *"ELECTRONIC PROCESSES IN NON-CRYSTALLINE MATERIALS"*, Oxford: Clarendon (1971)
- [9] Lambe J., and Klick C.C., *J. Phy. Rad.* 17 (1956) P.663
- [10] Klassens H.A., *Nature* 158 (1946) p. 483
- [11] Piper W.W. and Willams F.E., "Electroluminescence" *Soild State Phy.* Vol. 6, Academic Press, New York (1958)
- [12] Figgis B.N., *"INTRODUCTION TO LIGAND FIELDS"* John Wiley & Sons. Inc. New York (1966)
- [13] Voronko Yu K., Denker B. Osiko V.V., *Crystals. Phys. Tverd Tela*, 13 (1971) p.2193
- [14] Lea K.R., Leask M.J.M. and Wolf W.P., *Phys. Chem. Solids*, 23 (1962) p.1381
- [15] Zhong C.Z. and Bryant F.J., *J. Phy. C.*, 13 (1980) P. 4997
- [16] Stevens K.W.H. and Elliot R.J., *Proc. Roy. Soc. (London)* A 218 (1953) p.553
- [17] Stevens K.W.H., *Proc.Roy. Soc.*, A65 (1952) p. 209
- [18] Freeman A.J. and Wastson R.E., *Phy. Rev.*187 (1962)
- [19] Pringsheim P., *"FLUORESCENCE AND PHOSPHORESCENCE"*, Inter Sc. Pub. New York (1949)
- [20] Klick C.C. and Schulman J.H., *"LUMINESCENCE IN SOLIDS"*, in "Soild State Physics - Advance in Research applications", Frederi Seitz and Davis Thuhall (Ed), Vol.5, Acad. Press Inc., New York (1953).
- [21] Dexter D.L., *J. Chem. Phy.* 21 (1953) p- 836
- [22] Dexter D.L. and Schulman J.H., *J.Chem. Phy.*22 (1957)p.1063
- [23] Randall J.T. and Wilkins M.H.F., *Proc. Roy. Soc.* A184 (1945)p.366
- [24] Bube F.H.,*Phy. Rev.*, 80 (1950) p.655.
- [25] Singha O.P. and Sivaraman Indian *J.of Pure and Appl. Phys.* 10 (1972)p.134
- [26] Randall J.T. and Wilkins M H F., *Proc. Phy. Soc.* A184 (1945) p.390
- [27] Medlin W.I., *"THERMOLUMINESCENCE OF GEOLOGICAL MATERIALS"* Academic Press, new York (1968)

- [28] Muer D. de, Physics 48 (1970) p.1
- [29] Townsend p.d. *"THERMOLUMINESCENCE IN GEOLOGICAL MATERIALS"* Acad. Press, New York (1968)
- [30] Curie D., *"LUMINESCENCE IN CRYSTALS"*, John Wiley & Sons Inc., New York (1963)
- [31] Urbach F., Cornell Symp. Vol.115, John Wiley & Sons Inc. New York (1948)
- [32] Booth A.H., Canadian J. Phy. 32 (1954) p. 214
- [33] Hoogenstraaten W., *"Electron traps in Zinc sulphide phosphors"*, Ph.D. thesis, Amstrdam (1958)
- [34] Bohun A., Czechosl J. phy. 6 (1956),p.628
- [35] Bohun A., Czechosl. J.Phy. 4 (1954) p.2
- [36] Halperin A., and Braner A. A., Phy. Rev. 117 (1960) p.408
- [37] Halperin A. and Braner A.A., Phy. Rev. 108 (1956) p.1498
- [38] Grosswiener I.i., J. Appl. Phy. 24 (1953) p.570
- [39] Chen R., J. Appl.Phy. 40 (1969) p.570
- [40] Louchtchik, *"CRYSTALLO PHOSPHORS"*, (Ed) Acad. Fiz., Tarton, (1955)
- [41] Chen R., J. Appl. Phy. 41 (1970) p. 5227.

## **CHAPTER II**

## REVIEW OF PREVIOUS WORK

A brief description of luminescence and its theoretical aspects has been given in the first chapter. As indicated in the previous chapter, understanding of the mechanism involved in luminescence and related fields is essential in making use of this natural phenomenon for scientific and technological advancements of mankind. Development of devices like flat panel displays demands the synthesis of new phosphor materials having good quantum yield. Amongst a large number of materials, alkaline earth sulphides (AES) are the most efficient phosphors which can be put into practical use. AES phosphors which are known as Lenard phosphors in earlier literature belong to the group of phosphors which were found to fluoresce in the visible region under UV excitation [1]. Most of the earlier works on luminescence and related properties of these sulphides are available in the literature [2-5]. Although several hundred papers have been published so far on the preparation and characterization of these sulphides there does not seem to be an agreement on the results of the studies even on the same material. This chapter gives an overview of the work which has already been carried out on the preparation and characterization of AES phosphors in recent years.

AES phosphors were prepared by several workers in the past [6-10]. Most of the preparation procedures involved the reduction of host sulphates by carbon or  $H_2S$ . However the stability of these phosphors was poor and in most of the cases only 80% yield was obtained [11]. It has been pointed out by Lehmann [12] and Kato et.al. [13] that these materials, when properly prepared and activated with suitable impurities, may become efficient phosphors for many opto-electronic applications. Normally these sulphides are prepared by firing the host sulphates/carbonates/oxides with reducing agent in the temperature range  $800^{\circ}C$  to  $1200^{\circ}C$  under different controlled ambient atmospheres, for a duration of about one to four hours. The optimum yields of the sulphides in the end product could be obtained by making several trials by varying the temperature and duration of firing and by adding different types of reducing agents and flux materials. Recently Green et.al.[14] reported that CaS phosphors prepared by the reduction of sulphates in  $H_2/H_2S$  atmosphere and refired in the presence of flux  $Na_2CO_3/S, NH_4Cl/CaF_2$  are found to give a good quantum yield as compared to the previous methods of preparation.

The role of flux materials in the preparation of industrial phosphors is well known. Depending upon the nature of phosphors, the flux materials are suitably chosen to provide a proper media for an effective incorporation of the activating impurities in the system. Materials like alkali fluorides, sulphates, borax etc. have been used in the past to prepare AES phosphors [15-17]. With a special reference to the role of fluxes, studies were made by J.D. Ranade and B.K. Kathal [18] which led to the important conclusion that the flux only serves to alter relative importance of different groups of traps and not their mean depth. The emission is affected only by the atoms of flux cluster around the activator atoms and bring about changes in the number of centres. The variation of flux results in slight change of operative trap depth from phosphor

to phosphor. This leads to the view that within a single group of traps in these phosphors there may exist sub-groups which are probably very close to each other and may follow quasi-uniform distribution of traps in themselves. Chakravarthi et.al.[19]. studied the effect of NaF, Na<sub>2</sub>SO<sub>4</sub> and KF fluxes on AES phosphors and observed that fluxing ions going into the lattice do not interact in such a way as to shift the trapping levels. However, when KF was used as a flux, two distinctly separate peaks were observed with relative heights depending on the amount of flux. This result confirms the conclusion that the traps are distributed in depth and the fluxing ions may interact in such a way with the lattice as to redistribute the trapping levels. According to Chakravarthi et.al the initial increase in flux percentage helps to increase the number of luminescence centres, but further increase leads to the formation of centres responsible for radiationless transitions. R.P. Rao [20] recently used NaCl as the flux for preparing BaS:Cu, Bi system and found to give good yield for TL output for a flux concentration in the range of 25% to 30%.

The theories of luminescence emission assume that the activator is an important part of the luminescence centre. Usually the emission band is attributed to interaction between host lattice and the emission centre. By knowing the shift of emission peaks with the activator concentration it is possible to estimate whether the activator is incorporated substitutionally or interstitially. The advancement of ligand field theory and the discovery of energy transfer mechanisms helped the understanding and interpretation of luminescence. Shulman et. al. [21] showed that the resonance energy transfer is possible even when the activators and co-activators are separated by nearest neighbour distance. Dexter [22] gave an extensive theoretical treatment of energy transfer mechanism extending to forbidden transitions.

Sensitization of luminescence is another process involved in energy transfer responsible for most of the luminescence emissions in AES phosphors [2,3]. Impurity sensitization has been shown to be due to the radiationless transitions between sensitizer and co-activator [3]. As far as the luminescence characteristics of BaS is concerned, only in 1966, the work in this direction has been started. Stroganova et.al [23-25] reported the preparation and luminescence spectra of BaS:Mn, BaS:Cu and BaS:Bi under excitation with a.c. and d.c. electric fields, UV light and x-rays. They suggested that the form of light pulses depends on the activator, not on the matrix. The mechanism involved here is the ground state electrons from the traps in the opposite edge of the host materials returning to the ionised centres by the electric field. Lenard [1] reported two phosphorescence bands of BaS:Cu at 5400 Å and 6200 Å. Lehmann [26] in his studies on cathodoluminescence of BaS:Cu observed only one band at 5815 Å. Laud and Kulkarni suggested a model for the emission spectra of BaS:Cu under 365 nm excitation for the two emission bands observed at 5270 Å and 5680 Å. [27]. They obtained the band gap of BaS as 3.9eV. Laud & Kulkarni observed a shift in the band position towards longer λ-side (5705 Å) as the Cu<sup>+</sup> concentration was increased which indicates substitutional Cu<sup>+</sup> ions. Kanari, in 1973 [28] reported that copper activated AES are normally efficient phosphors

in which a quantum efficiency of photoluminescence of about 50% or more can be obtained. An extensive study on BaS phosphors doped with Cu and Bi impurities was made by Rao et.al. [29-34] during the past few years. Their studies involved phosphorescence, thermoluminescence (TL), thermally stimulated conductivity etc. under UV, X-ray,  $\gamma$ -ray and low energy electron excitations. The TL traps with intense TL glow peaks observed in BaS phosphors doped with Bi and Cu are associated with native defects, which have a close relationship with impurities. From decay and TL analysis it is concluded that the electron and hole traps are located near each other. The TSC results indicate that the distribution of the corresponding traps must involve the liberation of electrons from the traps to the conduction band, destroying the related trapped hole centres in the process of recombination. Most of the conclusions drawn points out that the traps responsible for luminescence emission are associated with the host lattice such as sulphur ion vacancies. Under UV excitation BaS:Cu system showed a TL peak at 80°C while no such result was obtained for BaS powder. Under x-ray excitation also, BaS:Cu gave a glow peak around a temperature 80°C and number of peaks in the temperature range of 120°C to 300°C. This suggests that the traps are related to Cu impurities generating localized levels in the forbidden gap. From TL and decay curves they obtained the trap depth 'E' as 0.5 eV and the escape frequency factor  $S \sim 10^6/\text{sec}$ . However, the trapping parameters 'E' and 'S' calculated from TL glow curves by various authors were not in agreement even for the same material. In recent years significant progress has been made in the development of new materials for radiation dosimetry. These include alkaline earth sulphide phosphors too. Rao [35-37] found that the mixed system (Ba, Cu, Sr)S when doped with Cu and Bi were efficient due to its peak at 278°C and has potentiality for use in dosimetry.

The decay of phosphorescence of UV excited AES was studied by several other workers [38-43]. These investigations mostly dealt with the kinetics of decay processes and the related distribution of the traps in the system. Effect of flux and the duration of firing on the intensity of phosphorescence of BaS:Cu phosphors were studied by Razadan [44] who observed a decrease in intensity of decay with the increase of duration of firing and increase of flux content which was attributed to the formation of copper-borax complexes during the preparation. Khare and Ranade [15] reported their results on the characteristic decay of phosphorescence of BaS:Bi using excitation at 438 nm light. The samples found to exhibit two stage decay processes and analysed as the superposition of exponentials.

Thermoluminescence of BaSO<sub>4</sub> phosphors has been the subject of many investigations. TL of natural barite samples has been studied by Prokic [46] and rare-earth doped synthetic samples by Krystek, Luthra etc. [47-49]. It was found that rare-earth ions are the best co-activators for the AES phosphors. The glow peaks induced by rare earth ion in BaSO<sub>4</sub> lattice are found to be determined only by the valence state of the rare-earth ion. Many dopants especially Sm, Eu, Tb, Dy and Tm in BaSO<sub>4</sub> are reported to give extremely bright TL having efficiency comparable to that of other highly sensitive phosphors such as CaSO<sub>4</sub>:Dy and

$\text{CaSO}_4:\text{Tm}$ , which are at present being used in radiation dosimetric applications [50]. As the effective atomic number of the  $\text{BaSO}_4$  phosphors is relatively high, ( $\sim 45.8$ ), the TL sensitivity for low photon energies is an order higher than other phosphors and hence has been suggested for dosimetry of low energy X-rays [44]. Nagpal [51] studied TL of  $\text{BaSO}_4$  doped with Y, La, Ce, Pr, Nd, Sm, Eu, Tb, Dy etc under  $\gamma$  and micro wave radiations. TL emission spectral bands of these phosphors systems are identified as arising due to transitions between different energy levels of the dopant ions. They are characteristics of  $\text{RE}^{3+}$  and arise between the known energy levels belonging to the  $4f^n$  electron configuration. Ajay et.al [52] studied the effect of rare-earth impurities like Ce and Sm on BaS phosphor under UV (320nm) excitation. For BaS:Sm phosphors the emission spectra show the broad emission band with peak at 550 nm, while for BaS:Ce at lower concentration two peaks at 515 nm and 595 nm. They concluded that the emission of Ba:Ce is due to characteristics of  $\text{Ce}^{3+}$  while in the case of BaS:Sm emission it can be attributed to the perturbed intrinsic nature, due to the recombination of electrons and holes taking place near the vacancy impurity complex ( $V_{\text{Ba}}-\text{Sm}_{\text{Ba}}$ ).

Studies on electroluminescence spectra of CaS phosphor doped with specific rare-earth impurities like Sm, Dy, Er etc. were found to give well resolved emission purely characteristics of rare-earth ion energy levels [53,54]. Analysis of such spectra based on the calculations of crystal field splitting was used to identify the probable impurity sites responsible for emission. Rare-earth impurities containing some metallic impurities are found to give some significant results in sulphide phosphors [55]. With this in view, a number of scientists have studied the combined effect of rare-earth impurities along with metallic ones like Cu, Mn, etc. in the CaS and SrS [56-61] phosphors, while such studies are found to be very rare in the case of BaS.

Of all the investigations reported on the studies of luminescence and related phenomena in AES phosphor systems till now, it was found that fluorescence studies on BaS based phosphor doped with rare-earth systems are rather very limited. In the present investigations we have made an attempt in this direction by choosing BaS as the host material, and  $\text{Cu}^+$  and  $\text{RE}^{3+}$  impurities like Ce, La, Pr, Nd, Sm, Gd, Dy etc. as the dopants. Results obtained from the present studies are given in later chapters.



## REFERENCES :

- [1] Lenard p, Schmidt and Tomaschek R., *"HAND BOOK ON EXPERIMENTAL PHYSICS"*, Vol.23, Leipzig; springer-Verlag (1928)
- [2] Marfunin A.S., *"SPECTROSCOPY, LUMINESCENCE AND RADIATION CENTERS IN MINERALS"*, Springer-Verlag, New York (1979)
- [3] Curie D., *"LUMINESCENCE IN CRYSTALS"* John Wiley & Sons Inc., New York (1963)
- [4] Pringsheim p., *"FLUORESCENCE AND PHOSPHORESCENCE"* Intersc. Publ. New York (1949)
- [5] Leverenz H.W., *"AN INTRODUCTION TO LUMINESCENCE OF SOLIDS"*, John Wiley & Sobs Inc. (1950)
- [6] Pearlman D., Goddard P.E. and Urbach F., *J. Optic. America*, 39 (1949) p.695
- [7] Bawalkar D.R., *Saugar Univ. J.* 1 (1951/1952) p.209
- [8] Keller S.P., Maper J.E. and Cheroff G., *Phy. Rev.* 108 (1957) p.663.
- [9] Watchel A., *J. Electrochem. Soc.* 105 (1958) p. 256
- [10] Avinor M. and Meijer G., *J. Phys. Chem. Solids*, 12 (1960) p. 211
- [11] Mellor W., *"A COMPREHENSIVE TREATISE OF INORGANIC THEORETICAL CHEMISTRY"*, Vol.3, Ed longman and Greek, London (1948)
- [12] Lehmann W., *J. Luminescence*, 5 (1972) p. 87
- [13] Okamoto F. and kato K., *J. Electrochem. Soc.* 130 (1983) p.432
- [14] Green A.G.J., Brightwell J.W., Viney I.V.F. and Ray B., *J. Crystal growth*, 86 (1988) p. 639
- [15] Razdan, K.N., *Indian J. Pure and Appl. Phy.* 2 (1964) p. 271
- [16] Verma S.K., *Indian J. Pure and Appl. Phy.* 9 (1971) p.738
- [17] Yamashita N. and Asano S., *J. Phy. Soc. Jpn.* 41 (1976) p.536
- [18] Ranade J.D. and Kanthal B.K., *Indian J. Pure and Appl. Phy.* 9 (1971) p. 456
- [19] Chakravarthi A.K., Mor S.L. and Ranade J.D., *Indian J. Pure and Appl. Phys.* 12 (1974) p. 603
- [20] Rao R.P. and Rao D.R., *Bull. Mat. Sc.*5 (1983)p.29
- [21] Shulman I.H., Genter R.L and Dafby, E.W., *J. Electrochem. Soc.*, 97 (1950) p.127
- [22] Dexter D.L. *J. Chem. Phy.* 21 (1953) p.836
- [23] Stroganova T.N. and Rubolkin, *Bull. Acad. Sc. (USSR), Phy. Sc. (USA)*, 30, No.9 (1966) p. 1575
- [24] Stroganova T.N. and Chernyaskine B.G., *Optics and Spectroscopy (USA)* 22 (1967) p. 280
- [25] Stroganova T.N. and Chernyaskine B.G., *Optics and spectroscopy (USA)* 11 (1966) p. 142
- [26] Lehmann W., *J. Electrochem. Soc.* 117 (1970) p. 1389

- [27] Laud B.B. and Kulkarni V.W., *Phy. Stat. Sol(a)*, 51 (1979) p.269
- [28] Kanari P.S., *Indian J. Pure and Appl. Phy.* 11 (1973)p.499
- [29] Rao R.P., *J. Mat. Sc.* 10 (1986) p.3357
- [30] Rao R.P. and Rao D.R., *Physica Scripta*, 25 (1982) p. 592
- [31] Rao R.P., *Mat. Res. Bull.*, 21 (1986) p.299
- [32] Rao R.P., *Radiat. Effects*, 44 (1983) p. 444
- [33] Rao R.P. and Rao D.R., *Mat. Chem. and Phy.* 9 (1983) p. 501
- [34] Rao R.P., Rao D.R. and Banerji H.D., *Res. Bull.*, 13 (1978)p. 491
- [35] Rao R.P., *Radiat. Prot.* 17 (1986) p.403
- [36] Rao R.P., Gasiot J. and fellard J.P., *J. Lum.* 31,32 (1989) p. 23
- [37] Rao R.P., de Marcia and Gasiot J., *Radiat. Prot. Dosm.* 6 (1983) p. 64
- [38] Balakrishna and Kanari P.S., *Indian J. Pure and Appl. Phy.* 13 (1975) p. 71
- [39] Jain and Ranade J.D., *Indian J. of Pure and Appl. Phy.*, 11 (1973) p. 602
- [40] Singha O.P. and Sivaraman S. *Indian J. Pure and Appl. Phy.* 10 (1972) p. 134
- [41] Bawalkar D.R. and Malhotra B.R., *Indian J. Pure and Appl. Phy* 7 (1969) p.163
- [42] Patil A.G. and Lawanger R.D., *J. Lum.*, 22 (1981) p. 377
- [43] Sharma D. and Amar Singh, *Indian J. Pure and Appl. Phy.*, 7 (1969) p. 310
- [44] Razadan K.Z., *Indian J. Pure and Appl. phy.* 8 (1964) p. 271
- [45] Khare V.K., *Indian J. Pure and Appl. Phy.* 6 (1971) p. 856
- [46] Prokic, M.J., *Phy. Chem. Solids*, 40 (1979) p.405
- [47] Krystek M., *Phy. Stat. Sol. (a)*, 57 (1980) p.177
- [48] Luthra J.M. and Gupta N.M., *J. Lum.* 9 (1974) p.94
- [49] Dixon R.L. and Ekstrand K.E., *J. Lum.* 8 (1974) p.383
- [50] Nambi K.S.V., Bapat V.N. and Ganguly A.K., *J. Phy. C* 7 (1974) p.4403
- [51] Nagpal J.S. and Geetha Varadarajan, *Int. J. Appl. Radiat.* 33 (1982) p. 175
- [52] Ajay S. Reddi K. and Rao D.R. *Physica Scripta*, 29 (1984) p.254
- [53] Pillai S.M. and Vallabhan C.P.G., *Phy. Stat. Solidi (b)*, 134(1986) p. 383
- [54] Pillai S.M. and Vallabhan C.P.G., *J. Phy C-Solid state Phy.* 17 (1984) p.219
- [55] Mor S.L. and Bhatwalkar D.R., *Indian J. Pure and Appl. Phy.* 8 (1970) p.320
- [56] Aswathi M.C. and Thakar J.L., *Indian J. Pure and Appl. Phy* 24 (1986) p.100
- [57] Malhotra B.R. and Bhawalkar D.R., *Indian J. Pure and Appl. Phy.* 7 (1969) p.573
- [58] Yasuhiro Nako, *J. Phy. Soc. Jpn.*, 48 (1980) p.534
- [59] Kulkarni V.W., Patwardan S.S., and Ghanbahadur R.Y., *Physica Scripta*, 25 (1982) p.496
- [60] Rao R.P., *J. Lum.*, 40 (1988) p. 848
- [61] Jain S.C. and Bhawalkar D.R., *Indian J. Pure and Appl. Phy.* 13 (1975) p.74.

## **CHAPTER III**

## PHOSPHOR SYNTHESIS AND EXPERIMENTATION

### 3.1 Introduction

The most important objective of research activities in the field of luminescence phenomenon is the development of efficient phosphor materials with good quantum yield. This requires (i) pure chemicals for sample preparation (ii) furnace which is capable of attaining high temperatures either in reducing or oxidising atmosphere depending on the method of preparation (iii) suitable sources of excitation etc. Synthesis of an efficient phosphor necessitates a number of optimum conditions due to the fact that the final objectives are quite challenging. Hence extensive trials on the preparation and characterization of phosphors of different host materials doped with activators and co-activators become unavoidable before any worthwhile result is obtained.

Alkaline earth sulphide (AES) phosphors have been known for quite long time as versatile and excellent phosphor materials. They possess simple f.c.c crystal structure and offer themselves as good host materials in the preparation of industrial phosphors by incorporating different impurities [1-2]. Because of their wide band gap (3.8 eV-5.2eV), the excited states of the dopants are not densely distributed between the valence band and the conduction band. These sulphides, when doped with impurities such as rare-earths, are found to give good quantum efficiency of luminescence. As compared to other members of the AES group, the work on phosphors based on BaS is less. Hence, in the present investigations we have selected BaS as the host material.

In this chapter a detailed account of various sub-systems need for experimental set up is given. This involves the descriptions of a high temperature vacuum furnace (for phosphor preparation), the phosphor preparation methods, experimental cell, excitation sources, detection and recording set up for studying the fluorescence, phosphorescence and thermoluminescence characteristics of the phosphors. The experimental set up to record the emission spectra is described with the help of block diagrams followed by descriptions of various subsystems which include monochromator, PMT, pre-amplifier, chart recorder etc.

### 3.2 Vacuum Furnace

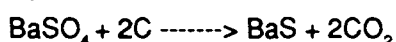
For the preparation of efficient phosphor samples an important parameter to be considered is the temperature of firing. This necessitates the design and fabrication of a high temperature muffle furnace.

The furnace was constructed with a 7cm diameter silica tube having length of about 90cm. Both ends of the tube were suitably adapted using cylindrical metal(S.S) couplings.

A fused thermocouple was attached to one end to read the central zone temperature, while the other end of the coupling was given provisions for evacuating the furnace / for maintaining a suitable atmosphere of the desired gas. A Kanthal wire element of 18 gauge was wound around the tube at the central portion about 15cm in length and was mounted within the sillimanite which formed the muffle of the furnace. A square block of Aluminium enclosure covering the sillimanite gravel provides the external heat insulation. The furnace was given a.c heating through a regulated relay power supply. At an input voltage of 230 V it can attain a maximum temperature of 1100°C within four hours. A temperature control unit was also attached to the power supply so that the temperature of the furnace can be set to a any desired constant temperature. The constant temperature zone was about 8 cm in length at the centre part. This furnace can be evacuated upto a pressure of  $10^{-3}$ Torr. A photograph of the furnace is given in fig.3.1.

### 3.3 Sample Preparation

The starting materials used for the phosphor synthesis in the present case are  $\text{BaSO}_4$  (99.99% purity - which was supplied by E. Merck, Bombay) and spectroscopically pure grade carbon powder. All the phosphor samples are prepared using this  $\text{BaSO}_4$  by the reduction process



A proper reducing atmosphere was maintained throughout the process by keeping sufficient quantity of carbon in a separate crucible which minimizes the formation of oxides on the exposed surface. The firing temperature was selected by making several trials in the range 750-1000°C and it was observed that the firing at the temperature range 900 - 950°C produces a good yield of BaS [3]. Thus the charge was fired for one hour at 950°C under vacuum ( $10^{-3}$  Torr).

During the preparation, for proper crystallization of the phosphor, fluxes are very essential. In this preparation we used sodium thiosulphate as the flux material. The role of flux in phosphor synthesis is to provide a medium which lowers the crystallization temperature for the incorporation of the activating impurities [4]. But the increase in amount of flux above an optimum value leads to deterioration of luminescence emission [5]. With this views in mind we prepared a set of BaS phosphors with varying concentrations of flux and determined the value of optimum flux concentration which gave a moderate intensity of emission.

The nature of luminescent centres can be well understood by incorporating suitable activators and co-activators which will enhance the emission efficiency. In this respect copper was found to be a good dopant in BaS for creating both interstitial and substitutional vacancies and rare - earths were found to be good co-activators due to its characteristic emission in the visible region [6]. In its trivalent form, the rare-earth ion in BaS creates donor levels while the copper in its monovalent form creates acceptor levels. Hence copper and rare-earth ions in

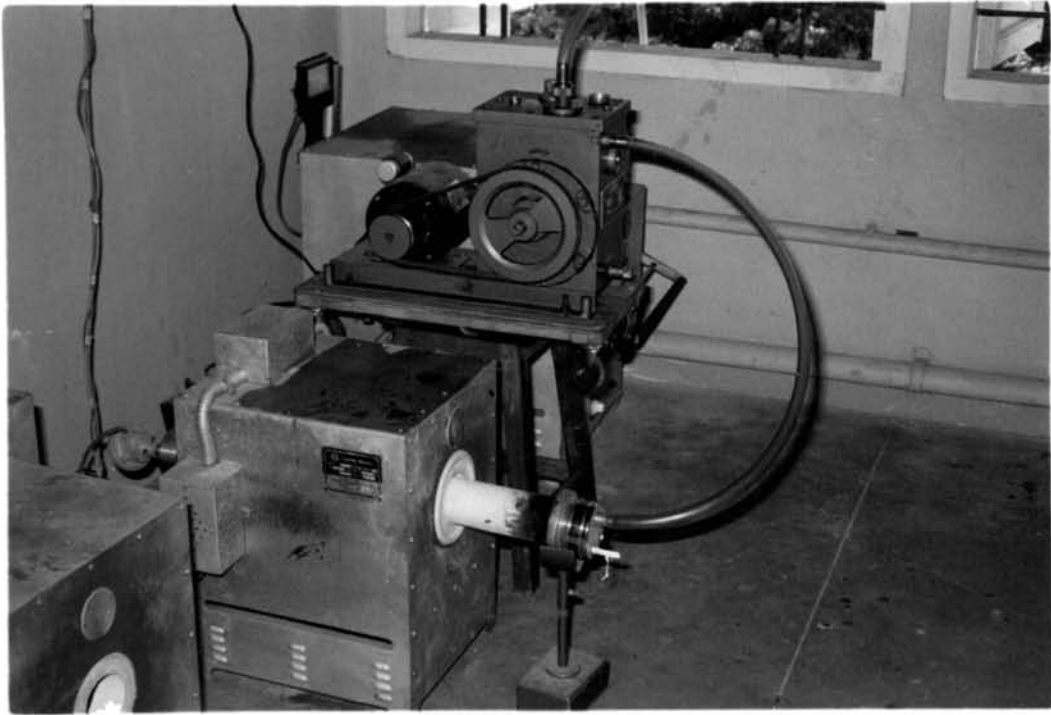


**Fig 3.1** The high temperature vacuum furnace used for preparation of the phosphor samples

the form of RE<sup>3+</sup> and Cu<sup>+</sup> were selected as the activators and co-activators for the present investigations. RE<sup>3+</sup> considered for the present studies are Ce<sup>3+</sup>, La<sup>3+</sup>, Pr<sup>3+</sup>, Nd<sup>3+</sup>, Sm<sup>3+</sup>, Gd<sup>3+</sup> and Dy<sup>3+</sup>. For better sample incorporation, we have taken rare-earths and copper in the form of aqueous solutions of their respective chlorides (RECl<sub>3</sub> and CuCl). RECl<sub>3</sub> was precipitated from RE oxides of 99.9% purity (supplied by IRE, India) by adding excess amount of concentrated HCl and the mixture was slowly heated upto 300°C till the complete evaporation of the acid.

Using the same starting material, BaSO<sub>4</sub>, the phosphor samples for the present investigations were prepared by two methods. In the first one, the method usually followed by most of the earlier workers [7], the activators and co-activators were added along with the flux in proper concentrations to the starting material. This slurry was well mixed and given a slow heating upto 120°C and the dried mass was then crushed and thoroughly mixed using a mortar and pestle. This charge was then taken in flat bottom alumina crucibles and introduced into the central zone of the high temperature furnace at 950°C and fired in carbon atmosphere for about one hour. In the second method, to a weighed amount of BaS obtained from the initial reduction process, the activators and the flux in the form of aqueous solutions, in proper concentrations were added and the slurry was dried giving a slow heating upto 200°C. This charge was then thoroughly mixed and the powder thus obtained was taken in alumina crucibles and given a second firing by introducing into the high temperature zone of the furnace at 1050°C for about 90 minutes under vacuum (10<sup>-3</sup>Torr). In both the cases, after firing, the phosphors were suddenly quenched to room temperature. It was then well crushed, thoroughly grinded and the powder thus obtained was taken in a pelletiser and given a uniform pressure of 2.5 tonnes/cm<sup>2</sup> using an electrically driven hydraulic press. The pelletiser was so designed that the final form of the phosphor samples for the measurements are obtained as pellets of 3mm thickness and 10mm diameter. Fig.3.2 shows the accessories used for pelletising the phosphor samples.

Different sets of phosphor samples were prepared in different concentrations using combinations of RE<sup>3+</sup> and Cu<sup>+</sup> as the dopants. The lists of phosphors prepared are given in tables 3.1 and 3.2.

### 3.4 Experimental Cell

The experimental cell is essentially a vacuum chamber, suitably designed and fabricated using a cylindrical mild steel tube of 20cm diameter and is provided with four windows of 2cm diameter on the four sides facing at right angles to each other. The windows are closed with flat quartz discs with allen-head screws and proper O-ring seals. The chamber is closed with top and bottom discs, which are fitted with allen-head screws and suitable O-ring seals. A hollow copper tube of 2cm diameter and 3mm wall thickness bent in U-form is placed into the chamber through the top disc, brazed in such a way that the open ends are kept outside. To the U-shaped

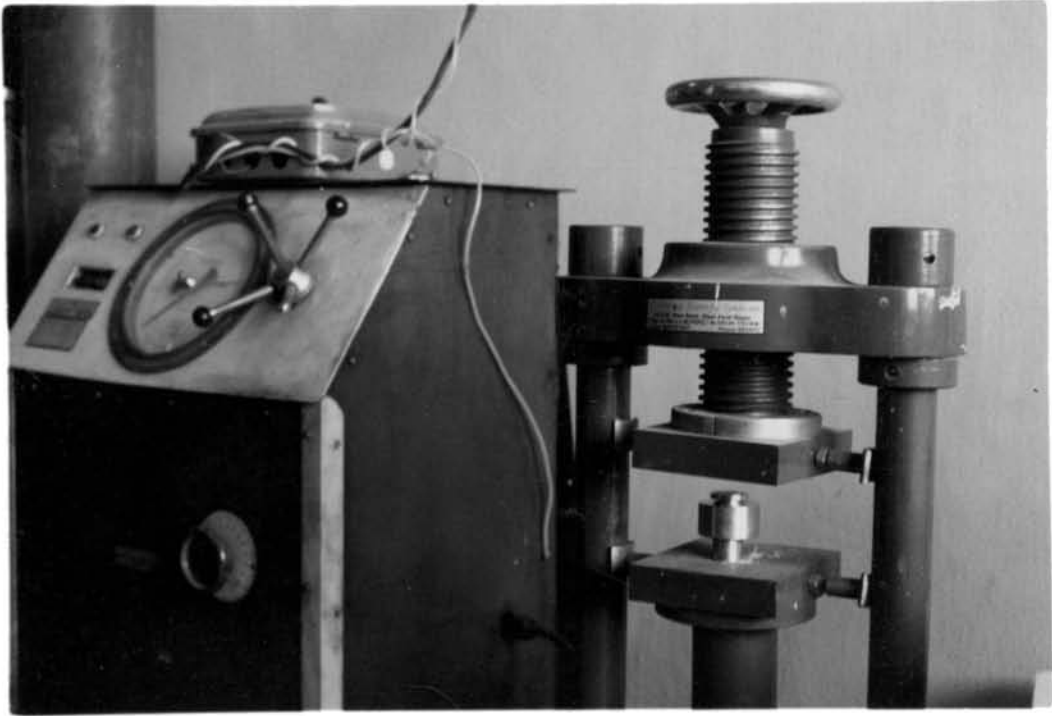


**Fig 3.2** Accessories used for pelletising the phosphor samples



**Table 3.1**  
**List of the phosphor samples prepared by 1st Method [7]**

Type of Phosphor	Sample Notation	Concentrations of the dopants (Mol % by wt. of BaS)	
		Cerium	Copper
BaS	S <sub>0</sub>	0	0
BaS:Ce	SR <sub>1</sub>	0.009	0
	SR <sub>2</sub>	0.182	0
	SR <sub>3</sub>	0.210	0
	SR <sub>4</sub>	0.702	0
	SR <sub>5</sub>	1.812	0
	SR <sub>6</sub>	2.104	0
	SR <sub>7</sub>	2.905	0
	SR <sub>8</sub>	3.601	0
	SR <sub>9</sub>	4.305	0
BaS:Cu	SC <sub>1</sub>	0	0.011
	SC <sub>2</sub>	0	0.202
	SC <sub>3</sub>	0	0.612
	SC <sub>4</sub>	0	2.521
	SC <sub>5</sub>	0	3.303
	SC <sub>6</sub>	0	4.812

Contd...

Type of Phosphor	Sample Notation	Concentrations of the dopants (Mol % by wt. of BaS)	
		Cerium	Copper
(BaS:Ce):Cu	SS <sub>41</sub>	0.702	0.110
	SS <sub>42</sub>	0.702	0.202
	SS <sub>43</sub>	0.702	0.811
	SS <sub>44</sub>	0.702	2.521
	SS <sub>45</sub>	0.702	3.303
(BaS:Cu):Ce	SS <sub>56</sub>	0.009	3.303
	SS <sub>57</sub>	0.401	3.303
	SS <sub>58</sub>	2.141	3.303

bottom portion another copper disc (4x4cm square, 4mm thick) is brazed, which contains the sample holder part, exactly facing the quartz windows. The sample holder is specially designed using a copper block and is attached to the copper disc by means of suitably adapted screws. It has special provisions for holding a copper-constantan thermocouple, which is taken from the sample holder part and its leads are taken out to the top disc by means of proper connectors. For high temperature studies, a heater coil of suitable size is also kept inside the copper sample holder so that by means of a.c voltage the sample can be heated upto 250°C. The electrical leads for a.c heating are also taken out through the top disc using B.N. connectors. In order to minimize the heat loss due to conduction, a perfect insulation of the sample holder path from the top portion is made using a teflon shielding in between. The sample cell can be used for low temperature studies too. Low temperatures can be attained by pouring liquid nitrogen into the U-shaped copper tube from the top. Then the teflon sheilding from the sample holder part must be removed so that the copper block containing the sample holder is exactly in touch with the copper tube. A vacuum of the order of 10<sup>-5</sup> Torr can be achieved by connecting the chamber to a rotary-diffusion combination through a side tube. The cell can be used for measurement at different temperatue regions viz ,LNT., RT and high temperatures upto 250°C. Fig.3.3 (a) and (b) shows the sample cell with the accessories.

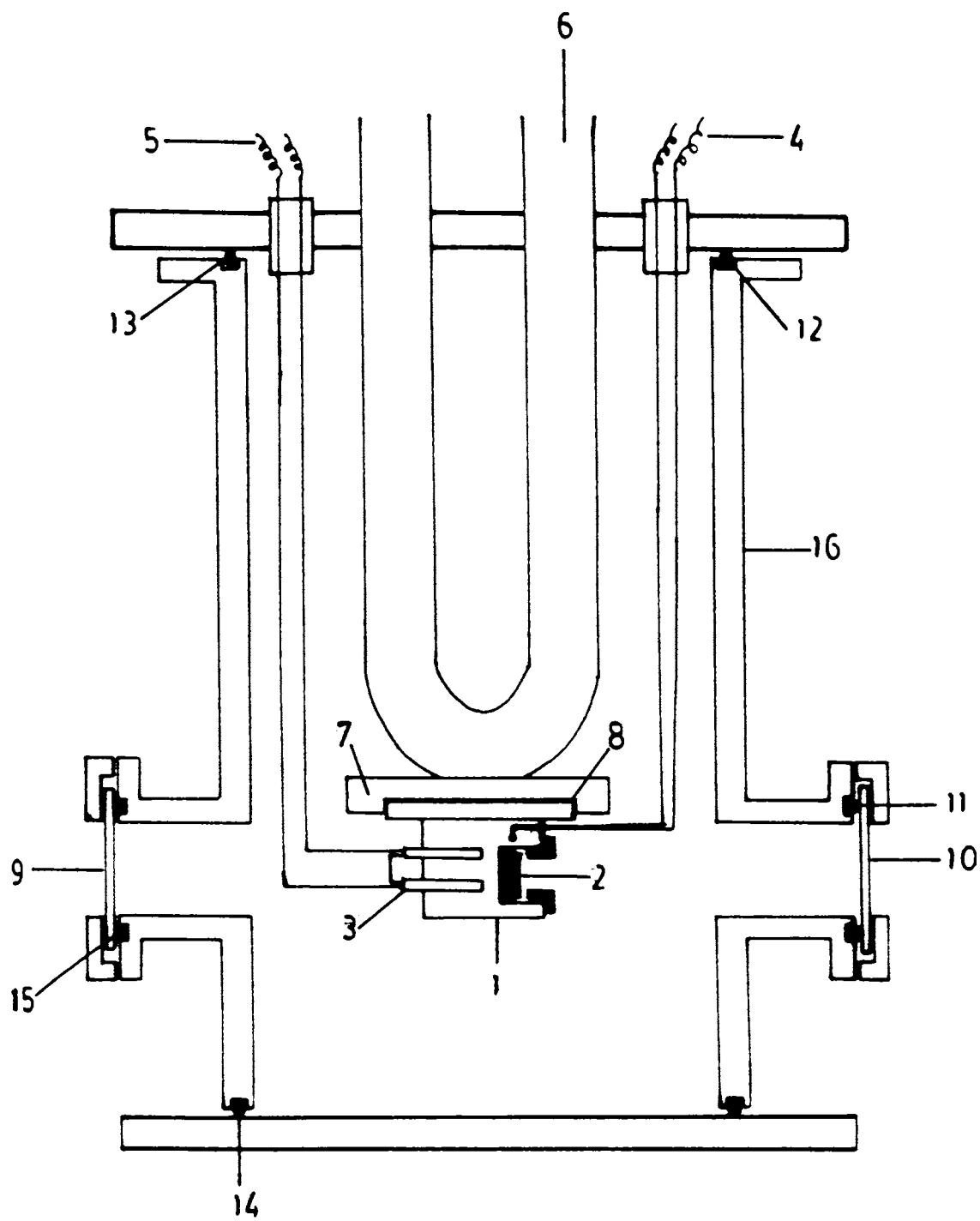
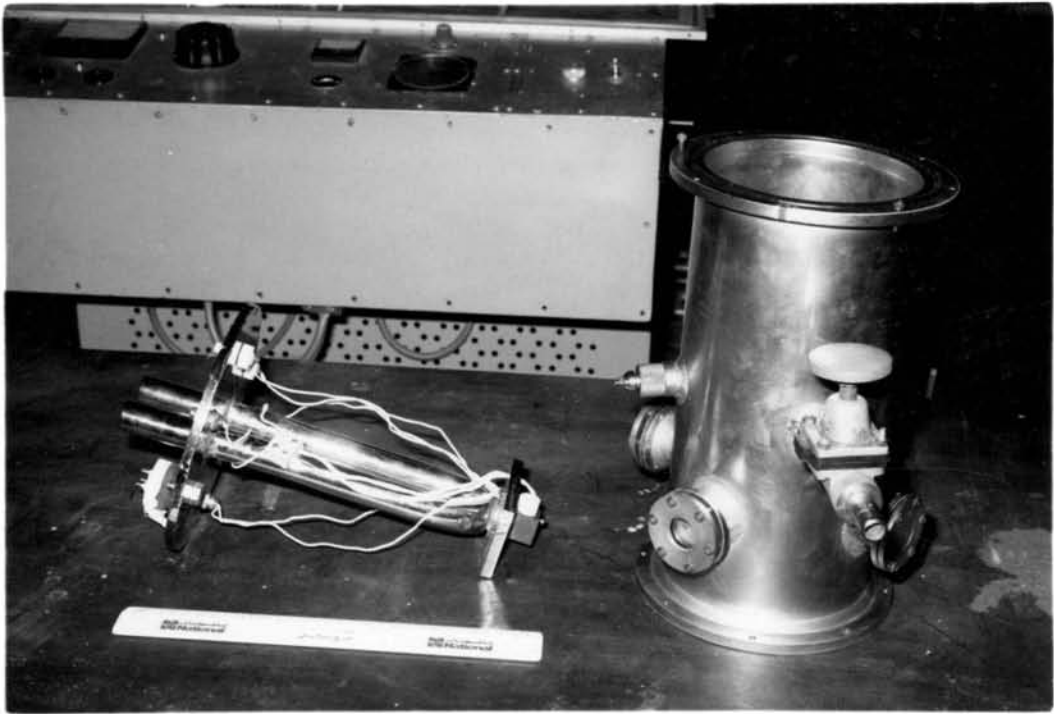


Fig 3.3 (a) Schematic digram of the experimental cell  
 1. Sample holder. 2. Sample. 3. Heater coil. 4. Leads for thermocouple. 5. BNC Leads for electrical connection  
 6. Liquid Nitogen trap.7. Copper disc.8. Teflon shielding.  
 9.-10. Quartz windows.11-15 O-ring seals. 16 M.S. Chamber.



**Fig 3.3 (b) The experimental cell**

Table 3.2.								
List of phosphor samples prepared by the 2nd method								
Type Of Phosphor	Sample Notation	Concentration of the dopants (Mol % by of BaS)						
		Rare - earths (RE <sup>3+</sup> )						Copper (Cu <sup>+</sup> )
		La	Pr	Nd	Sm	Gb	Dy	
BaS	B <sub>0</sub>	0	0	0	0	0	0	0
BaS:La	BL <sub>2</sub>	3	0	0	0	0	0	0
	BL <sub>3</sub>	1.5	0	0	0	0	0	0
	BL <sub>4</sub>	1	0	0	0	0	0	0
	BL <sub>6</sub>	0.01	0	0	0	0	0	0
	BL <sub>7</sub>	0.001	0	0	0	0	0	0
BaS:Pr	BP <sub>1</sub>	0	5	0	0	0	0	0
	BP <sub>2</sub>	0	3	0	0	0	0	0
	BP <sub>3</sub>	0	1.5	0	0	0	0	0
	BP <sub>5</sub>	0	0.5	0	0	0	0	0
	BP <sub>6</sub>	0	0.01	0	0	0	0	0
	BP <sub>7</sub>	0	0.001	0	0	0	0	0
	BP <sub>8</sub>	0	0.0005	0	0	0	0	0
BaS:Pr	BN <sub>2</sub>	0	0	3	0	0	0	0
	BN <sub>3</sub>	0	0	1.5	0	0	0	0

Cont'd...

Type Of Phosphor	Sample Notation	Concentration of the dopants (Mol % by of BaS)						
		Rare - earths (RE <sup>3+</sup> )						Copper (Cu <sup>+</sup> )
		La	Pr	Nd	Sm	Gb	Dy	
BaS:Pr	BN <sub>5</sub>	0	0	0.5	0	0	0	0
	BN <sub>6</sub>	0	0	0.01	0	0	0	0
	BN <sub>7</sub>	0	0	0.001	0	0	0	0
BaS:Sm	BS <sub>1</sub>	0	0	0	5	0	0	0
	BS <sub>2</sub>	0	0	0	3	0	0	0
	BS <sub>3</sub>	0	0	0	1.5	0	0	0
	BS <sub>5</sub>	0	0	0	0.5	0	0	0
	BS <sub>6</sub>	0	0	0	0.01	0	0	0
	BS <sub>7</sub>	0	0	0	0.001	0	0	0
BaS:Gd	BG <sub>1</sub>	0	0	0	0	5	0	0
	BG <sub>2</sub>	0	0	0	0	3	0	0
	BG <sub>5</sub>	0	0	0	0	0.5	0	0
	BG <sub>6</sub>	0	0	0	0	0.01	0	0
	BG <sub>7</sub>	0	0	0	0	0.001	0	0
BaS:Dy	BD <sub>3</sub>	0	0	0	0	0	1.5	0
	BD <sub>4</sub>	0	0	0	0	0	1	0

Contd...

Type Of Phosphor	Sample Notation	Concentration of the dopants (Mol % by of BaS)						
		Rare - earths (RE <sup>3+</sup> )						Copper (Cu <sup>+</sup> )
		La	Pr	Nd	Sm	Gb	Dy	
BaS:Dy	BD <sub>5</sub>	0	0	0	0	0	0.5	0
	BD <sub>6</sub>	0	0	0	0	0	0.01	0
	BD <sub>7</sub>	0	0	0	0	0	0.0001	0
BaS:Cu	BC <sub>1</sub>	0	0	0	0	0	0	1
	BC <sub>2</sub>	0	0	0	0	0	0	0.5
	BC <sub>3</sub>	0	0	0	0	0	0	0.05
(BaS:Sm);Pr	BSP <sub>1</sub>	0	1.5	0	1	0	0	0
	BSP <sub>2</sub>	0	0.5	0	1	0	0	0
	BSP <sub>3</sub>	0	0.05	0	1	0	0	0
	BSP	0	1	0	1	0	0	0
(BaS:Pr):Sm	BPS <sub>1</sub>	0	1	0	1.5	0	0	0
	BPS <sub>2</sub>	0	1	0	0.5	0	0	0
	BPS <sub>3</sub>	0	1	0	0.05	0	0	0
(BaS:Pr):Gd	BPG <sub>1</sub>	0	1	0	0	1.5	0	0
	BPG <sub>2</sub>	0	1	0	0	0.5	0	0
	BPG <sub>3</sub>	0	1	0	0	0.05	0	0

Contd...

Type Of Phosphor	Sample Notation	Concentration of the dopants (Mol % by of BaS)						
		Rare - earths (RE <sup>3+</sup> )						Copper (Cu <sup>+</sup> )
		La	Pr	Nd	Sm	Gb	Dy	
(BaS:Pr):Gd	BPG	0	1	0	0	1	0	0
(BaS:Sm):Gd	BSG	0	0	0	1	1	0	0
	BSG <sub>2</sub>	0	0	0	1	0.5	0	0
	BSG <sub>3</sub>	0	0	0	1	0.05	0	0
(BaS:Nd):Pr	BNP	0	1	1	0	0	0	0
	BNP <sub>1</sub>	0	1.5	1	0	0	0	0
	BNP <sub>2</sub>	0	0.5	1	0	0	0	0
(BaS:Nd):Sm	BNS	0	0	1	1	0	0	0
	BNS <sub>1</sub>	0	0	1	1.5	0	0	0
	BNS <sub>2</sub>	0	0	1	0.5	0	0	0
(BaS:Nd):Dy	BND	0	0	1	0	0	1	0
	BND <sub>2</sub>	0	0	1	0	0	0.5	0
	BND <sub>3</sub>	0	0	1	0	0	0.05	0
(BaS:Sm):Dy	BSD	0	0	0	1	0	1	0
	BSD <sub>2</sub>	0	0	0	1	0	0.5	0
	BSD <sub>3</sub>	0	0	0	1	0	0.05	0

Cont'd...



Type Of Phosphor	Sample Notation	Concentration of the dopants (Mol % by of BaS)						
		Rare - earths (RE <sup>3+</sup> )						Copper (Cu <sup>+</sup> )
		La	Pr	Nd	Sm	Gb	Dy	
(BaS:Cu):Sm	BCS <sub>1</sub>	0	0	0	1.5	0	0	0.5
	BCS	0	0	0	1	0	0	0.5
	BCS <sub>2</sub>	0	0	0	0.5	0	0	0.5
(BaS:Cu):Pr	BCP <sub>1</sub>	0	1.5	0	0	0	0	0.5
	BCP	0	1	0	0	0	0	0.5
	BCP <sub>2</sub>	0	0.5	0	0	0	0	0.5
(BaS:Cu):Nd	BCN <sub>1</sub>	0	0	1.5	0	0	0	0.5
	BCN	0	0	1	0	0	0	0.5
	BCN <sub>2</sub>	0	0	0.5	0	0	0	0.5
(BaS:Cu):Gd	BCG <sub>1</sub>	0	0	0	0	1.5	0	0.5
	BCG	0	0	0	0	1	0	0.5
	BCG <sub>2</sub>	0	0	0	0	0.5	0	0.5
(BaS:Cu):Pr:Sm	BC(Pr,Sm)	0	0.5	0	0.5	0	0	0.5
(BaS:Cu):Sm:Gd	BC(Sm,Gd)	0	0	0	0.5	0.5	0	0.5
(BaS:Cu): Pr:Sm:Gd	BC(Pr,Sm,Gd)	0	0.5	0	0.5	0.5	0	0.5
BaS:Pr:Sm:Gd	B(Pr,Sm, Gd)	0	0.5	0	0.5	0.5	0	0

### 3.5. Excitation Sources

The emission output of phosphors depends on the exciting wavelength. The exact region of excitation wavelength can be selected only on the basis of optical absorption spectrum. The absorption spectra of the prepared phosphor samples show intensified absorption in the UV region (details of the absorption spectra measurements are given in the next chapter). These phosphors are excited using UV sources such as (i) mercury lamp (with its outer glass cover removed) and (ii) a pulsed N<sub>2</sub> laser

#### 3.5.1 Mercury lamp.

In ordinary commercial mercury lamps, the glass cover of the bulb absorbs most of the UV radiations. Hence the glass cover is removed and the filament is covered with a rectangular aluminium sheet provided with window in front so as to allow the UV radiations to come out. A parabolic reflector made of aluminium is also kept behind the mercury source facing the window to enhance the output light intensity. Mercury vapour lamp contains intense emission lines in UV and visible regions. Using an appropriate interference filter, 365nm line of Hg is focussed on to the phosphor sample by means of proper optics.

#### 3.5.2 Nitrogen laser system

A pulsed nitrogen laser system designed and fabricated in our laboratory [8] which is capable of giving out intense radiation at the wavelength 337.1nm was used as another source to excite the phosphor samples. Main parts of this laser system constitute (a) double parallel plate non-Blumlein type transmission line (b) laser cavity (c) power supply (d) triggered spark gap (e) trigger circuit (f) Gas line and (g) EMI shielding and cabin

##### (a) Parallel plate transmission lines

Double parallel-plate non-Blumlein transmission lines are used for the present nitrogen laser system. Each parallel-plate transmission line is a double sided copper clad glass epoxy sheet with a dielectric thickness of 1.6mm which acts as energy storage capacitors. A channel is etched on one side of the copper clad sheet and the laser cavity is placed in this channel, fixed to the copper clad sheet, through copper strips. The copper clad sheets on either side of the cavity serves as energy storage capacitors. These can easily withstand voltages upto 15 KV. In our case the maximum voltage given to the transmission line was 14 KV without any dielectric break down.

(b) laser cavity

It is designed and constructed using aluminium side walls separated by perspex sheets. The inner dimensions of the cavity are 90 cm length, 3cm width and 5.5cm height. In the aluminium wall, channels were cut and aluminium electrodes of length 80 cm were fixed with an inter-electrode distance at two ends as 10mm and 11mm. This was used for initiating the discharge always at one end of the tube. The perspex sheet is fixed to the side walls of the cavity by means of machine screws. The cavity was made air-tight by using teflon tape and Araldite<sup>®</sup> adhesive. The windows of the cavity are attached by the perspex flanges and neoprene O-rings. A front coated mirror was placed at one end of the cavity where the discharge strikes first and to the other end of the cavity from where, the laser emission is obtained, an optically flat quartz glass plate was fixed. Gas inlet and outlet were provided in the cavity through which nitrogen gas can be filled and maintained at required pressure. The transmission lines were connected to the cavity by copper strips.

(c) Power supply

The circuit diagram of the power supply is given in fig.3.4. The power was fed to the energy storage capacitors through a half-wave rectifier, by means of which the capacitors on either side of the cavity are charged. A step-up transformer charges the transmission lines to a maximum voltage of about 14KV through the rectifier chain.

(d) Spark gap

The heart of  $N_2$  laser is the spark gap. The spark gap was specially designed and fabricated with aluminium electrodes with an inter-electrode distance of 3mm. The whole unit was made as small as possible so that the inductance of the spark gap is minimum (few nano Henries). Heavy cooling fins were also provided by the special design of aluminium enclosure. Ceramic insulator along with central aluminium pin forms the trigger of the spark gap. Gas inlet and outlet are provided to maintain the gas pressure in the gap. It is attached to the transmission lines through copper strips.

(e) Trigger circuit

It is reported that the energy storage efficiency of  $N_2$  laser powered by a half wave rectifier, is found to increase when triggered in the negative half of the charging cycle [9]. A simple circuit which triggers the spark gap in the negative half cycle was employed in this laser system.

(f) Gas line

The nitrogen gas line is shown in fig.3.5. The gas lines are made of high pressure rubber tubes and the connections to the spark gap and cavity are given through proper inlets and outlets.

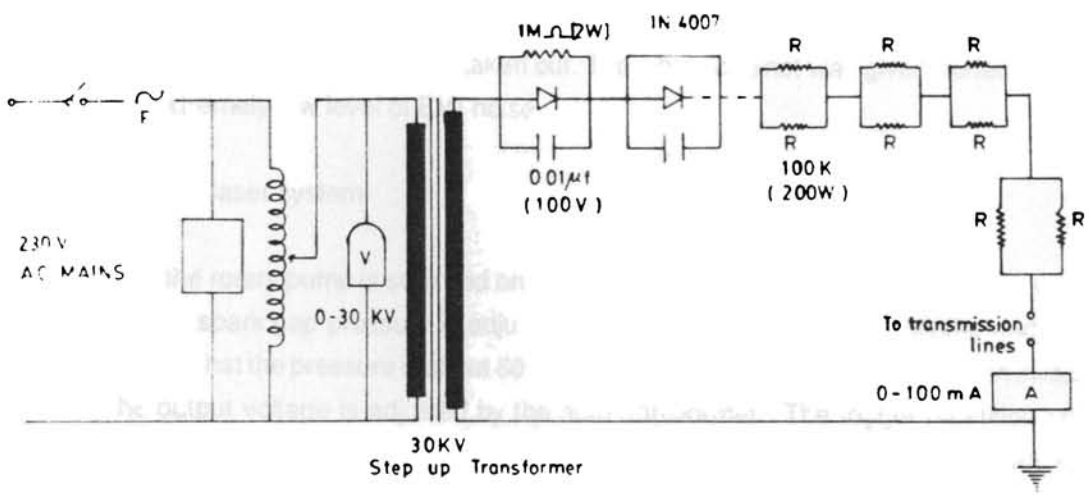


Fig. 3.4 Nitrogen laser power supply

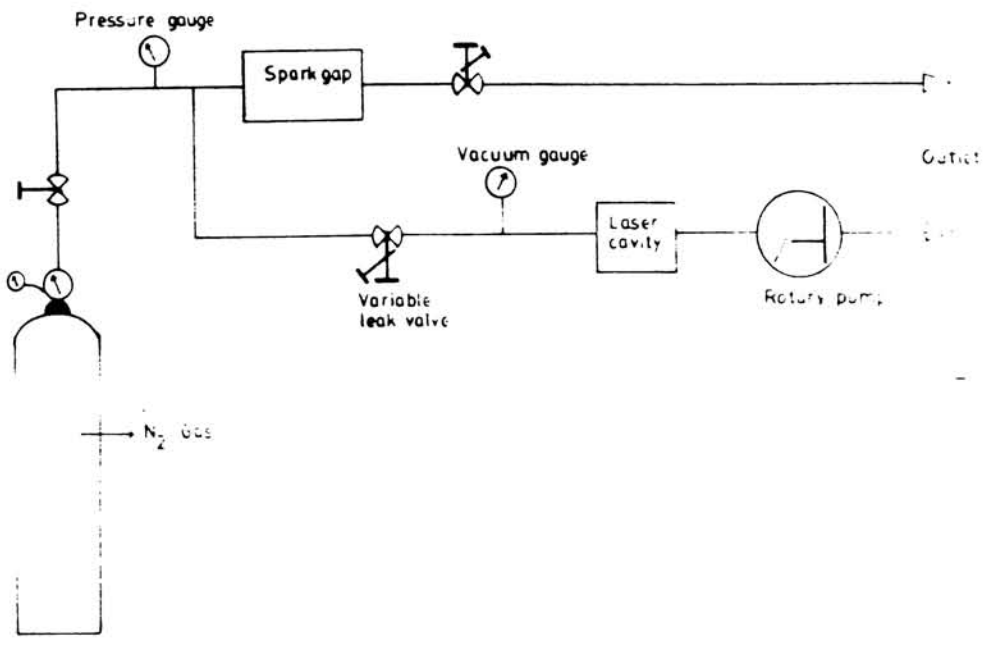


Fig. 3.5 Nitrogen gas line

(g) EMI shielding

The heavy electrical discharge in the spark gap and in the cavity produces EMI noise. This is due to the discharge of high voltage within a few nanoseconds when peak current is extremely high. The transmission lines, cavity and spark gap were enclosed in a metal cabinet and the output laser beam alone was taken out. The whole cabinet was given perfect earthing which gave extremely low level of EMI noise.

Operation of the laser system

First the rotary pump is switched on. The  $N_2$  gas pressure inside the cavity is suitably adjusted. Then spark gap pressure is adjusted through the valve at gas cylinder and by the needle valve so that the pressure is about 60 Torr. The power supply to  $N_2$  laser is then switched on and the output voltage is adjusted by the auto transformer. The trigger repetition rate is selected using the selector switch and the trigger switch is switched on. Laser action starts when trigger switch is put to "ON" position.

The special design of the spark gap and the new triggering mechanism gives better efficiency and performance to the laser system. It gave a maximum output power of 300 KW for 337.1nm radiation, when operating with a voltage of about 12 KV, at 25pps, and 10ns pulse width. The output beam profile is roughly a rectangular one, which can be focused to the sample by using a cylindrical lens. The whole laser system is shown in fig.3.6.

### 3.6. Experimental Details

The studies on fluorescence, phosphorescence and thermoluminescence characteristics were carried out on the phosphor samples. Fig.3.7 (a), (b) and (c) show the schematic block diagrams of the experimental arrangements for recording fluorescence, phosphorescence and thermoluminescence spectra.

Fluorescence of the samples are collected at  $90^\circ$  with respect to the direction of the exciting radiation so as to minimise the interference of the fluorescence signal with the exciting radiation. The fluorescence emission collected was focussed exactly to the slit of the monochromator which was coupled to a highly sensitive PMT followed by pre-amplifier and chart recorder.

For phosphorescence decay measurements, the samples were mounted on a specially designed sample holder, which can be easily and quickly turned towards the slit of the PMT within a minimal time in a very precise way soon after the excitation source is cut off. In the case of decay measurements, all this samples were excited to the saturation level (~ 3 to 5 minutes) and afterwards turned towards the slit of a highly sensitive PMT and the decay curves are charted by the chart recorder.



**Fig 3.6 Nitrogen Laser System**

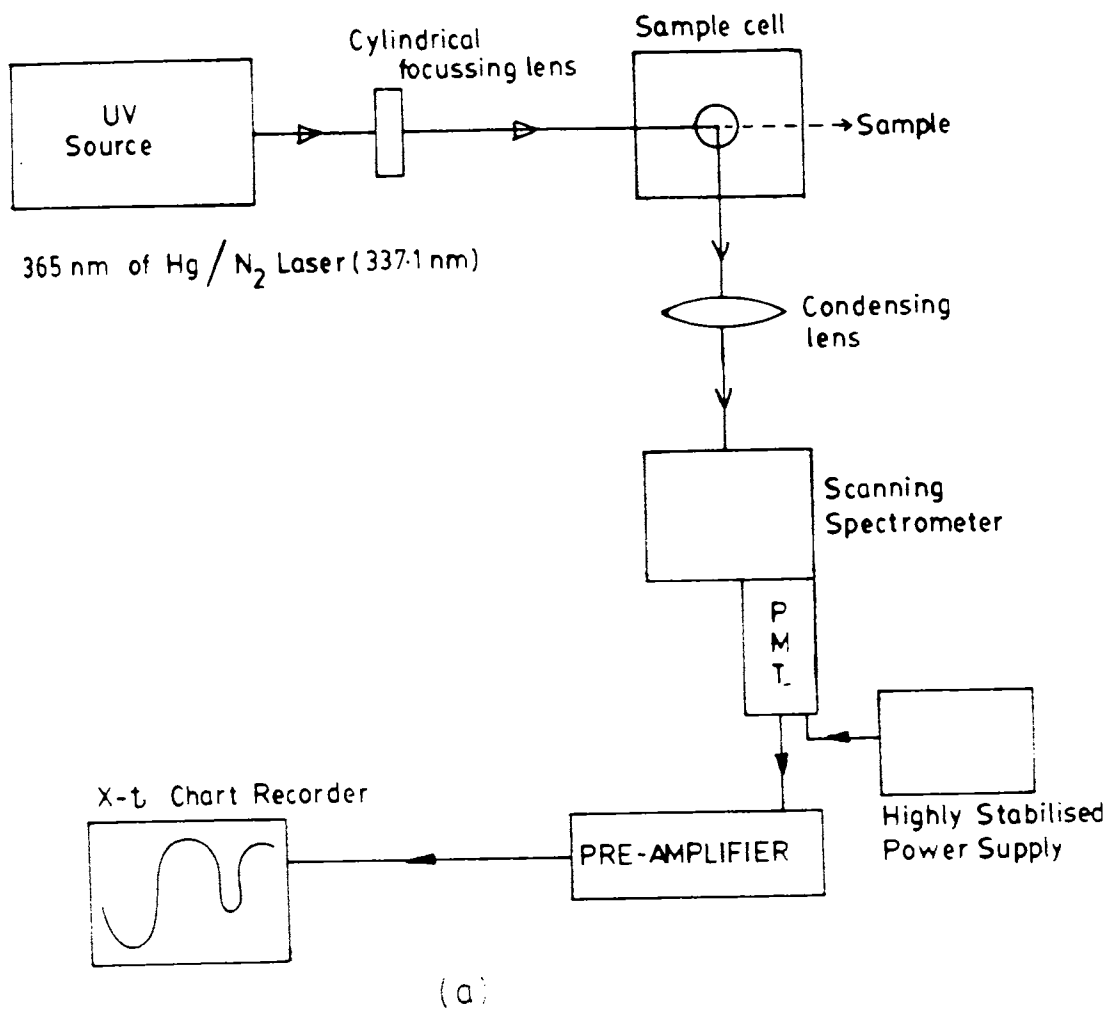
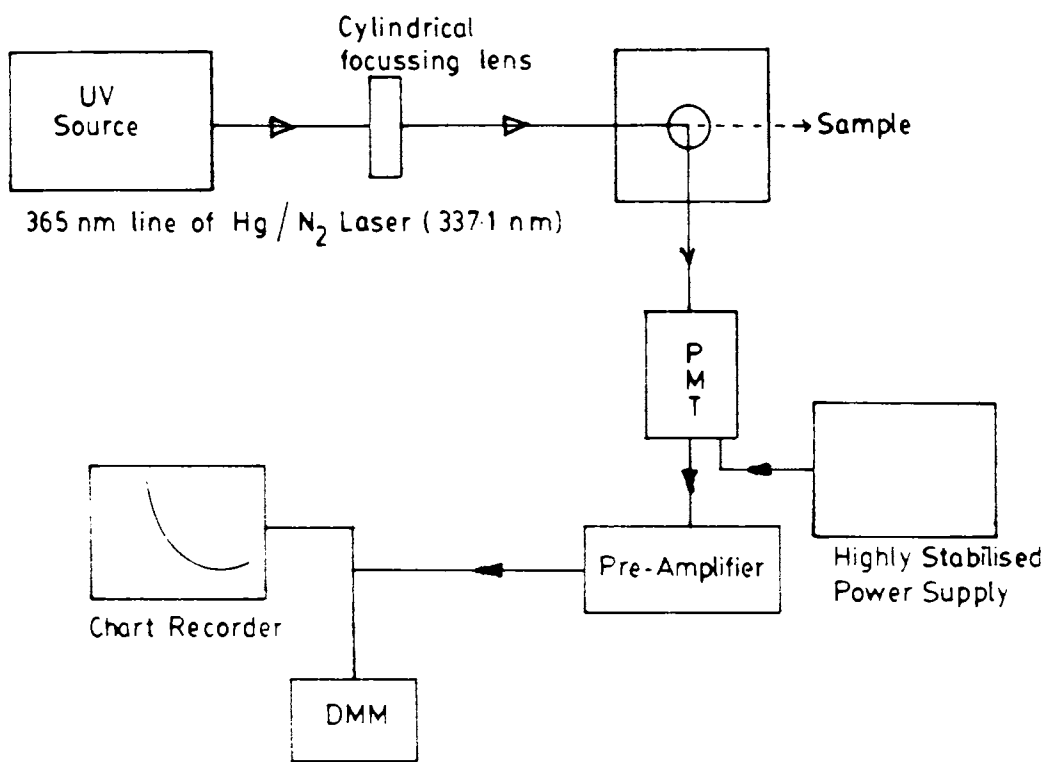


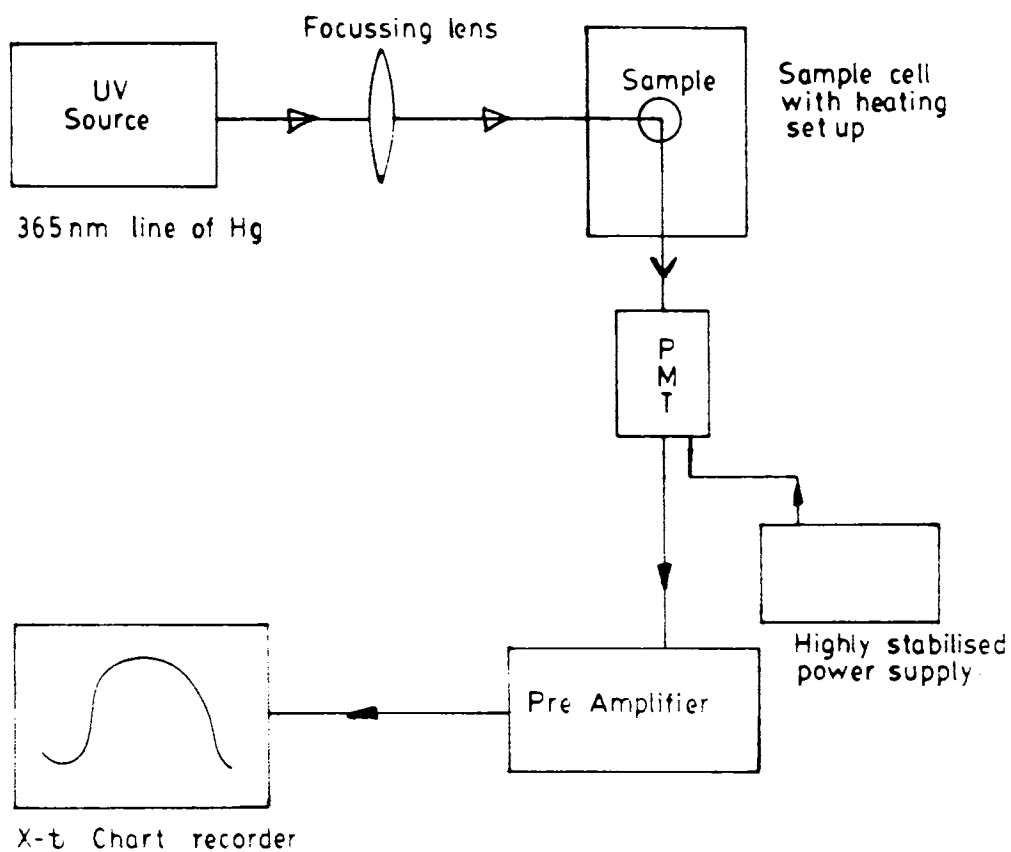
**Fig. 3.7 Schematic experimental arrangement for recording fluorescence spectra.**



(b)

**Fig. 3.7 Schematic experimental arrangement for recording phosphorescence decay**





(c)

**Fig. 3.7 Schematic experimental arrangement for recording thermoluminescence spectra**

In the case of thermoluminescence studies after exciting the sample to the saturation level, the excitation source was cut off and left the sample to decay for about 5 to 10 minutes. Then it is turned towards the slit of the PMT. The sample was heated with a uniform rate and the emission intensity was recorded with the help of a chart recorder as a function of time - (which can be converted into temperature by knowing the heating rate).

### **3.7 Data Acquisition Techniques**

The data acquisition was made with utmost precision. This involved highly sensitive and very precisely calibrated instruments such as scanning spectrometer, photomultiplier tube, pre-amplifier and chart recorder.

#### **3.7.1. Scanning spectrometer**

For the wavelength scanning of fluorescence emission, a medium resolution scanning instrument was needed. This purpose was served by a 0.5m scanning spectrometer (Jarrel - Ash model 82-000). This spectrograph provided a smooth scanning motion in eight speeds ranging from 20 Å/min to 500 Å/min. It gave 16Å/min. dispersion in the first order with maximum resolution of 0.2Å. It covered a spectral range of 4000Å to 9000Å using a reflection grating with 1800 grooves/mm blazed at 500 Å and is driven by a reversible motor [10].

The apparatus consists of two slits - an inlet slit  $S_1$  and exit slit  $S_2$ . The light enters through  $S_1$  and passes to a concave mirror having 150mm diameter and 0.5 meter focal length, gets collimated and reflected to fall on the grating chip, where it undergoes dispersion and again reflects back to the mirror and comes out through the exit slit  $S_2$  (fig.3.8). The wavelength of the monochromatic light emerging at the exit slit is changed by simply rotating the grating about its centre.

#### **3.7.2. Photomultiplier tube**

The output from the monochromator was detected by an EMI photomultiplier tube (model 9683KQB) with S-20 cathode. This tube was directly mounted at the exit slit of the monochromator. The PMT used in the present studies was PR-1400RF model operated at 1.3KV d.c. Since the output gain of the PMT highly depends on the voltage, any variation in the applied voltage causes a noticeable change in its gain. Hence a highly stabilized power supply (EMI PM 28B) was used to operate the PMT, which maintained a constant output voltage across the terminals, in spite of the variation of the input load. The tube was also provided with a good RF shielding. This PMT has got a fairly constant quantum efficiency in the spectral region 350-800nm where all the present investigations were carried out. Before recording the spectra the PMT was given sufficient cooling so that the dark current of the tube is reduced to a minimum value.

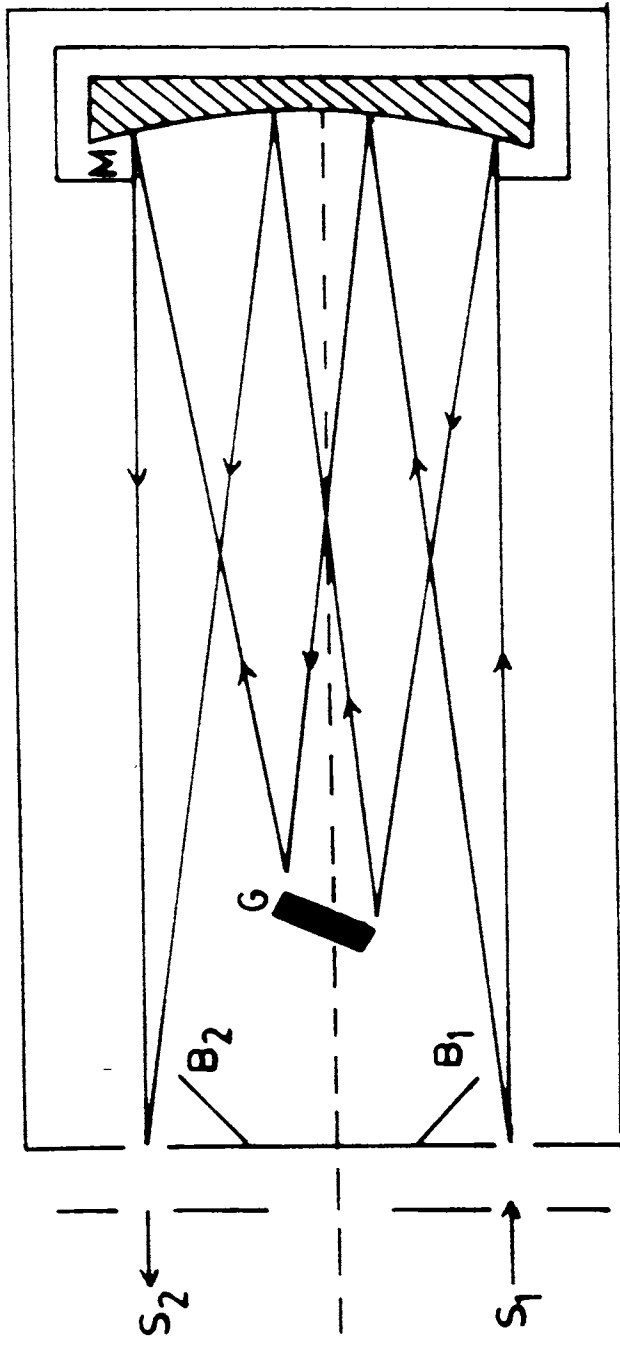


Fig. 3.8 Light path of grating spectrometer

### 3.7.3 Pre-amplifier

Very low intensity light emission from the low efficient phosphors should be amplified using a noise free, high gain amplifier. For this purpose a simple low noise drift free d.c. amplifier using an integrated circuit was fabricated [11]. The circuit is shown in fig.3.9. In this configuration the FET input operational amplifier NE 536 acts as current to voltage converter. Since the integrated circuit has a very large input impedance ( $\sim 10^{14}\Omega$ ) it does not load the large resistance  $R_f$  connected in the feed back circuit. The circuit performance is unaffected by the resistance  $R_b$  used to compensate for the bias current, since the PMT has an output impedance greater than  $10^{12}\text{ohms}$ . The low leakage, low value condenser  $C_f$  suppresses possible oscillations. The RC filter circuit at the output of the amplifier should have a time constant appropriate with the type of signal to be detected. The circuit was perfectly wired on an epoxy board taking care to see that input terminals of the IC are well isolated to reduce the effect of leakage current. A 7.5cm x 5cm x 5cm. M.S box with BNC for input and output terminals contained the entire assembly along with two 9V batteries used as the power supply. This d.c. supply avoids all the possible pick-up noises.

When used with 10 mV strip chart recorder, the system is capable of measuring clearly a change in current as low as 2pico amperes. The PMT dark current could be compensated by adjusting the off-set  $R_{\alpha}$  (10 turn pot). By using suitable variable resistors  $R_1$  and  $R_2$  the output voltage to the chart recorder can be adjusted.

### 3.7.4. Recorder

The amplified output of the PMT is fed to a strip chart recorder (Omniscribe Fisher Recordall series- 5000 model x-t recorder). The sensitivity of this recorder is 0.5mV/cm and has six scanning speeds in the range 2.5 cm/min to 25 cm/min.

In the case of recording the fluorescence emission spectra, the scanning speeds of the monochromator and the chart recorder are suitably adjusted so that a good resolution is obtained. The output of the recorder gives fluorescence emission intensity as a function of wavelength whereas for the phosphorescence decay measurements the recorder charts the decay intensity as a function of time. In TL measurements also, the recorder is calibrated in such a manner that it charts TL intensities as a function of time. But in this case as the time increases the temperature of the sample also increases at a uniform rate which depends on the heating rate applied to the sample holder.

Fig.3.10 shows a photograph of the experimental set up for recording the spectra and fig. 3.11 the flow chart of the experimental scheme employed for the present analysis.

Observations, results and their interpretations are included in the forth coming chapters.

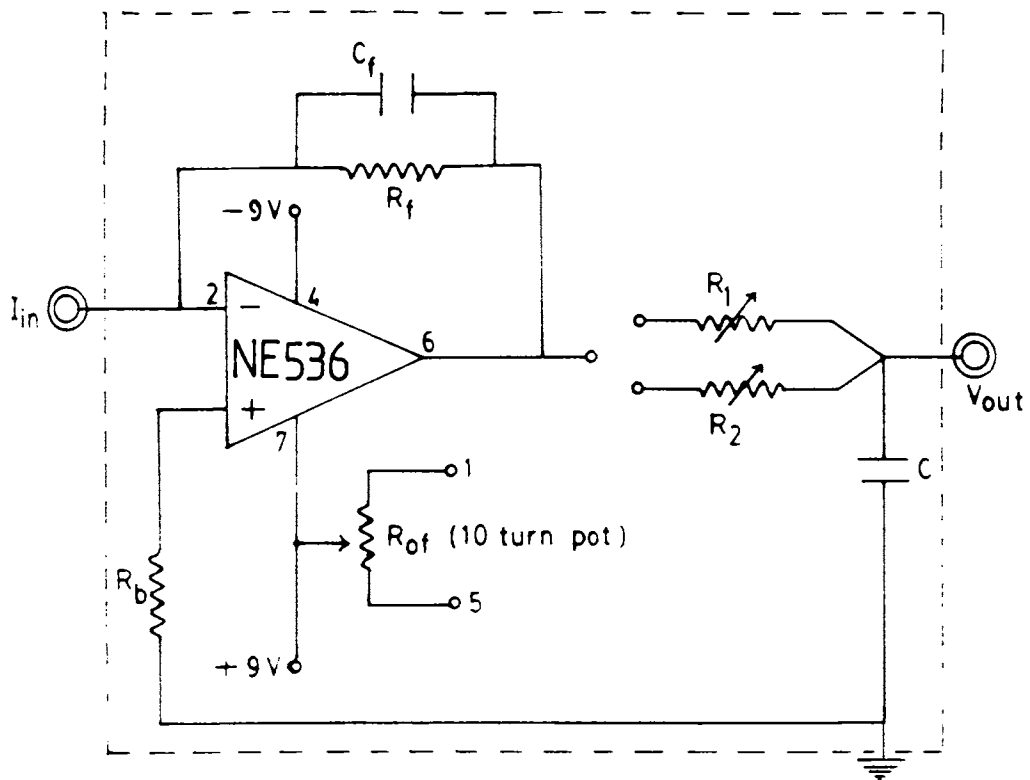


**Fig. 3.9** Circuit diagram of PMT pre-amplifier



**Fig 3.10** The photograph showing the experimental set up used for recording the spectra

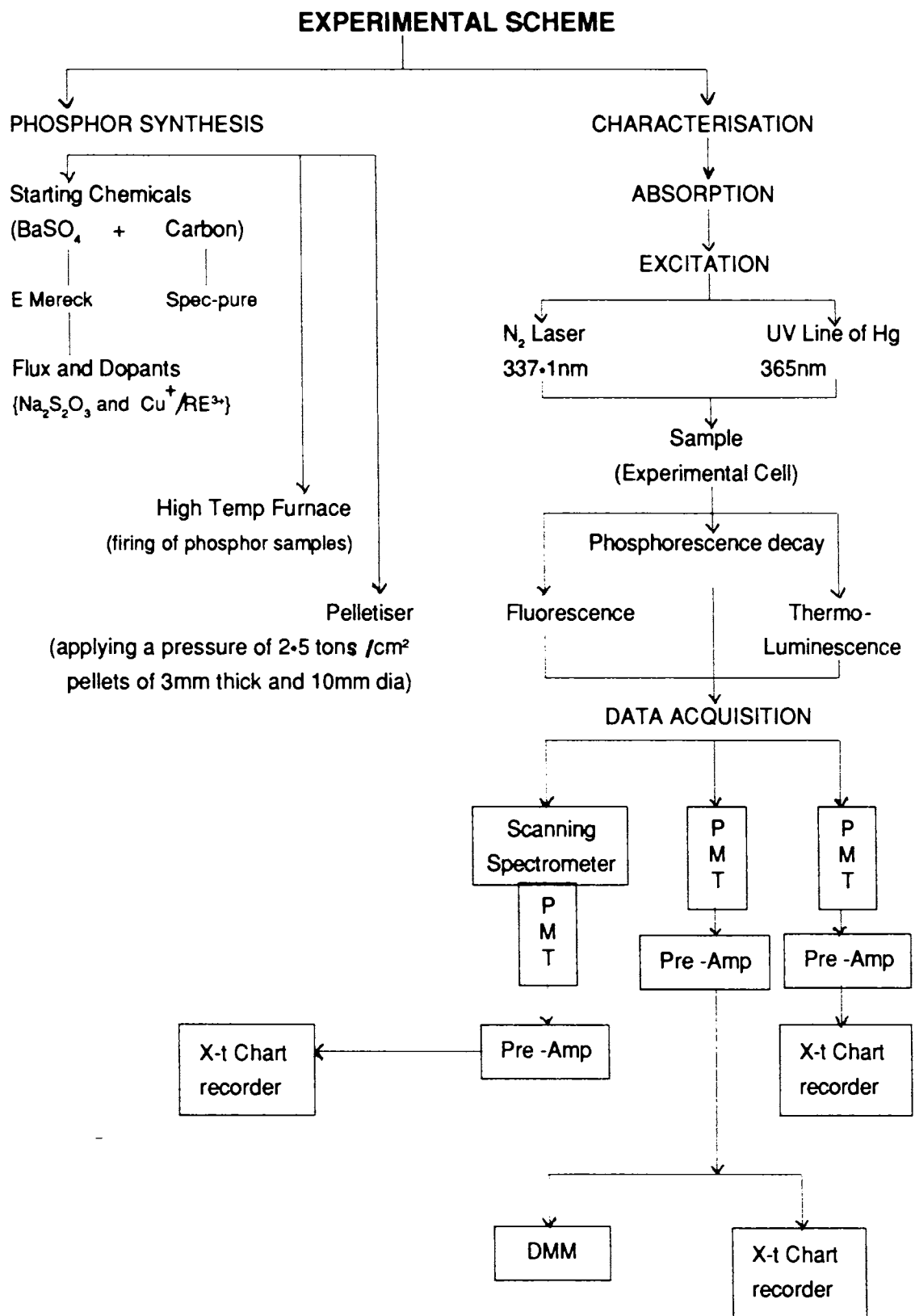


**Fig. 3.11** Flow chart of experimental scheme employed for the present analysis

## REFERENCES :

- [1] Lehmann W., J. Electrochem. Soc. 177 (1970) p.1389
- [2] Gasiot J., Braunlich P and Fillard J.P., Appl. Phys. Lett. 406 (1982) p.376
- [3] Rao R.P., J. Mater. Sci. Lett. 2 (1983)p.106
- [4] Rao R.P., Bull. of Mater. Sc. 5 (1983)p.29
- [5] Chakravarthi A.K., Mor S.L. and Ranade J.D., Indian J. Pure and Appl. Phys. 12 (1974) p.608
- [6] Blasse G., "HAND BOOK ON THE PHYSICS AND CHEMISTRY OF RARE-EARTHS" (ed) K.A.Gachneidner Jr and Eyring L.R. Vol. 4, NorthHolland, New York (1979)
- [7] Bhawalkar D.R. and Sivarman, Indian J. of Pure and Appl. Phys. 9 (1971) p.18
- [8] Ravisankar M. "Fabrication and parametric studies of a triggered  $N_2$  laser and investigations on the influence of dissolved constituents of sea water on the optical attenuation using the nitrogen laser pumped Dye laser" Ph.D. thesis, Cochin University of Science and Technology, 1988.
- [9] Thaattey, J. Phys. E -Scient. Instrum. 14(1981) p.1299
- [10] Jarell- Ash. Instruction Manual, Engineering Publ. no. 82-00/IM-RW 7. (1971)
- [11] Pillai S.M , Raghavan C., Sudha Kartha and Vallabhan C.P.G, J. of Instrum. Soc. of India 12 (1982) p.7.



## **CHAPTER IV**

# LASER INDUCED FLUORESCENCE FROM

## BaS:RE PHOSPHORS

### 4.1. Introduction

The phosphors, as indicated earlier, owe their practical importance due to their property of absorbing incident energy and converting it into visible radiations. The studies on absorption and emission spectra of phosphors are helpful in understanding the energy levels involved in the process and deductions can be made on the nature of luminescence centres

In this chapter the results of investigations carried out on  $N_2$  laser induced fluorescence emission from Barium sulphide phosphor doped with different rare-earth (RE) impurities and copper are presented in detail. The analysis and results are explained under three different sections. In section A, the details of absorption spectra taken for the phosphor samples under consideration are given. Section B gives an account of spectral features observed in fluorescence emission of undoped BaS, BaS:RE, BaS:RE<sub>1</sub>:RE<sub>2</sub>, BaS:Cu, BaS:Cu:RE, BaS:Cu:RE<sub>1</sub>:RE<sub>2</sub> phosphor systems and their analysis. Here RE stands for rare-earth ions such as La<sup>3+</sup>, Pr<sup>3+</sup>, Nd<sup>3+</sup>, Sm<sup>3+</sup>, Gd<sup>3+</sup> and Dy<sup>3+</sup>. Finally, in section C, the energy level splitting observed in the cases of BaS:Sm and BaS:Pr phosphors due to crystal field interactions are discussed at length.

The results presented in this chapter pertains to the phosphor systems prepared by method II as described in the last chapter. Details of the prepared phosphor sets are listed in Table 3.2. In these samples the flux- ( $Na_2S_2O_3$ ) concentration was kept fixed at 2 Mol% by wt of BaS.

### SECTION A

#### 4.2. The Absorption Spectra

As an initial step for the analysis, the absorption spectra of the phosphor samples were taken using a Hitachi 3410 model UV-Vis-NIR spectrophotometer. This spectrophotometer is of dual beam type which can record absorption/transmission spectra in the wavelength region 2600-200 nm.

The absorption spectra of the solid phosphors were taken as follows. A small quantity of the phosphor sample in powder form was added to one or two drop of liquid paraffin to form an emulsion. This paste was then uniformly spread over a filter paper cut to the exact size of the sample holder of the spectrophotometer. On the same quality of filter paper, the liquid

paraffin alone is spread uniformly and this was used as the reference. The absorption spectra of all the phosphor samples show considerably intense absorption in the UV region; while there is comparatively very low absorption in visible range. There is no variation in the region of absorption in the case of undoped and doped phosphors. However, there is some variation in absorption intensity depending upon the concentrations of the dopant as seen in fig.4.1 (A) to (D), which show, the absorption spectra charted in UV region for  $B_0$  (undoped BaS), BaS:RE, BaS:RE<sub>1</sub>:RE<sub>2</sub>, BaS:Cu phosphor systems. The region of absorption gives an idea about the excitation wavelength which will give fluorescence emission in the visible region. Also the variation in intensities of absorption give a measure of the intensity of fluorescence output too. So these spectra revealed that excitation in UV region starting from 365 nm will give emission in the visible range depending upon the levels which are excited.

## SECTION B

### 4.3. N<sub>2</sub> Laser Induced Fluorescence

As is well known, IIA-VIA compounds become efficient phosphors when activated with rare-earth metal ions. Since the band gap of alkaline earth sulphides (AES) are comparatively large, the excited states of the activator are not densely distributed between valence and conduction bands. Also these host materials provide different environment around the impurity ions. In order to understand the role of rare-earth impurity ions and their relationship with the host lattice, we have studied BaS phosphor doped with different rare-earth ions. Moreover, the simultaneous incorporation of specific metallic impurities along with the rare-earth ions in these type of phosphors are gained considerable practical importance recently [1]. So we studied the effect of Cu<sup>+</sup> and RE<sup>3+</sup> impurities in BaS, in different combinations too.

Using a pulsed nitrogen laser system (output wavelength 337.1 nm), fluorescence emission spectra were recorded for a system of phosphors viz., BaS, BaS:RE, BaS:RE<sub>1</sub>:RE<sub>2</sub>, BaS:Cu, BaS:Cu:RE, BaS:Cu:RE<sub>1</sub>:RE<sub>2</sub> etc. at room temperature (28°C). The details of experimental set up are given in chapter III.

#### 4.3.1. Spectral Features and Analysis

##### (a) Self activated BaS

In the preparation of phosphors, even though the fluxes are very essential for proper crystallization, the high concentration causes the quenching of host lattice emission [2]. With this view in mind, we prepared BaS phosphors with different concentrations of flux-(Na<sub>2</sub>S<sub>2</sub>O<sub>3</sub>)-ranging from 2 Mol% by wt of BaS to 30 Mol% by wt of BaS. The emission spectra of these

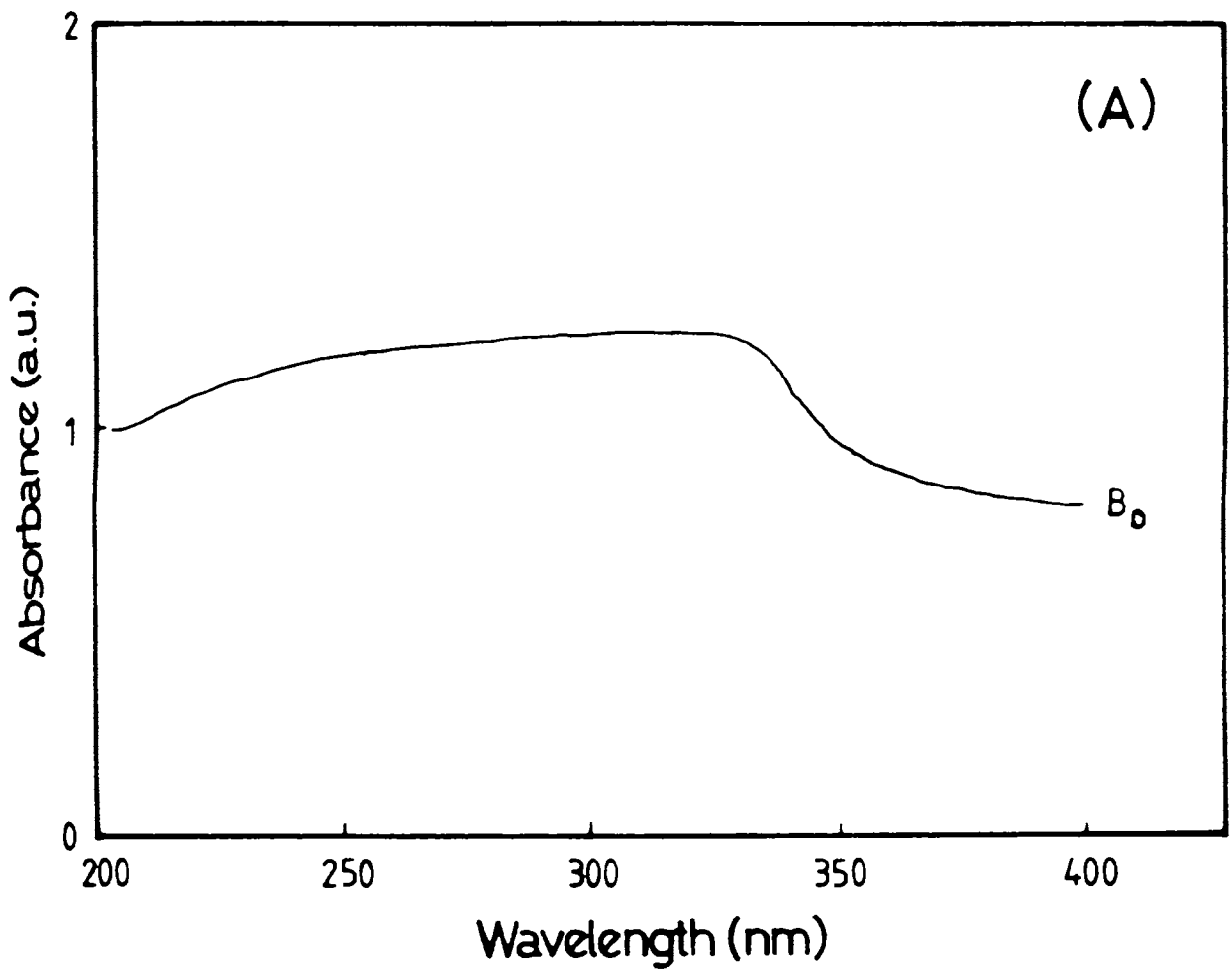


Fig. 4.1 (a) Absorption spectrum of undoped BaS phosphor

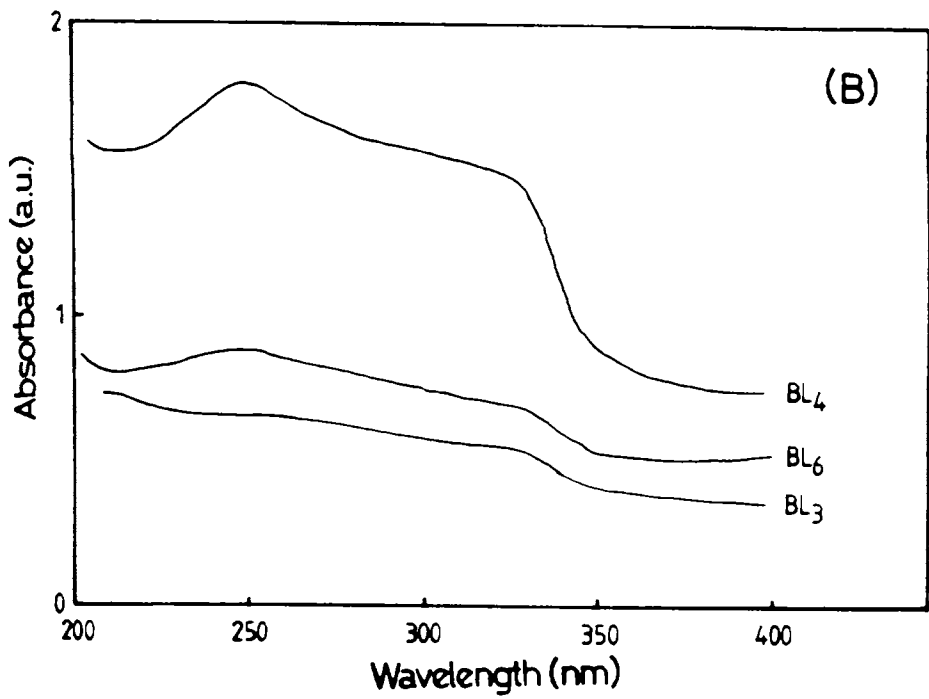


Fig. 4.1 (b) Absorption spectra of BaS:La phosphors

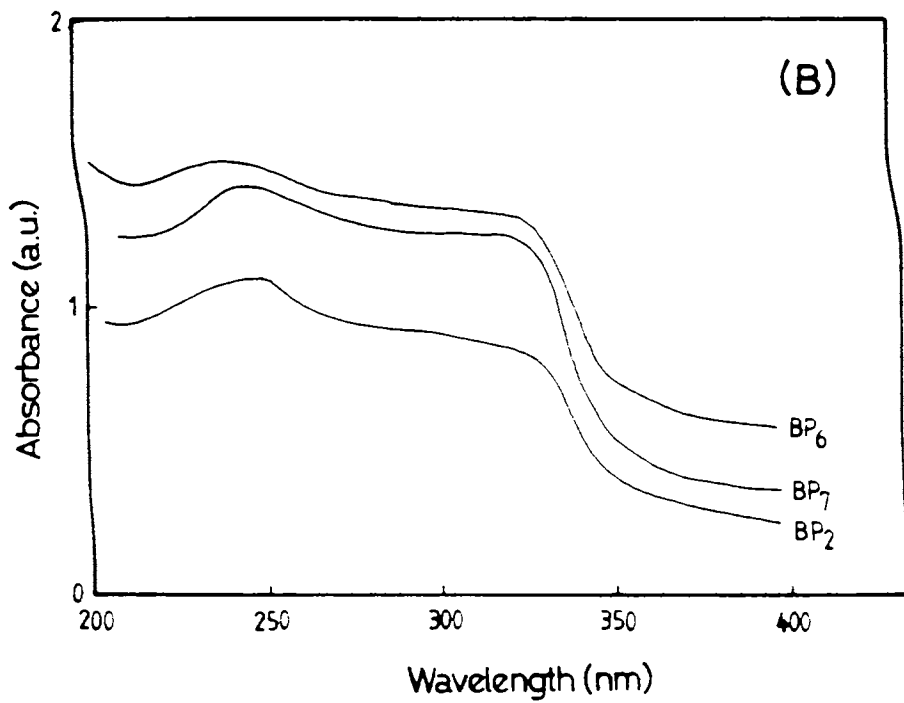


Fig. 4.1 (b) Absorption spectra of BaS:Pr phosphors

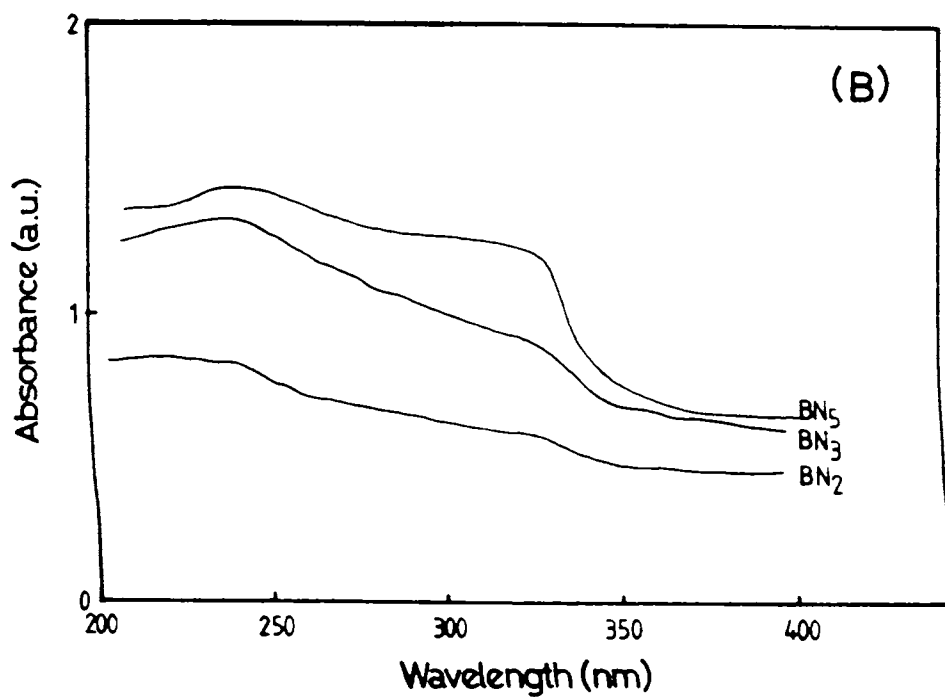


Fig. 4.1 (b) Absorption spectra of BaS:Nd phosphors

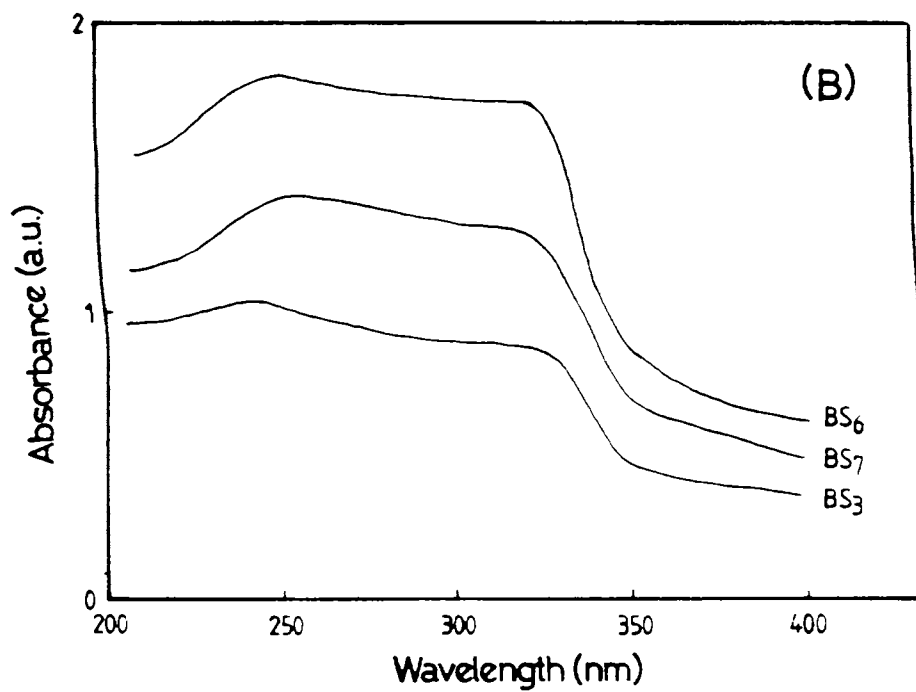


Fig. 4.1 (b) Absorption spectra of BaS:Sm phosphors

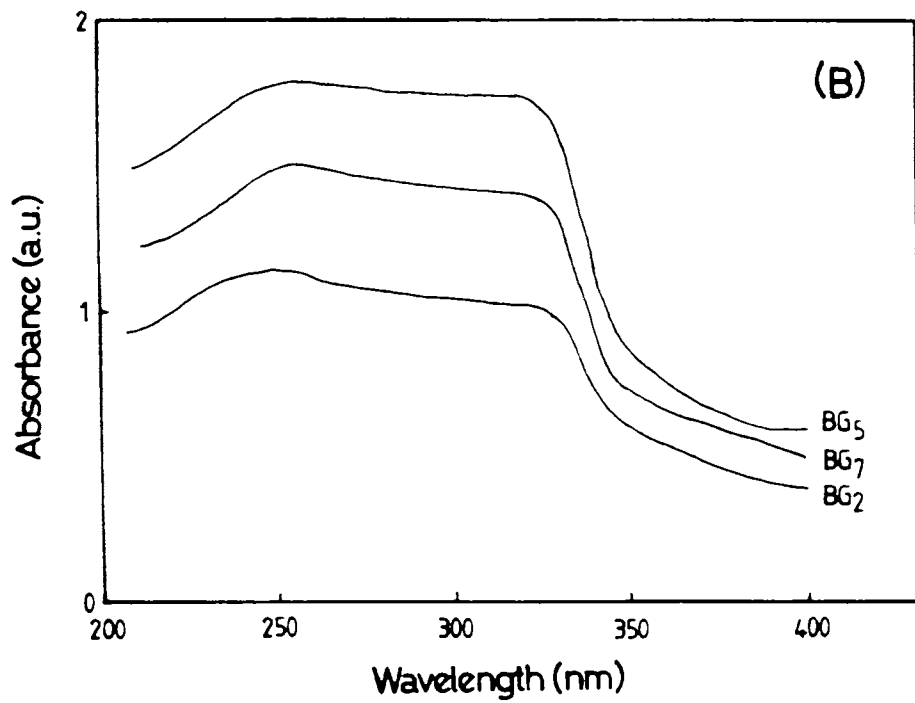


Fig. 4.1 (b) Absorption spectra of BaS:Gd phosphors

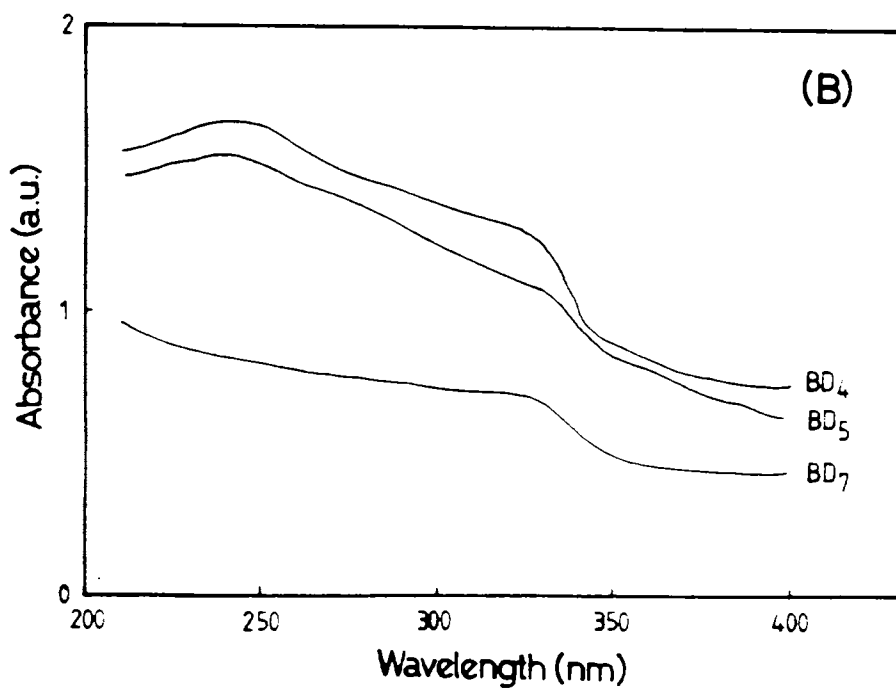


Fig. 4.1 (b) Absorption spectra of BaS:Dy phosphors

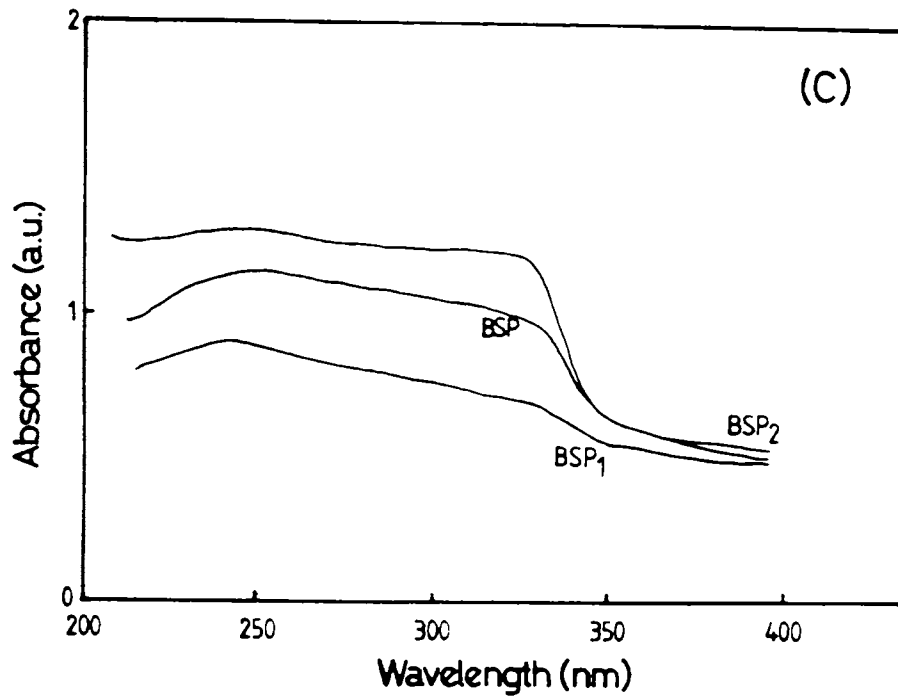


Fig. 4.1 (c) Absorption spectra of BaS:Sm:Pr phosphors

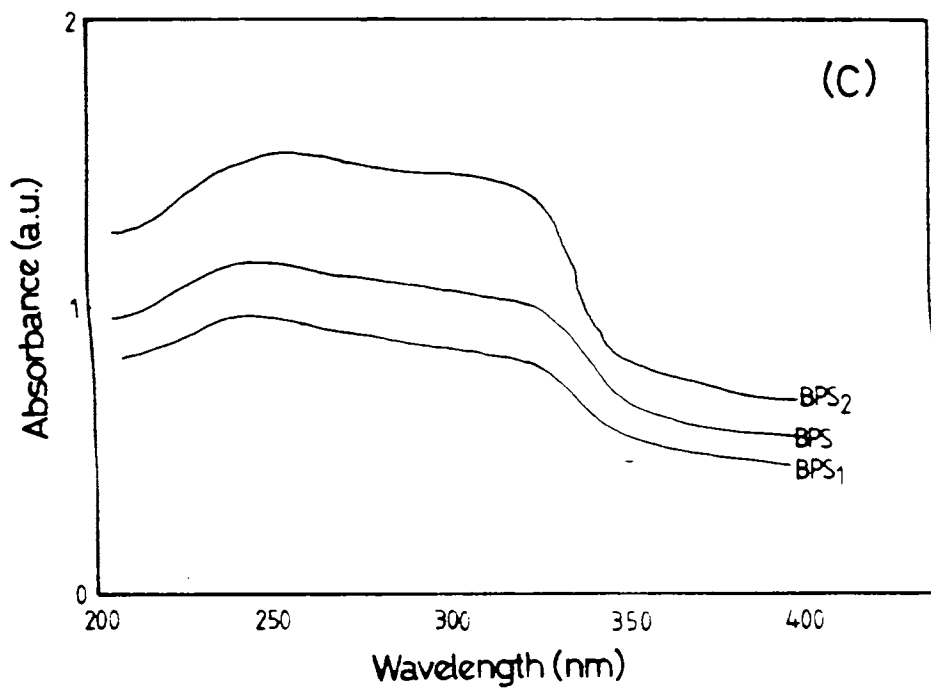


Fig. 4.1 (c) Absorption spectra of BaS:Pr:Sm phosphors



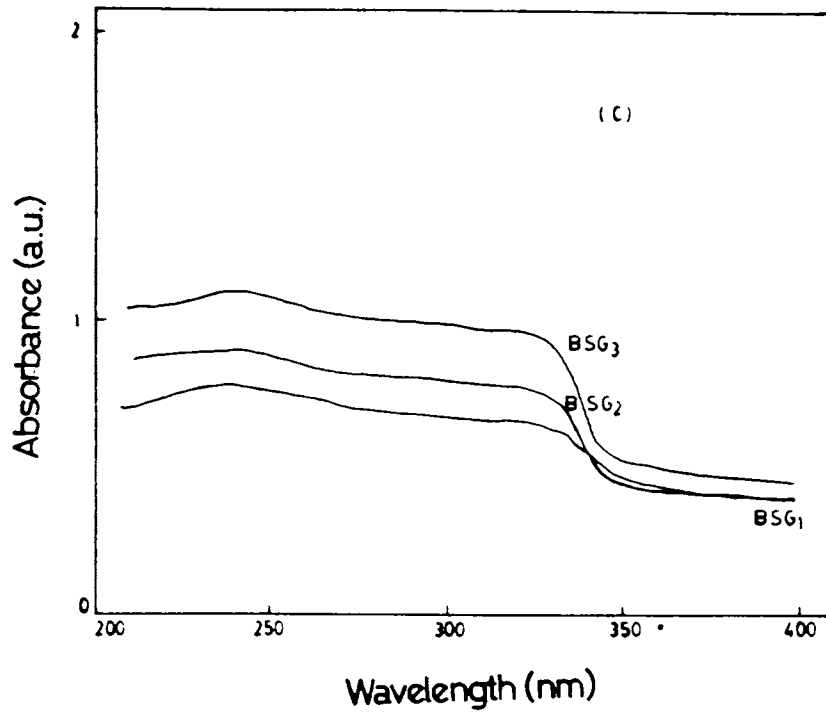


Fig. 4.1 (c) Absorption spectra of BaS:Sm:Gd phosphors

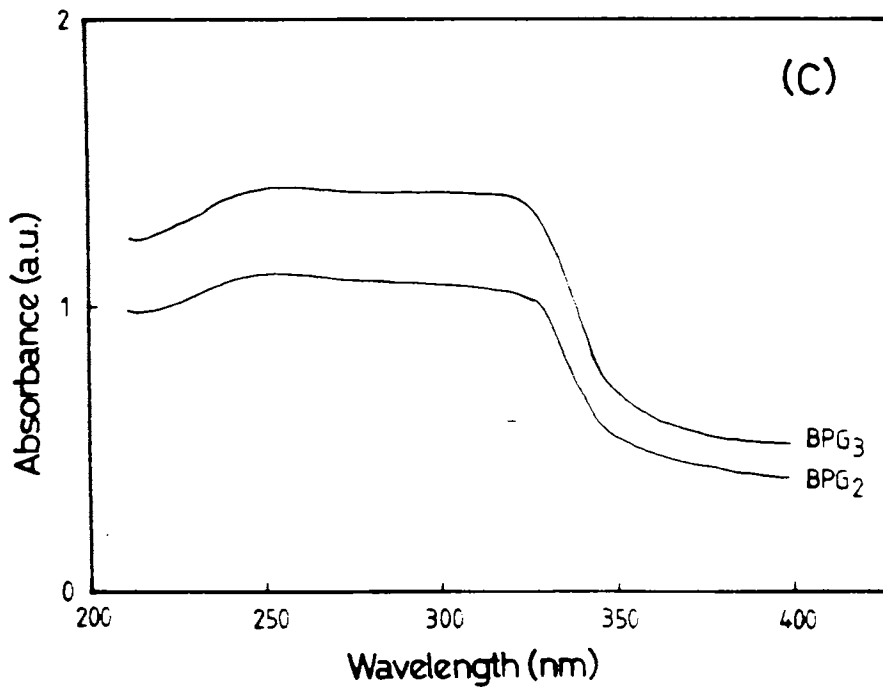


Fig. 4.1 (c) Absorption spectra of BaS:Pr:Gd phosphors

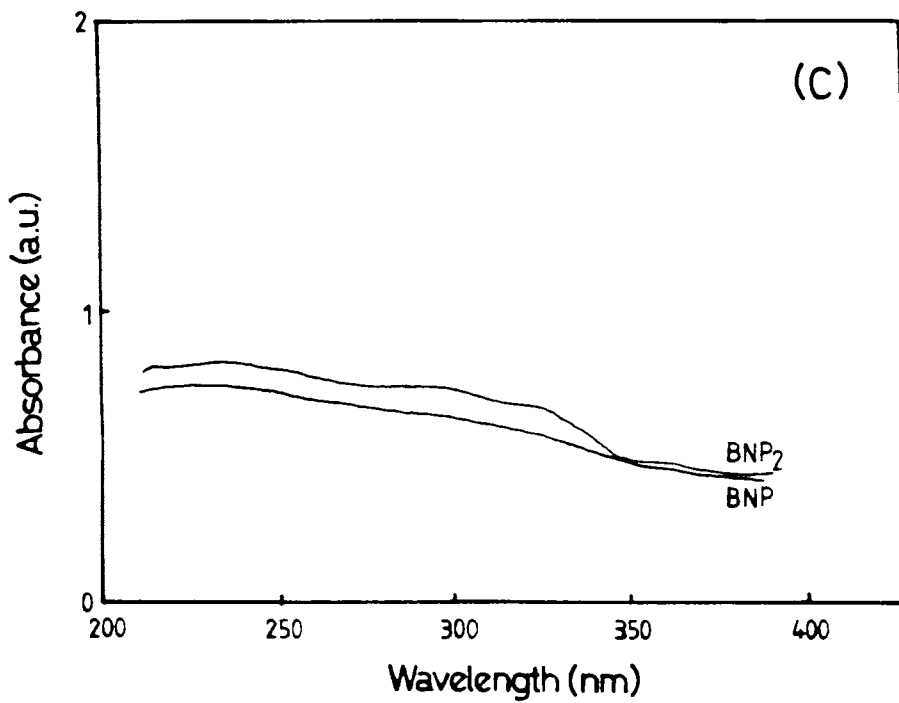


Fig. 4.1 (c) Absorption spectra of BaS:Nd:Pr phosphors

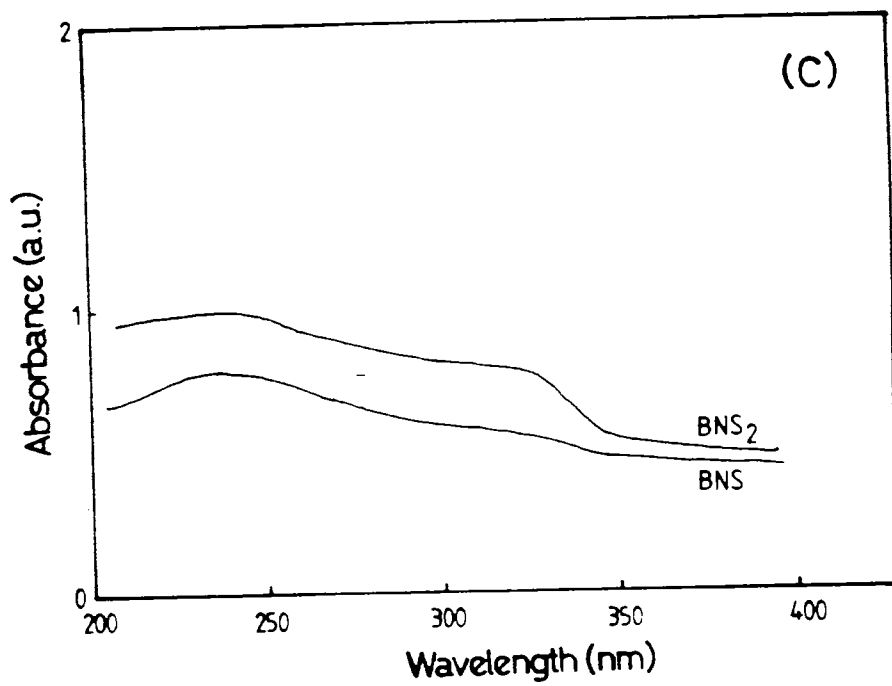


Fig. 4.1 (c) Absorption spectra of BaS:Nd:Sm phosphors

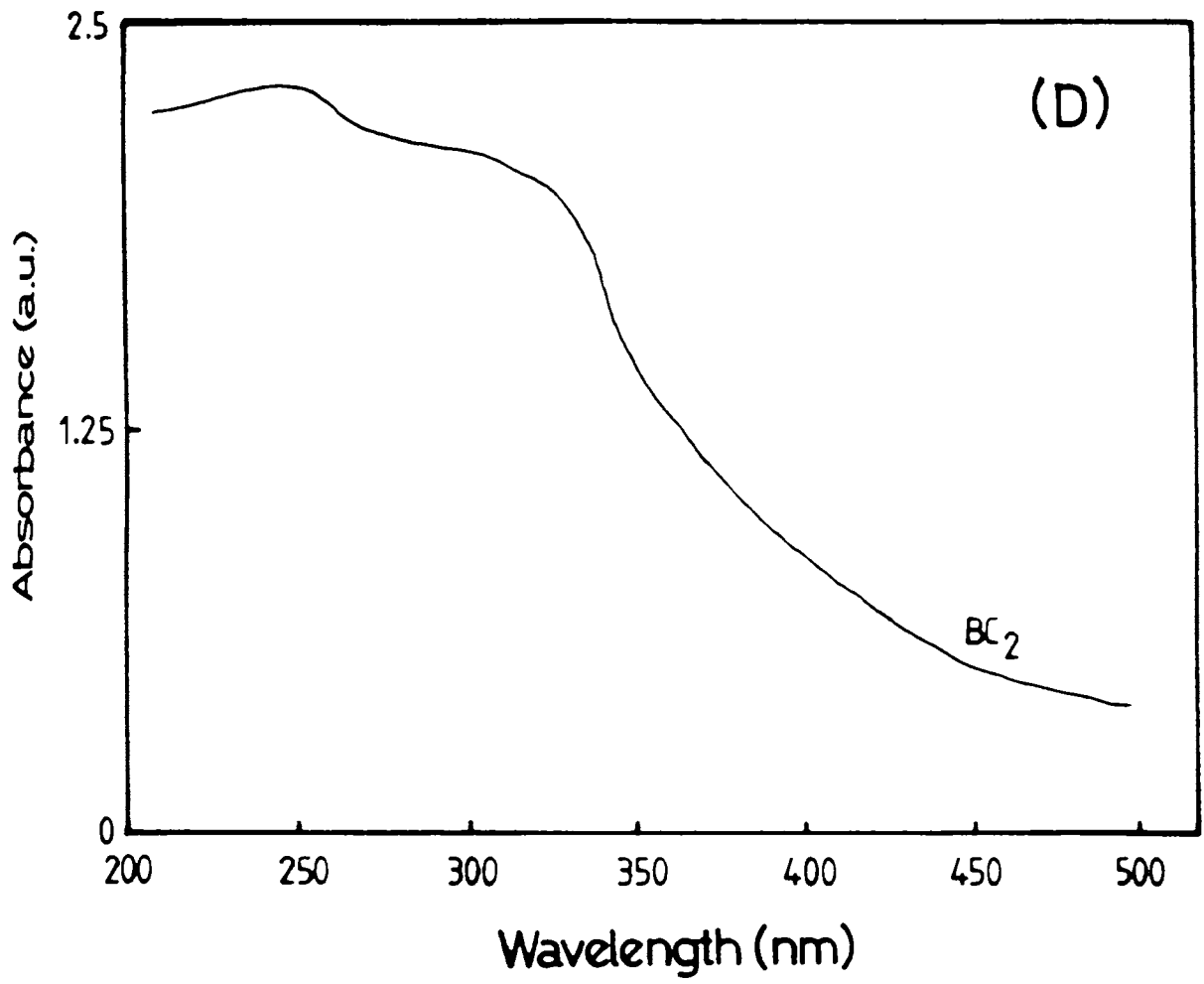


Fig. 4.1 (d) Absorption spectra of BaS:Cu phosphor

samples are in general found to be broad in nature with two bands in the 450-540 nm and 560-650 nm regions (fig.4.2 ) Depending on the concentration of flux, the intensities of these bands are found to vary. As the flux concentration increases, the band in blue-green region becomes more and more intensified with peak position at ~450 nm, while the other band has no such dependence on the concentration of flux. For the flux concentration at 2 Mol% by wt of BaS, both bands show a moderate intensity of emission. So we used this concentration of the flux, when the phosphors were doped with copper and different rare-earth impurities.

Excitation with N<sub>2</sub> laser output of 337.1 nm is effective in causing band to band transitions in BaS. Electrons and holes which are generated in this process will migrate through the lattice and will get trapped by the host lattice vacancies from where the fluorescence emission by radiative transitions results. The broad nature of the emission bands is due to the lattice vibrations which assist rapid depopulation of the energy states in subsequent radiative transitions. The increase in emission intensity of the band in blue green region with increase in flux concentration suggests that this band is due to the host lattice vacancies created due to the addition of flux. The flux in the form of sodium thiosulphate in BaS is effective in creating more and more V<sub>Ba<sup>2+</sup></sub> levels. So the blue band peaking at 450 nm region can be attributed to recombination of the holes trapped at V<sub>Ba<sup>2+</sup></sub> levels with electrons from the conduction band. The other possible vacancy sites in the band gap region of BaS are due to sulphur vacancy positions (V<sub>S<sup>2-</sup></sub>) or the complex levels like V<sub>Ba<sup>2+</sup></sub> + V<sub>S<sup>2-</sup></sub> arising due to S<sup>2-</sup> in the vicinity of a cation vacancies and Ba<sup>2+</sup> in the vicinity of anion vacancies. Electrons and holes trapped in these levels and their recombination can be attributed to the emission observed in 560-650 nm region.

#### (b) Rare-earth doped BaS phosphors.

When rare-earth (RE) dopants are added individually, i.e., in the case of BaS:RE phosphor systems, the fluorescence emission characteristics of BaS was found to be modified. Fig. 4.3(A) to (F) show the fluorescence emission spectra of BaS:RE phosphor systems studied. All the RE doped phosphors show an overall increase in emission intensity. The characteristic emissions of RE<sup>3+</sup> ions were found to be superposed over the broad emission bands of BaS. In the cases of BaS:Sm and BaS:Pr phosphors the well resolved emission lines characteristic of Sm<sup>3+</sup> and Pr<sup>3+</sup> are seen unlike in the other cases of BaS:RE systems. The emission intensity of 450-540 nm band gets more enhanced in BaS:La, BaS:Nd, BaS:Gd, and BaS:Dy phosphor systems in comparison with BaS:Pr and BaS:Sm phosphors. Fig.4.4 shows the variation in peak intensity ratio of 560-650nm band to 450-540 nm band for various RE<sup>3+</sup> concentrations of BaS:RE systems. In the case of BaS:Dy phosphor, at high concentrations of the dopant, there is a pronounced increase in the intensity for 560-650 nm band with complete suppression of the 450-540 nm band.

It is seen that the concentration of the dopants has a considerable effect on the emission

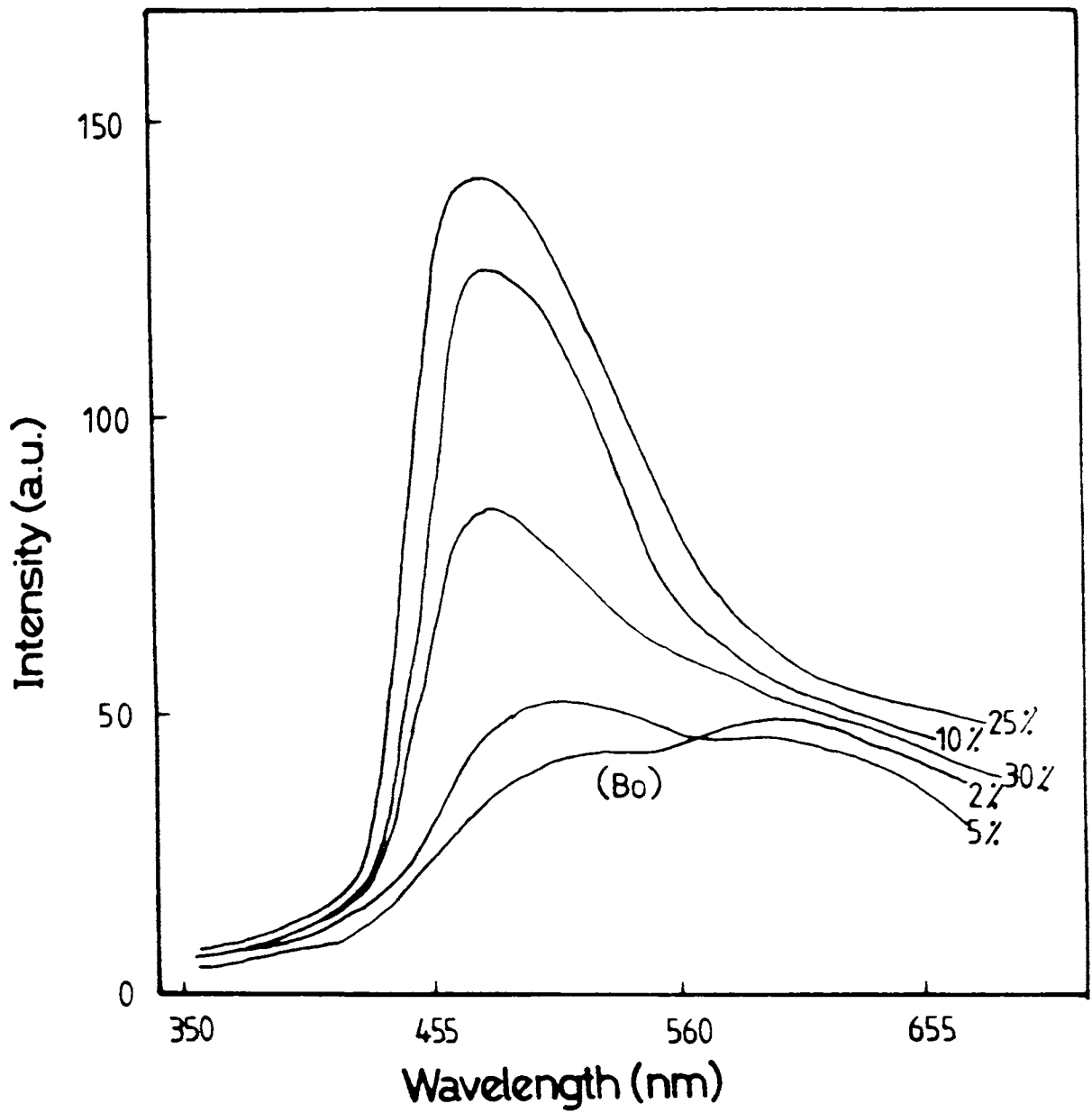


**Fig. 4.2** Fluorescence emission spectrum of self-activated BaS phosphor under N<sub>2</sub> laser excitation for various flux (Na<sub>2</sub>S<sub>2</sub>O<sub>3</sub>) concentrations

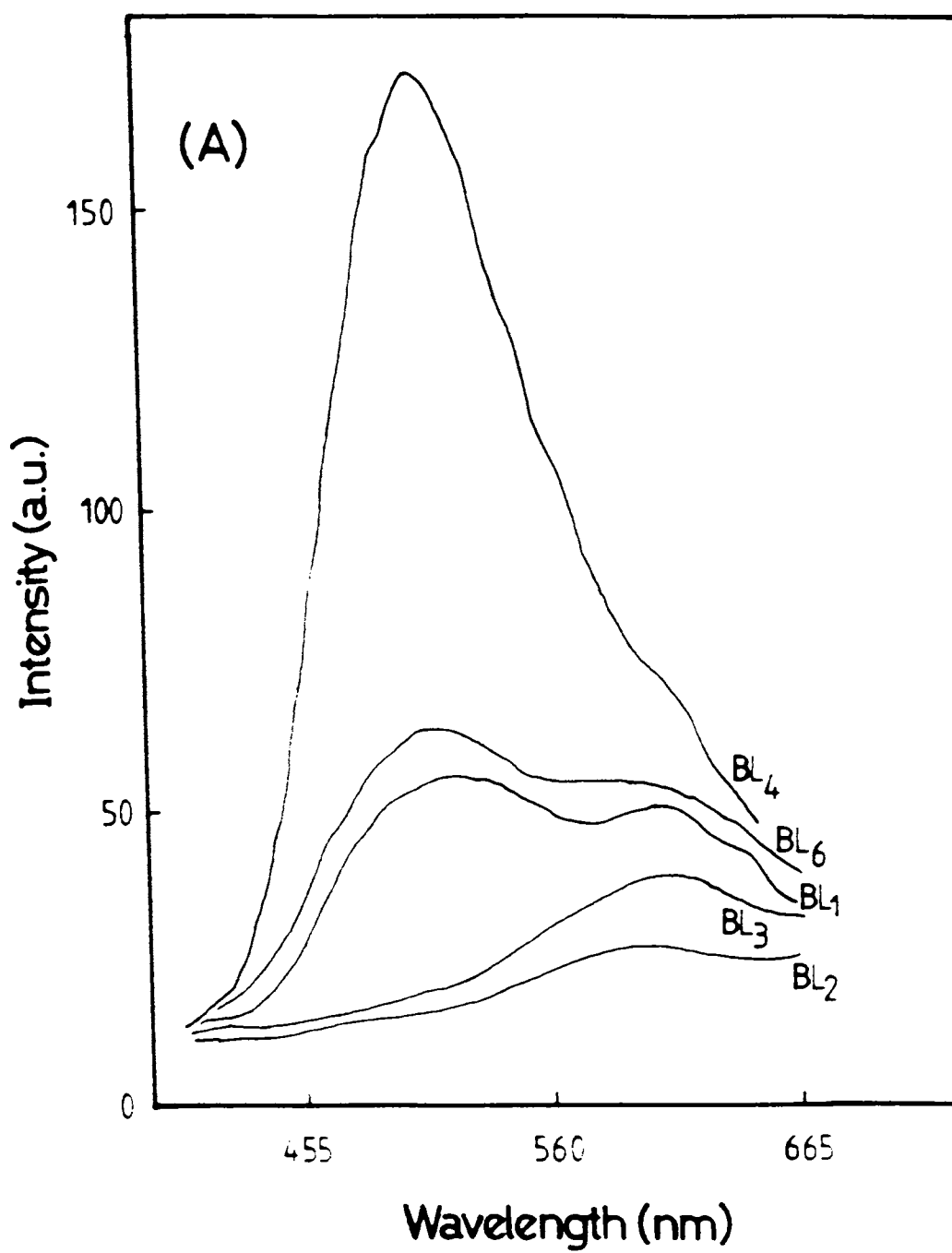


Fig. 4.3 (a) Fluorescence emission spectra of BaS:La phosphors under N<sub>2</sub> laser excitation

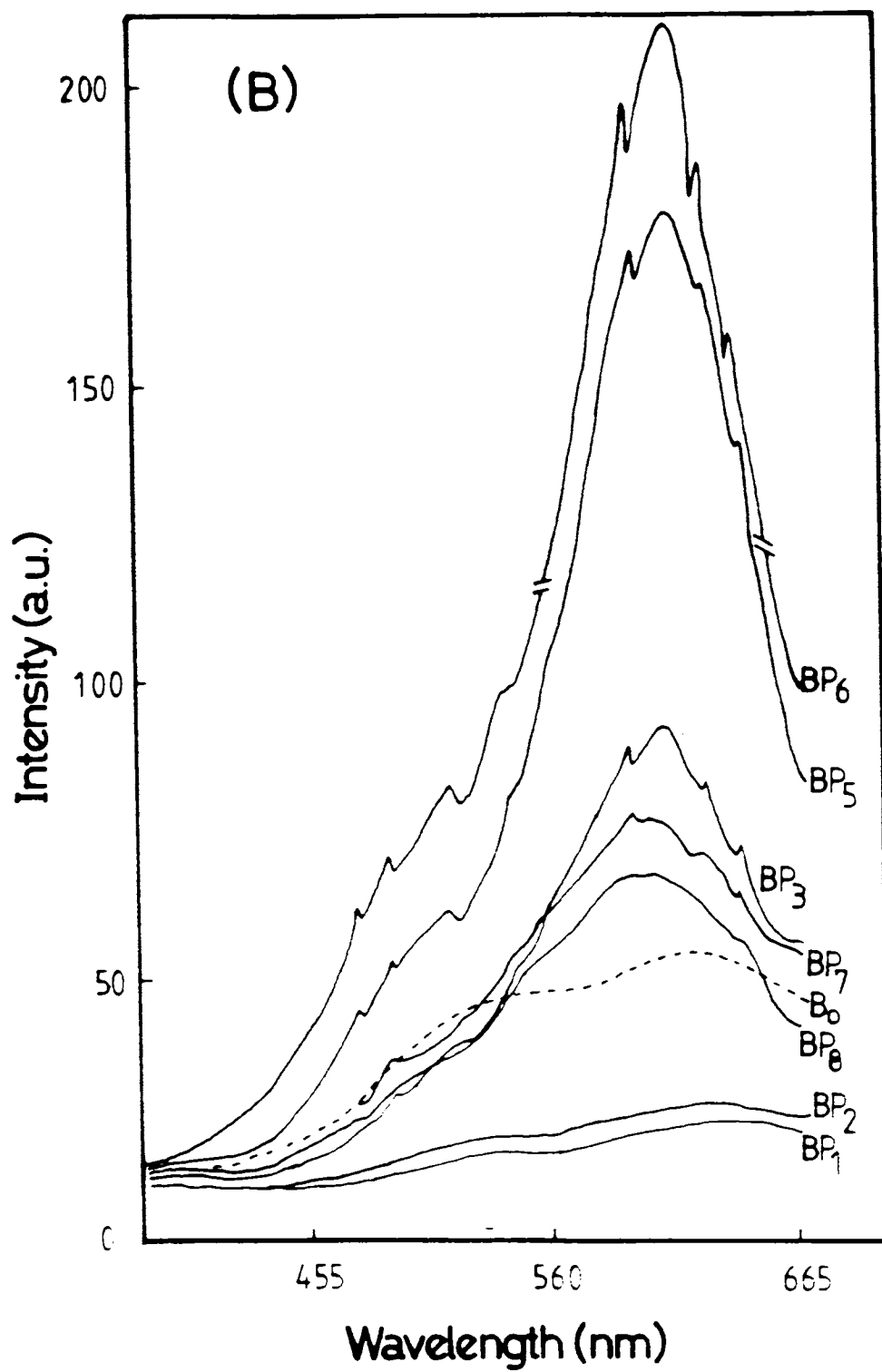


Fig. 4.3 (b) Fluorescence emission spectra of BaS:Pr phosphors under  $N_2$  laser excitation (-  $B_0$  denotes undoped BaS)

- G5039 -

T  
535.374 : 669.893.001.5  
REF

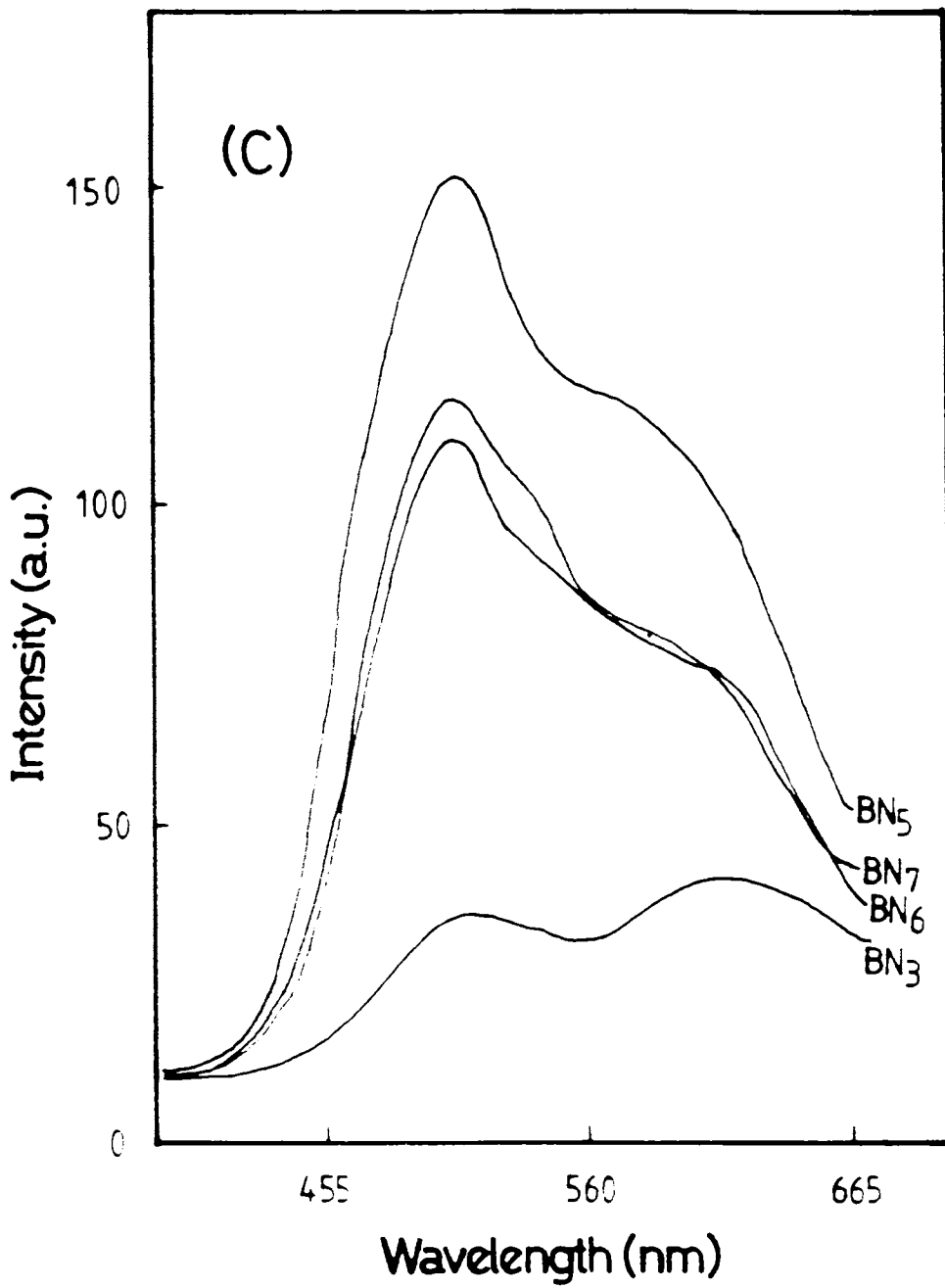


Fig. 4.3 (c) Fluorescence emission spectra of BaS:Nd phosphors under  $N_2$  laser excitation



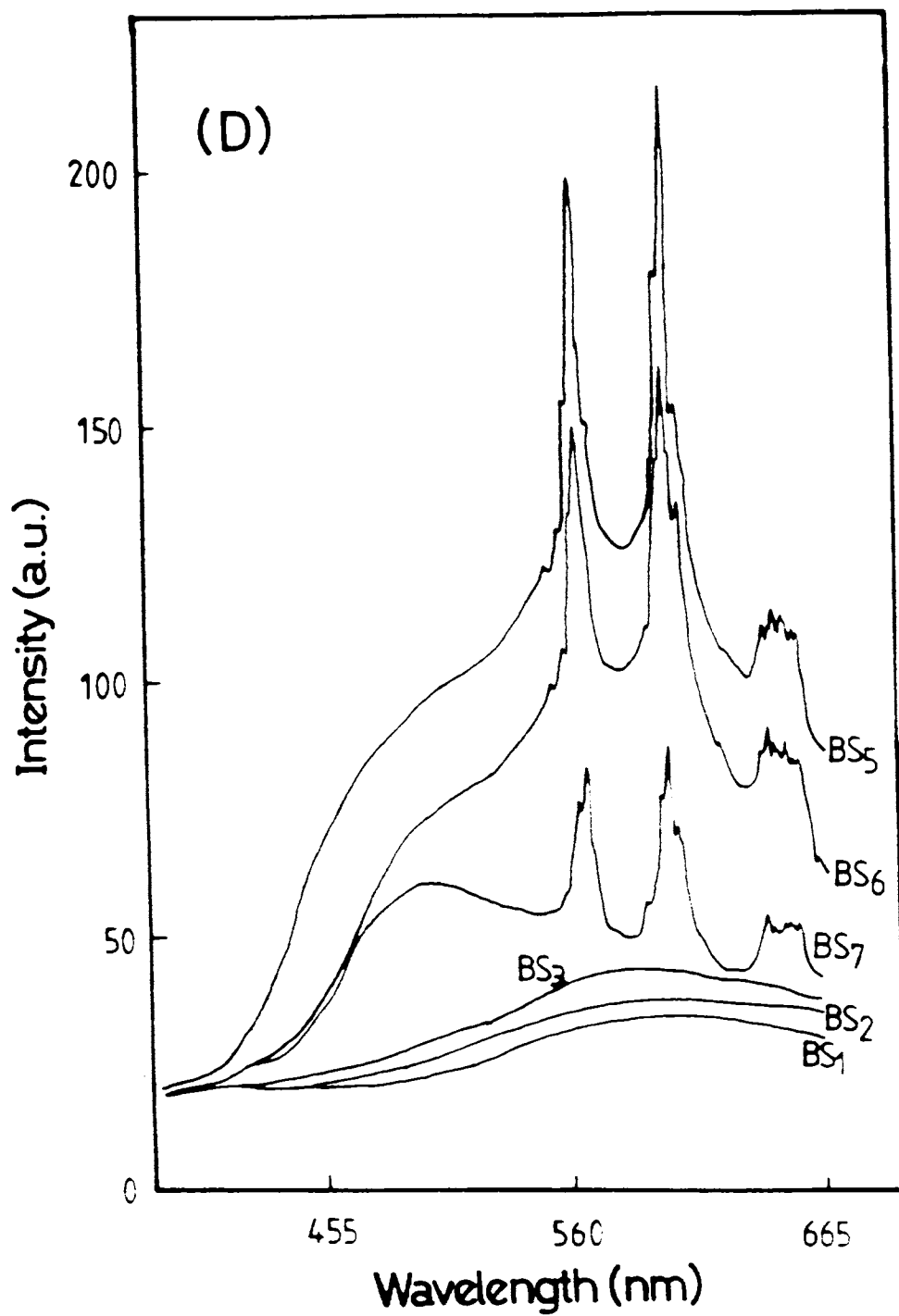


Fig. 4.3 (d) Fluorescence emission spectra of BaS:Sm phosphors under N<sub>2</sub> laser excitation

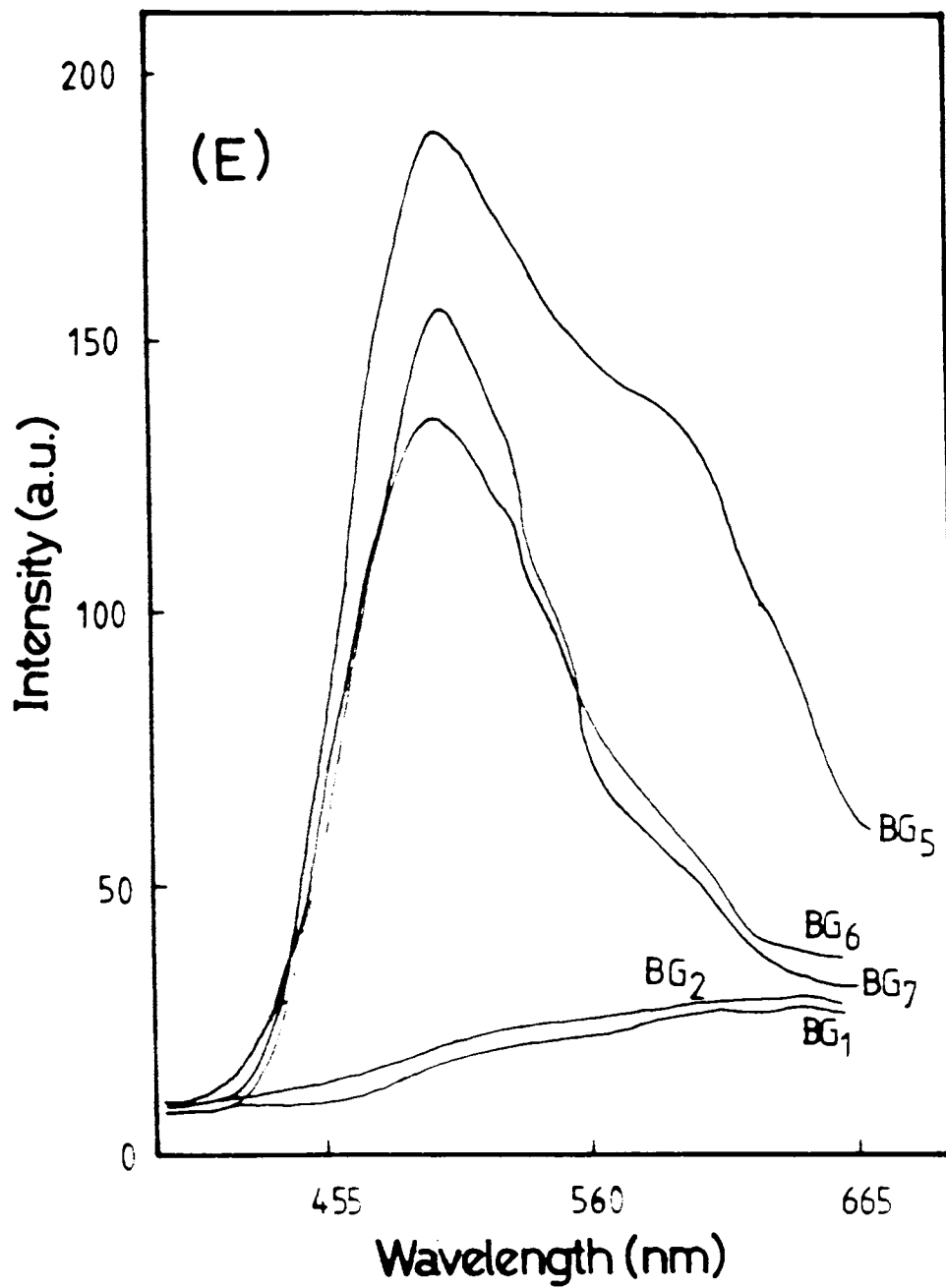


Fig. 4.3 (e) Fluorescence emission spectrum of BaS:Gd phosphors under  $N_2$  laser excitation

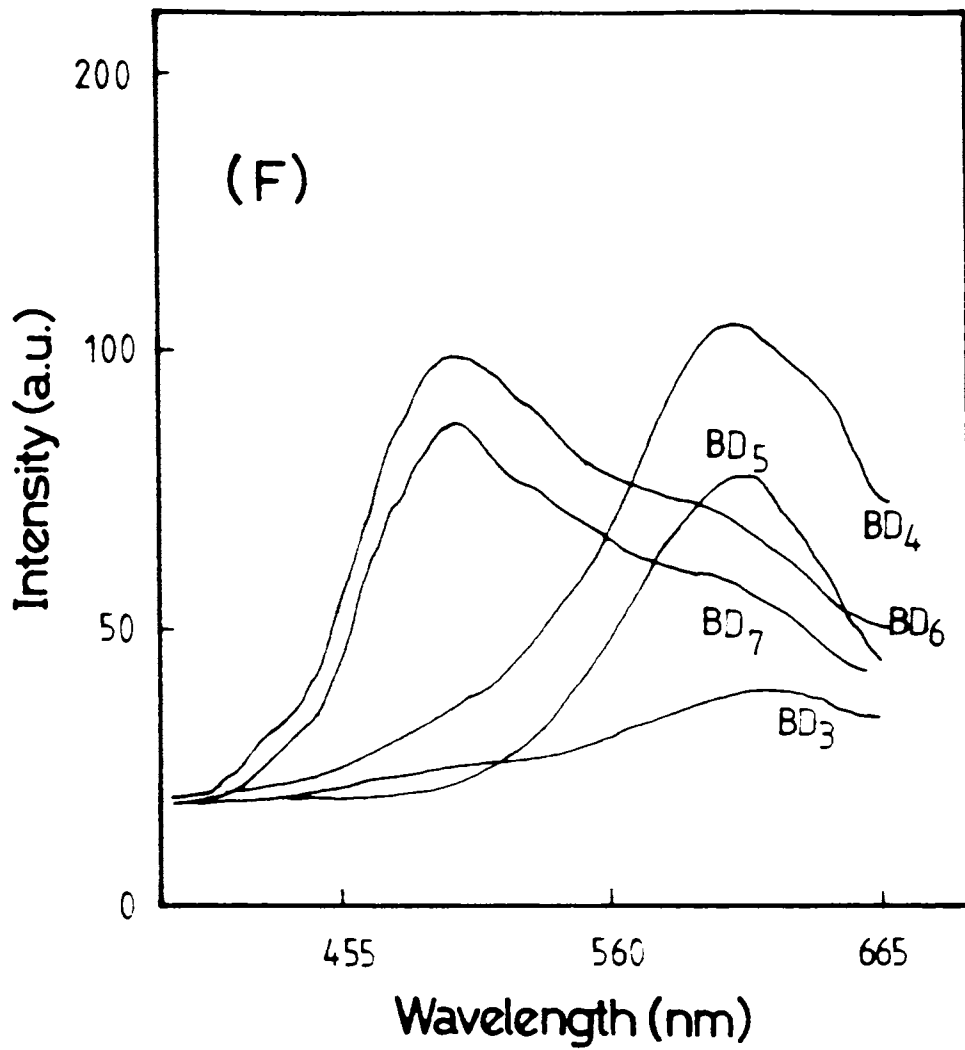
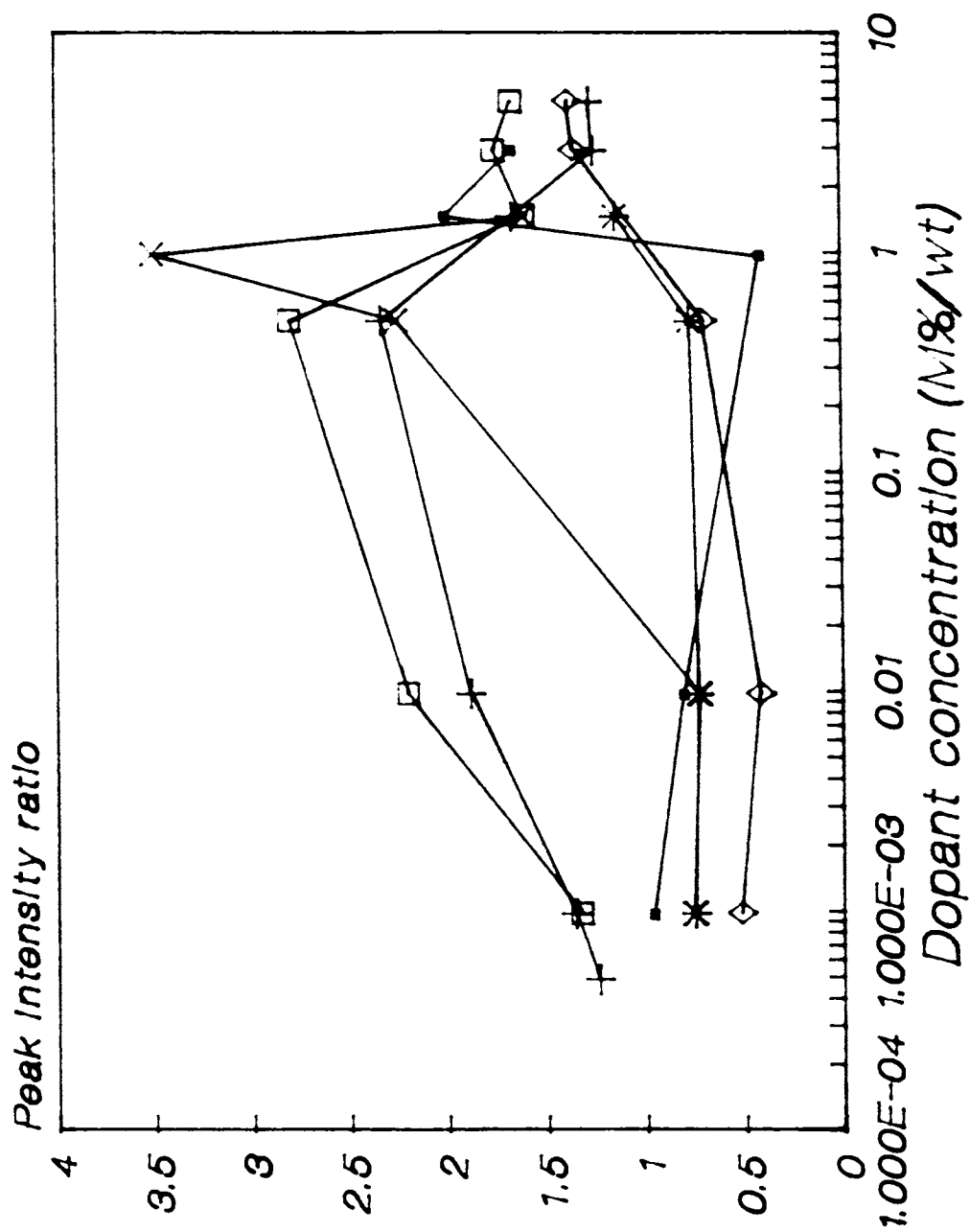


Fig. 4.3 (f) Fluorescence emission spectra of BaS:Dy phosphors under  $N_2$  laser excitation.



$$\left[ \frac{I(560-650\text{nm})}{I(450-540\text{nm})} \right]$$

Fig. 4.4 Graph showing peak intensity ratio of the two bands vs concentration, for BaS:RE phosphors

intensity as well as on the nature of emission bands. The concentration of dopants in each type of BaS:RE was varied in the range of 0.0005 Mol% to 5 Mol% by wt of BaS. In each type of the phosphor systems studied, the total intensity of emission becomes maximum for an optimum concentration of the dopant and then decreases with further increase in concentration. This is due to the well established phenomenon of concentration quenching [3]. Fig.4.5 gives a clear picture of the variations in total intensities of emission in each type of the BaS:RE phosphor systems with respect to the concentration of the dopants. In the figure the base (X-axis) represents the rare-earth dopants in the order of increase of ionic radii, Y-axis represents total intensity of emission (in arbitrary units are given at the top of each bar diagram) while the Z-axis represents the sample number denoting dopant concentration in Mol% by wt of BaS. In all cases, the fluorescence emission intensity was found to decrease drastically when concentration of the dopant reaches above 3 Mol% by wt of BaS. Also no perceptible change in peak positions of the bands with change in concentration was detected in the spectra.

The optimum concentration of the dopant which gives the maximum intensity of emission varies in each type of the phosphor. At very low concentrations of the dopant, the overall efficiency of luminescence is less due to the less number of active centres. As the concentration goes on increasing the efficiency of luminescence also increases due to the fact that  $RE^{3+}$  acts as a sensitizer which aids the formation of defects in the lattice. Again the decrease in luminescence yield beyond a certain concentration is attributed to the cluster formation of doped impurities and increase in non-radiative processes. As mentioned before, BaS with 3.8 eV band gap undergoes a direct band-to-band transition under  $N_2$  laser excitation. Electrons and holes generated in this process will migrate through BaS lattice and will be trapped by  $RE^{3+}$  ions followed by radiative recombination between electrons and holes giving rise to fluorescence emission. The band in the 450-540 nm region was found to increase in intensity irrespective of the type of  $RE^{3+}$  dopant. Hence it can be attributed to some host lattice vacancy created during the incorporation of the activator in accordance with the charge compensation theory of Kroger and Hellingman [4]. When  $RE^{3+}$  enter into BaS lattice by replacing  $Ba^{2+}$ , the necessary charge compensation is attained by cation vacancies ( $V_{Ba^{2+}}$ ). The vacancies formed due to the preparation of the phosphor may remain either isolated or randomly distributed or form complexes depending upon the concentration of  $RE^{3+}$  incorporated in the material. Hence the  $RE^{3+}$  impurities and the associated defects create localized levels in the forbidden gap of the host lattice which act as electron / hole centres as well as recombination centres. The concentration of such trapped electron/hole centres depend on the concentration of the  $RE^{3+}$  incorporated. Moreover, in the case of BaS:RE phosphors the open d-orbitals of rare-earth metal impurity will approximately get mixed up with the conduction band, since for BaS, the conduction band has got a dominant character of d-orbital [5]. Similarly 4f orbitals of  $RE^{3+}$  will get hybridized with valence band. Hence one can anticipate an efficient energy transfer taking place between  $RE^{3+}$  ions and host lattice. This mechanism is responsible for the increased efficiency of fluorescence emission in BaS:RE phosphors. Again another feature noticed is that, of all the

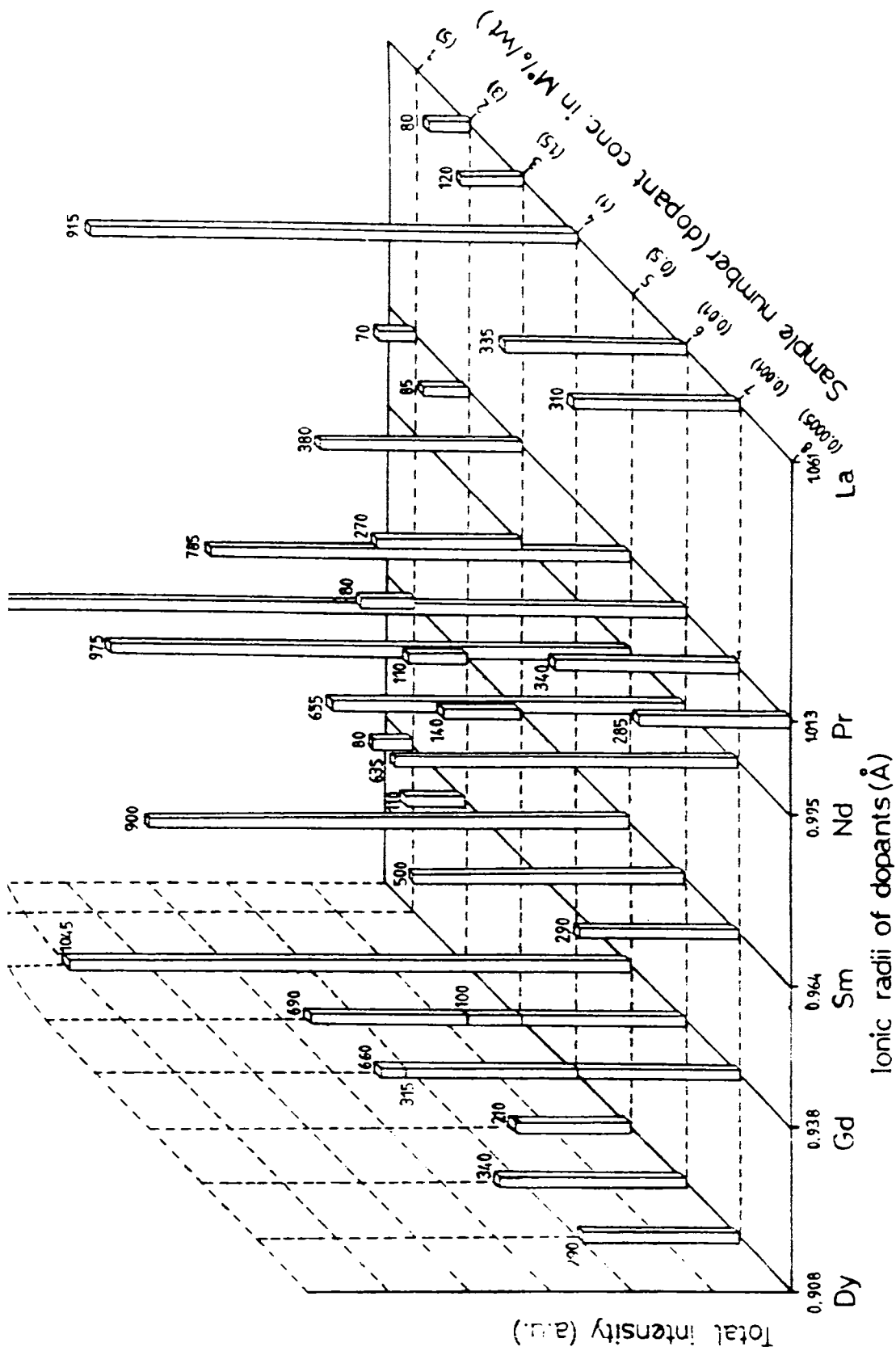


Fig. 4.5 A representation showing the variation of total intensity of emission of BaS:RE system with respect to concentrations of the dopants.

dopants studied, in the case of  $Gd^{3+}$  the blue-green emission intensity is enhanced to the maximum extent as seen in fig. 4.6. This means that  $Gd^{3+}$  incorporates more  $V_{Ba^{2+}}$  sites in BaS lattice as compared to other dopants.

$S^{2-}$  in the vicinity of the cation vacancy and  $Ba^{2+}$  in the vicinity of an anion vacancy site may form complexes like  $V_{Ba^{2+}} + V_{S^{2-}}$ , giving rise to additional localized levels in the forbidden gap of BaS lattice. The recombination of the holes trapped in these levels with electrons trapped in  $V_{S^{2-}}$  vacancy levels causes the emission of 560-650 nm band in the case of undoped BaS, as reported earlier.

Depending on the ionic radius of  $RE^{3+}$ , incorporation of  $RE^{3+}$  in BaS lattice favours the creation of  $S^{2-}$  vacancies, when goes into an interstitial site. Ionic radii of  $RE^{3+}$  varies from 1.061 Å to 0.908 Å [6]. For example  $Dy^{3+}$  has ionic radius of 0.908 Å which is less compared to interstitial radius (0.93 Å) of BaS lattice [7]. Hence  $Dy^{3+}$  can go into an interstitial site, thereby, creating more of  $V_{S^{2-}}$  levels. This is the reason that, at high concentrations of  $Dy^{3+}$  there is a prominent increase in emission intensity for 560-650 nm band in BaS:Dy phosphor (fig. 4.3 (F)-BD<sub>4</sub> and BD<sub>5</sub>). It is also reported that  $Dy^{3+}$  ion in AES has got characteristic emissions in the regions 470-500 nm and 550-590 nm, with more intensity of emission for 550-590 nm band due to  ${}^4G_{9/2} \rightarrow {}^6H_{13/2}$  transitions [8]. So the enhanced intensity of yellow-red emission in BaS:Dy phosphor at high concentrations can be attributed to the overlapping of 550-590 nm emission too.

The cation and anion radii in BaS have got values as 1.35 Å and 1.82 Å respectively [9]. So an  $RE^{3+}$  ion which has an ionic radius much less compared to this, (ie. for doped  $RE^{3+}$ , the ionic radii values lie in between 1.061 Å and 0.908 Å ) when it enters a BaS lattice, occupies substitutional site of  $Ba^{2+}$ . This causes the creation of more  $V_{Ba^{2+}}$  levels causing the increased emission intensity of 450-540 nm band as observed in BaS:RE phosphors irrespective of the type of  $RE^{3+}$ . But the chances of an  $RE^{3+}$  ion occupying an  $S^{2-}$  vacancy site cannot be completely ruled out, even though it is not a stable position for a positive ion. This assumption is, however, supported by the observation of an analogous defect centre formation in alkali halide crystals where the interstitial halogen atoms have been found to be trapped by cation vacancies [10]. Moreover, the high ionicity and the observed violation of charge compensation principles in AES are the factors that give further support to this assumption [11].

In the case of BaS:Sm and BaS:Pr phosphor systems, well resolved characteristic emission lines are found to superpose over the self-activated emission bands of BaS (fig. 4.3. (B)&(D)). Here the emission lines are explained as purely due to  $4f \rightarrow 5d$  transitions of  $RE^{3+}$  ion. However, the energy level positions of these ions get modified due to crystal field interaction, which causes stark splitting as well as shifting of ion energy level positions.

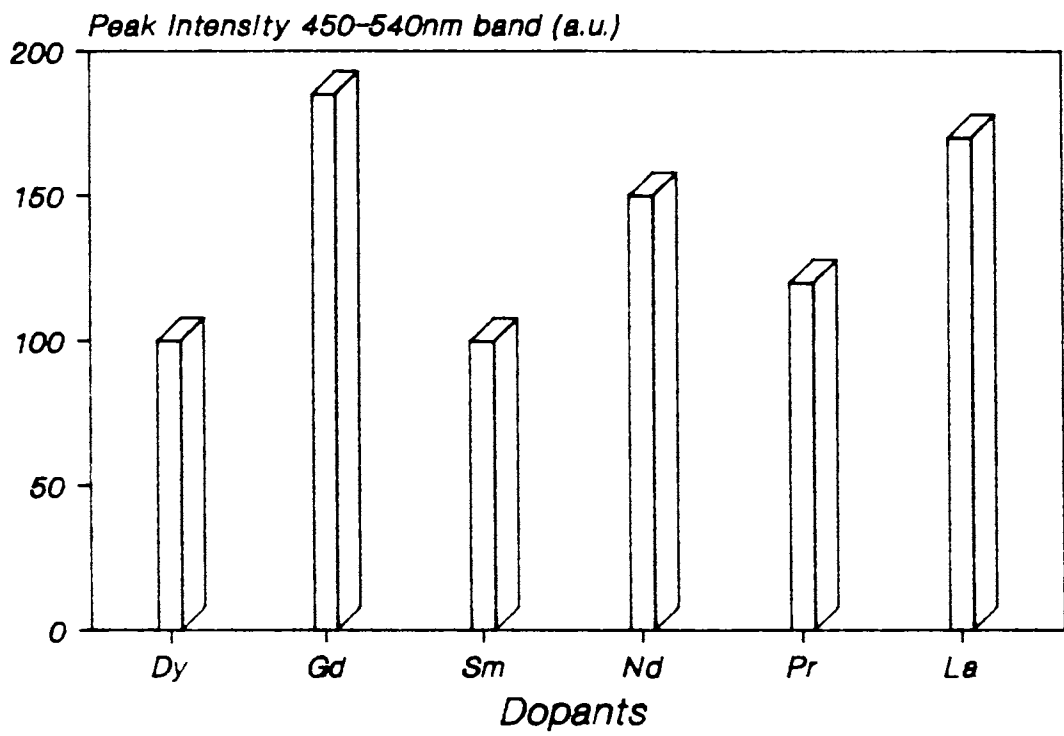


Fig. 4.6 A plot showing intensity of 450-540nm band in each type of rare - earth dopants in BaS



The three groups of lines obtained in BaS:Sm phosphor are attributed to the transitions from  ${}^4G_{5/2}$  to various lower levels viz.,  ${}^6H_{5/2}$ ,  ${}^6H_{7/2}$ ,  ${}^6H_{9/2}$ . The emission lines observed in BaS:Pr phosphor are attributed to the transitions  ${}^3P_1 \longrightarrow {}^3H_5$ ,  ${}^3P_0 \longrightarrow {}^3H_4$  and  ${}^1D_2 \longrightarrow {}^3H_4$  of  $Pr^{3+}$  ion [12]. Details of the spectral analysis based on the crystal field splitting of the energy levels are discussed in "Section C" of this chapter.

To get a clear picture about the energy transfer mechanisms and the dependence of emission on the concentrations of the dopant, the spectra of doubly doped phosphors were also taken. Fig. 4.7(A) to (G) show the emission characteristics of BaS:RE<sub>1</sub>:RE<sub>2</sub> systems studied. In all the cases of doubly doped phosphors, when doped heavily and equally (1 Mol% by wt of BaS) the overall intensity of emission is less with complete suppression of 450-540 nm band while the second band at 560-650 nm region has got certain amount of intensity. This shows the effective energy transfer between host lattice centres and RE<sup>3+</sup> luminescence centres. In the case of BaS:Pr:Sm phosphor, depending on the concentrations of the dopant, the characteristic emission becomes prominent. When Pr<sup>3+</sup> concentration goes below Sm<sup>3+</sup> concentration, the characteristic emission of Sm<sup>3+</sup> appear with increased intensity. When Sm<sup>3+</sup> concentration goes below Pr<sup>3+</sup> concentration, the emission lines of Pr<sup>3+</sup> are seen with increased intensity. Since the characteristic emission lines of Pr<sup>3+</sup> and Sm<sup>3+</sup> are found to be more or less in the same region, depending upon the concentrations of the dopant, there is an overlapping of both the emission lines as seen in fig. 4.7 (A) & (B). It is evident that the characteristic emission of RE<sup>3+</sup> has got a sensitive dependence on the concentration of the dopant. In BaS:Sm:Gd and BaS:Pr:Gd samples, where the concentration of Sm<sup>3+</sup> and Pr<sup>3+</sup> were fixed at 1 Mol% by wt, and that of Gd<sup>3+</sup> varied, it was observed that at a particular concentration of Gd<sup>3+</sup> the band in 450-540 nm also appear (eventhough with less intensity) along with the characteristic Pr<sup>3+</sup>/Sm<sup>3+</sup> emission (fig. 4.7 (c) & (D)). Similarly in BaS:Pr:Nd and BaS:Sm:Nd phosphors, where the concentrations of Nd<sup>3+</sup> was varied, depending on the concentration of Nd<sup>3+</sup> along with Pr<sup>3+</sup>/Sm<sup>3+</sup> characteristic emissions, 450-540 nm band was also seen (fig. 4.7 (E) & (F)). A comparison between the intensities of band in doubly doped phosphor systems shows that only Dy<sup>3+</sup> combination (ie. BaS:Sm:Dy, BaS:Nd: Dy) have marked intensity of emission in 560-650 nm region (fig. 4.7 (G)). This again confirms the fact that Dy<sup>3+</sup> easily occupies the interstitial sites in BaS and hence increases the V<sub>s2</sub> levels. In short, the relative intensities of emission of the two bands are influenced markedly by energy transfer between RE<sup>3+</sup> luminescence centres.

### (C) Copper doped BaS phosphors.

Copper activated AES are normally efficient phosphors in which quantum efficiencies of luminescence of 50% or more can be achieved [13]. In order to incorporate copper in the monovalent form (Cu<sup>+</sup>) in BaS lattice, CuCl was added in the preparation of BaS:Cu phosphors. Due to the high instability of Cu<sup>+</sup>, there are chances of Cu<sup>2+</sup> ions too, entering the lattice.

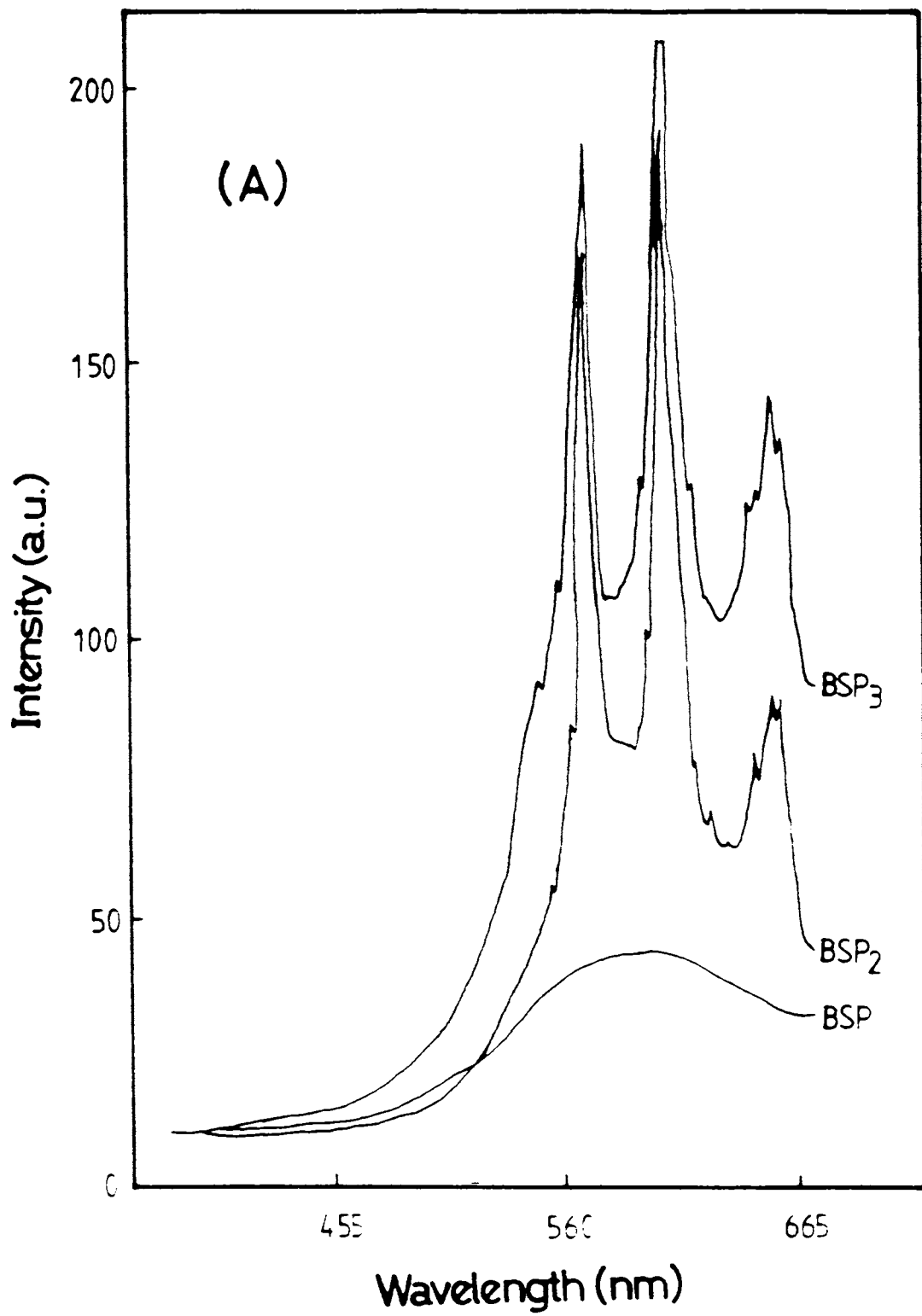


Fig. 4.7(a) Fluorescence emission spectra of BaS:Sm:Pr phosphors under N<sub>2</sub> laser excitation

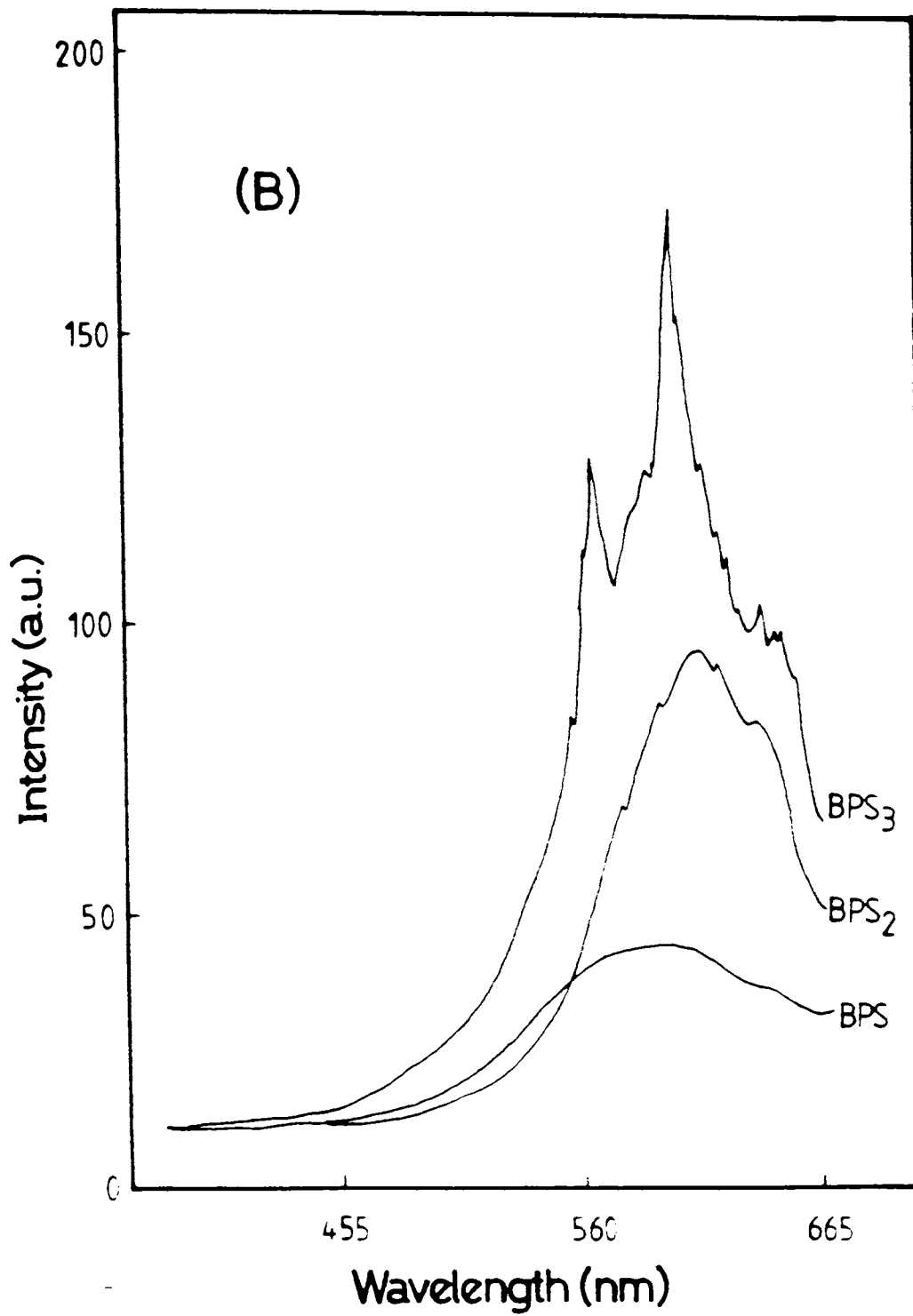


Fig. 4.7(b) Fluorescence emission spectra of BaS:Pr:Sm phosphors under N<sub>2</sub> laser excitation

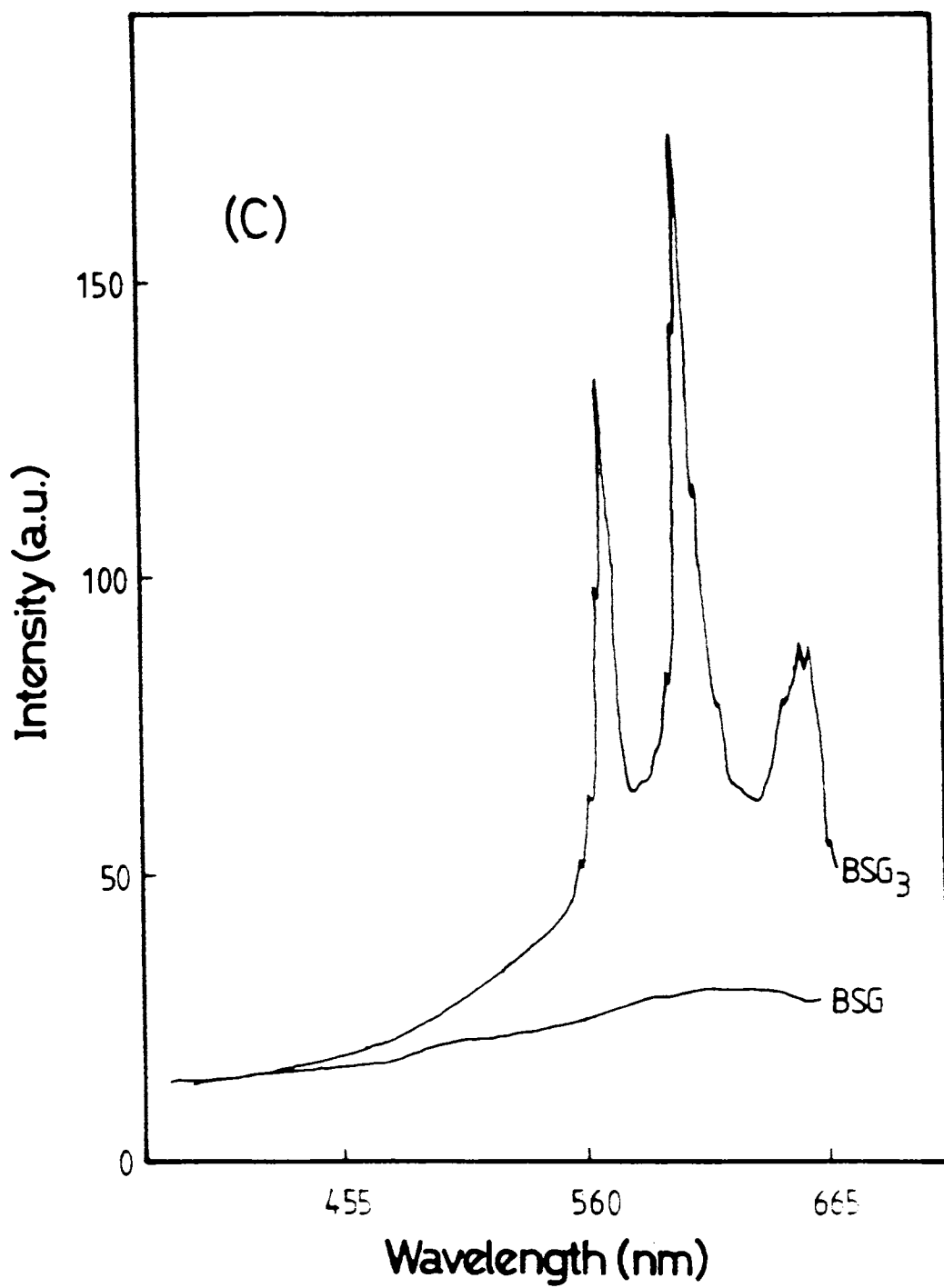


Fig. 4.7(c) Fluorescence emission spectra of BaS:Sm:Gd phosphors under N<sub>2</sub> laser excitation

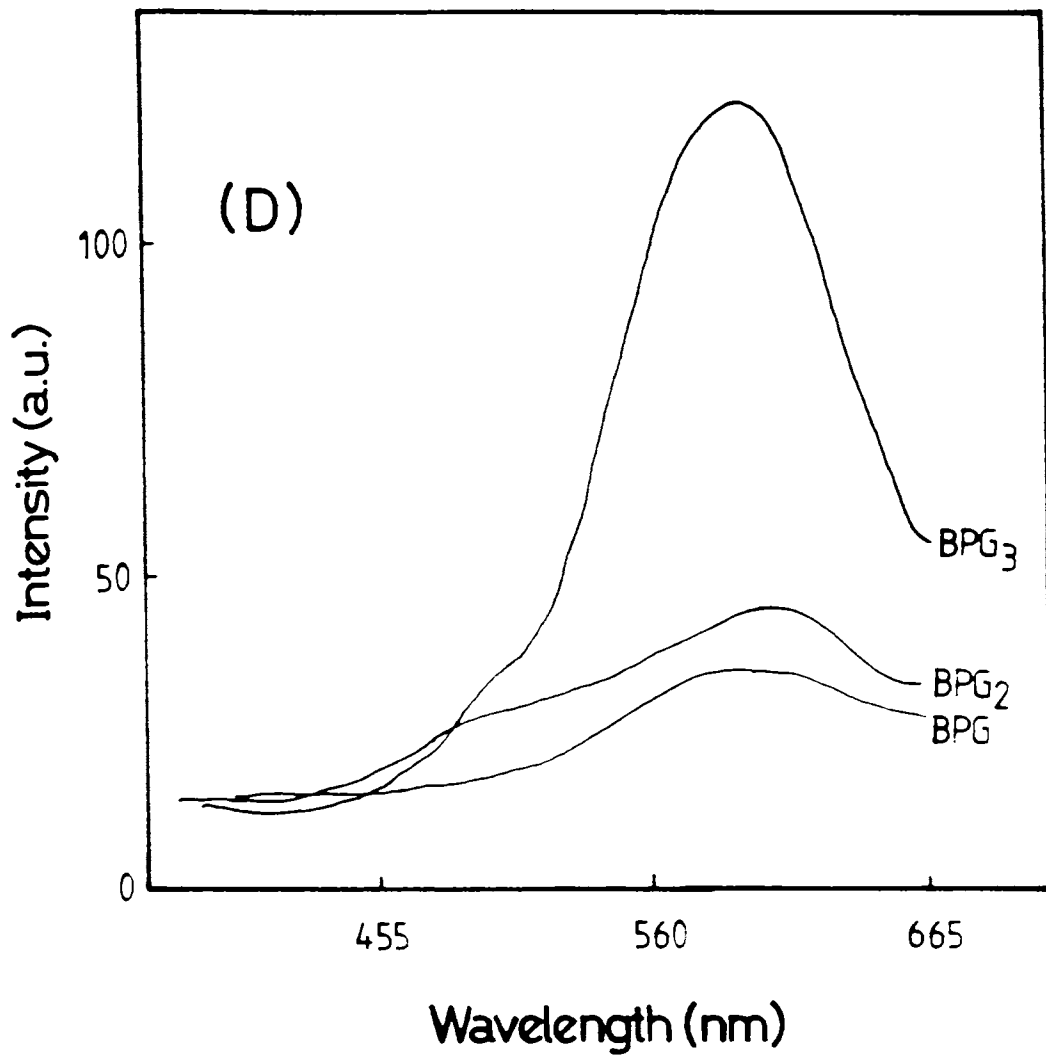


Fig. 4.7(d) Fluorescence emission spectra of BaS:Pr:Gd phosphors under N<sub>2</sub> laser excitation

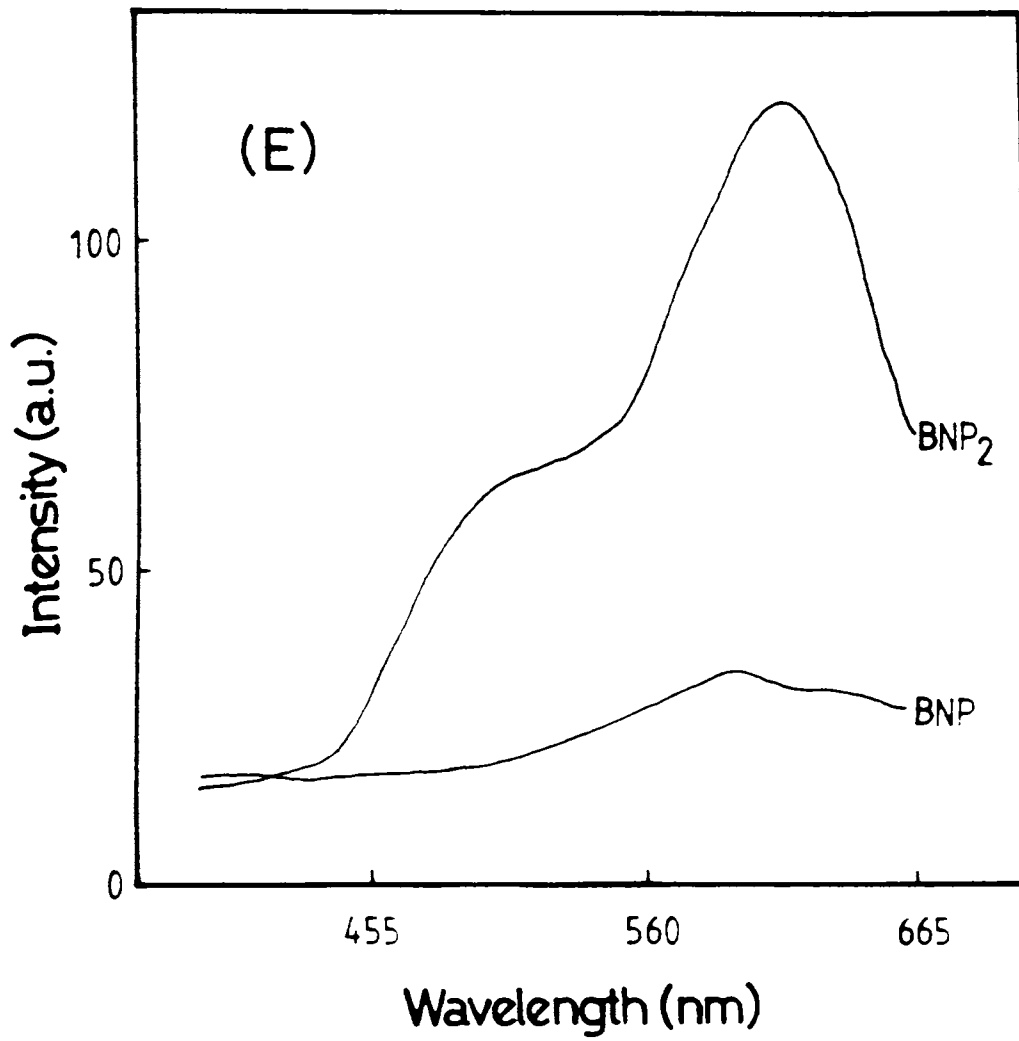


Fig. 4.7 (e) Fluorescence emission spectra of BaS:Nd:Pr phosphors under N<sub>2</sub> laser excitation

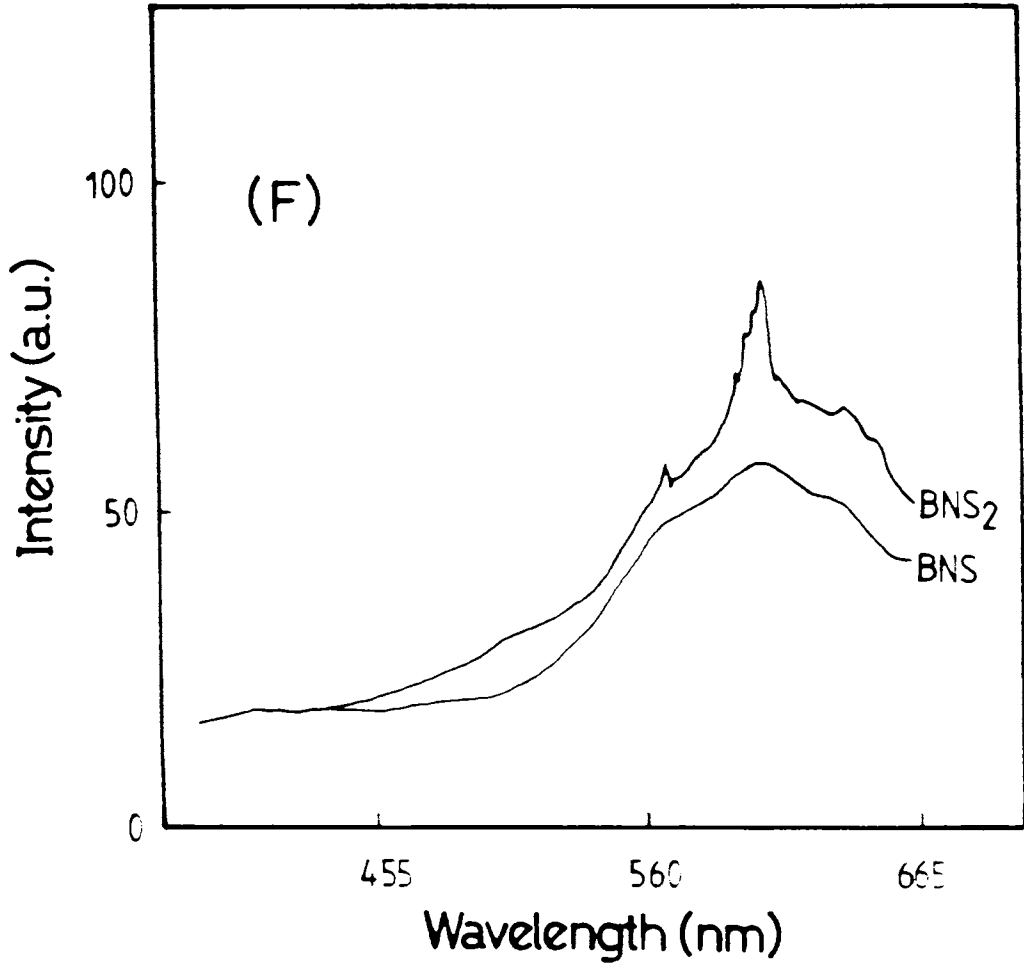


Fig. 4.7 (f) Fluorescence emission spectra of BaS:Nd:Sm phosphors under N<sub>2</sub> laser excitation

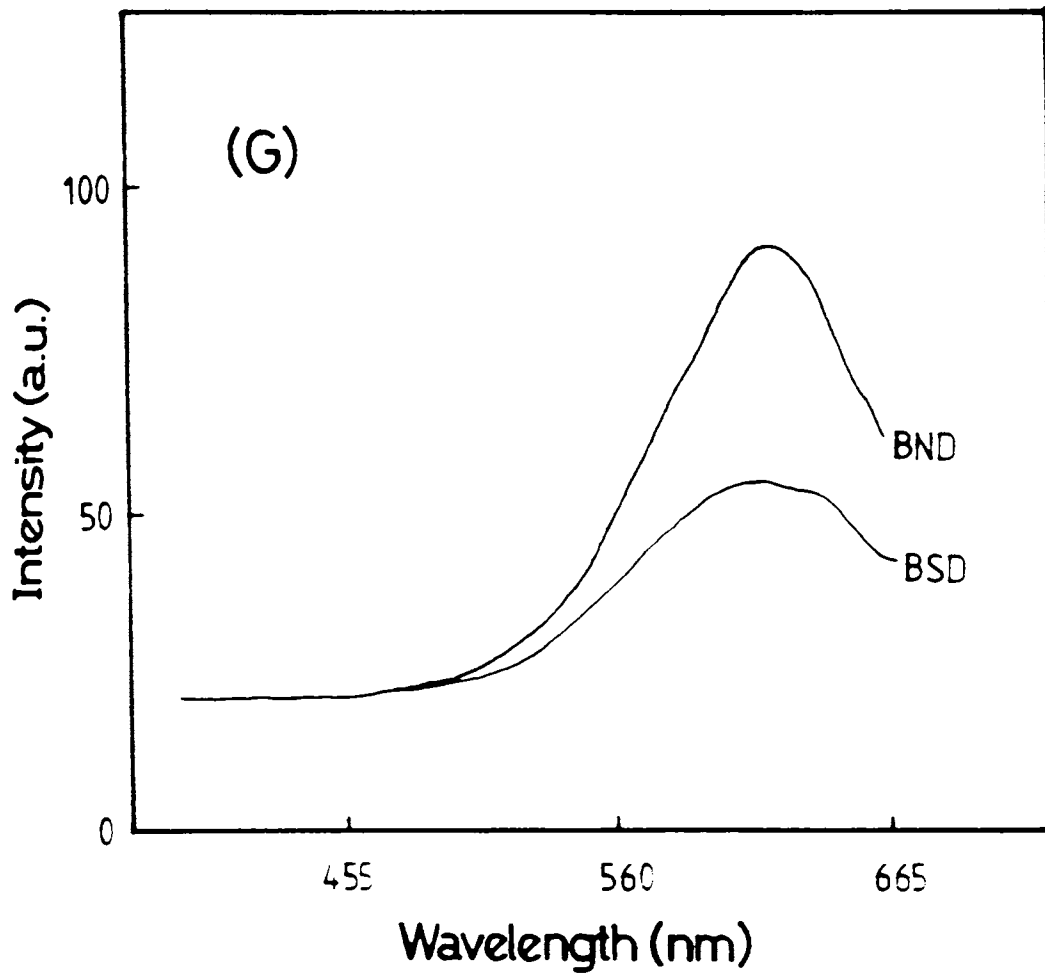


Fig. 4.7(g) Fluorescence emission spectra of BaS:Nd:Dy and BaS:Sm:Dy phosphors under N<sub>2</sub> laser excitation



But the high temperature employed for the preparation of the phosphor completely rules out the formation of  $\text{Cu}^{2+}$  centres in BaS, since above  $900^\circ\text{C}$  the thermal decomposition of cupric compounds to cuprous is more appreciable [14]. Also since copper is added in CuCl form, the presence of Cl<sup>-</sup> centres in BaS causes the conversion of  $\text{Cu}^{2+}$  if any, to  $\text{Cu}^+$  form. Fig.4.8 show the fluorescence emission spectra of BaS:Cu phosphors. In these spectra the emission efficiency of 560-650 nm region was found to get enhanced with complete suppression of 450-540 nm band.

$\text{Cu}^+$  (ionic radius less than  $0.93\text{\AA}$ ) in BaS goes into the lattice either substitutionally or interstitially. The effect of  $\text{Cu}^+$  in substitutional site is to create more and more  $\text{S}^{2-}$  vacancies ( $\text{V}_{\text{S}^{2-}}$ ). The enhanced intensity of emission in yellow region can be accounted due to this fact. As  $\text{Cu}^+$  enters in BaS lattice, there is considerable reduction in cation vacancy levels ( $\text{V}_{\text{Ba}^{2+}}$ ) which led to the complete suppression of the 450-540 nm band in the emission spectra of BaS:Cu phosphors. A close examination of BaS:Cu fluorescence spectrum shows certain emission peaks at 560.8nm, 610.4 nm and 640.9 nm. etc. superposed over 550-650 nm region. Introduction of  $\text{Cu}^+$  in cubic crystal field of BaS causes the perturbation of  $\text{O}_h$  symmetry of BaS and hence the free electronic states of  $\text{Cu}^+$  get modified due to strak splitting. This gives rise to certain localized levels within the forbidden gap of BaS. The emission lines seen in BaS:Cu phosphor can be assigned due to the transitions within  $\text{Cu}^+$  energy levels itself or from  $\text{V}_{\text{S}^{2-}}$  levels to these  $\text{Cu}^+$  energy levels. The probable energy level scheme suggested to explain these emission lines is given in fig.4.9. The highly intense peak at 575 nm region can be either from  ${}^3\text{T}_{2g}$  ( ${}^3\text{D}$ ) of  $\text{Cu}^+$  to  $\text{V}_{\text{Ba}^{2+}} + \text{V}_{\text{S}^{2-}}$  complex level or from  $\text{V}_{\text{S}^{2-}}$  levels to  ${}^1\text{A}_{1g}$  ( ${}^1\text{S}$ ) ground state of  $\text{Cu}^+$ , with more probability for the latter. The emission line at 640,9 nm may be due to the recombination of the holes trapped at  $\text{Cu}^+$  ground state ( ${}^1\text{A}_{1g}$ ) and the electrons trapped at the localized Cl<sup>-</sup> centres in BaS. In explaining the electroluminescence spectra of ZnS:Cu, Pillai and Vallabhan [15] also reported an emission at 640nm as due to recombination of Cl<sup>-</sup> and  $\text{Cu}^+$  centres.

#### d) Rare- earth and Copper doped BaS Phosphors

In BaS, when  $\text{Cu}^+$  is incorporated as the activator, charge compensation criteria require the simultaneous incorporation of a donor impurity- a trivalent ion- a co-activator [16]. In order to find the nature of luminescence centres responsible for emission, the fluorescence spectra of BaS:Cu:RE and BaS:Cu:RE<sub>1</sub>:RE<sub>2</sub> phosphor systems were also taken (where RE stands for rare-earth such as  $\text{Pr}^{3+}$ ,  $\text{Nd}^{3+}$ ,  $\text{Sm}^{3+}$ ,  $\text{Gd}^{3+}$  etc). In these phosphor systems the Cu concentration was kept constant at 0.5 Mol% by wt of BaS, while the concentrations of RE<sup>3+</sup> impurities were varied in the range of 1 Mol% by wt to 0.05 Mol% by wt of BaS. These studies revealed two main interesting features viz., sensitized luminescence and energy transfer from RE<sup>3+</sup> to  $\text{Cu}^+$  centres. The influence of  $\text{Cu}^+$  on the emission spectra of BaS:RE system is in fig.4.10. There is an enhanced emission intensity in the yellow region peaking at 575 nm with

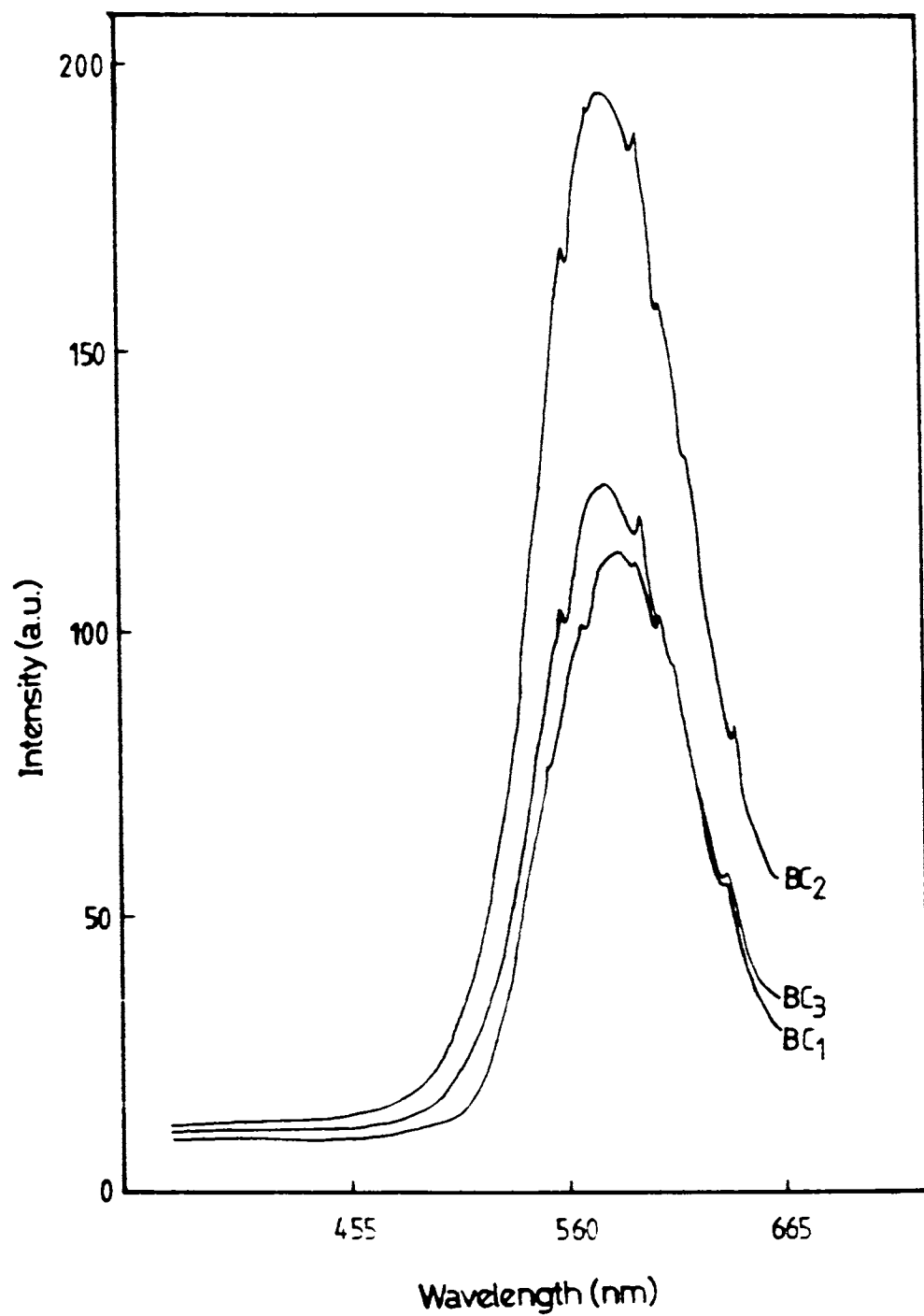


**Fig. 4.8** Fluorescence emission spectra of BaS:Cu phosphors under N<sub>2</sub> laser excitation

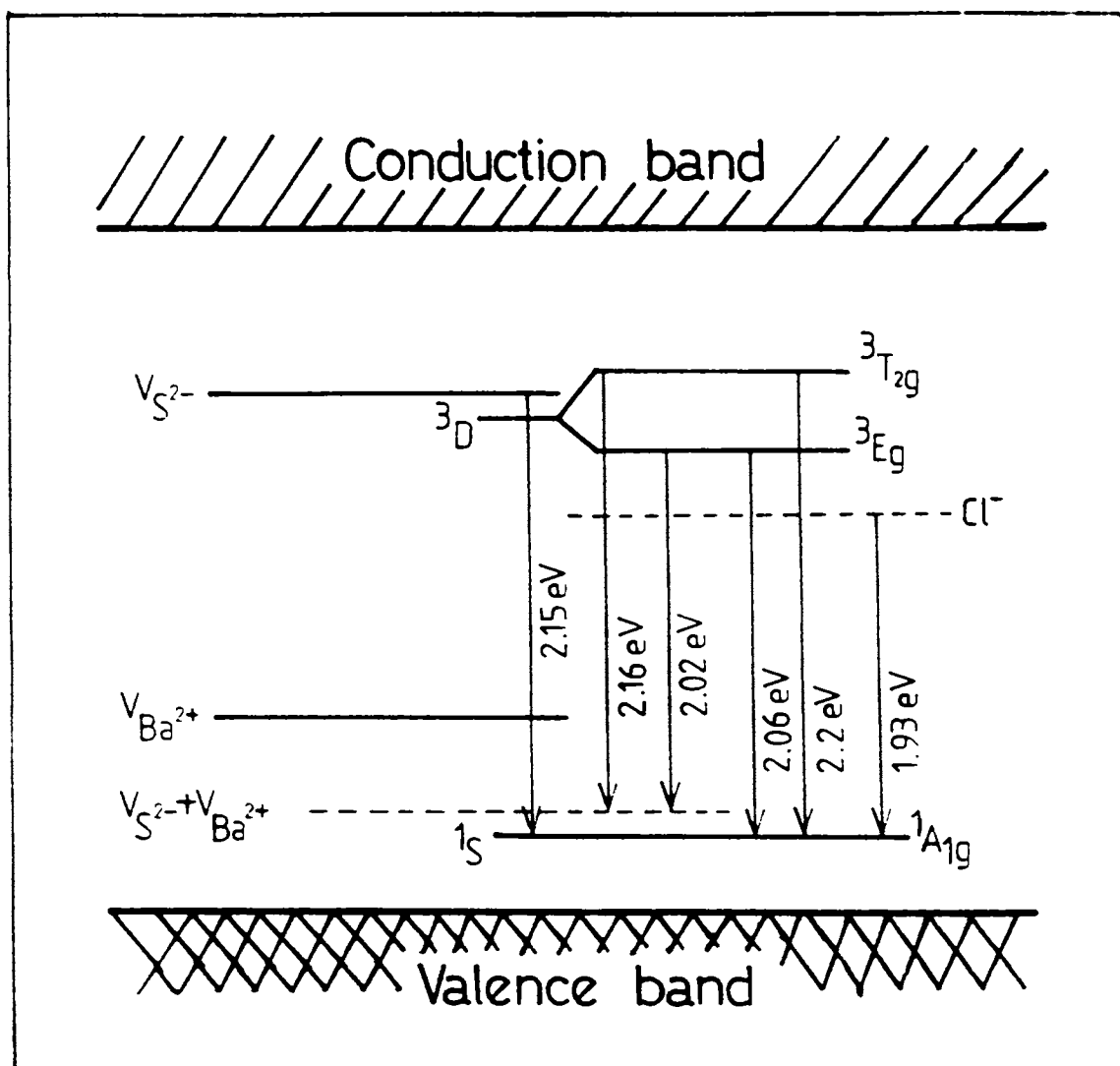
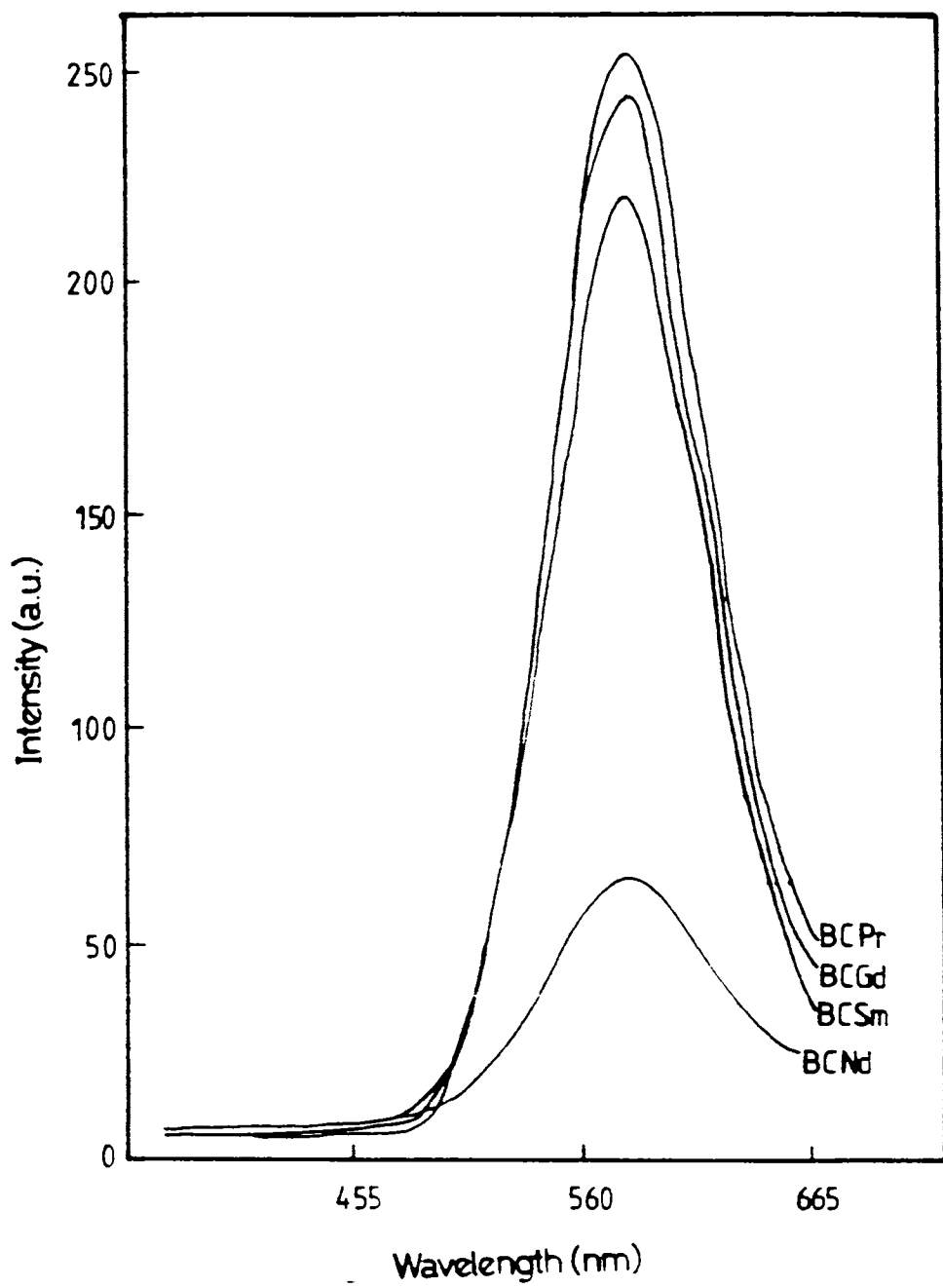
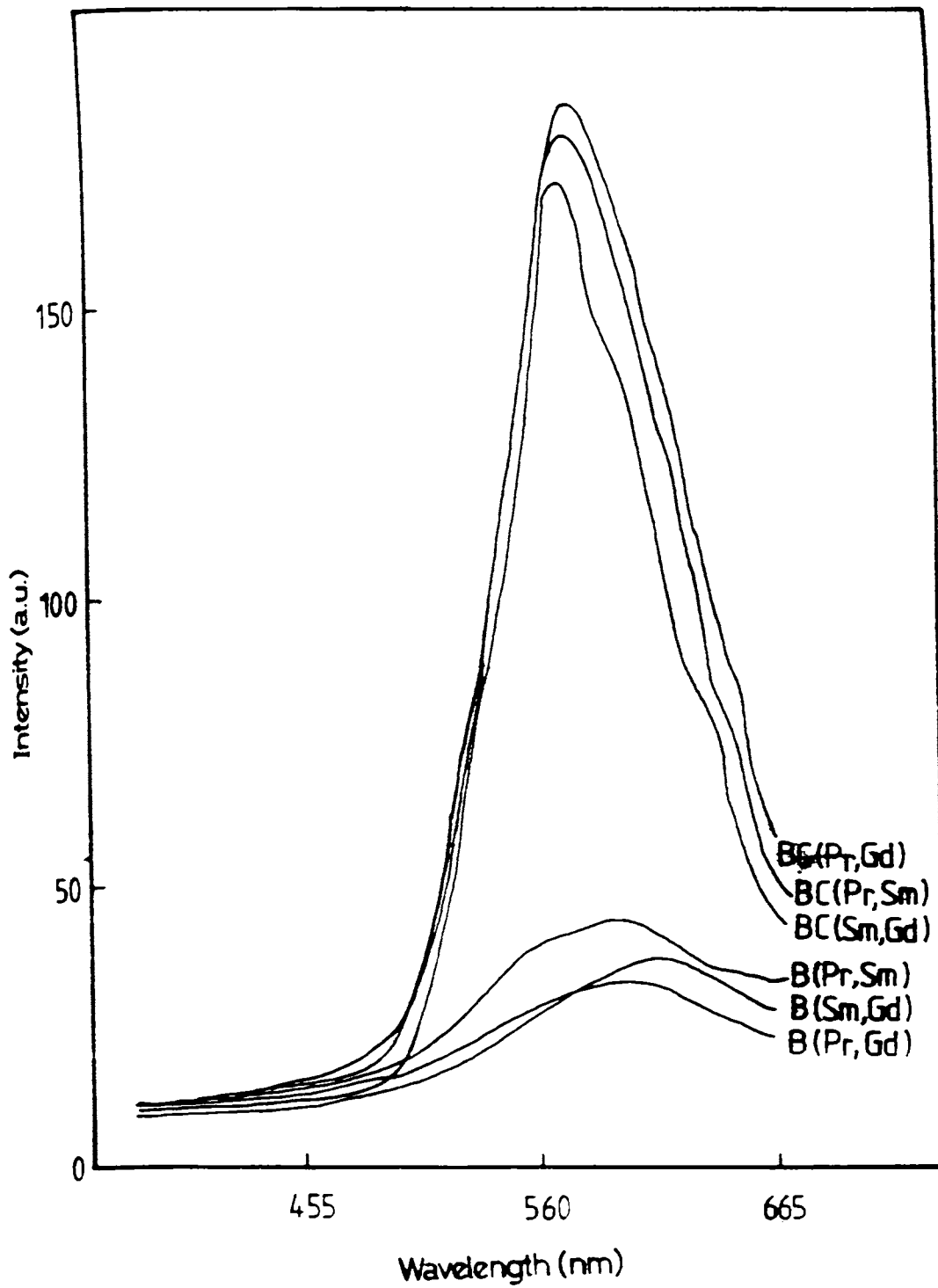


Fig. 4.9 Emission model for BaS:Cu fluorescence Spectrum



**Fig. 4.10** Fluorescence emission spectra of BaS:Cu:RE phosphors under N<sub>2</sub> laser excitation



**Fig. 4.11** Fluorescence emission spectra of  $\text{BaS:Cu:RE}_1:\text{RE}_2$  phosphors under  $\text{N}_2$  laser excitation

complete disappearance of  $RE^{3+}$  characteristic lines. This is due to the resonant energy transfer from  $RE^{3+}$  centres to  $Cu^+$  centres because of the close matching of energy levels of both the centres in BaS. Along with  $RE^{3+}$  co-activators,  $Cu^+$  in BaS, yield high value of quantum efficiency. In the case of mixed RE doped BaS phosphors (ie. in  $BaS:RE_1:RE_2$  systems) which show very broad emission bands with less intensity, the incorporation of  $Cu^+$  (ie in  $BaS:Cu:RE_1:RE_2$ ) enhances the fluorescence efficiency as shown in fig.4.11. This is due to the sensitization effect of  $Cu^+$  centres in BaS. When compared to  $BaS:Cu:RE$ ,  $BaS:Cu:RE_1:RE_2$  show a broadening of emission band in the red region with more predominance to 640 nm emission. This again confirms that the emission at 640 nm arises due to  $Cl^-$  and  $Cu^+$  centres recombination. In  $BaS:Cu:RE_1:RE_2$ , the more is the formation of  $Cl^-$  centres in BaS lattice, since we are adding  $RE^{3+}$  also in the form of  $RECl_3$ .

In short  $Cu^+$  along with  $RE^{3+}$  in BaS acts as an efficient phosphor giving intense emission in yellow red region due to the sensitization effect of  $Cu^+$  centres by  $RE^{3+}$ .

## SECTION C

### 4.4. Fluorescence Of BaS:Sm And BaS:Pr Phosphors - Fine structure analysis

As stated in the last section the fluorescence emission spectra of BaS:Pr and BaS:Sm show well resolved emission lines purely characteristic of  $Sm^{3+}/Pr^{3+}$  ion energy levels. The observed proportionate increase in intensities of these emission lines with increase in dopant concentration also clearly indicates that these emission originate essentially from the transitions occurring in  $Sm^{3+}/Pr^{3+}$  ions.

#### (a) BaS:Sm phosphor

The fluorescence emission of BaS:Sm phosphors revealed three groups (A, B and C in fig. 4.12) of well separated bands superposed over the broad emission band 560-650 nm of BaS phosphor. The four lines seen in group A at 560nm, six lines in group B at 600 nm and another six lines in group C at 650 nm regions can be attributed to  $Sm^{3+}$  transition from  ${}^4G_{5/2}$  to various lower levels viz,  ${}^6H_{5/2}$ ,  ${}^6H_{7/2}$  and  ${}^6H_{9/2}$  (fig. 4.13). Fine structure revealed in these bands are due to the crystal field interaction on free-ion energy levels of  $Sm^{3+}$ . Since BaS has got simple f.c.c. structure  $Ba^{2+}$  site will experience a cubic crystal field with an octahedral co-ordination. The free-ion energy levels of  $Sm^{3+}$  ions in  $Ba^{2+}$  site will split into sub-levels due to crystal field effect.

Analysis of crystal field splitting can be made by the method used by Zhong and Bryant [17] and Pillai and Vallabhan [8]. Within a manifold of angular momenta  $J$  of  $4f^n$  electron configuration, the general operator equivalent potential with cubic symmetry can be written as [18]

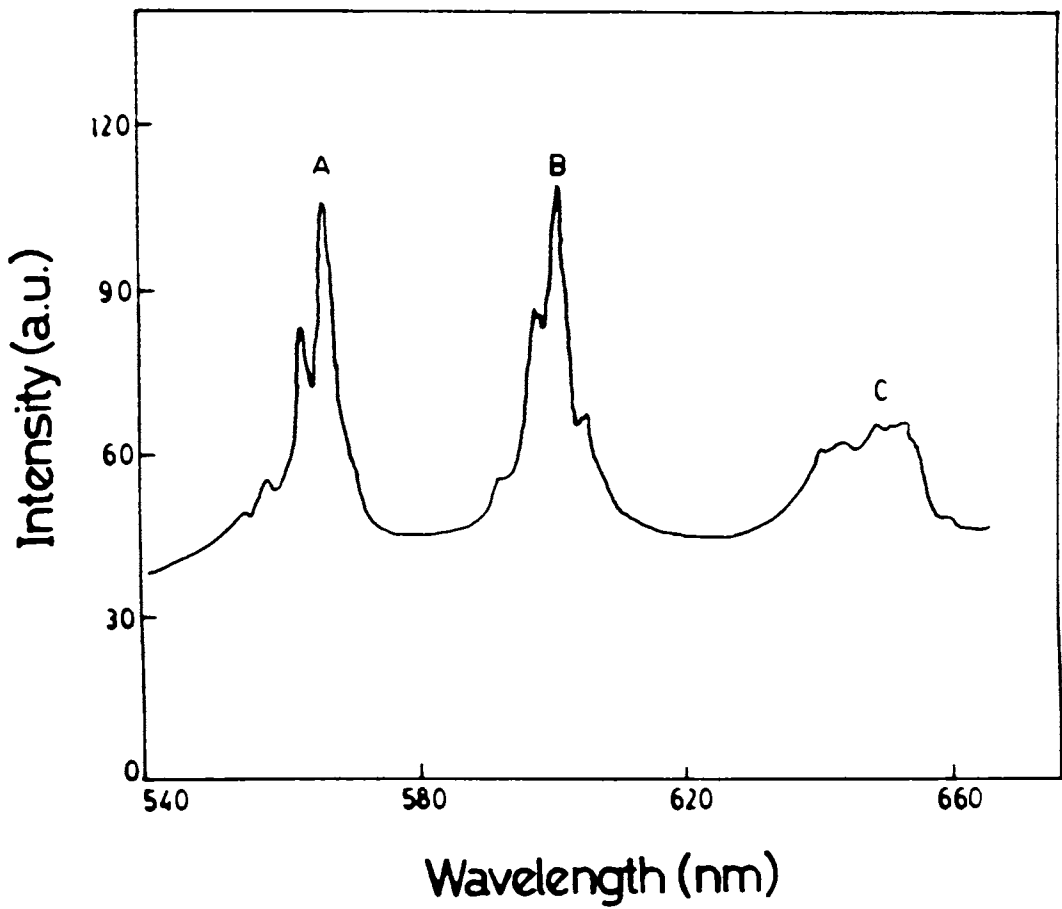


**Fig. 4.12** Fine structure spectrum of BaS:Sm phosphor

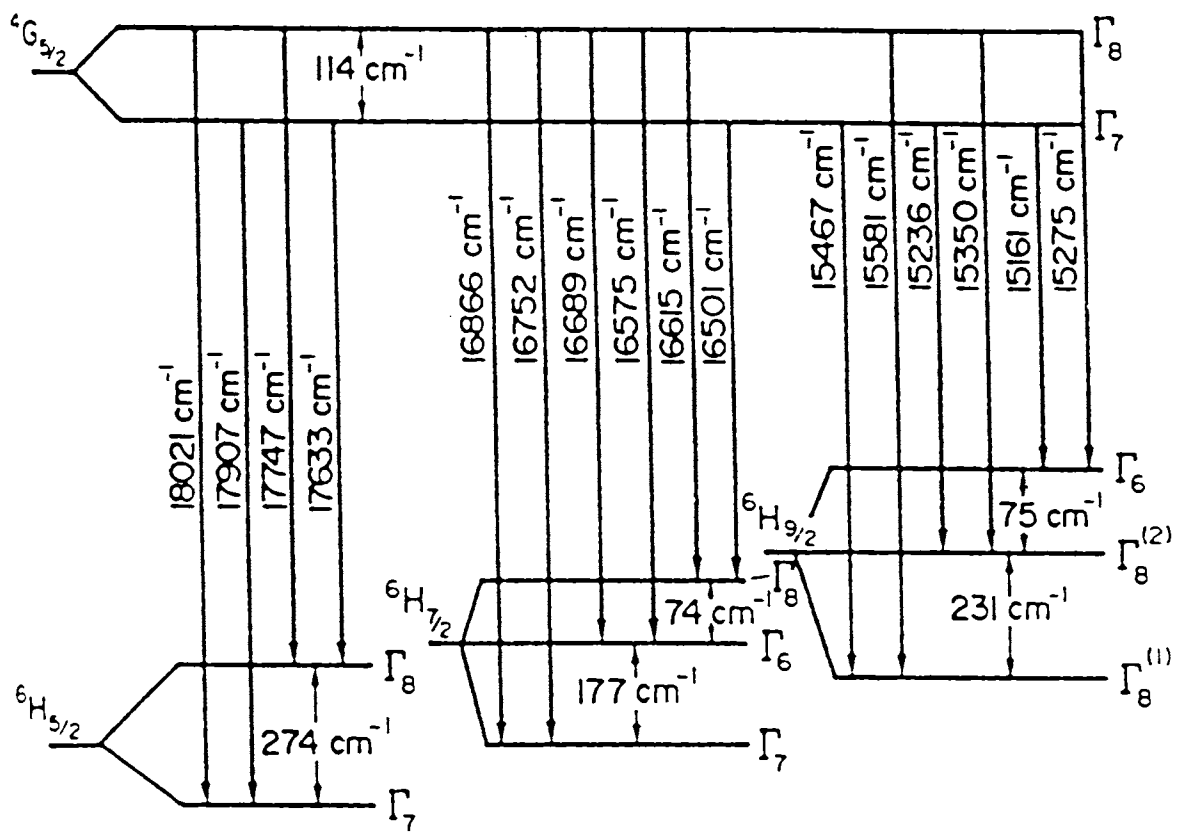


Fig. 4.13 Energy level multiplet structures of  $Sm^{3+}$  in BaS lattice. Term values are given as obtained from the analysis. Various transitions are also shown.



$$H = B_4 ( O_4^0 + 5 O_4^4 ) + B_6 ( O_6^0 - 21 O_6^4 ) \quad 4.(1)$$

where  $O_m^l$  are the usual spherical harmonic functions, using the modified notation,

$$H = W \left[ x \frac{O_4}{F(4)} + (1 - |x|) \frac{O_6}{F(6)} \right] \quad 4.(2)$$

$$\text{Where } O_4 = O_4^0 + 5 O_4^4 \quad ; \quad O_6 = O_6^0 - 21 O_6^4 \quad 4.(3a)$$

and  $F(4)$  and  $F(6)$  are defined through

$$B_4 F(4) = Wx \quad ; \quad B_6 F(6) = 1 - |x| \quad 4.(3b)$$

with  $-1 < x < 1$  and  $W$  the scale factor.

The pattern of crystal field splitting is determined by  $B_4$  and  $B_6$  which are given by

$$B_4 = A_4 \langle r^4 \rangle \beta \quad ; \quad B_6 = A_6 \langle r^6 \rangle \gamma \quad 4.(4)$$

where  $\langle r^4 \rangle$  and  $\langle r^6 \rangle$  are the mean fourth and sixth powers of radii of 4f electrons of  $\text{Sm}^{3+}$  ion and  $\beta$  and  $\gamma$  are the Stevens multiplicative constants [19].  $A_4$  and  $A_6$  the geometrical co-ordination factors and are given by point charge crystal field model (given in chapter 1, Table 1.1). Freeman and Watson [20] gave the values of  $\langle r^4 \rangle$  and  $\langle r^6 \rangle$  for  $\text{Sm}^{3+}$  ion as  $1.897a_{\text{H}}^4$  and  $8.775a_{\text{H}}^6$  respectively (chapter 1, Table 1.2)

Free-ion terms with  $J=5/2$  will split into two sub-levels viz.  $\Gamma_8$  and  $\Gamma_7$  in octahedral crystal field. The four lines observed in group A is due to  ${}^4G_{5/2} \rightarrow {}^6H_{5/2}$  transitions of  $\text{Sm}^{3+}$  ion can therefore be explained by taking into consideration the doublet structure of upper and lower levels with separation as  $114 \text{ cm}^{-1}$  and  $274 \text{ cm}^{-1}$  respectively. The six lines observed in group B are the transitions due to radiative de-excitation of  ${}^4G_{5/2} \rightarrow {}^6H_{7/2}$  between the two sub-levels of  ${}^4G_{5/2}$  ( $\Gamma_8$  and  $\Gamma_7$ ) and the three sub-levels of  ${}^6H_{7/2}$  ( $\Gamma_6$ ,  $\Gamma_8$  and  $\Gamma_7$ ) having multiplet separation  $74 \text{ cm}^{-1}$  and  $177 \text{ cm}^{-1}$ . Similarly the six lines observed in group C can be attributed to the transition  ${}^4G_{5/2} \rightarrow {}^6H_{9/2}$  where  ${}^6H_{9/2}$  split into three sub-levels viz.  $\Gamma_6$ ,  $\Gamma_8^{(8)}$ ,  $\Gamma_8^{(1)}$  with multiplet separation as  $75 \text{ cm}^{-1}$  and  $231 \text{ cm}^{-1}$ . The multiplet structures of observed energy levels assigned for  $\text{Sm}^{3+}$  in BaS are shown in fig. 4.13. These lines are then compared with the splitting pattern for  $J=7/2$  and  $J=9/2$  terms, best fitted for the values of  $x=0.955$  and the scale factor  $W=8.447 \text{ cm}^{-1}$ , for  ${}^4G_{5/2} \rightarrow {}^6H_{7/2}$  transitions and  $W=11.84 \text{ cm}^{-1}$  for  ${}^4G_{5/2} \rightarrow {}^6H_{9/2}$

transitions. In fig. 4.14 (a) and (b) the broken lines corresponds to this position. The term values and observed and calculated values of the assigned transitions are given in Table 4.1.

Table 4.1					
Transitions involved corresponding to the fine structure spectrum of Sm <sup>3+</sup> in BaS lattice.					
Group	Transitions		Wave length ( nm )	Wave number ( $\nu$ cm <sup>-1</sup> )	
	Upper State	Lower State		Observed	Calculated
A $^4G_{5/2} \text{ ----} \rightarrow ^6H_{5/2}$	$\Gamma_8 \longrightarrow \Gamma_7$		554.9	18021	18021
	$\Gamma_8 \longrightarrow \Gamma_8$		563.3	17752	17747
	$\Gamma_7 \longrightarrow \Gamma_7$		558.3	17911	17907
	$\Gamma_7 \longrightarrow \Gamma_8$		567.1	17633	17633
$^4G_{5/2} \text{ ----} \rightarrow ^6H_{7/2}$	$\Gamma_8 \longrightarrow \Gamma_7$		592.7	16866	16866
	$\Gamma_8 \longrightarrow \Gamma_8$		599.2	16888	16869
	$\Gamma_8 \longrightarrow \Gamma_6$		601.9	16614	16615
	$\Gamma_7 \longrightarrow \Gamma_7$		597.0	16750	16752
	$\Gamma_7 \longrightarrow \Gamma_8$		603.0	16583	16575
	$\Gamma_7 \longrightarrow \Gamma_6$		606.0	16501	16501
$^4G_{5/2} \text{ ----} \rightarrow ^6H_{9/2}$	$\Gamma_8 \longrightarrow \Gamma_8^{(1)}$		641.8	15581	15581
	$\Gamma_8 \longrightarrow \Gamma_8^{(2)}$		651.5	15349	15350
	$\Gamma_8 \longrightarrow \Gamma_6$		654.7	15274	15275
	$\Gamma_7 \longrightarrow \Gamma_8^{(1)}$		646.8	15469	15467
	$\Gamma_7 \longrightarrow \Gamma_8^{(2)}$		656.2	15239	15236
	$\Gamma_7 \longrightarrow \Gamma_6$		659.5	15163	15161

Calculations using the measured values of  $x$  and  $W$  gave the relevant crystal field parameters as:

$$B_4 = 0.1346 \quad ; \quad B_6 = 3.016 \times 10^{-4};$$

and

$$A_4 \langle r^4 \rangle = 53.74 \text{ cm}^{-1} \quad \text{for } J = 7/2 \text{ term}$$

and

$$B_4 = 0.188453 \quad ; \quad B_6 = 2.114 \times 10^{-4};$$

and

$$A_4 \langle r^4 \rangle = 75.345 \text{ cm}^{-1} \quad \text{for } J = 9/2 \text{ term, respectively}$$

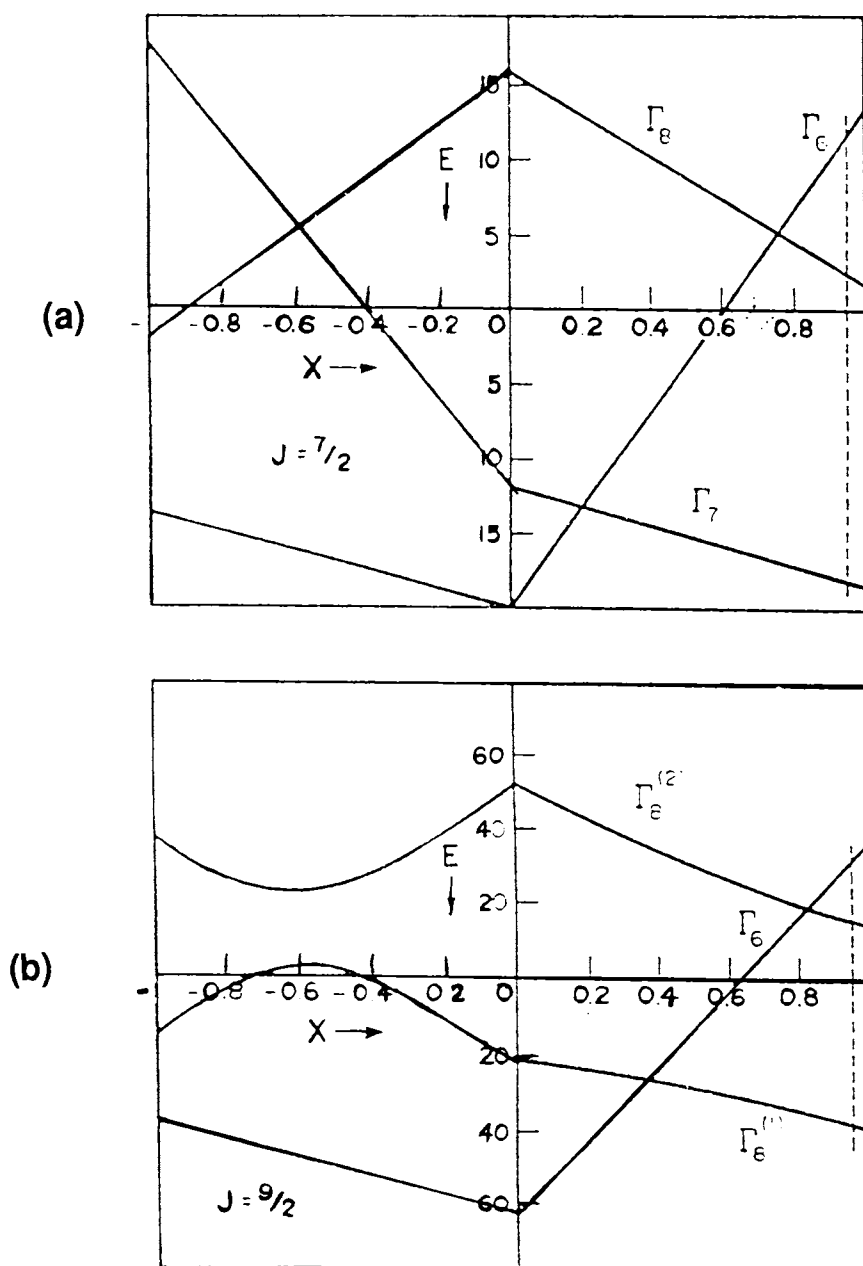


Fig. 4.14 Splitting patterns of (a)  ${}^6H_{7/2}$  and (b)  ${}^6H_{9/2}$  manifold of  $\text{Sm}^{3+}$  ion in BaS lattice.  $E$  is in  $\text{cm}^{-1}$ ;  $x$  is a dimensionless parameter defined in text, the broken lines indicate the values of  $x$  used to evaluate scale factor  $W$  (in  $\text{cm}^{-1}$ ) required for experimental determination of crystal field parameters.

In conclusion, we have analysed the fine structure of  $\text{Sm}^{3+}$  in BaS lattice by laser induced fluorescence. The splitting patterns obtained for  $\text{Sm}^{3+}$  energy levels in BaS lattice show the activator ions ( $\text{Sm}^{3+}$ ) occupies  $\text{Ba}^{2+}$  substitutional sites. Calculated values of the crystal field parameters using the experimental data support this fact.

**(b) BaS:Pr phosphor**

The BaS:Pr fluorescence emission spectrum also shows some well resolved lines superposed over the broad emission band of BaS (fig.4.15). In order to identify the lattice site of luminescence centre and the crystal field splitting pattern of energy levels involved in the emission, a detailed analysis of the spectrum was carried out, as in the case of BaS:Sm phosphor. The observed emission lines can be attributed to  ${}^3\text{P}_1 \rightarrow {}^3\text{H}_5$ ,  ${}^3\text{P}_0 \rightarrow {}^3\text{H}_4$  and  ${}^1\text{P}_2 \rightarrow {}^3\text{H}_4$  transitions of  $\text{Pr}^{3+}$  ion. The energy level scheme which explains the observed transitions assigned to various sub-levels of  $\text{Pr}^{3+}$  ion in BaS lattice are given in fig.4.16 and in table 4.2. The occurrence of sub-levels is due to the splitting of free-ion terms of  $\text{Pr}^{3+}$  ion under the influence of the crystal field.

Table 4.2				
Transitions involved corresponding to various sub-levels of $\text{Pr}^{3+}$ ions in BaS lattice.				
Group	Transitions Upper State    Lower State	Wave length ( nm )	Wave number ( $\nu \text{ cm}^{-1}$ )	
			Observed	Calculated
${}^3\text{P}_1 \rightarrow {}^3\text{H}_4$	${}^3\text{P}_1 \rightarrow {}^3\text{H}_4$ ( $\Gamma_1$ )	473.9	21101	21100
${}^3\text{P}_0 \rightarrow {}^3\text{H}_4$	${}^3\text{P}_0 \rightarrow {}^3\text{H}_4$ ( $\Gamma_1$ )	485.6	20593	21600
	${}^3\text{P}_0 \rightarrow {}^3\text{H}_4$ ( $\Gamma_3$ )	515.1	19410	19409
${}^3\text{P}_0 \rightarrow {}^3\text{H}_5$	${}^3\text{P}_0 \rightarrow {}^3\text{H}_5$	536.4	18642	18600
${}^1\text{P}_2 \rightarrow {}^3\text{H}_4$	${}^1\text{D}_2 \rightarrow {}^3\text{H}_4$ ( $\Gamma_1$ )	595.9	16781	16780
	${}^1\text{D}_2 \rightarrow {}^3\text{H}_4$ ( $\Gamma_5$ )	609.1	16415	16415
	${}^1\text{D}_2 \rightarrow {}^3\text{H}_4$ ( $\Gamma_4$ )	622.0	16076	16076
	${}^1\text{D}_2 \rightarrow {}^3\text{H}_4$ ( $\Gamma_3$ )	641.1	15590	15589

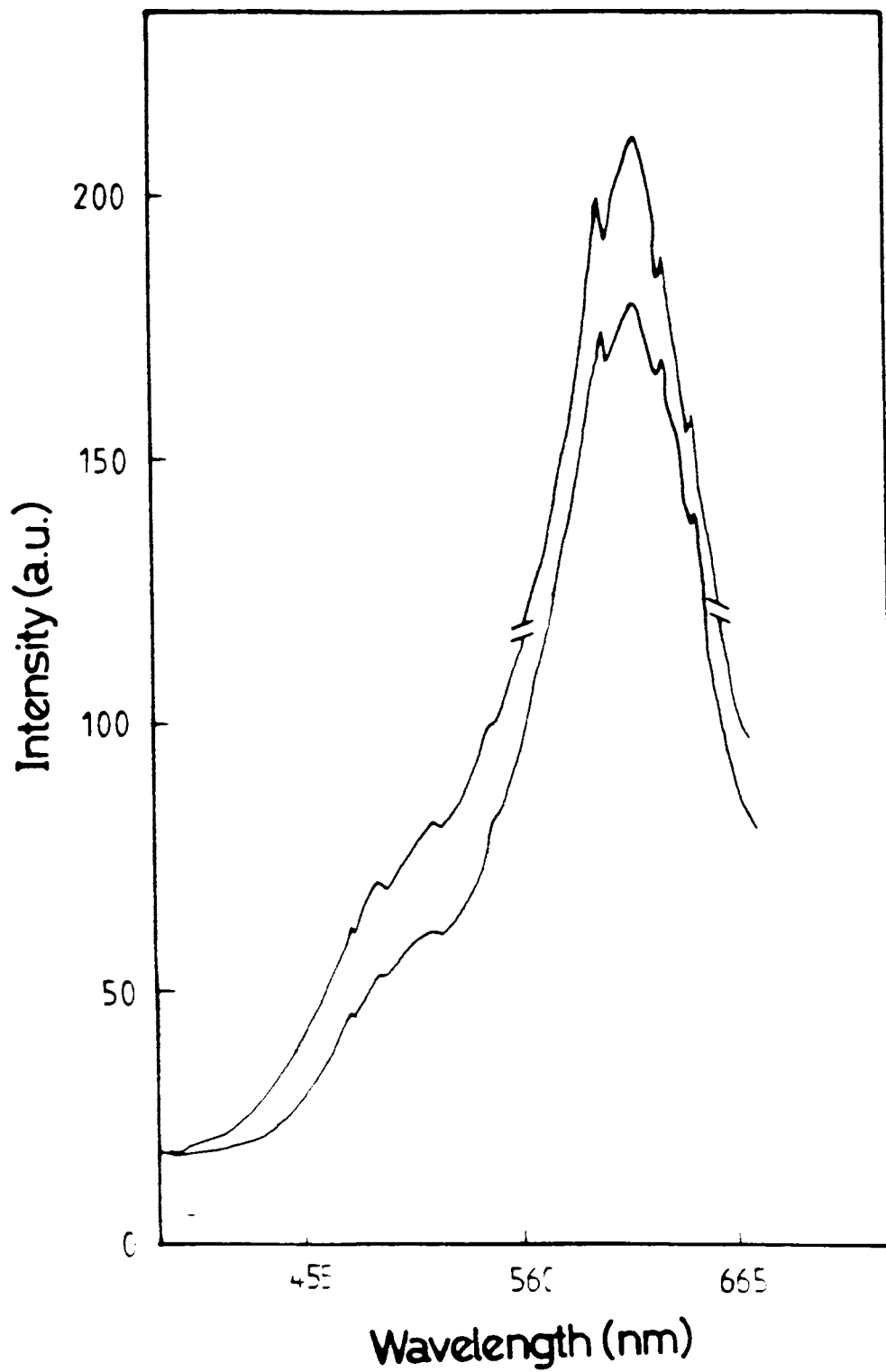


**Fig. 4.15** Emission lines observed in BaS:Pr phosphor under  $N_2$  laser excitation.

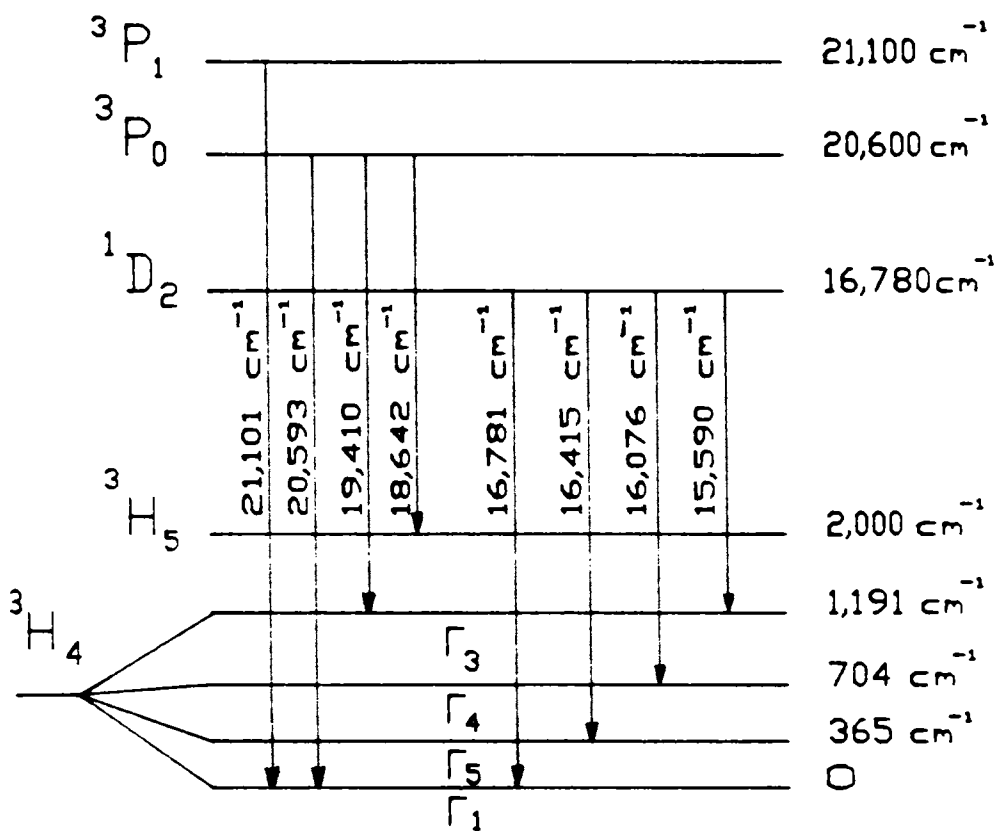


Fig. 4.16 Energy level scheme for the assigned transitions in BaS:Pr phosphor

Analysis was carried out by taking the ground state splitting alone into the consideration; the sub-levels being designated as  $\Gamma_1$ ,  $\Gamma_5$ ,  $\Gamma_4$  and  $\Gamma_3$ . The exact fit of the energy level separation for the observed transitions occur at the values of  $x = 0.224$  and the scale factor  $W = 12.80 \text{ cm}^{-1}$  for the splitting pattern of  $J = 4$  term. In the fig.4.17, the broken line corresponds to this position. The value of the crystal field parameters calculated using the above measured values of  $x$  and  $W$  obtained, are as follows:

$$\begin{aligned}
 B_4 &= 4.78 \times 10^2 & ; & & B_6 &= 5.7 \times 10^4 ; \\
 A_4 \langle r^4 \rangle &= -65.06 \text{ cm}^{-1} \\
 \text{and} \\
 A_6 \langle r^6 \rangle &= 9.345 \text{ cm}^{-1}
 \end{aligned}$$

In short, the present studies reveal an energy transfer between host lattice and  $\text{Sm}^{3+}/\text{Pr}^{3+}$  centres.  $\text{Sm}^{3+}/\text{Pr}^{3+}$  easily occupies the substitutional site of  $\text{Ba}^{2+}$  giving its characteristic emission lines superposed over the host-lattice emission.

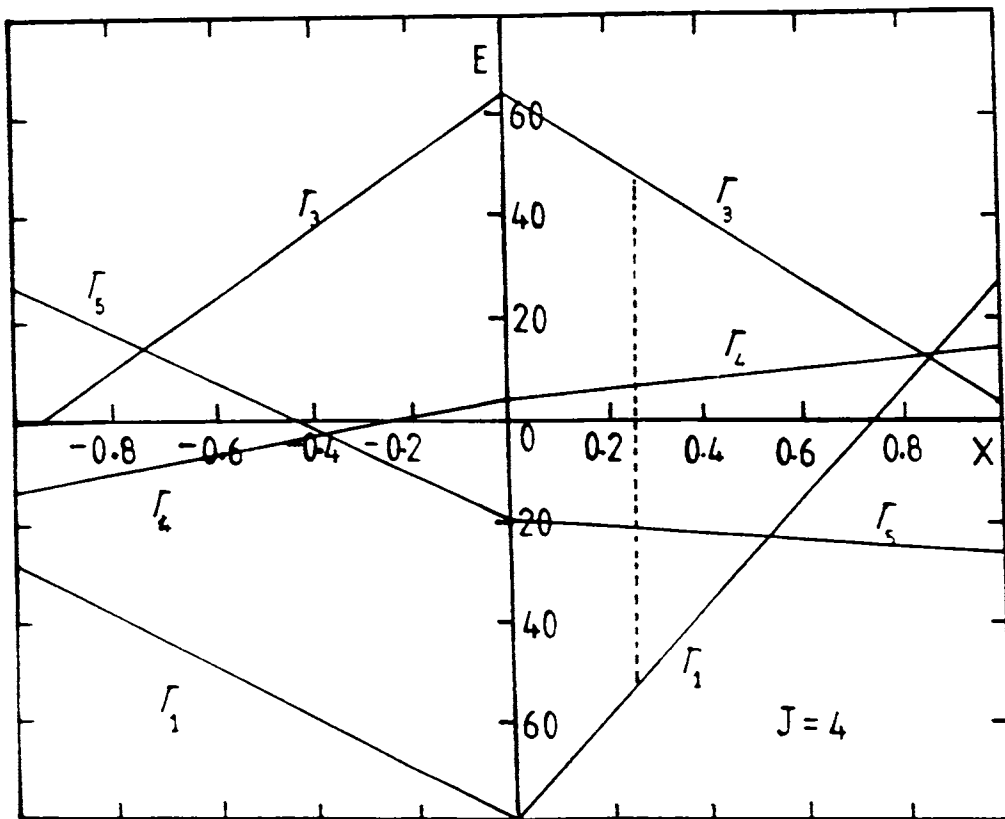


Fig. 4.17 Energy level splitting pattern of  ${}^3H_4$  manifold of  $Pr^{3+}$  ion in BaS lattice



## REFERENCES

- [1] Kulkarni V.W., S.S. Patwardhan and Ghanbather R.Y., *Phy. Scripta.* 25, (1982) p.496
- [2] Smith A.L., *J. Electrochem. Soc.* 46 (1949) p.75
- [3] Dexter D.L., and Schulman, J.H., *J. Chem. phys.* 27, (1954) p.1063
- [4] Kroger and Hellingman, *J. Electrochem. Soc.* 95 (1945) p.68
- [5] Yoshio Keneto and Tako, *J. of Cry. Growth*, 86 (1988) p.72.
- [6] Thomson L.C., *HAND BOOK OF PHYSICS AND CHEMISTRY OF RARE-EARTHS, Vol.3 - NONMETALLIC COMPOUNDS* (ed) D. K. Gschenedner Jr. and L. Eyring North Holland (1979)
- [7] Willi Lehmann, *J. electrochem. Soc. "Solid State Science"* 117 (1979) 1390
- [8] Pillai S.M. and Vallabhan C.P.G., *Phy. Stat. Solidi (b)*134 (1986) p.383
- [9] Agarwal and Jai Sanker, *Indian J. of Pure and Appl. Phy.* 110 (1973) p.708
- [10] Kabler M.N. "*POINT DEFECTS IN SOLIDS*" Vol. 11, London (1972)
- [11] Willi Lehmann, (1983), Private communication
- [12] Marfunin "*SPECTROSCOPY, LUMINESCENCE AND RADIATION CENTERS IN MINERALS*" Springer Verlag, New York (1979)
- [13] Willi Lehmann, *J. of electrochem. Soc. "Solid State Science"* 117 (1979) p.1389
- [14] Lattimer W.M., and Heldebrand J.A., "*BOOK OF INORGANIC CHEMISTRY*" Macmillian Co. New York (1946)
- [15] Pillai, S.M., and Vallabhan, C.P.G. *Solid State Comm.* 47 (1983) p.1389
- [16] Kroger and Dikhoff, *J. Physica* 16 (1950) p.29.
- [17] Zhong C.Z. and Bryant T.J., *J. Phy. C* 13 (1980) p. 4497
- [18] Lea K.R., Leask M.J.M., and Wolf W.P., *J. Phy. Chem. Solids* 23 (1962) p. 1381
- [19] Stevens, *Proc. Phy. Soc.* A65 (1952) p.209
- [20] Freeman and Watson, *Phy. Rev.* 127 (1962) p.2058.

## **CHAPTER V**

## FLUORESCENCE AND THERMOLUMINESCENCE STUDIES USING ULTRA-VIOLET LAMP EXCITATION

In this chapter fluorescence and thermoluminescence studies made on copper and cerium doped Barium sulphide phosphor by exciting with 365 nm line from a UV lamp. are presented.

### 5.1. Fluorescence Emission Studies

Different sets of BaS:Ce, BaS:Cu, BaS:Ce:Cu phosphor samples were prepared following the method 1 [1] described in chapter III. Details of the samples are given in table 3.1. In all the phosphor samples prepared in this method the flux ( $\text{Na}_2\text{S}_2\text{O}_3$ ) concentrations was kept at 25% by wt of  $\text{BaSO}_4$  which was found to give a maximum fluorescence efficiency. The fluorescence spectra of the phosphor samples were charted at room temperature (28°C) using the experimental set up described in chapter III. All the emission spectra were scanned in the visible region from 400 nm to 700 nm.

#### 5.1.1. Spectral Features

The self-activated spectrum of BaS shows emission bands in blue and yellow-red regions with maxima at 450 nm, 585 nm and 613.4 nm respectively (fig. 5. 1). In the emission spectra of BaS:Cu phosphors, the band in the blue region was found to be completely suppressed while the other bands became more intense. It can be seen that as the copper concentration increases the bands at 585 nm and 613.4 nm regions merge together to give a single band starting from 550 nm to 660 nm with peak position at ~ 600nm (fig. 5.2). Another important feature to be noticed in the spectra is that, at higher concentrations of the dopant, a well defined shoulder appears at 560nm region. When the copper concentration reaches above 3.303% by wt., the intensity of emission was found to decrease as due to usual concentration quenching phenomena [2].

Cerium doped BaS phosphors do not show any characteristic emission lines of cerium in the fluorescence spectra. As the concentration of cerium increases, bands in both the regions gain in intensity along with a broadening of the band in the red region (fig. 5.3). In this case also, the concentration quenching effect is observed. For doubly doped phosphor systems (BaS:Cu:Ce), the quantum efficiencies of fluorescence emission was found to be comparatively high. Here the blue band as well as red band show considerable increase in intensity with more predominance to red band, peaking at 600 nm (fig. 5.4).

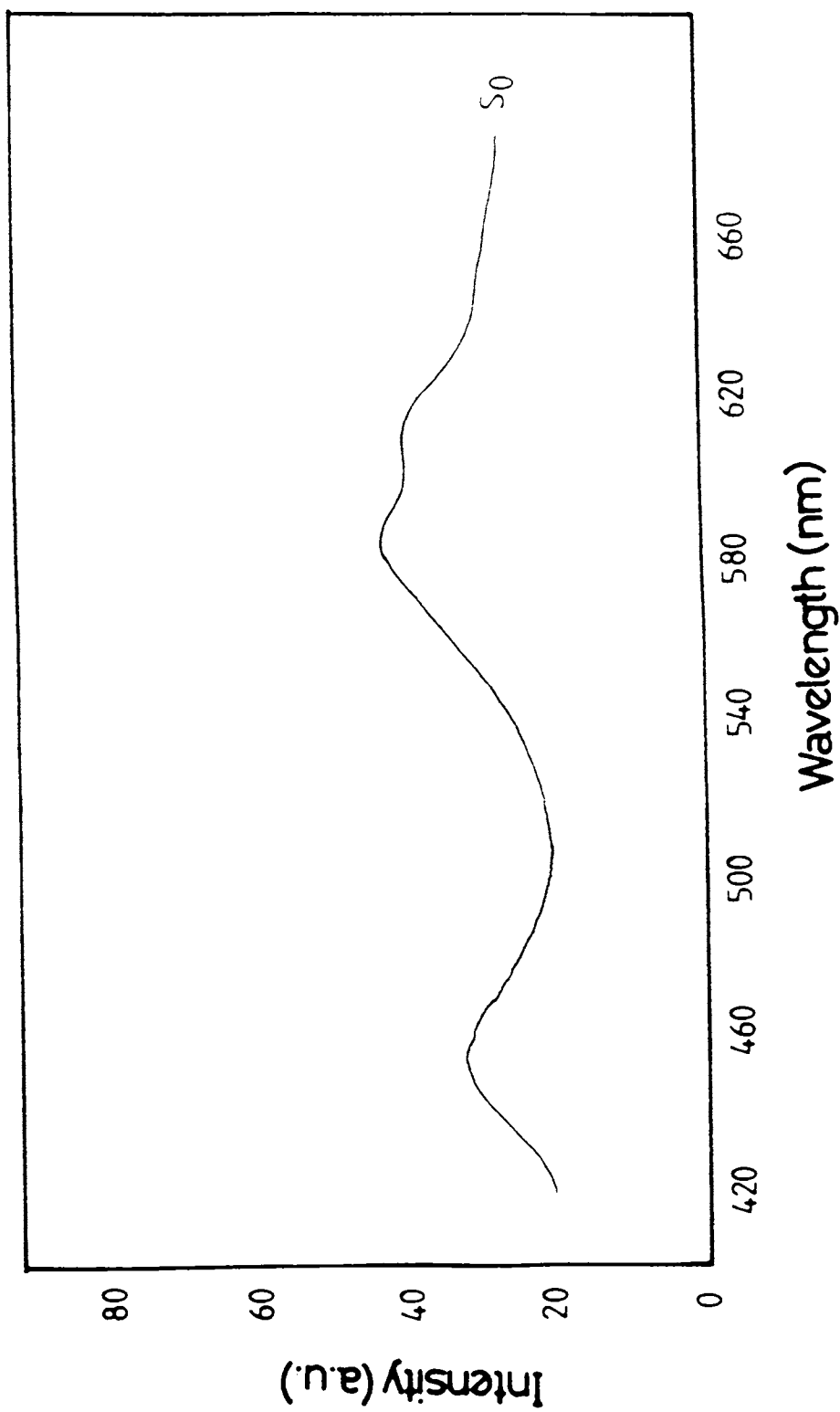


Fig 5.1 Fluorescence emission spectrum of self-activated BaS (S<sub>0</sub>) under 365nm excitation.

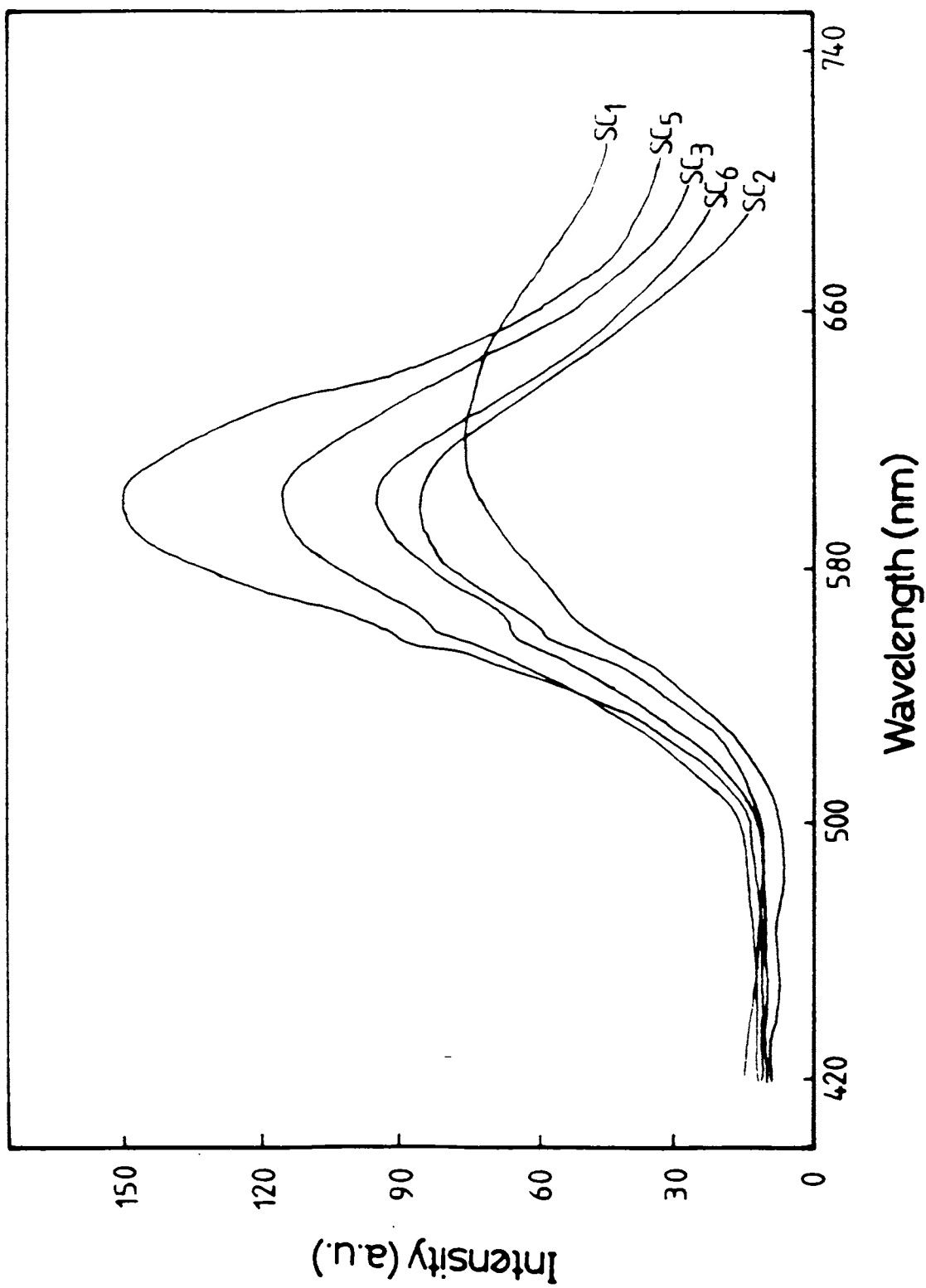


Fig 5.2 Fluorescence emission spectra of Bas:Cu phosphors under UV(365nm) excitation.

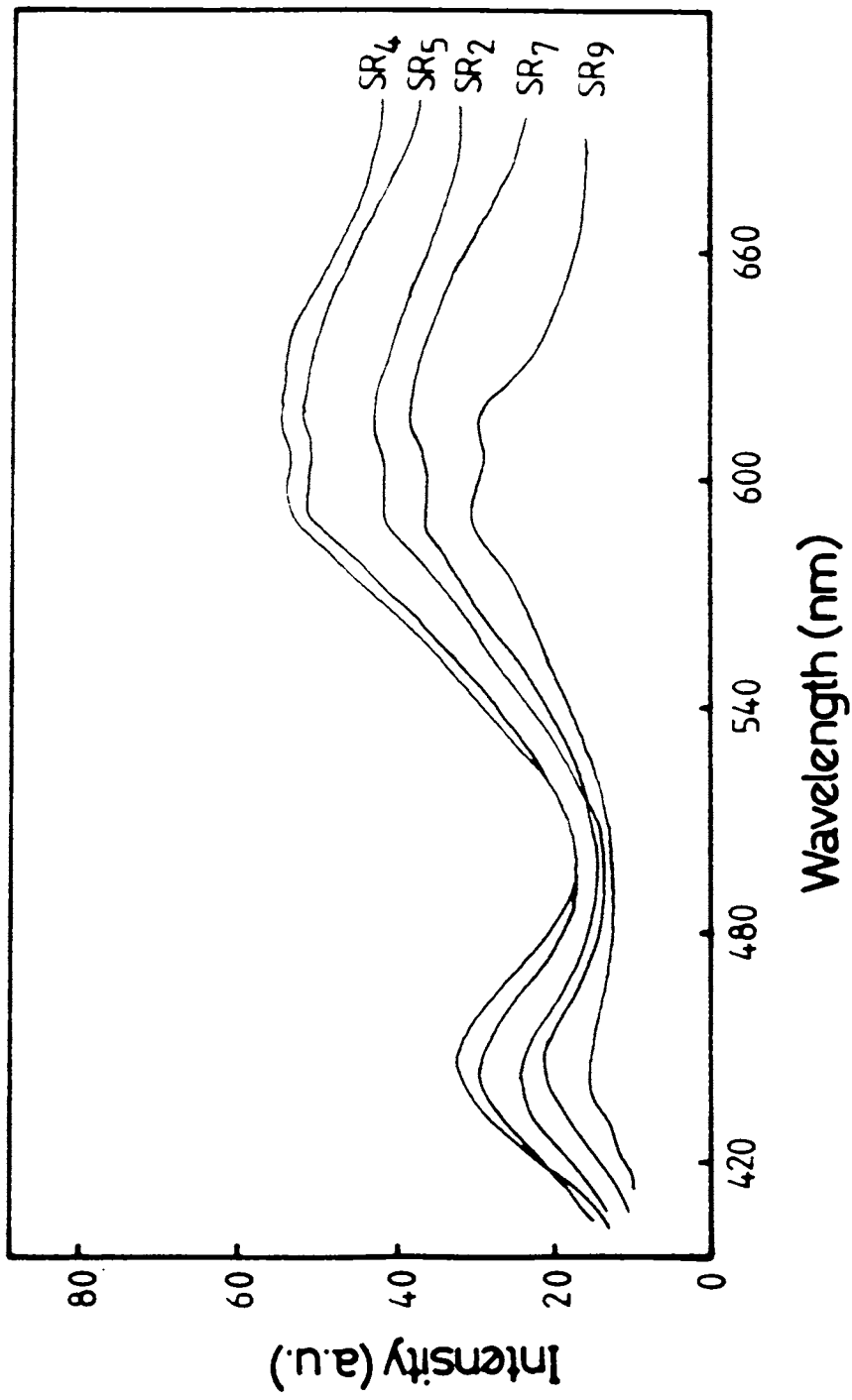


Fig 5.3 Fluorescence emission spectra of BaS:Ce phosphors underUV (365nm) excitation

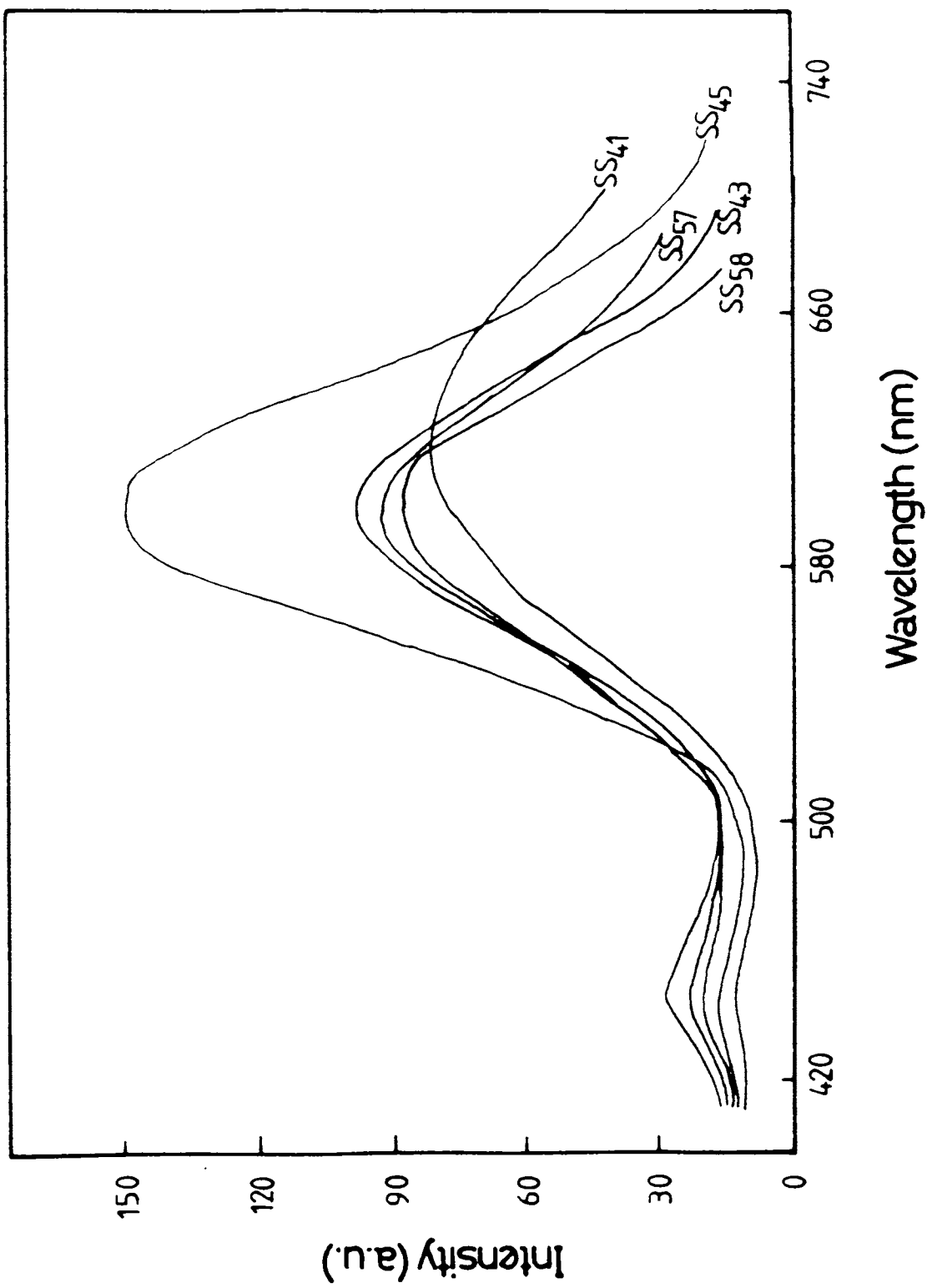


Fig 5.4 Fluorescence emission spectra of BaS:Ce:Cu phosphors under UV (365nm) excitation.

### 5.1.2. Emission Model

The band gap of BaS was found to be  $\sim 3.8$  eV [3], and UV radiation of 365 nm does not have sufficient energy to cause a band to band transition in BaS. So we expect a vacancy level near the valence band (level A, in fig.5.5(a)) causing the excitation of electrons to the conduction band. The flux in the form of sodiumthiosulphate will create more cation vacancies in the lattice. The recombination of localized holes in these cation vacancy levels with electrons in the conduction band causes the emission of 450 nm band. The increase in intensity of this emission in the case of BaS:Ce phosphors also support this assumption. The addition of cerium which goes as a trivalent cation in BaS lattice increase  $V_{Ba^{2+}}$  levels so as to have charge compensation. Hence the effect of  $Ce^{3+}$  is to sensitize the blue emission. Eventhough no characteristic emission lines of cerium are seen, the overall efficiency of fluorescence emission increases and a broadening of the band in yellow-red region is also observed in BaS:Ce emission spectra. This is because of an energy transfer between luminescence centres in the host lattice due to presence of  $Ce^{3+}$  sites. The band observed at 613.4 nm in self activated BaS, can be attributed to the annihilation of localized electrons in the vicinity of anion vacancy and holes trapped at the level A. The difference between these two band energies give the location of anion and cation vacancy levels in the forbidden gap.  $S^{2-}$  in the vicinity of cation vacancy, and  $Ba^{2+}$  in the vicinity of anion vacancy, will form a complex  $V_{Ba^{2+}} + V_{S^{2-}}$  giving rise to an additional level in the forbidden gap, the position of which is very near to the valence band. The recombination of holes trapped in this level with electrons trapped in  $V_{S^{2-}}$  level will give the band at 585 nm (fig. 5.5).

$Cu^+$  in BaS can occupy as substitutionally or interstitially. Effect of  $Cu^+$  in the lattice reduce the population of cation vacancy sites. This causes the disappearance of the blue band as  $Cu^+$  is introduced in BaS lattice. The intensified emission seen in BaS:Cu spectra are explained by taking into consideration, the splitting of  $Cu^+$  energy levels due to BaS crystal field [4]. The intense red emission peaked at 600 nm is due to the transition  ${}^3E_g ({}^3P) \longrightarrow {}^1A_{1g} ({}^1S)$  and the shoulder band seen at 560 nm can be attributed to  ${}^3T_{2g} ({}^3D) \longrightarrow {}^1A_{1g} ({}^1S)$  of  $Cu^+$  energy levels in the forbidden gap of BaS (fig.5.5(b)). Actually the effect of  $Cu^+$  in BaS is to activate the red emission. Also it is found that the spectral intensity depends very much on the concentration of dopants.

In short, the spectra obtained show a clear evidence for the effect of  $Cu^+$  and  $Ce^{3+}$  on BaS lattice.  $Cu^+$  is found to be a more effective sensitizer of host lattice centre as compared to  $Ce^{3+}$ . The spectra show that the effect of doping increases the fluorescence efficiency of the phosphor. The high quantum yield of fluorescence emission observed in the case of doubly doped phosphor system give the conclusion that  $Cu^+$  in BaS acts as a good activator, whereas  $Ce^{3+}$  as a good co-activator.



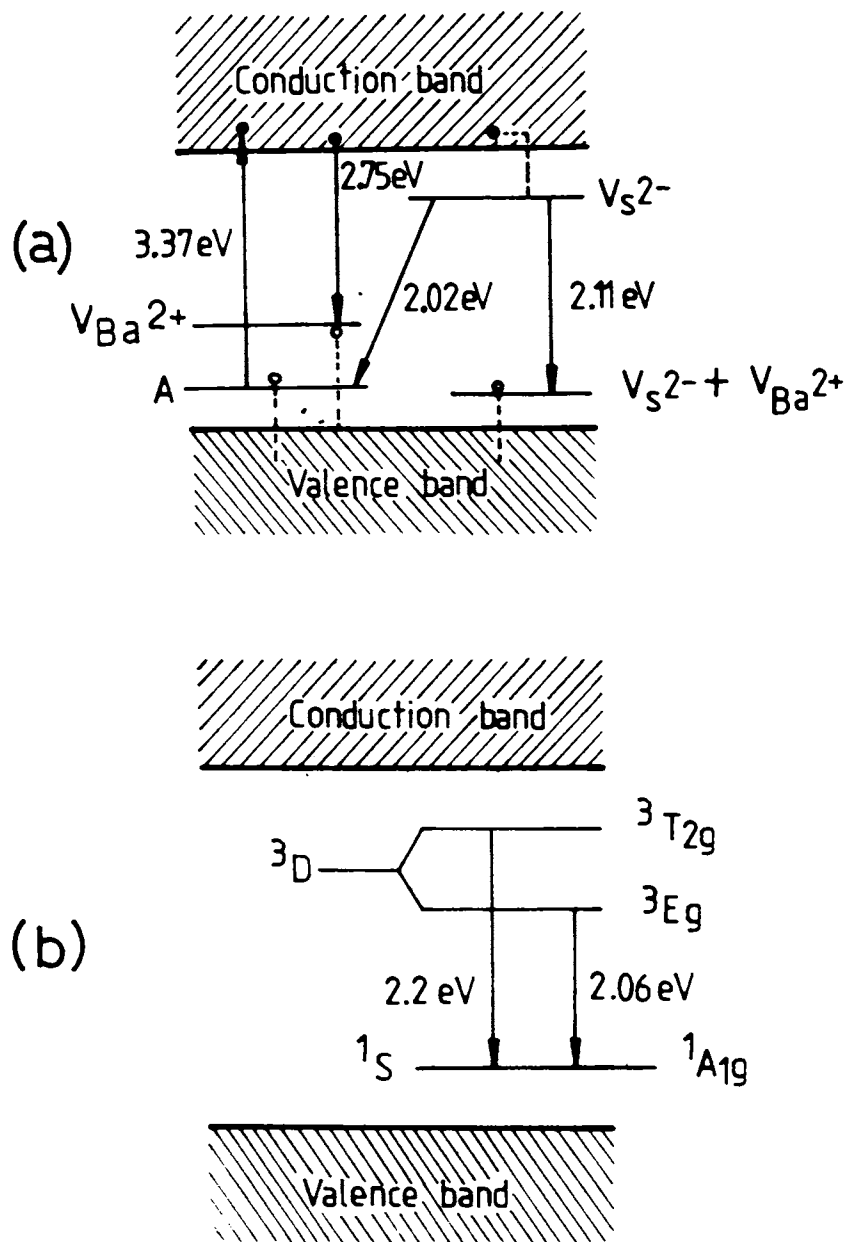


Fig 5.5 Emission models for (a) self-activated emission of BaS  
(b) copper emission centres in BaS

## 5.2. Thermoluminescence(TL) Studies

To have a clear understanding about the mechanism involved in luminescence process, the thermoluminescence (TL) spectra of the samples were also studied. For TL measurements, sample pellets were placed in a specially designed sample holder having provisions for heating the sample at a uniform rate. This purpose is served by keeping a small heater coil inside the copper sample holder which is in good contact with the sample. Temperature of the sample can be readily read by means of a copper-constantan thermocouple which is kept in contact with the sample holder. In TL study, after excitation to a saturation level, samples were left to decay for about 5 min, and then were heated at a uniform rate. During this time the TL emission intensity was recorded with the help of PMT and chart recorder (details of experimental arrangement are already given chapter III). TL spectra of the phosphor samples were recorded above room temperature at two different linear heating rates 0.15° K/sec and 0.1°K/sec. Fig 5.6 and fig 5.7 show the TL spectra recorded for some of the phosphor samples studied.

No considerable TL emission was seen in the case of pure BaS phosphor; while singly doped phosphors showed a weak TL output. In case of BaS:Ce:Cu phosphors, appreciable TL emission was obtained. The glow curves show only one peak with maximum intensity of emission around 350° K (fig.5.7). It is seen that the presence of Cu enhances the TL output of BaS:Ce phosphors. The intensity of glow was found to be maximum for the dopant concentrations 0.702% by wt. of BaS for cerium and 0.11% by wt. of BaS for copper. At high concentrations of Cu in BaS:Ce the TL efficiency was found to decrease. This is due to the fact that characteristic emission of Cu<sup>+</sup> reduces the role of vacancies in luminescence emission, while cerium enhances vacancy population. The intense TL emission observed for BaS:Ce:Cu phosphors suggest that the emission is controlled by these impurities. The lattice imperfections associated with the two kinds of impurities viz., Cu<sup>+</sup> and Ce<sup>3+</sup> are basically different in nature. The possible centres/sites for trapping the electrons liberated during irradiation are [Ce<sub>Ba</sub>]<sup>+</sup> and anion vacancies [V<sub>S</sub>]<sup>2-</sup> and complexes like [V<sub>S</sub> - Cu<sub>Ba</sub>]<sup>+</sup> and for holes, [Cu<sub>Ba</sub> - V<sub>Ba</sub>]<sup>2-</sup> and [V<sub>Ba</sub> - Ce<sub>Ba</sub>]<sup>+</sup> responsible for the TL glow peak. So the simultaneous incorporation of Cu and Ce will populate deeper traps more efficiently. The enhancement of the glow peak intensity in the beginning is due to the increase in the number of luminescent centres and traps with increase in activator concentration. The decrease in intensity of glow with increase of activator concentration was due to large number of levels produced which might give radiationless transitions. The decrease in glow peak intensity on further increase of concentrations of the activator may be due to concentration quenching [5,6]. It was also observed that the area under the TL curve first increases and then decreases with increase in activator concentration. This indicates the increase in number of traps with concentration in the beginning as the area under TL curve is proportional to the number of traps [7]. The decrease in area at higher concentration may be due to the concentration quenching rather than the decrease in number of traps. The single peak observed in cases of all the samples studied indicates that the probability for only

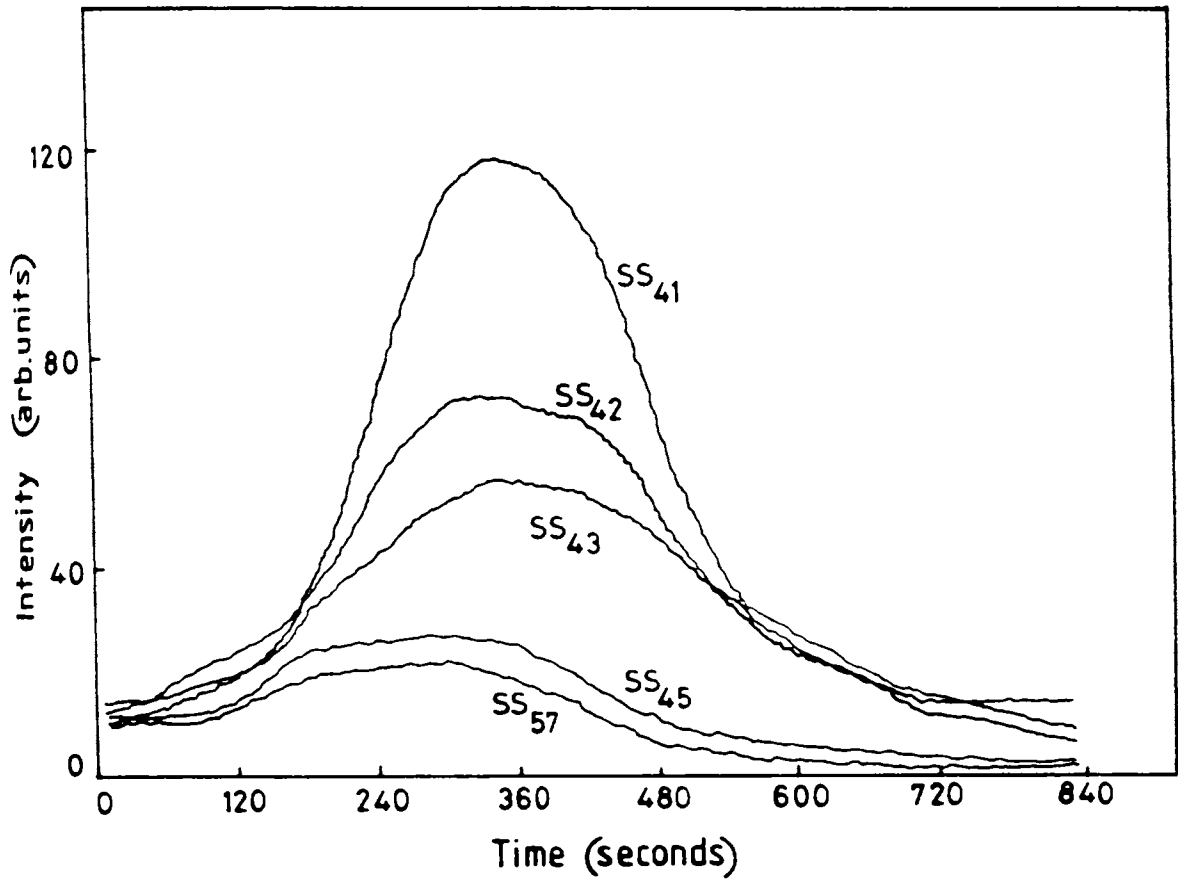


Fig 5.6 TL glow curves of BaS:Ce:Cu phosphors for heating rate ( $\beta$ )  $0.15^\circ/\text{sec}$ .

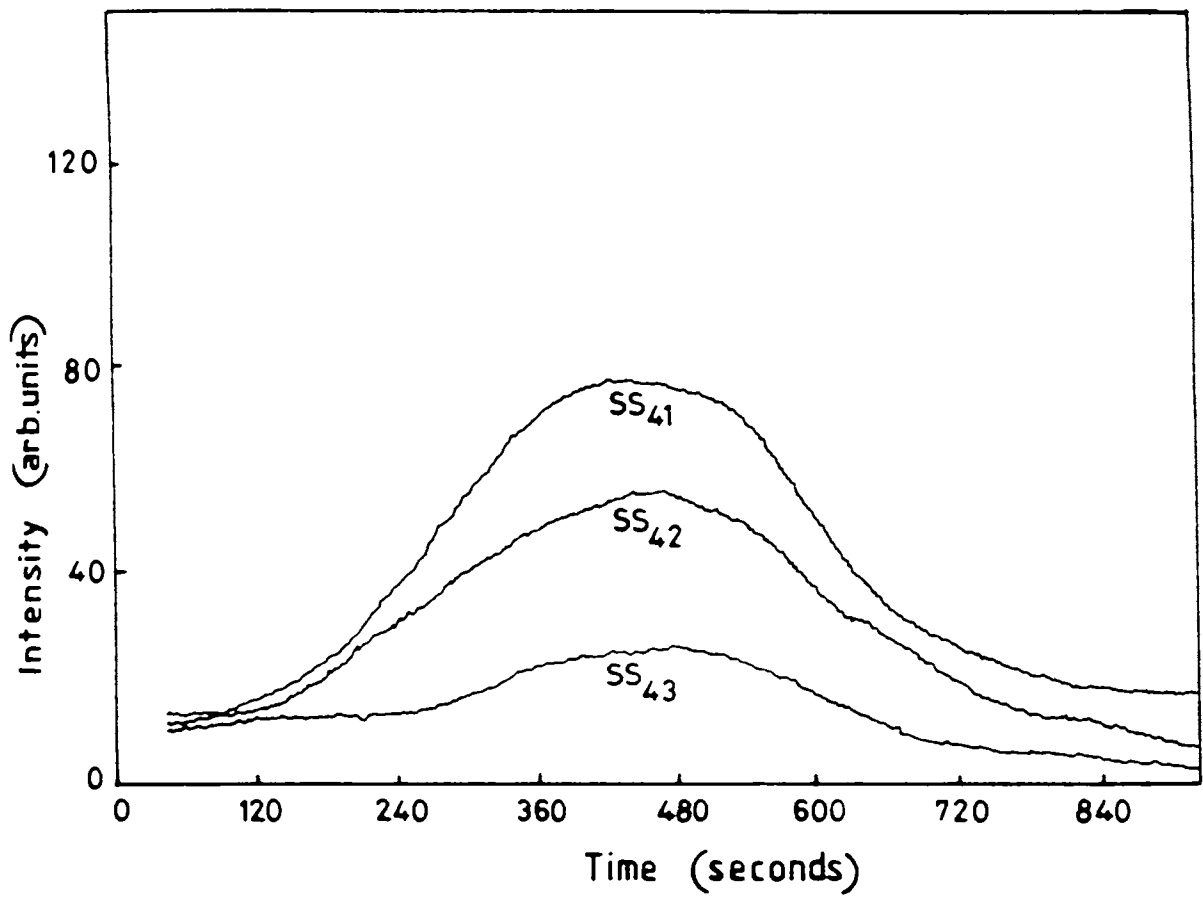


Fig 5.7 TL glow curve of BaS:Ce:Cu phosphors for heating rate ( $\beta$ ) 0.1°/sec

one trapping level under the present experimental conditions. The traps get emptied as the temperature rises; the shallow ones first and at each temperature  $T$  those with life times of a fraction of a second or so are responsible for the observed increase in intensity of the glow curve. The thermoluminescence intensity increases and reaches a maximum for the temperature  $T_m$  and then decreases to zero at higher temperature as the traps are emptied. The activation energy 'E' for the electron to escape from the trap and the escape frequency factor 'S' are calculated from the TL glow curves using different methods viz.,

- 1) Urbach method [8] given by

$$E = T_m / 500 \text{ which give the right order of values for E.}$$

- 2) Curie method [9] as

$$E = \frac{T_m (^{\circ}\text{K}) - T_0 (\beta/S)}{K (\beta/S)}$$

where  $T_0$  and  $K$ , the Curie parameters (give in Table 1.4)

- 3) Grosswiener's method [10], the equation for 1st order kinetics is

$$E = \frac{1.51 K T_m T_1}{T_m - T_1}$$

where  $T_1$  - the half intensity bandwidth temperature towards the rise in temperature of the glow peak.

- 4) Louchtchik's [11] method

$$E = K T_{m2} / (T_2 - T_m) \text{ for first order kinetics}$$

- 5) Chen's method [12]

$$E = 2.29 K T_m^2 / \omega \text{ where } \omega - \text{band width } (T_2 - T_1)$$

- 6) Randall and Wilkins method [13]

$$E = K T_m \log S$$

- 7) Booth, Bohun, and Hooganstraafen's method [14]

$$E = \frac{K T_{m1} T_{m2}}{T_{m1} - T_{m2}} \log \left[ \frac{\beta_1 \left[ \frac{T_{m2}}{T_{m1}} \right]^2}{b_2 \left[ \frac{T_{m1}}{T_{m2}} \right]} \right]$$

where  $\beta_1$  and  $\beta_2$  are the two heating rates and  $T_{m1}$  and  $T_{m2}$  the corresponding temperature maxima.

And for escape frequency factor, 'S'

a) Chen's method [12]

$$S = 2.67 (\beta/\omega) 10^{T_m}$$

b) Randall and Wilkins method [13]

$$S = \beta (E/KT_m^2) \exp (E/KT_m)$$

The trapping parameters calculated are compiled in Table 5.1. It is seen that the values of trap depth (~ 0.5 e V) and escape frequency factor (~ 10<sup>6</sup>/sec) agree well with the earlier reports on similar systems. [15]

Table 5.1

Trapping parameters from TL curves calculated using different formulae [8-14]

Sample No	heating rate (%K/Sec.)	Temp. Maximum of TL glow(°K.)	Trap depth E (eV) [Methods of estimation]								Escape frequency factor S ( /Sec) x 10 <sup>6</sup>	
			(1)	(2)	(3)	(4)	(5)	(6)	(7)	(a)	(b)	
SS <sub>41</sub>	0.15	352.25	0.7	0.57	0.66	0.51	0.56	0.40	0.52	1.1	1.5	
	0.1	345.76	0.69	0.62	0.58	0.52	0.51	0.36		0.32	0.602	
SS <sub>42</sub>	0.15	350.15	0.70	0.56	0.66	0.35	0.46	0.39	0.49	0.33	0.636	
	0.1	346.23	0.69	0.56	0.67	0.42	0.51	0.39		0.15	0.637	
SS <sub>43</sub>	0.15	354.0	0.70	0.57	0.53	0.43	0.46	0.40	0.76	0.33	0.337	
	0.1	349.0	0.69	0.56	0.64	0.59	0.59	0.39		2.07	1.8	
SS <sub>44</sub>	0.15	353.0	0.70	0.57	0.46	0.42	0.40	0.41	-	0.05	0.18	
	0.15	348.07	0.69	0.56	0.49	0.53	0.48	0.39	-	0.1	0.58	
SS <sub>56</sub>	0.15	347.61	0.69	0.56	0.48	0.62	0.51	0.39	-	0.04	0.58	
	0.15	346.69	0.69	0.56	0.48	0.62	0.52	0.39	-	0.04	0.37	
SS <sub>58</sub>	0.15	351.5	0.70	0.57	0.63	0.40	0.47	0.40	-	0.25	0.97	

## REFERENCES

- [1] Bhawalker D.R., and Malhotra B,R, Indian J of Pure and Appl Phy 7 (1969) p 163
- [2] Johnson P.D. and Williams F.E., J. Chem. Phys. 18 (1950) p.1477
- [3] Willi Lehmann J. Electrochem. Soc. -"Solid State Science" 117 (1979) p.1389
- [4] Figgis B.N. *"INTRODUCTION TO LIGAND FIELDS"* John Wiley Sons. Inc. New York (1966)
- [5] Leverenz. H.W., *"AN INTRODUCTION TO LUMINESCENCE OF SOLIDS"* John Wiley Sons, Inc. New York (1950)
- [6] Dexter D.L. and Schulman J.H., J. chem. Phy.27 (1954) p.1063.
- [7] Curie D. *"LUMINESCENCE IN CRYSTALS"* John Wiley Sons. Inc. New York (1963)
- [8] Urbach F., Cornell Symp Vol. 115, John Wiley Sons Inc. New York (1948)
- [9] Curie D. *"LUMINESCENCE IN CRYSTALS"* John Wiley Sons Inc. New York (1963)
- [10] Grossweiner L.I., J. Appl. Phy. 24 (1953) p.570
- [11] Louchtchik *"CRYSTALLOPHOSPHORS"* Academic fiz. Tartone (1955)
- [12] Chen, R., J. of Appl. Phy. 40 (1969) p.570
- [13] Randall J.T. and Wilkins M.H.F., Proc. Phy. Soc. A184 (1945) p.390
- [14] Hooganstraafen W. *"Electron traps in Zinc Sulphide phosphors"* Ph. D. Thesis, Amsterdam (1958)
- [15] R.P. Rao, J. of Mat. Sci. 21 (1986) p.3357.



## **CHAPTER VI**

## ANALYSIS OF PHOSPHORESCENCE DECAY CHARACTERISTICS

### 6.1 Introduction

The characteristics of phosphorescence emission have been widely used as a means of investigating the mechanism of luminescence. It offers significant information regarding the kinetics involved in the process and provides a direct means of studying electron traps in luminescent materials. Decay properties of alkaline earth sulphide (AES) phosphors have been studied in recent years [1-2]. Studies on this group of phosphors doped with one or more impurity elements have been reported by several workers [3-5]. After the discovery of sensitization effect [6], AES with double activators have acquired much importance.

This chapter reports the phosphorescence decay studies of BaS:RE and BaS:Cu:RE phosphor systems carried out at room temperature. All the phosphor samples were excited for about 5 minutes and then decrease in intensity of emission with time was recorded. Details of the experimental arrangement are given in chapter III.

### 6.2 Nature Of Phosphorescence Decay

The self-activated BaS shows phosphorescence emission (afterglow) only for about 50 seconds (fig. 6.1a). But the emissions from doped samples are found to decay for longer time of the order of minutes. In the case of BaS:RE phosphor systems studied the Pr doped BaS phosphors show comparatively intense afterglow and the decay lasts upto 250 seconds. For copper doped samples even though the decay lasts only for about 40-50 sec; the after glow has high intensity. But, when combined with rare-earth dopants (BaS:Cu:RE), enhancement in the decay time to the order of minutes were observed. BaS:Cu (Pr:Sm) phosphors show very intense phosphorescence emission which last upto 350 sec or more. It is found that the intensity of afterglow are very much dependent on the activator concentration.

The analysis of decay curves are made, based on the theory developed by Randall and Wilkins [7]. The emptying of traps assumes the probability of electron escaping from a trap given by

$$P = S \exp - (E/KT) \quad 6.(1)$$

where 'S' is the frequency factor (the attempt-to-escape frequency) and the exponential term is the Boltzmann factor involving the trap depth 'E' and temperature T. The attempt to-escape frequency may be interpreted as the number of times per second that the thermal quanta from crystal vibrations attempt to eject the electron from the trap, multiplied by the probability of

transition from the trap to conduction band. The Boltzmann factor is the probability of the electron having an energy sufficient to escape on any one of these attempts. The above equation assumes that (i) retrapping is negligible (ii) 'S' and 'E' are independent of temperature and (iii) radiative transition predominate once the electrons are freed. If there is a distribution of trap depths, the decay pattern will be due to the superposition of intensities, each of which is varying exponentially with time. This gives rise to a decay law of the form,

$$I = I_{01} \exp(-P_1 t) + I_{02} \exp(-P_2 t) + \dots + I_{0n} \exp(-P_n t) = I_0 t^{-b} \quad 6.(2)$$

where 'b' is the decay constant. This scheme representing superposition of exponentials has been adopted by several workers [1-2, 8-10]

In order to investigate the nature of decay, intensity(I) vs time, log I vs t, log I vs log t and I vs 1/t graphs were plotted. Figures 6.1, 6.2, 6.3 & 6.4 show these graphs for some representative samples. In all the phosphor samples studied the semi-log plots show non-linear behaviour excluding the possibility of simple exponential decay (fig.6.2 ((a) to (k))). However log I-log t plots show a linear behaviour with certain discontinuities (fig.6.3 ((a) to (h))). It is found that the number of discontinuities in log I-log t graphs corresponds to the number of straight lines into which the semi-log curve can be splitted. In order to estimate the degree of linearity, the correlation coefficient 'r' has been evaluated using the relation [11].

$$r = \frac{n \sum x_i y_i - \sum x_i \sum y_i}{\left[ n \sum x_i^2 - (\sum x_i)^2 \right]^{1/2} \left[ n \sum y_i^2 - (\sum y_i)^2 \right]^{1/2}} \quad 6.(3)$$

where  $x = \log t$ ,  $y = \log I$  and n-the number of observations.

The values of 'r' for the phosphors studied in the three regions of log I-log t plot comes out to be close to unity corresponding to the three exponentials of semi-log plot. This helps us to suggest that the decay is hyperbolic in nature in accordance with eq.6.(2). Again, in the case of the most of the phosphor samples, the plots I vs 1/t (fig.6.4 ((a) to (h))) show almost a linear relationship suggesting the kinetics of the decay process to be a monomolecular one [12]. The observed hyperbolic decay is due to the superposition of intensities of emission from traps of different depths. So on this basis, the decay curves can be analysed in terms of different exponentials following Bube's [13] 'peeling off' method (fig.6.2 ((a) to (k))).

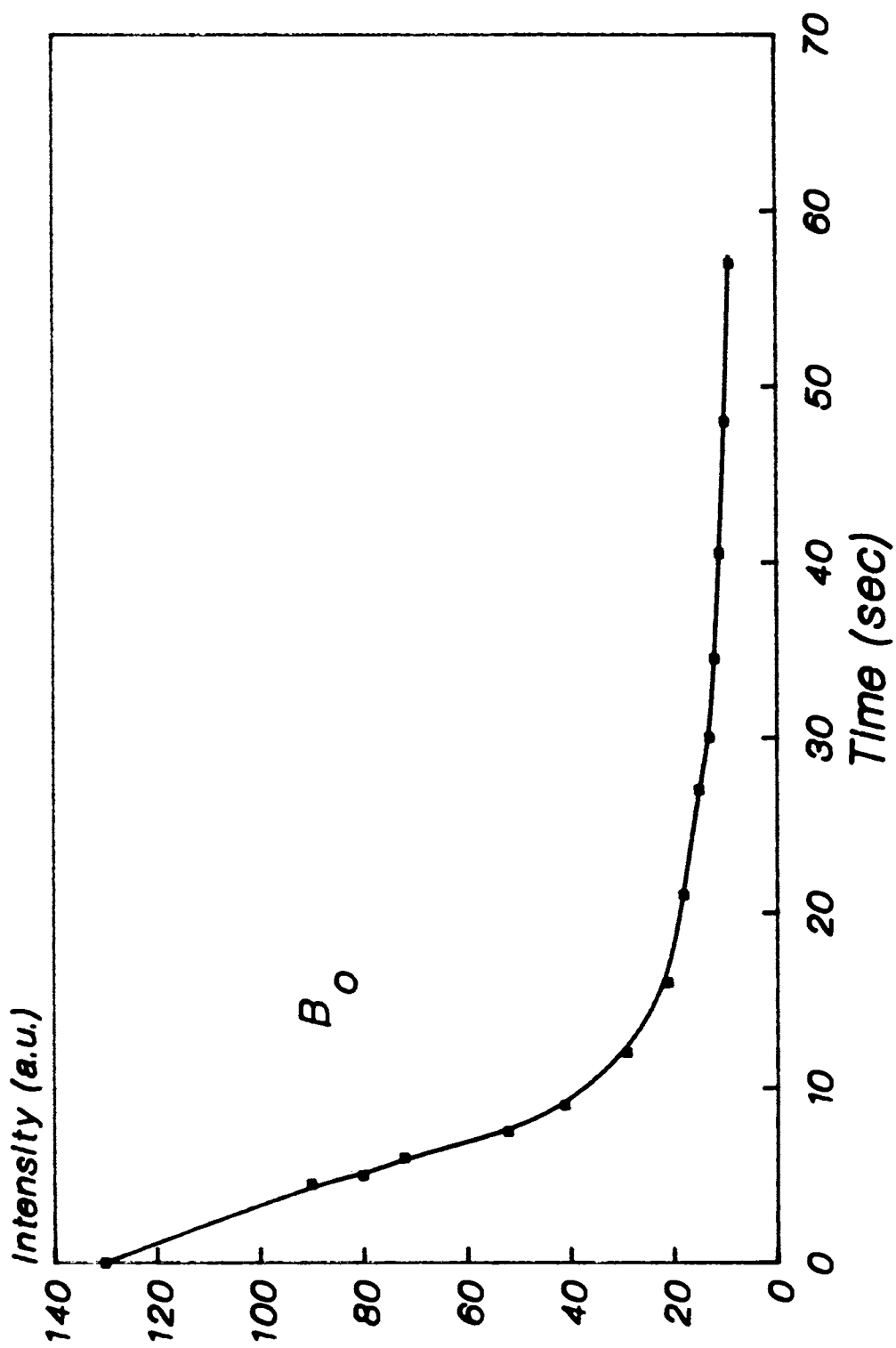


Fig 6.1 (a) Phosphorescence Intensity (I) vs time (t) plot for self-activated BaS phosphor

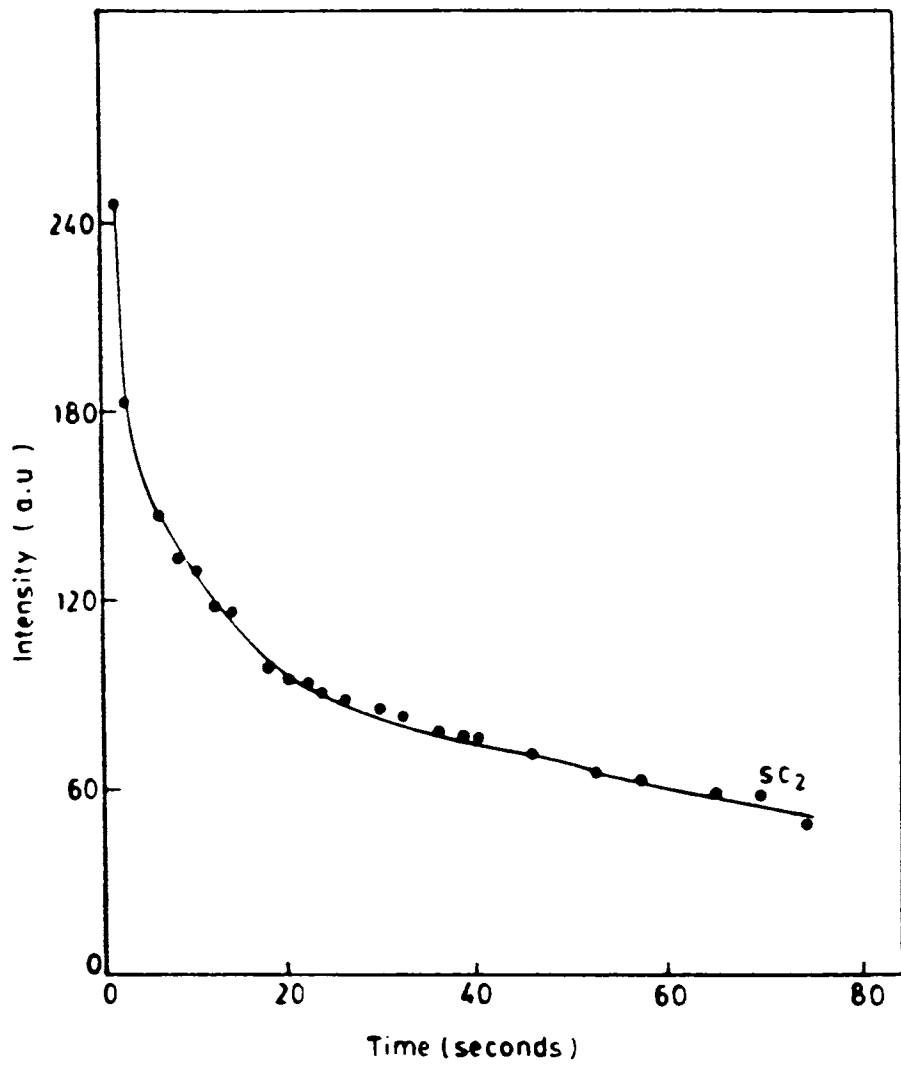


Fig 6.1 (b) Phosphorescence Intensity (I) vs time (t) plot for BaS:Cu phosphor

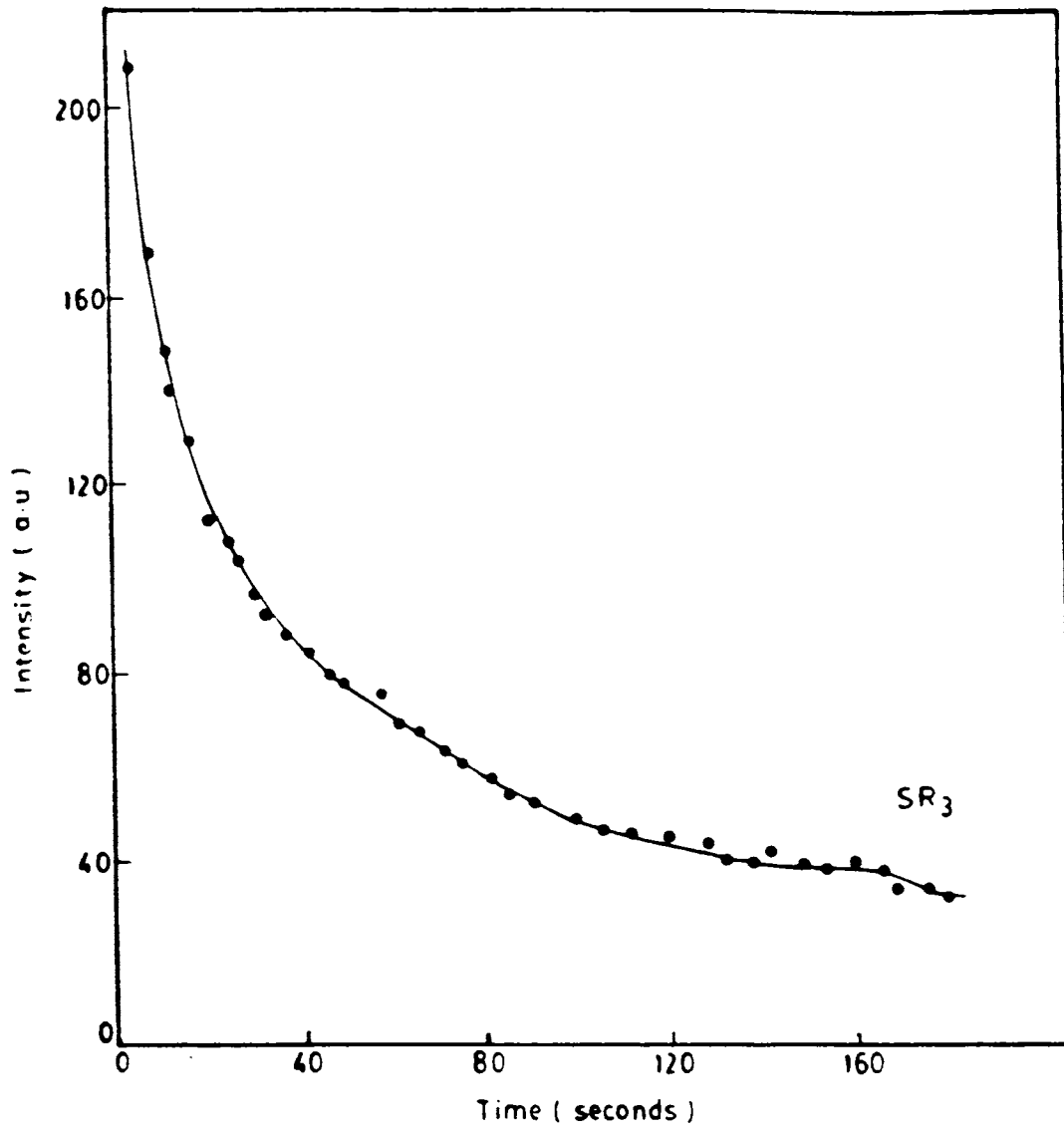


Fig 6.1 (c) Phosphorescence Intensity (I) vs time (t) plot for BaS:Ce phosphor

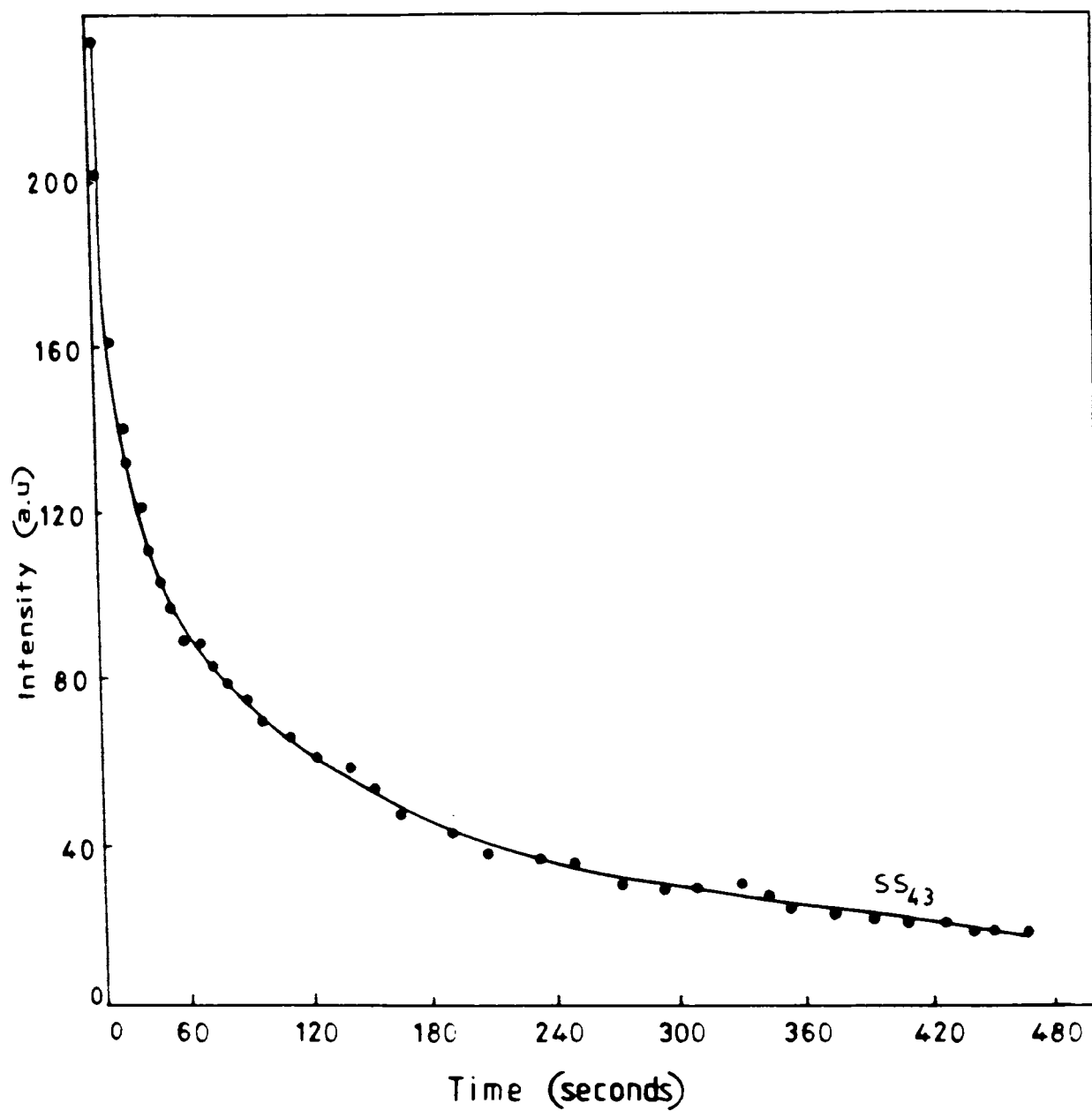


Fig 6.1 (d) Phosphorescence Intensity (I) vs time (t) plot for BaS:Ce:Cu phosphor

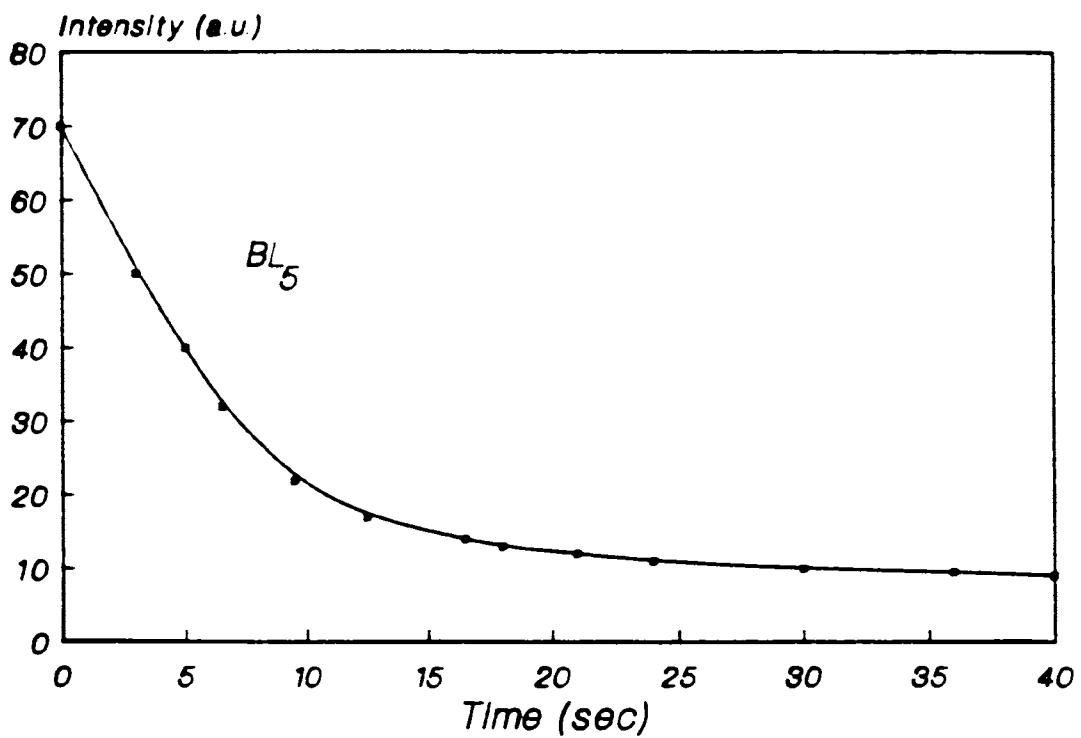


Fig 6.1 (e) Phosphorescence Intensity (I) vs time (t) plot for BaS:La phosphor

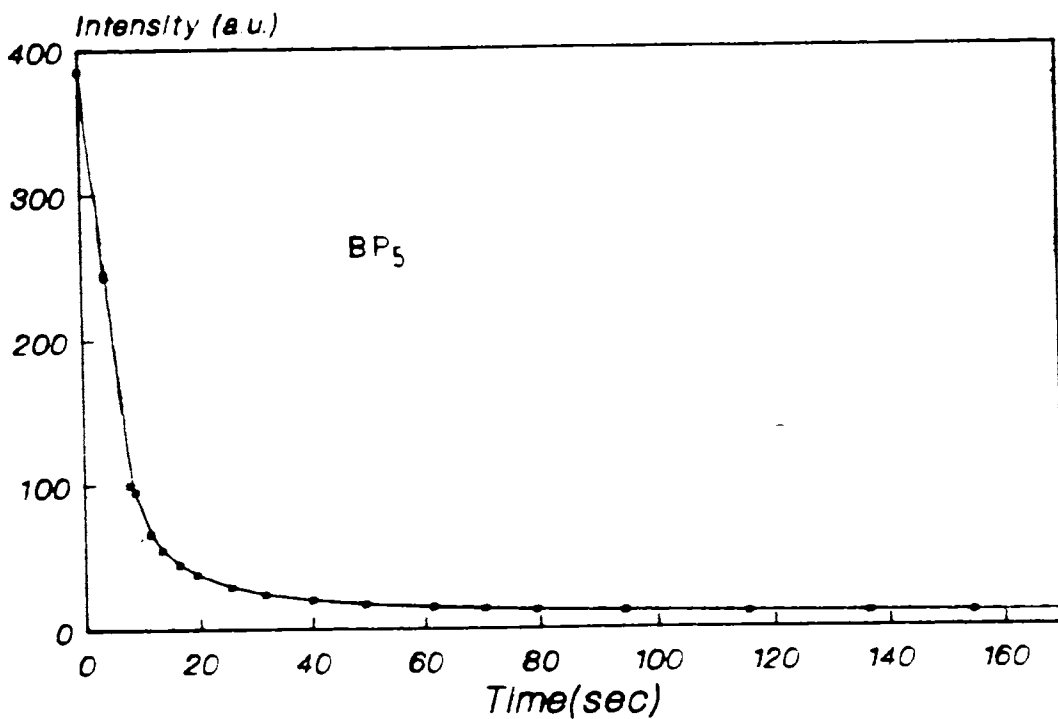


Fig 6.1 (f) Phosphorescence Intensity (I) vs time (t) plot for BaS:Pr phosphor



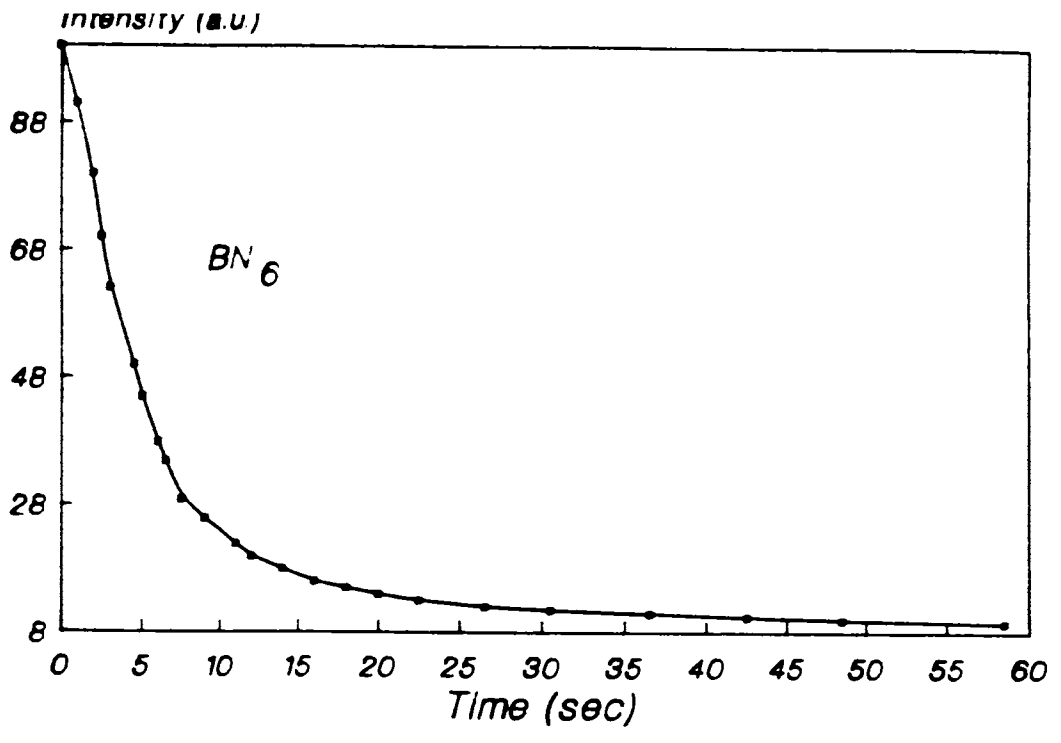


Fig 6.1 (g) Phosphorescence Intensity (I) vs time (t) plot for BaS:Nd phosphor

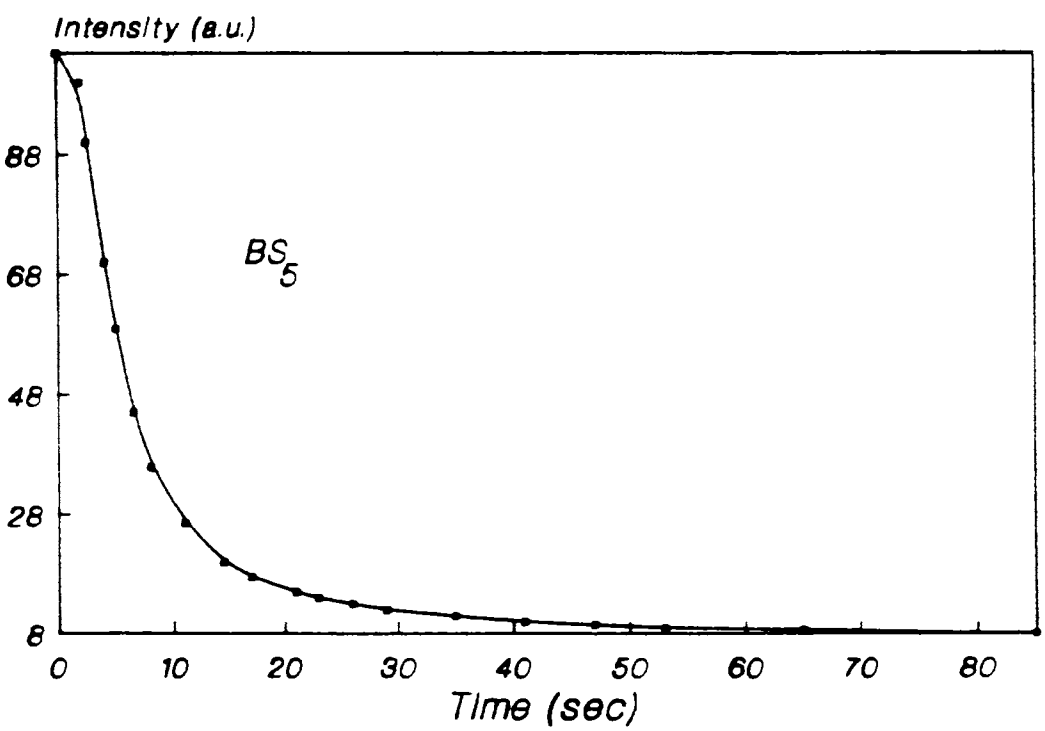


Fig 6.1 (h) Phosphorescence Intensity (I) vs time (t) plot for BaS:Sm phosphor

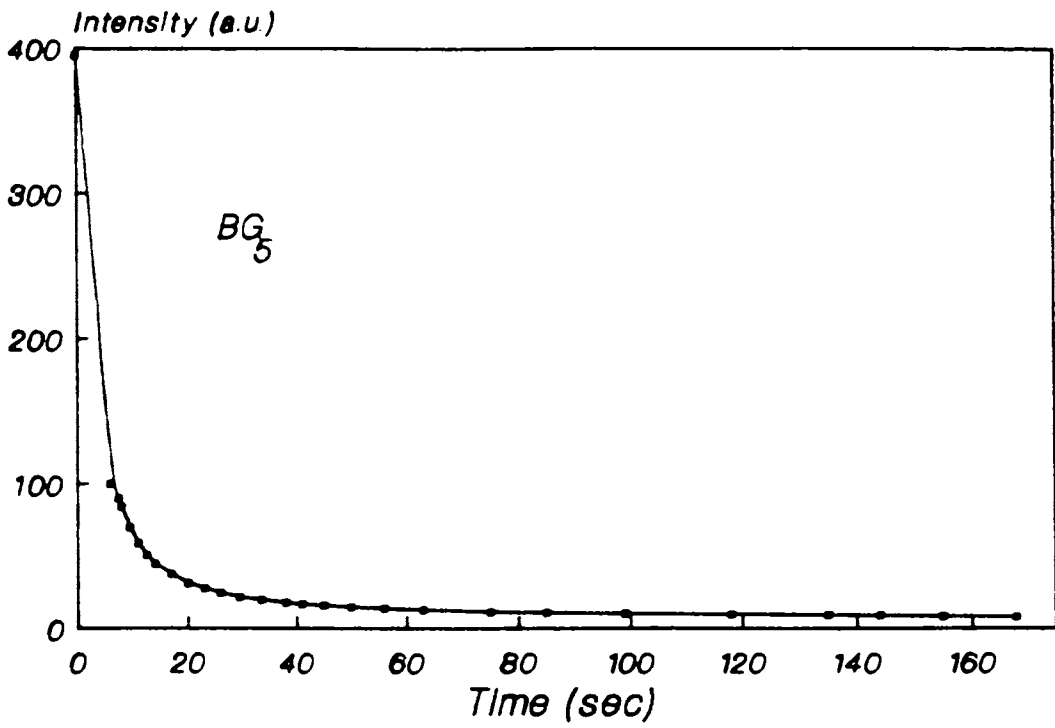


Fig 6.1 (i) Phosphorescence Intensity (I) vs time (t) plot for BaS:Gd phosphor

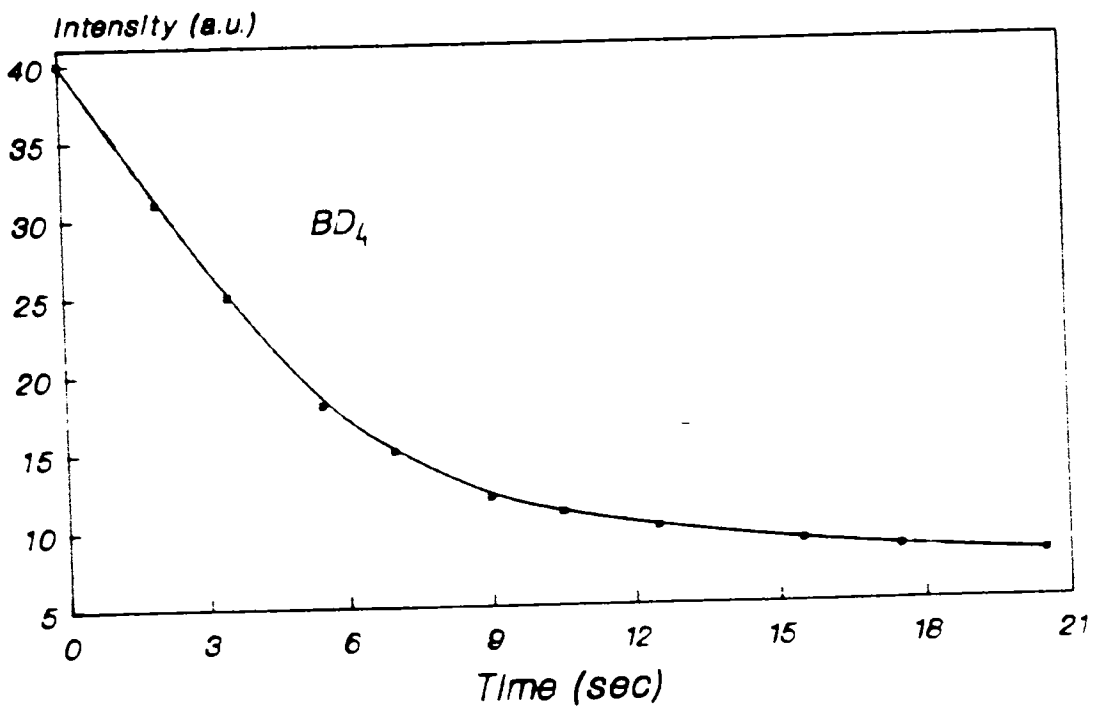


Fig 6.1 (j) Phosphorescence Intensity (I) vs time (t) plot for BaS:Dy phosphor

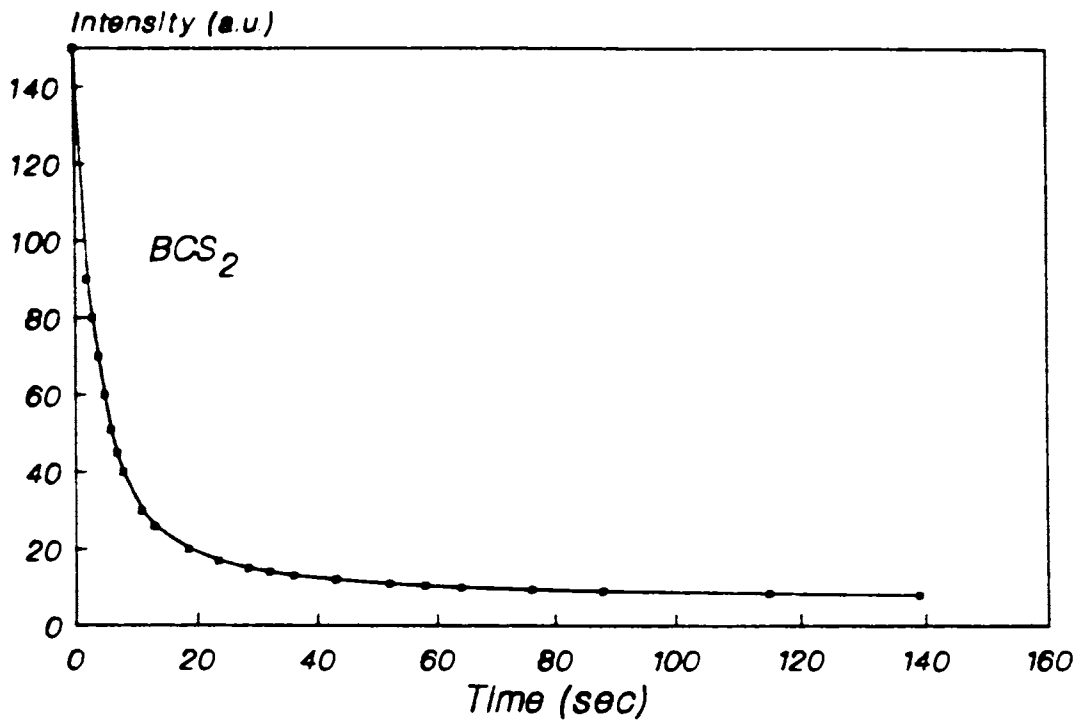


Fig 6.1 (k) Phosphorescence Intensity (I) vs time (t) plot for BaS:Cu:Sm phosphor

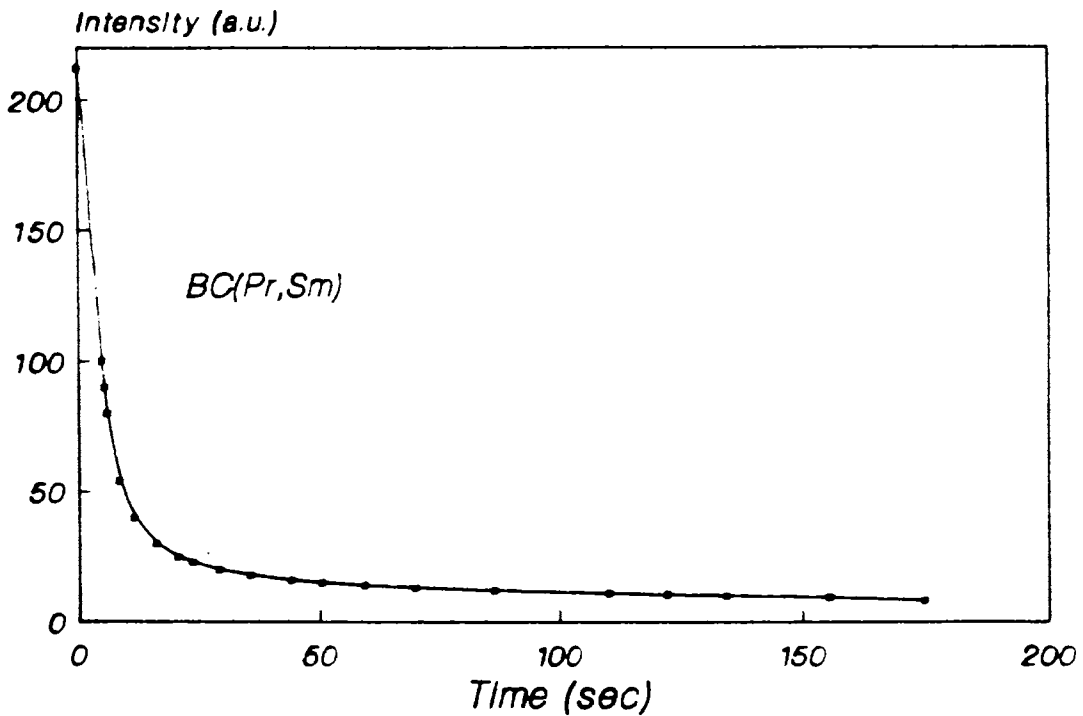


Fig 6.1 (l) Phosphorescence Intensity (I) vs time (t) plot for (BaS:Cu)Pr:Sm phosphor

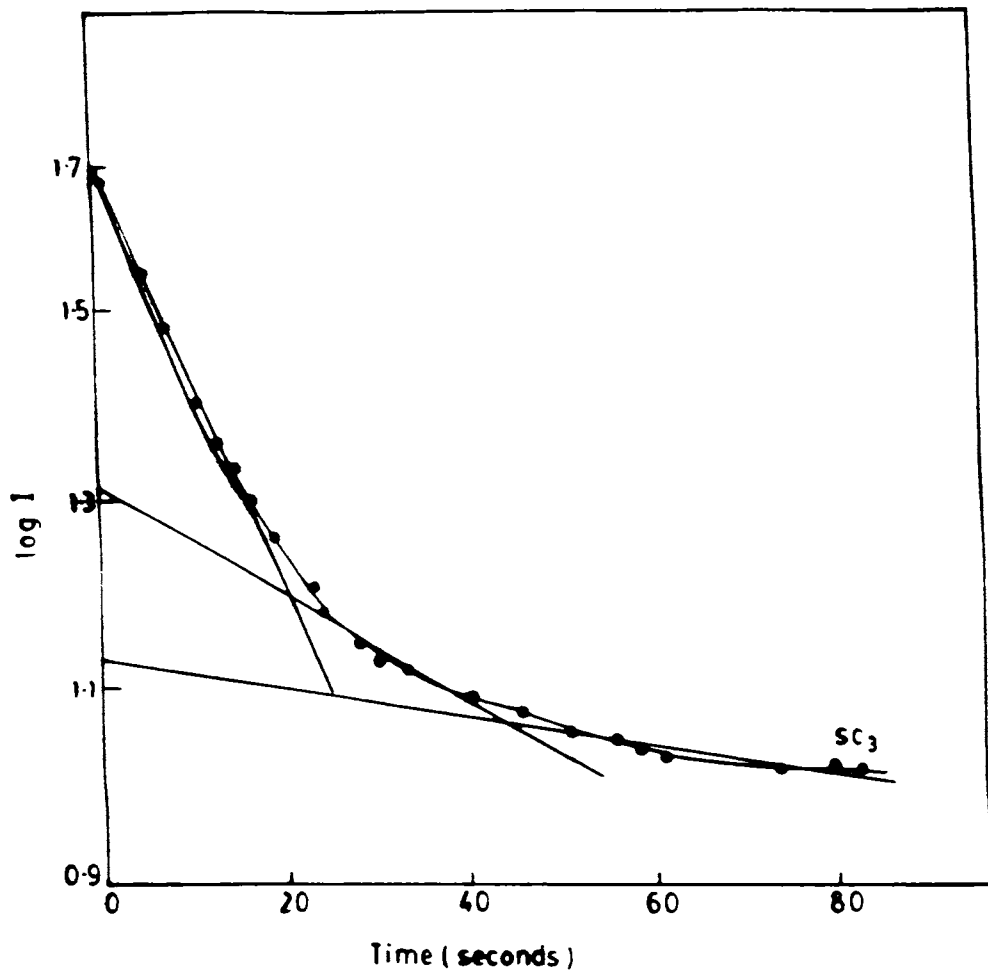


Fig 6.2 (a) Logarithm of decay intensity (log I) vs time (t) plot for BaS:Cu phosphor

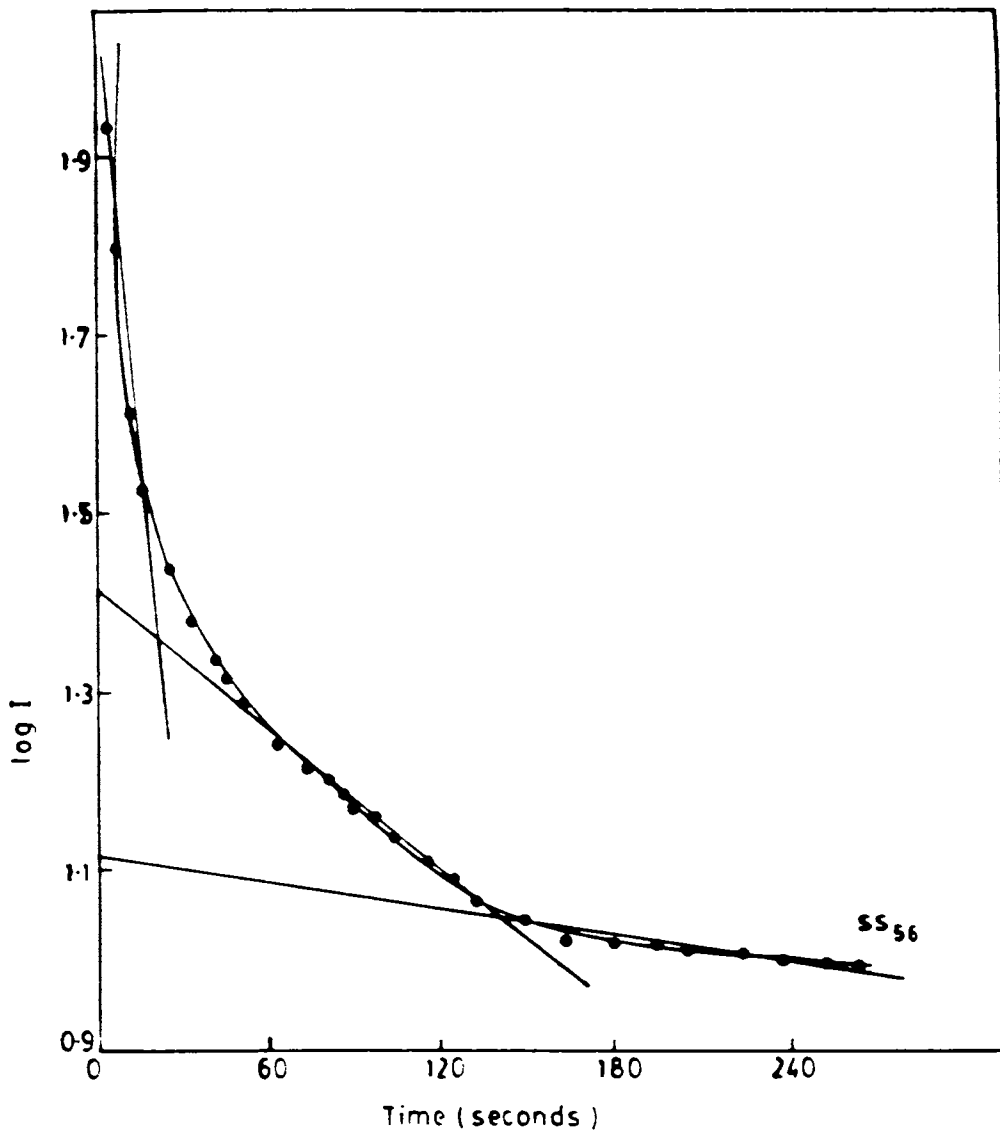


Fig 6.2 (b) **Logarithm of decay intensity (log I) vs time (t) plot for BaS:Ce:Cu phosphor**

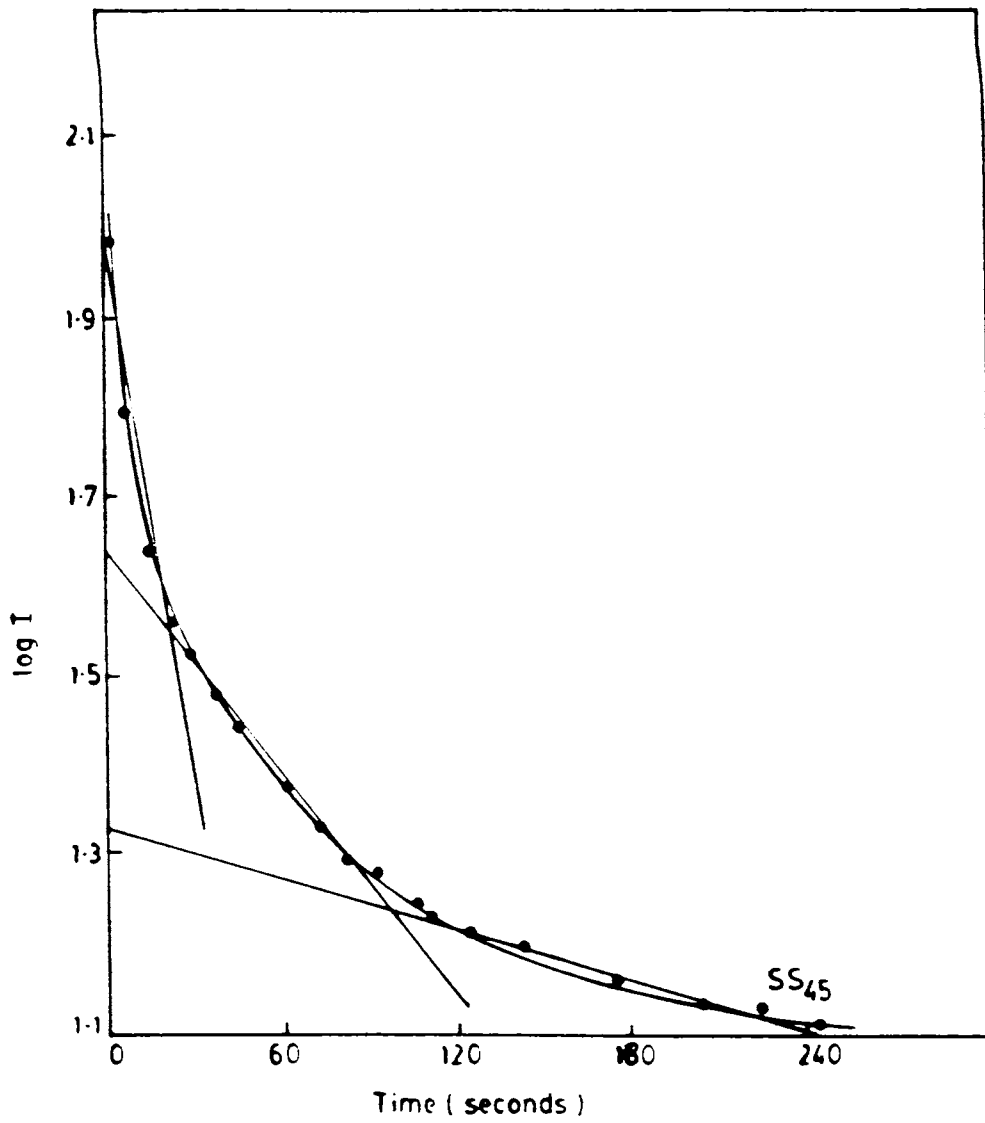


Fig 6.2 (c) Logarithm of decay intensity (log I) vs time (t) plot for BaS:Ce:Cu phosphor

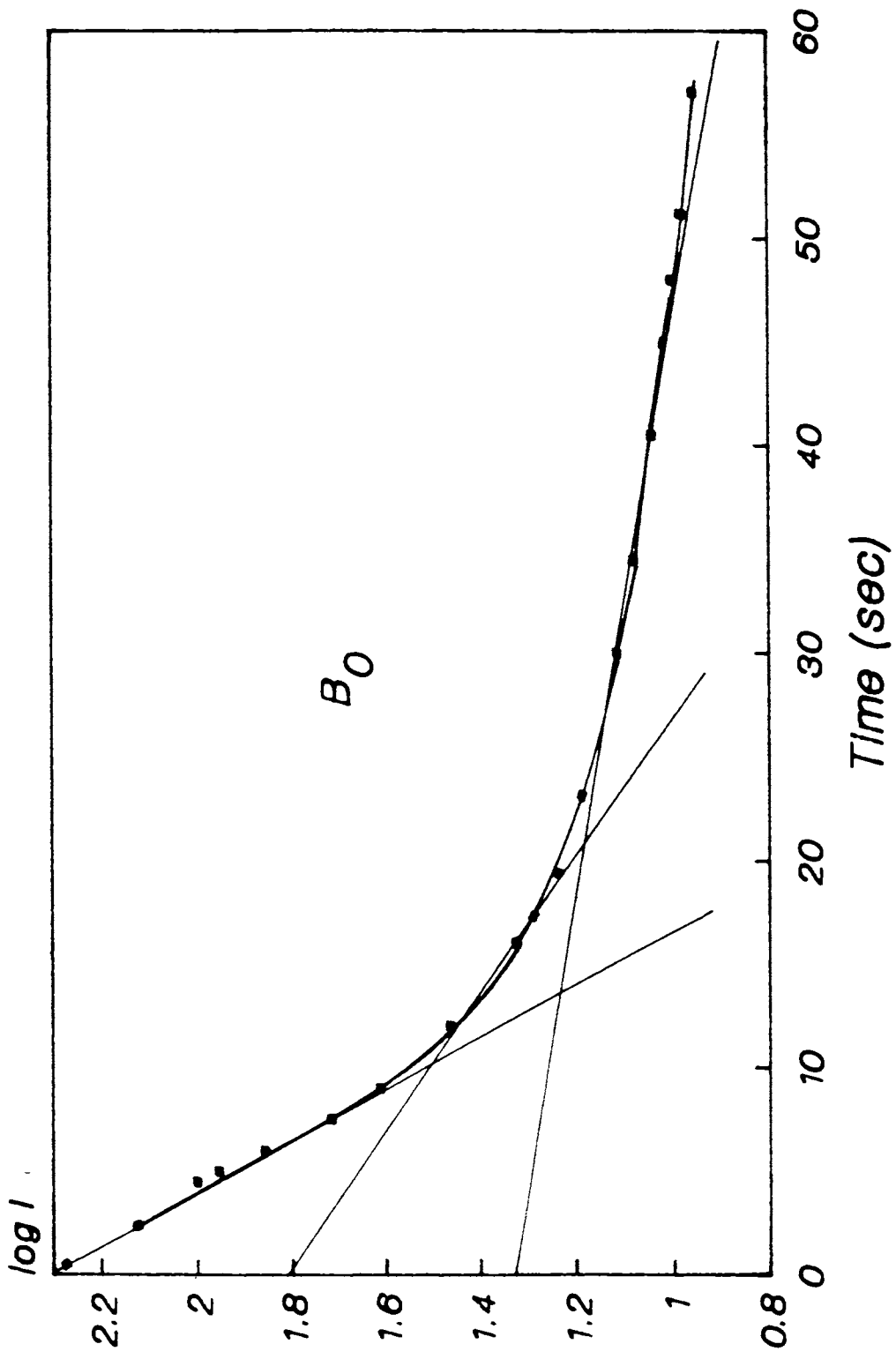


Fig 6.2 (d) Logarithm of decay intensity ( $\log I$ ) vs time (t) plot for BaS phosphor

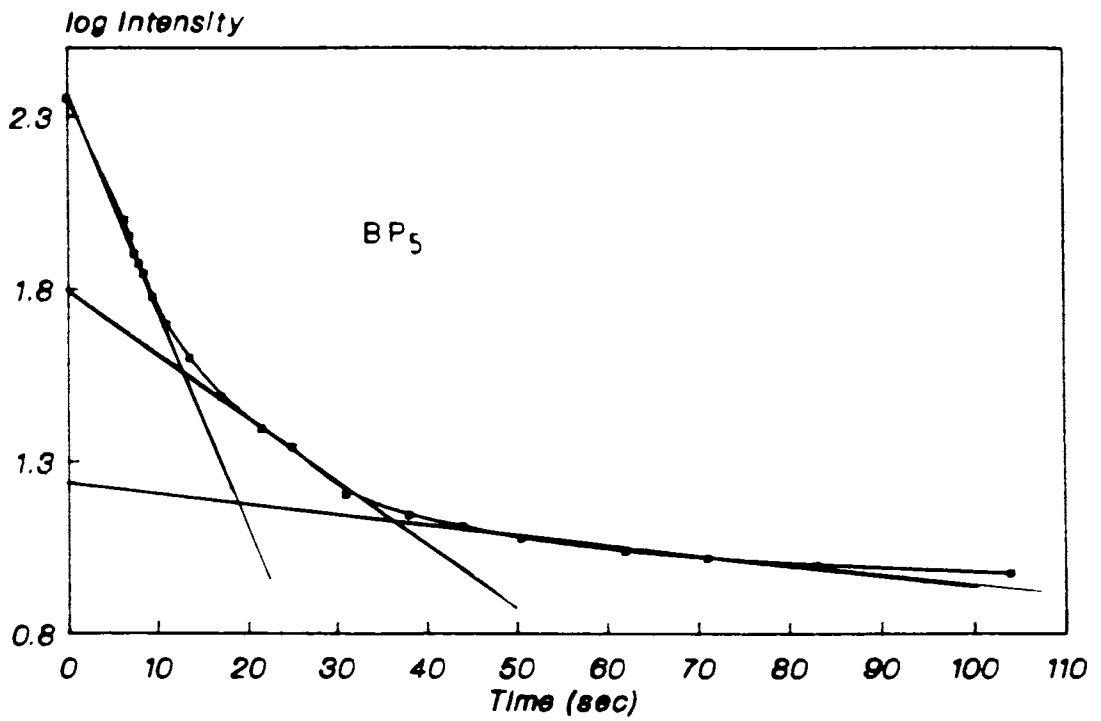


Fig 6.2 (e) Logarithm of decay intensity ( $\log I$ ) vs time ( $t$ ) plot for BaS:Pr phosphor

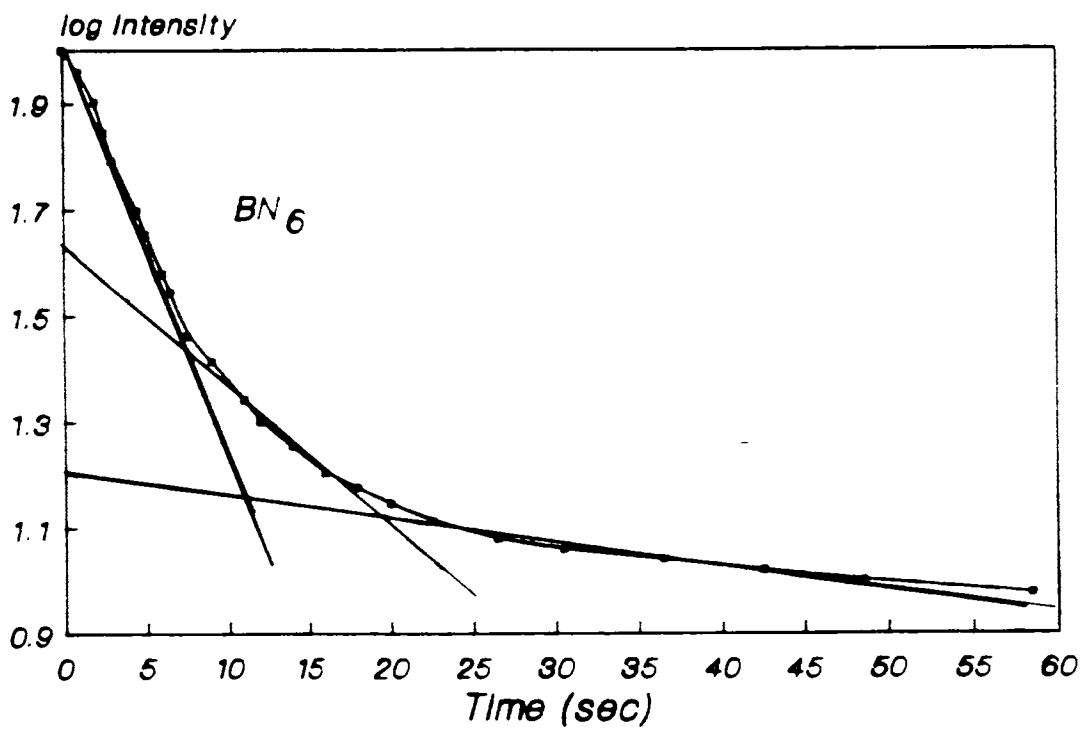


Fig 6.2 (f) Logarithm of decay intensity ( $\log I$ ) vs time ( $t$ ) plot for BaS:Nd phosphor



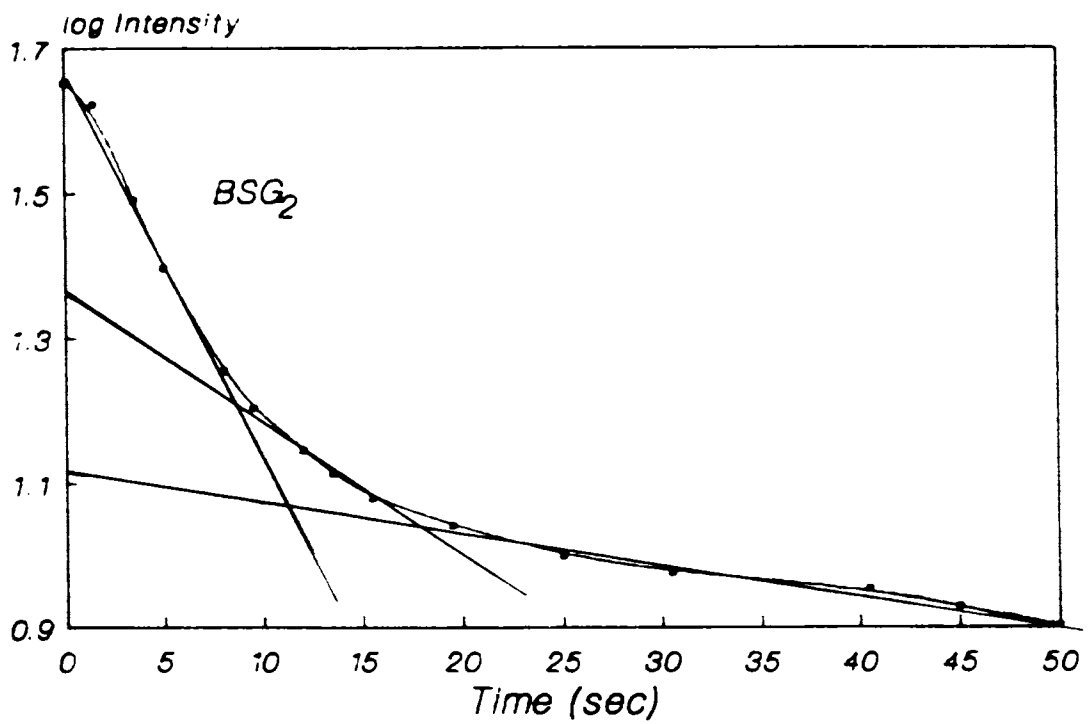


Fig 6.2 (g) Logarithm of decay intensity ( $\log I$ ) vs time ( $t$ ) plot for BaS:Sm:Gd phosphor

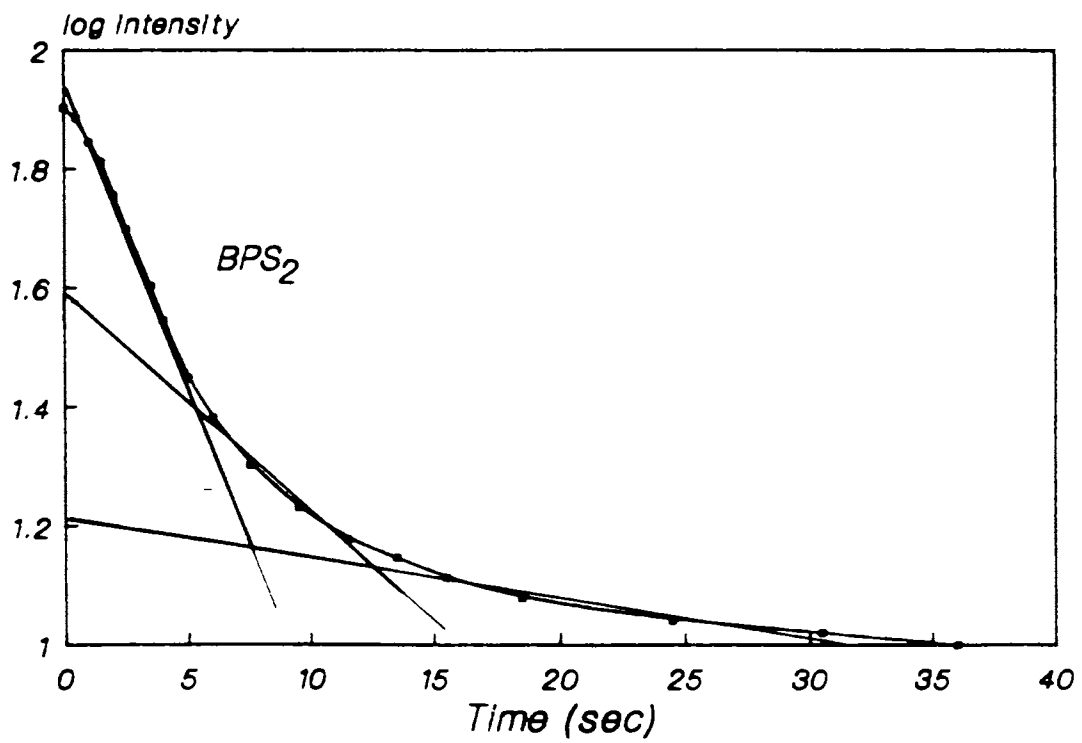


Fig 6.2 (h) Logarithm of decay intensity ( $\log I$ ) vs time ( $t$ ) plot for BaS:Pr:Sm phosphor

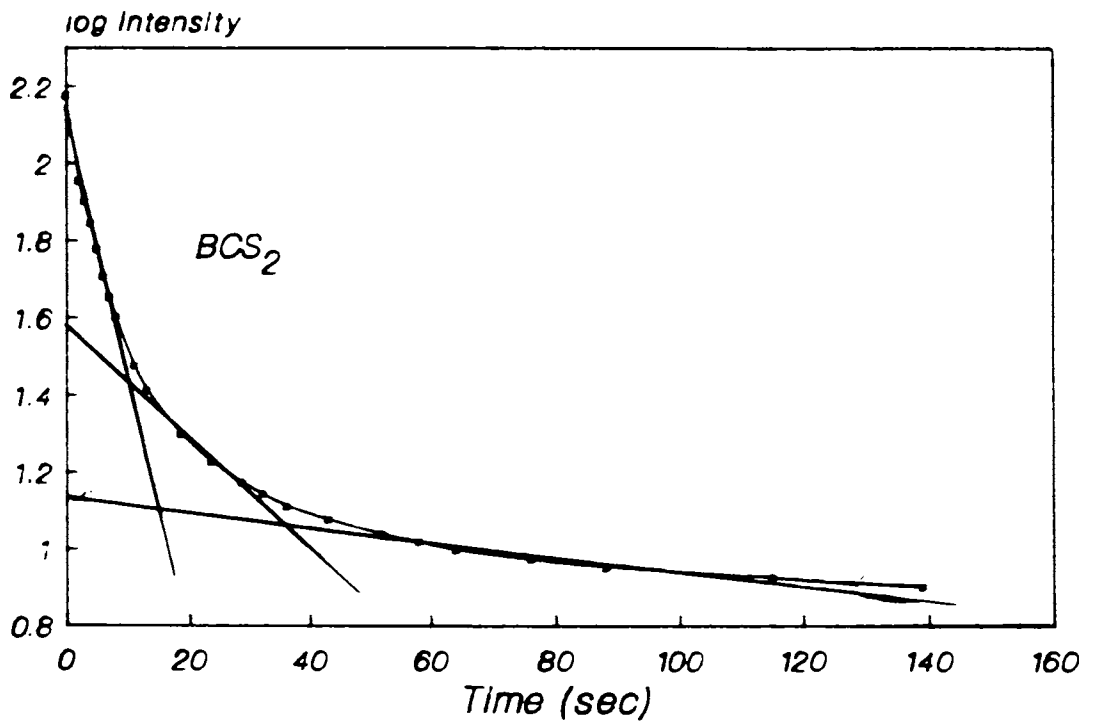


Fig 6.2 (i) Logarithm of decay intensity ( $\log I$ ) vs time ( $t$ ) plot for BaS:Cu:Sm phosphor

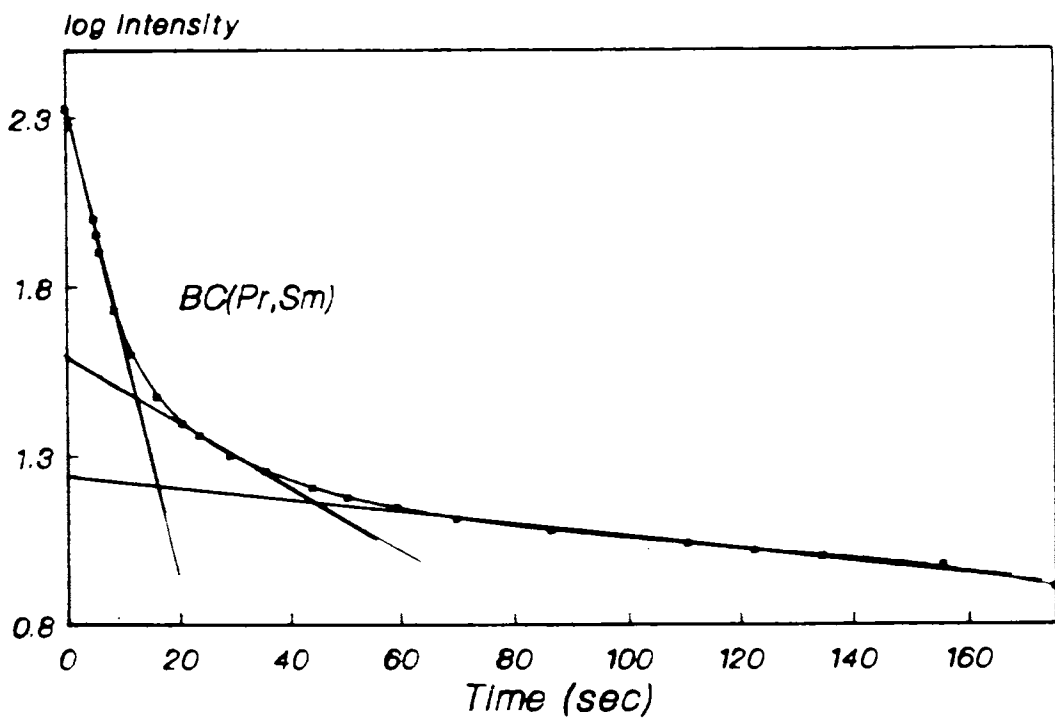


Fig 6.2 (j) Logarithm of decay intensity ( $\log I$ ) vs time ( $t$ ) plot for (BaS:Cu):Pr:Sm phosphor

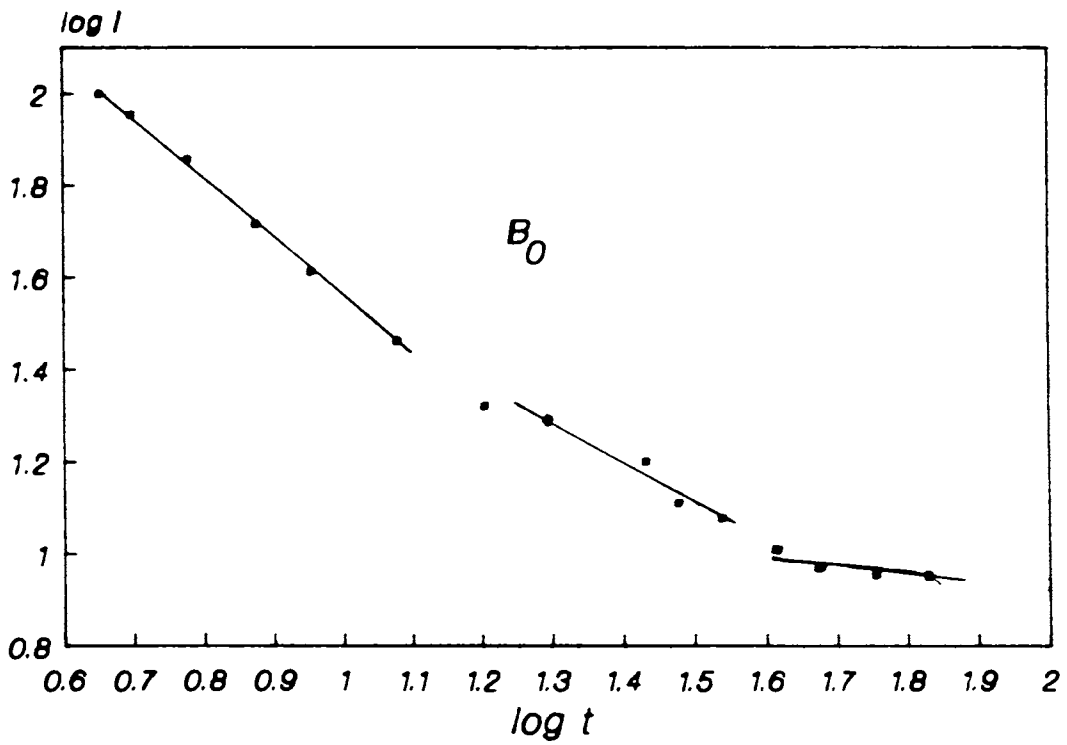


Fig. 6.3 (a) log I vs log t plot for self activated BaS phosphor

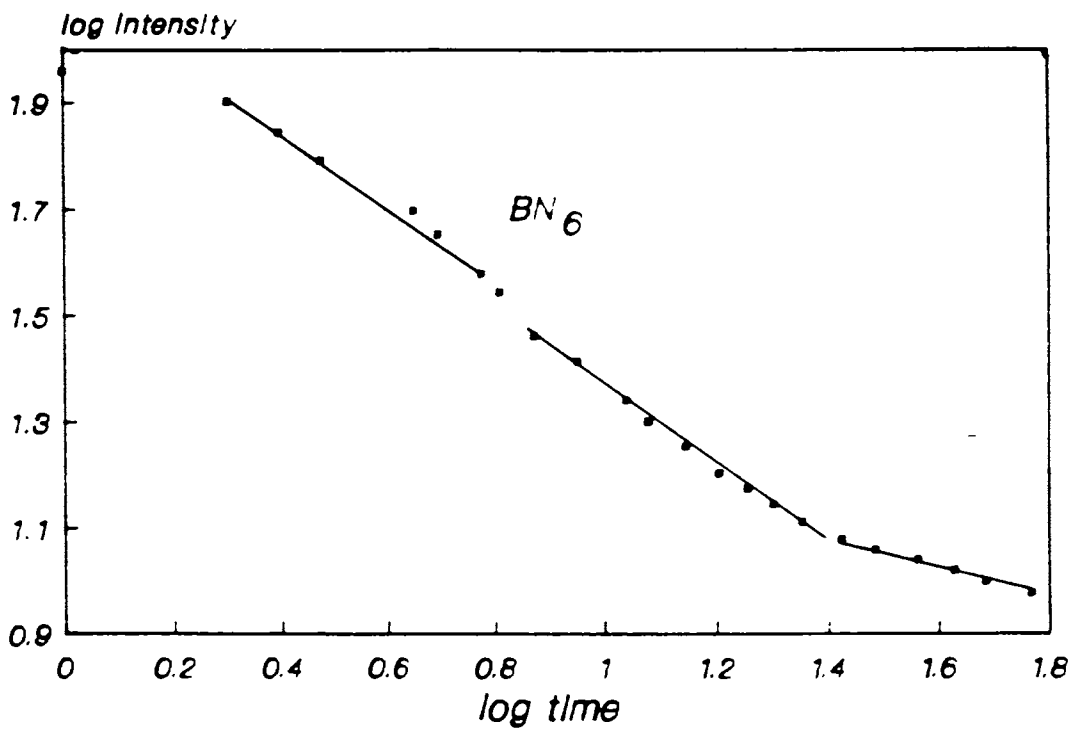


Fig 6.3 (b) log I vs log t plot for BaS:Nd phosphor

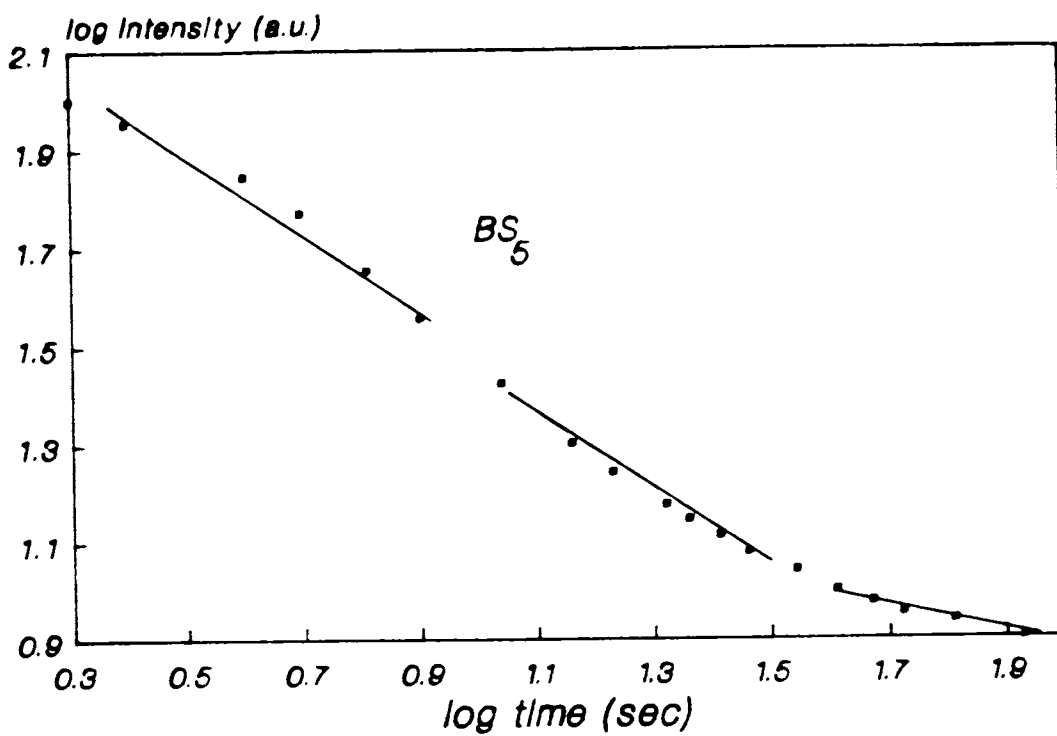


Fig. 6.3 (c) log I vs log t plot for BaS:Sm phosphor

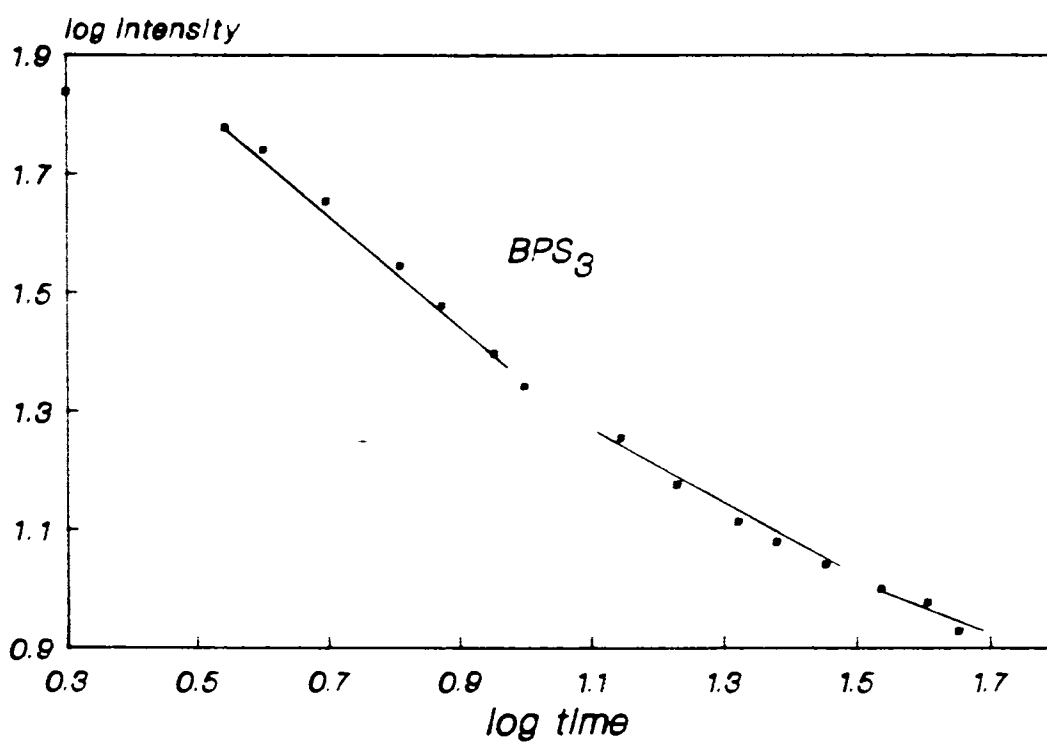


Fig. 6.3 (d) log I vs log t plot for BaS:Pr:Sm phosphor

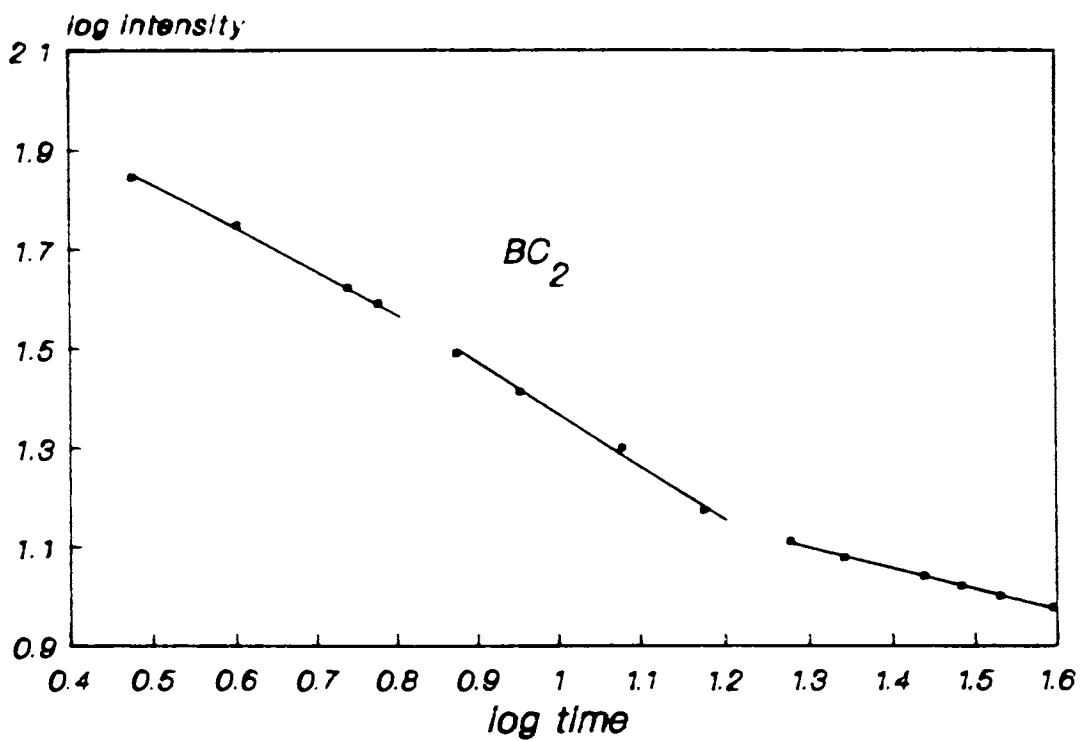


Fig. 6.3 (e) log I vs log t plot for BaS:Cu phosphor

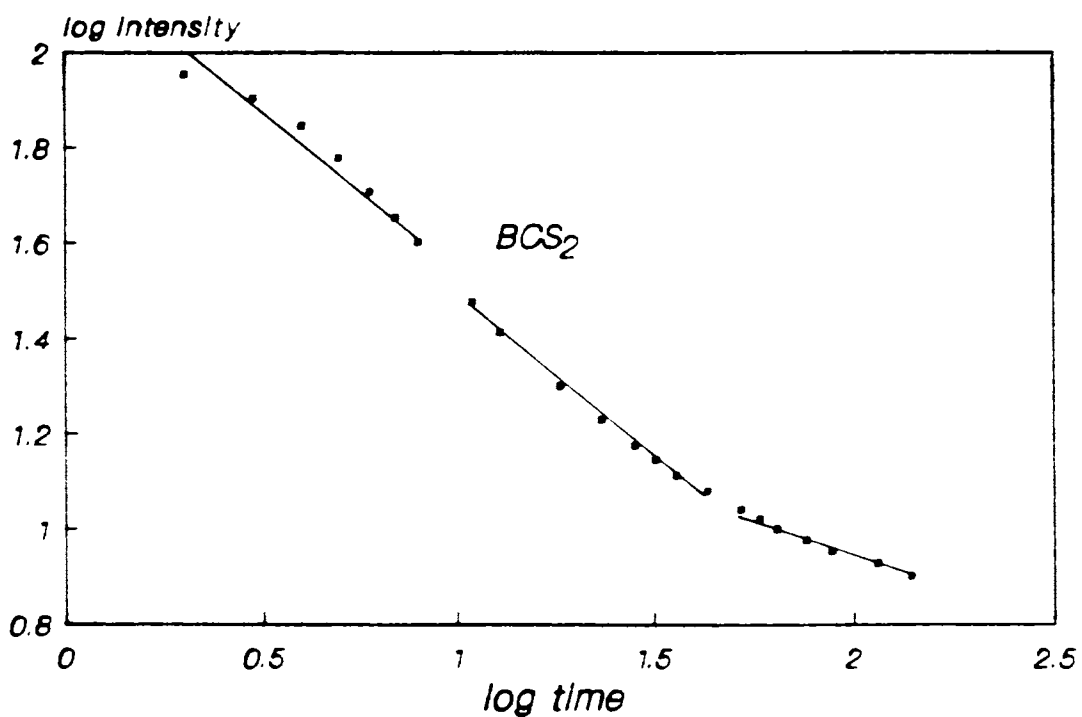


Fig. 6.3 (f) log I vs log t plot for BaS:Cu:Sm phosphor

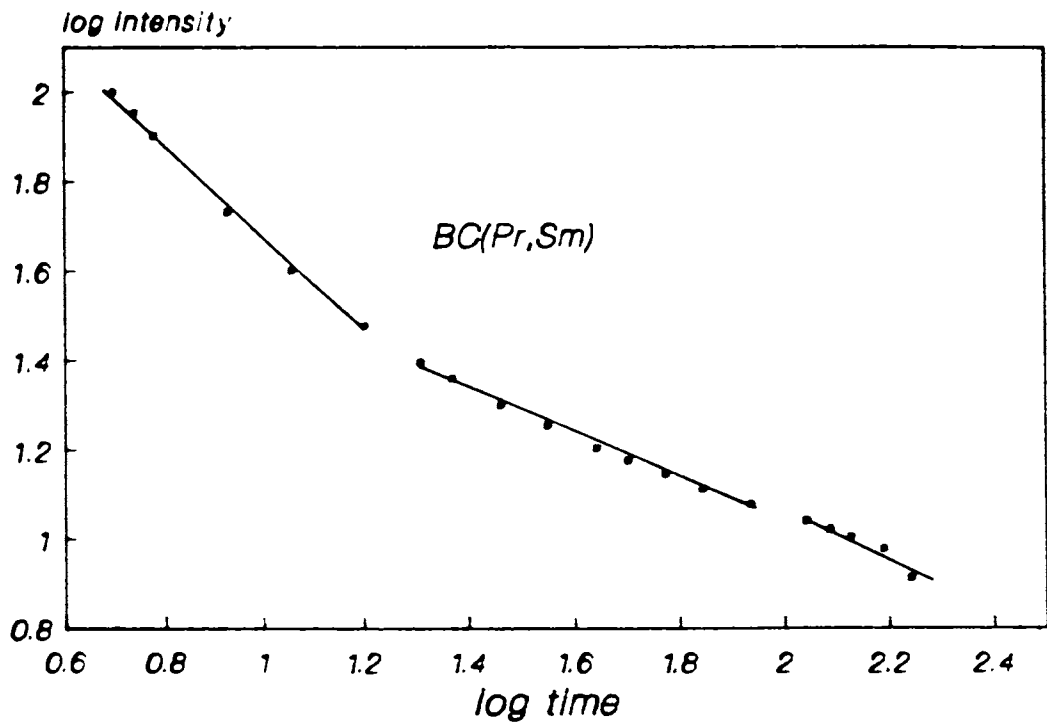


Fig. 6.3 (g) log I vs log t plot for (BaS:Cu): Pr:Sm phosphor

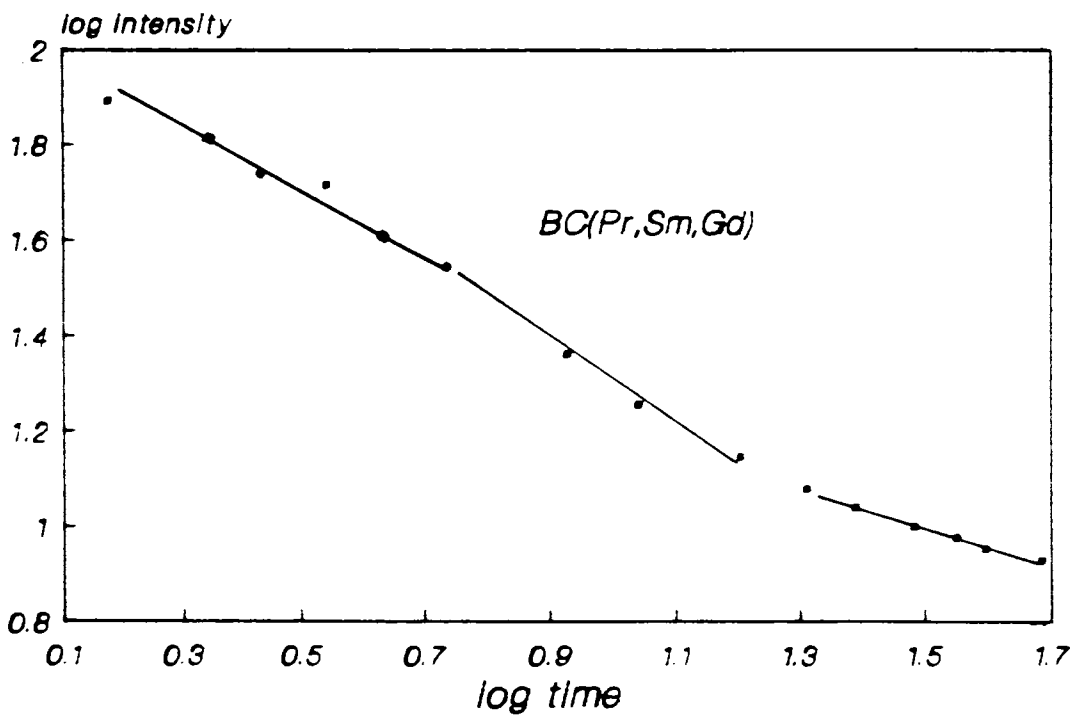


Fig. 6.3 (h) log I vs log t plot for (BaS:Cu):Pr:Sm:Gd phosphor

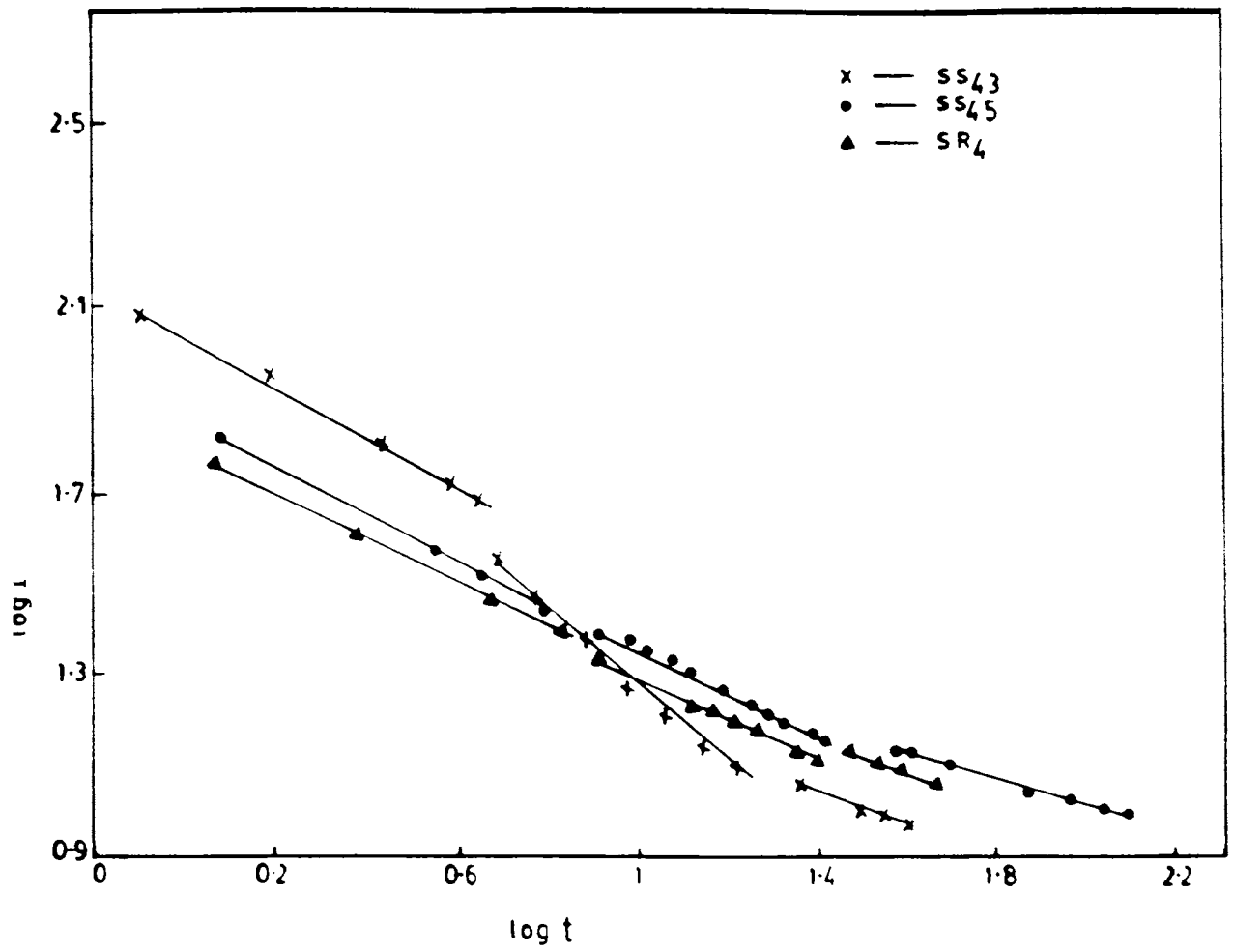


Fig 6.3(i) Logarithm of Intensity ( $\log I$ ) vs  $\log t$  plots for BaS:Ce:Cu and BaS:Ce phosphors

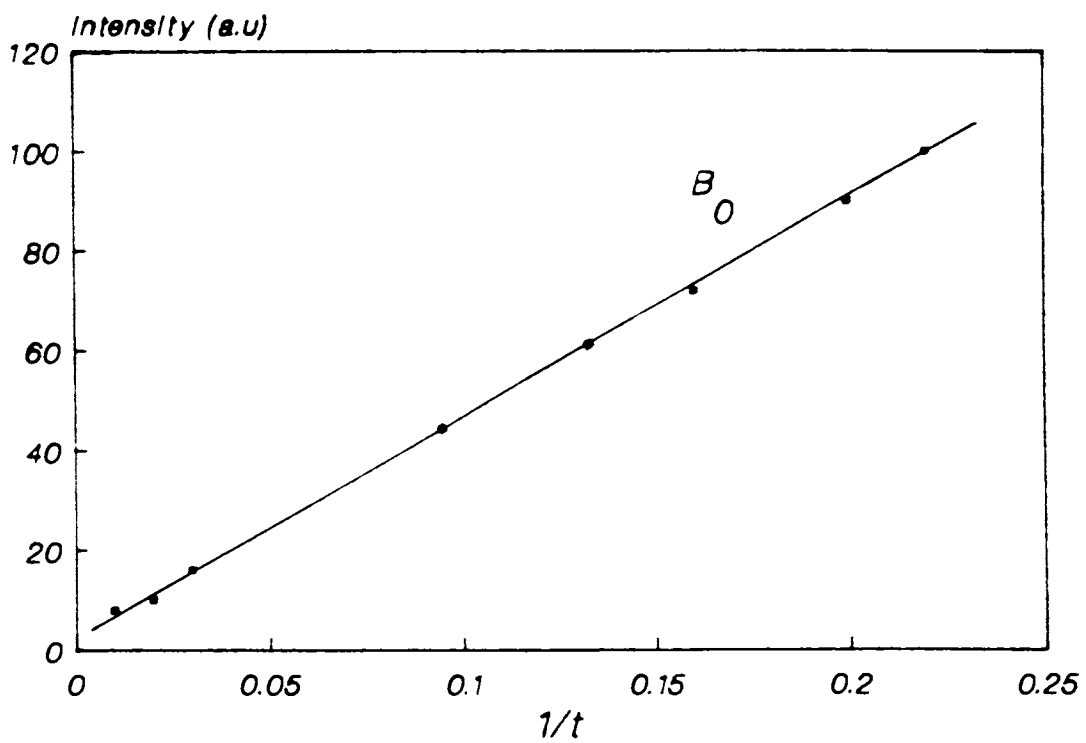


Fig 6.4 (a) I vs  $1/t$  plot for self activated BaS phosphor

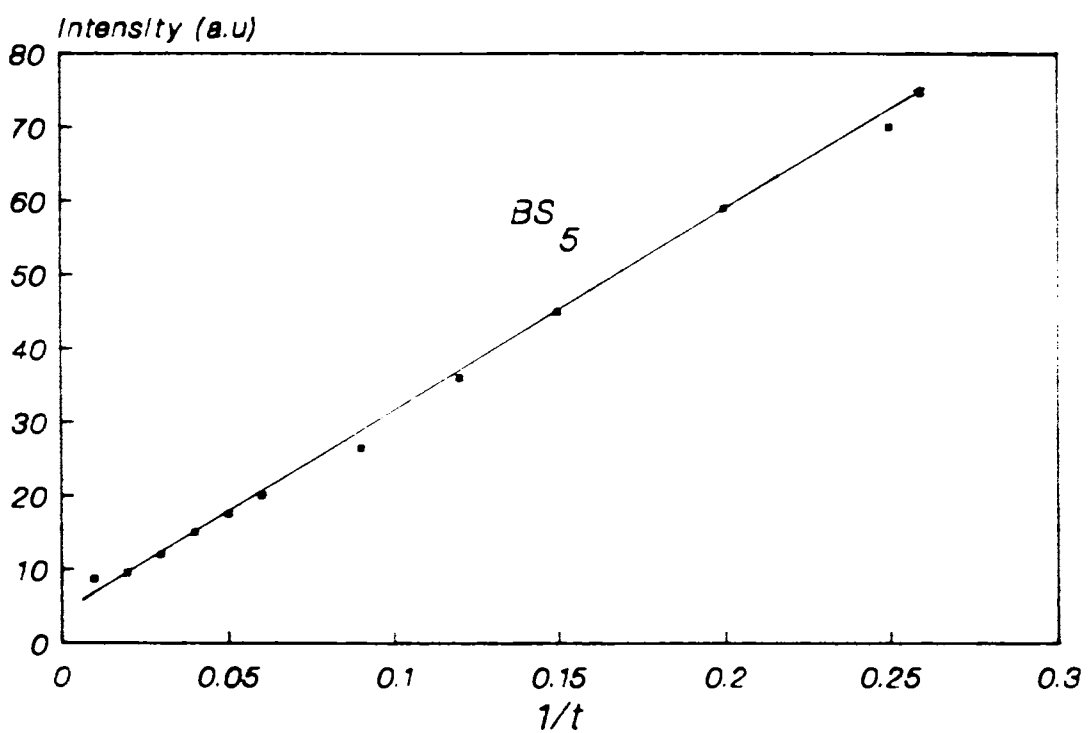


Fig 6.4 (b) I vs  $1/t$  plot for BaS:Sm Phosphor



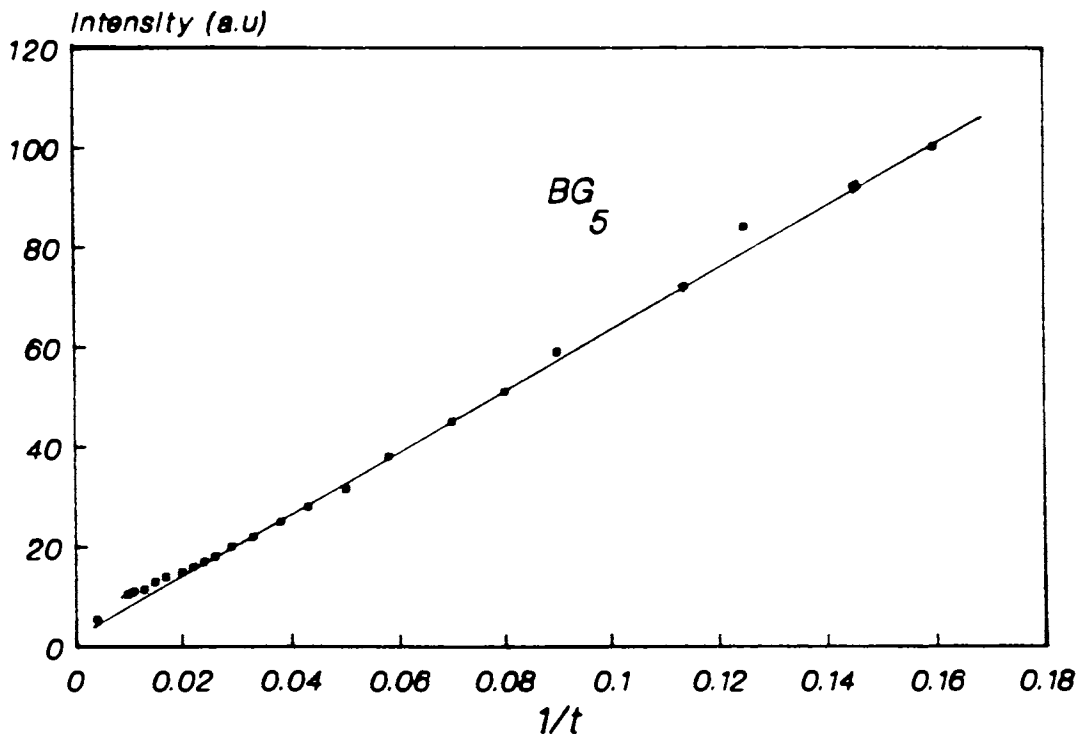


Fig 6.4 (c) I vs  $1/t$  plot for BaS:Gd Phosphor

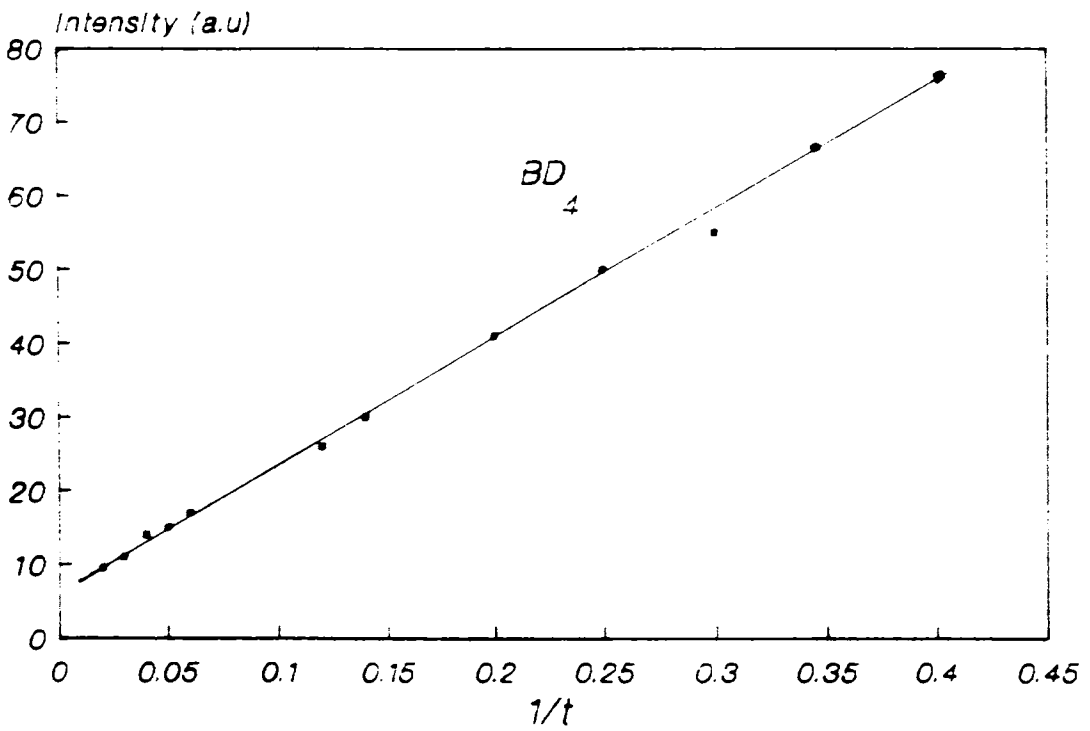


Fig 6.4 (d) I vs  $1/t$  plot for BaS:Dy Phosphor

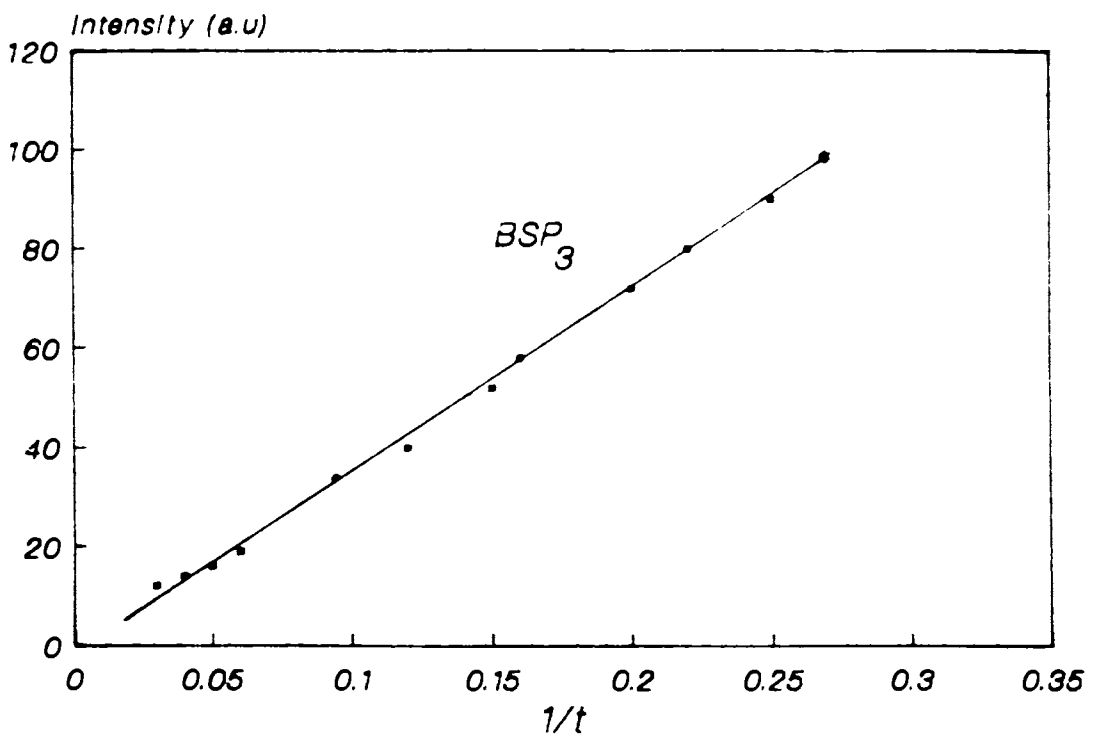


Fig 6.4 (e) I vs 1/t plot for BaS:Sm:Pr Phosphor

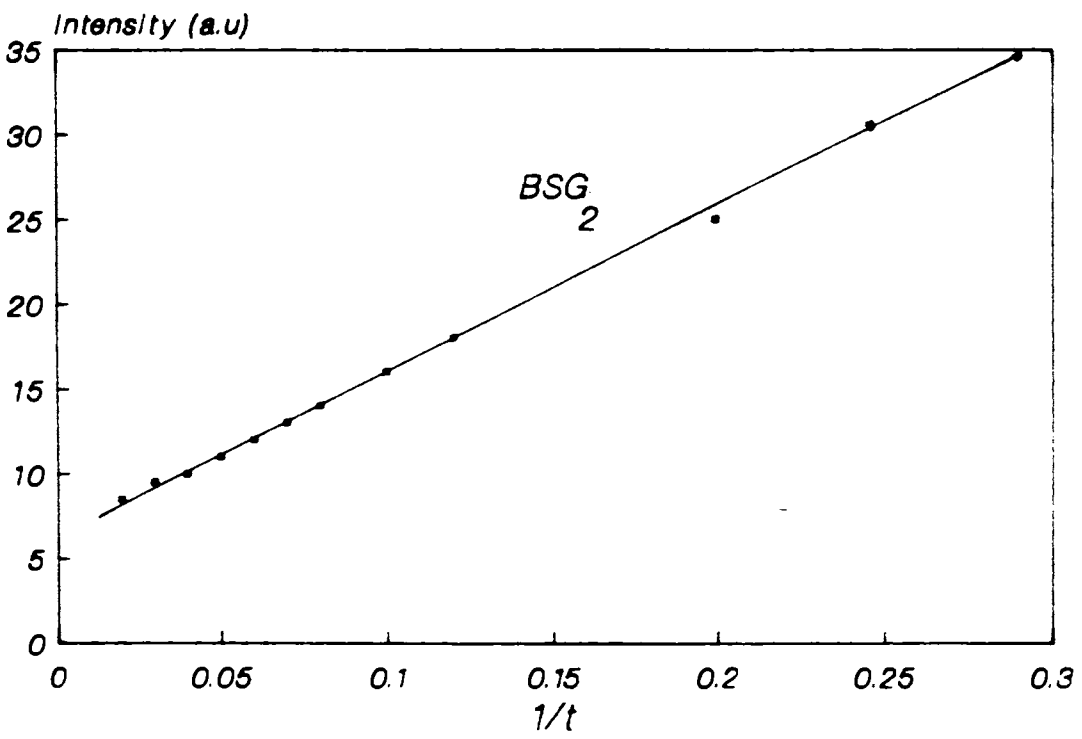


Fig 6.4 (f) I vs 1/t plot for BaS;Sm:Gd Phosphor

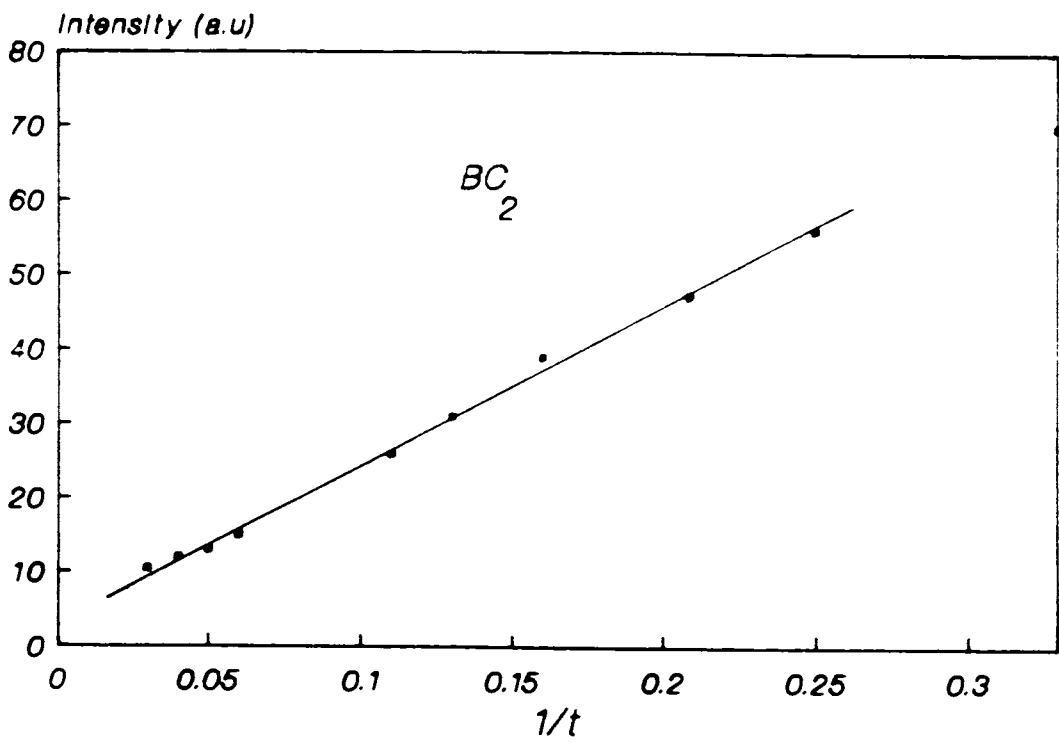


Fig 6.4 (g) I vs 1/t plot for BaS:Cu Phosphor

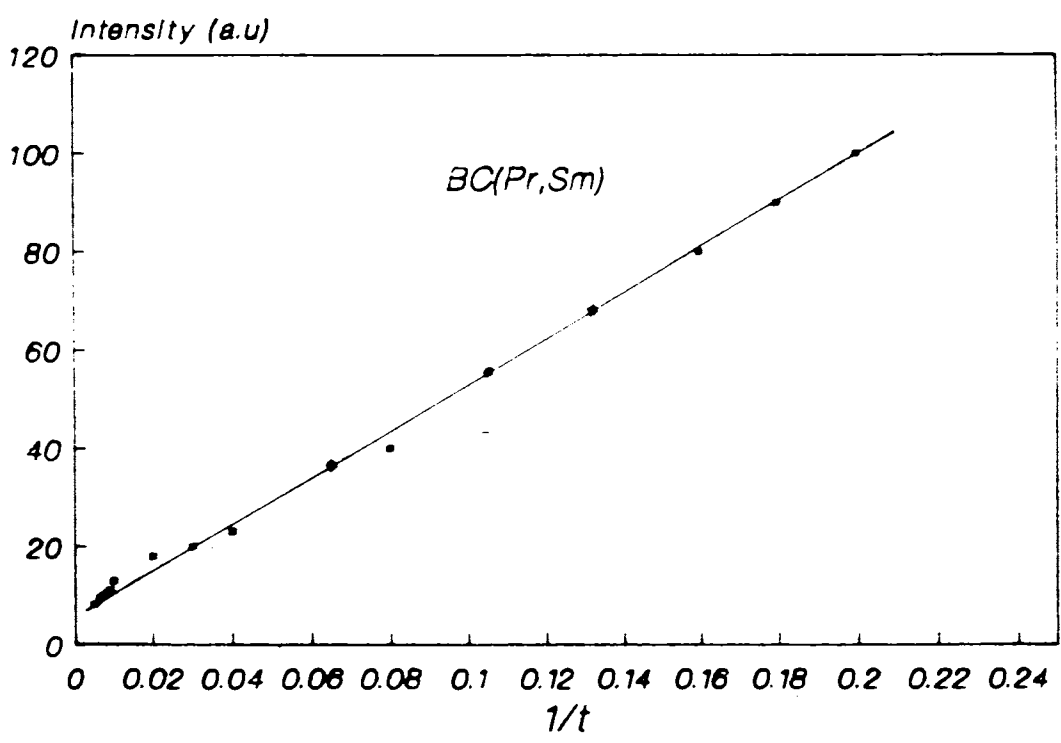


Fig 6.4 (h) I vs 1/t plot for (BaS:Cu)Pr:Sm Phosphor

### 6.3. Evaluation of Trap Depth - E (eV)

It has been found that the phosphorescence emission from phosphors under consideration can be described in terms of three exponentials. The trap depths corresponding to the three exponentials were calculated using the relation

$$E = KT \log (S/\alpha) \quad 6.(4)$$

where ' $\alpha$ ' is slope of the each linear portion of the semi-log plot. Here the escape frequency factor 'S' is taken as  $10^6$ /sec as obtained from TL analysis [given in the last chapter]. The calculated values of trap depths for these regions of the semi-log plots are given in Table 6.1 (a) and 6.1 (b).

Table. 6.1(a)						
Trapdepth values and Electron population ratios of phosphor samples prepared by method I						
Sample Notation	Trapth depth values 'E' (eV)			$N_n(t)_{t=0} / N_n(t)_{t=5}$ for three 'peeled off' components		
	Fastest exponential $E_1$	Middle exponential $E_2$	Slowest exponential $E_3$	Fastest exponential	Middle exponential	Slowest exponential
SR <sub>1</sub>	0.46	0.49	0.53	1.15	1.04	1.01
SR <sub>2</sub>	0.46	0.50	0.54	1.17	1.03	1.01
SR <sub>5</sub>	0.44	0.5	0.55	1.25	1.04	1.02
SR <sub>6</sub>	0.44	0.51	0.56	1.18	1.03	1.01
SR <sub>7</sub>	0.50	0.54	0.54	1.17	1.07	1.01
SR <sub>8</sub>	0.47	0.51	0.52	1.15	1.08	1.02
SC <sub>2</sub>	0.43	0.49	0.51	1.18	1.03	1.01
SC <sub>3</sub>	0.42	0.48	0.51	1.25	1.18	1.07
SC <sub>4</sub>	0.42	0.46	0.5	1.9	1.16	1.09
SC <sub>5</sub>	0.41	0.45	0.51	1.73	1.12	1.02

contd...

Sample Notation	Trapth depth values 'E' (eV)			$N_n(t)_{t=0} / N_n(t)_{t=5}$ for three 'peeled off' components		
	Fastest exponential $E_1$	Middle exponential $E_2$	Slowest exponential $E_3$	Fastest exponential	Middle exponential	Slowest exponential
SS <sub>41</sub>	0.41	0.49	0.51	1.95	1.11	1.02
SS <sub>42</sub>	0.44	0.47	0.55	2.13	1.07	1.03
SS <sub>43</sub>	0.45	0.47	0.53	3.21	1.03	1.07
SS <sub>45</sub>	0.43	0.46	0.54	2.41	1.46	1.09
SS <sub>56</sub>	0.40	0.44	0.57	2.5	1.33	1.07
SS <sub>57</sub>	0.42	0.43	0.51	1.98	1.11	1.07
SS <sub>58</sub>	0.43	0.44	0.55	2.11	1.33	1.09

Table. 6.1(b)						
Trapdepth values and Electron population ratios of phosphor samples prepared by method II						
Sample Notation	Trapth depth values 'E' (eV)			$N_n(t)_{t=0} / N_n(t)_{t=5}$ for three 'peeled off' components		
	Fastest exponential $E_1$	Middle exponential $E_2$	Slowest exponential $E_3$	Fastest exponential	Middle exponential	Slowest exponential
BL <sub>6</sub>	0.37	0.41	0.44	2.27	1.10	1.01
BP <sub>3</sub>	0.35	0.41	0.44	2.09	1.25	1.07
BP <sub>5</sub>	0.36	0.39	0.44	2.25	1.20	1.03
BP <sub>6</sub>	0.35	0.39	0.43	2.06	1.10	1.03
BP <sub>7</sub>	0.35	0.39	0.44	3.27	1.23	1.03

Sample Notation	Trapth depth values 'E' (eV)			$N_n(t)_{t=0} / N_n(t)_{t=5}$ for three 'peeled off' components		
	Fastest exponential $E_1$	Middle exponential $E_2$	Slowest exponential $E_3$	Fastest exponential	Middle exponential	Slowest exponential
BN <sub>2</sub>	0.36	0.40	0.44	2.68	1.24	1.07
BN <sub>3</sub>	0.37	0.41	0.44	2.29	1.25	1.05
BN <sub>5</sub>	0.35	0.41	0.43	2.29	1.13	1.03
BN <sub>6</sub>	0.35	0.40	0.43	2.33	1.22	1.03
BD <sub>3</sub>	0.38	0.41	0.44	2.09	1.28	1.10
BD <sub>4</sub>	0.36	0.40	0.48	2.97	1.24	1.06
BD <sub>5</sub>	0.37	0.40	0.43	2.42	1.36	1.08
BS <sub>1</sub>	0.37	0.40	0.42	2.92	7.20	1.10
BS <sub>6</sub>	0.35	0.40	0.43	2.40	1.18	1.04
BS <sub>7</sub>	0.36	0.41	0.42	2.28	1.36	1.08
BG <sub>6</sub>	0.34	0.39	0.43	3.50	1.18	1.03
BG <sub>5</sub>	0.34	0.38	0.42	3.04	1.16	1.04
BC <sub>1</sub>	0.37	0.40	0.44	1.78	1.36	1.05
BC <sub>2</sub>	0.37	0.40	0.43	2.56	1.32	1.07
BC <sub>3</sub>	0.37	0.40	0.44	3.50	1.43	1.05
BSG <sub>2</sub>	0.36	0.39	0.43	1.9	1.9	1.04

cont'd...

Sample Notation	Trap depth values 'E' (eV)			$N_n(t)_{t=0} / N_n(t)_{t=5}$ for three 'peeled off' components		
	Fastest exponential $E_1$	Middle exponential $E_2$	Slowest exponential $E_3$	Fastest exponential	Middle exponential	Slowest exponential
BNP	0.35	0.39	-	1.74	1.18	-
BNP <sub>2</sub>	0.35	0.39	0.42	2.62	1.19	1.06
BNS <sub>2</sub>	0.36	0.37	0.42	2.63	1.30	1.06
BND	0.39	0.41	0.44	2.24	1.19	1.03
BPG <sub>2</sub>	0.38	0.40	0.44	3.08	1.22	1.02
BPG <sub>1</sub>	0.38	0.40	0.43	1.85	1.50	1.06
BPS <sub>2</sub>	0.38	0.39	0.44	2.45	1.39	1.04
BPS	0.38	0.41	0.43	2.02	1.26	1.05
BPS <sub>3</sub>	0.36	0.40	0.43	2.20	1.21	1.06
BSP <sub>2</sub>	0.37	0.40	0.43	3.16	1.45	1.12
BSP <sub>3</sub>	0.36	0.40	0.44	5.52	1.56	1.06
BCP <sub>2</sub>	0.37	0.40	0.43	2.88	1.32	1.09
BCS <sub>2</sub>	0.35	0.40	0.44	2.48	1.23	1.07
BCG <sub>2</sub>	0.37	0.41	0.44	3.43	1.35	1.05
BC(Sm, Gd)	0.36	0.40	0.43	2.64	1.27	1.06
BC(Pr, Sm)	0.35	0.40	0.44	2.31	1.14	1.03
B(Pr, Sm, Gd)	0.36	0.38	0.44	2.13	1.14	1.04

It is seen that the effective trap levels are distributed in three groups in all these phosphor systems. Each of the exponentials is attributable to a certain trap depth. There is only a slight variation in the values of trap depths (in each group of levels) with change in activator or change of the activator concentration. Also these variations are found to be not of systematic character. This suggests that the addition of activators are not effective in introducing new trapping levels in the host lattice. It only modifies the relative distribution of the traps. The trap distribution can be thought of as consisting of various groups at different depths. The slight variation observed in trap depths in the case of different phosphor systems could be due to the influence of activators on the distribution of trap densities. Thus the trapping levels in the present system of phosphors could be attributed to host lattice defects. The traps are due to the defects incorporated during preparation. As the concentrations of the rare-earth dopant increase, the centre of gravity of the traps in these phosphors shifts towards the shallower side. The electronegativity and the ionic radii of these rare-earth ions are likely to occupy the substitutional sites in BaS. The trap depth values obtained and the presence of a monomolecular process in the emission indicate that the involved electron and hole traps are located near each other. The intense initial afterglow in these phosphors is due to the increase in number of luminescent centres and traps.

When compared with TL glow curve analysis (given in last chapter) it was found that the trap depths obtained for the slowest exponential of the decay curve agree well with the trap depth values obtained from TL analysis. Also the trap depth value above 0.59 eV is not obtained in decay analysis. This shows the smaller escape probability for the deeper traps at room temperature.

#### 6.4. Population Distribution Of Trapping Levels.

When more than one trap depth is involved, the decay rate depends on the population distribution of electrons in traps of various levels. The relative population of trapping levels  $N_n$  at  $t = 0$  can be obtained by the extrapolation of plots  $\log I$  vs time (fig 6.2 (a) to (k)) using the relation

$$N_n(t)_{t=0} = I_n(t)_{t=0} \tau_n \quad 6.(5)$$

where  $\tau_n = 1/P_n$  is the life time of the electrons trapped in the trap having depth  $E_n$ . The ratio  $N_n(t)_{t=0} / N_n(t)_{t=5}$  will give the relative population at  $t=0$  with respect to that at a later time  $t=5$  seconds and can be calculated from the three 'peeled off' components of the semi-log graph. Results are given in table 6.1(a) and 6.1(b). The variations in these values indicate that the deepest traps are more densely filled than the shallow ones. The high values of  $\tau_n$  for the slowest exponentials are due to the fact as time goes on the shallow traps become empty faster than the deeper ones. The calculated values of  $\tau_n$  also support this result (Table 6.2(a) and 6.2(b)).



**Table 6.2(a)**

**Decay constant values and life time ( $\tau$ ) for each group of traps corresponding to the three exponential regions. (for samples prepared by method I)**

Sample Notation	Decay Constant - 'b'			Life time - $\tau$ (sec)		
	$b_1$	$b_2$	$b_3$	$\tau_1$	$\tau_2$	$\tau_3$
SR <sub>1</sub>	0.3	0.3	0.3	.08	.32	8.3
SR <sub>3</sub>	0.3	0.25	0.2	.08	.36	11.2
SR <sub>5</sub>	0.13	0.14	0.02	.03	.34	18.0
SR <sub>6</sub>	1.1	0.8	0.1	.02	.32	20.0
SR <sub>7</sub>	0.5	0.7	0.3	.06	.36	22.1
SR <sub>8</sub>	0.26	0.3	0.28	.09	.38	26
SC <sub>2</sub>	0.7	0.3	0.2	.16	.21	12.4
SC <sub>3</sub>	0.8	0.38	0.4	.08	.25	.8
SC <sub>4</sub>	0.57	0.38	0.55	.02	.17	11.4
SC <sub>5</sub>	.55	0.5	0.4	.04	.08	9.4
SS <sub>41</sub>	1	1.1	0.3	.02	0.22	5.15
SS <sub>42</sub>	0.6	0.61	0.3	.04	0.1	9.2
SS <sub>43</sub>	0.8	0.7	0.4	.06	0.12	2.5
SS <sub>45</sub>	0.9	0.5	0.3	.01	.3	1.6

cont'd...

Sample Notation	Decay Constant - 'b'			Life time - $\tau$ (sec)		
	$b_1$	$b_2$	$b_3$	$\tau_1$	$\tau_2$	$\tau_3$
SS <sub>56</sub>	0.5	0.51	0.42	.01	.33	1.3
SS <sub>57</sub>	0.6	0.71	0.32	.04	.35	1.7
SS <sub>58</sub>	0.61	0.65	0.35	.06	.22	1.6

Table 6.2(b)						
Decay constant values and life time ( $\tau$ ) for each group of traps corresponding to the three exponential regions. (for samples prepared by method I)						
Sample Notation	Decay Constant - 'b'			Life time - $\tau$ (sec)		
	$b_1$	$b_2$	$b_3$	$\tau_1$	$\tau_2$	$\tau_3$
BL <sub>6</sub>	0.48	0.78	0.27	0.84	3.28	16.2
BP <sub>3</sub>	0.38	0.77	0.47	0.04	7.46	24.2
BP <sub>5</sub>	0.78	0.58	0.25	0.07	3.46	24.93
BP <sub>6</sub>	0.88	0.4	0.23	0.69	3.78	15.3
BP <sub>7</sub>	0.1	0.58	0.35	0.65	3.73	18.45
BN <sub>2</sub>	0.51	0.73	0.38	1.15	5.10	26.3
BN <sub>3</sub>	0.53	0.56	0.33	1.25	5.76	19.6
BN <sub>5</sub>	0.57	0.53	0.2	0.95	5.74	16.12
BN <sub>6</sub>	0.53	0.75	0.34	0.98	3.98	17.5

Sample Notation	Decay Constant - 'b'			Life time - $\tau$ (sec)		
	$b_1$	$b_2$	$b_3$	$\tau_1$	$\tau_2$	$\tau_3$
BD <sub>3</sub>	0.62	0.6	0.51	2.62	7.51	18.86
BD <sub>4</sub>	0.57	0.72	0.23	1.24	6.13	18.45
BD <sub>5</sub>	0.79	0.71	0.26	1.83	4.6	17.24
BS <sub>1</sub>	0.53	0.63	0.3	1.79	4.95	13.69
BS <sub>5</sub>	0.48	0.74	0.17	0.9	3.41	23.0
BS <sub>6</sub>	0.6	0.54	0.2	0.84	5.58	19.6
BS <sub>7</sub>	0.88	0.6	0.2	1.94	9.8	28.81
BG <sub>6</sub>	0.88	0.53	0.21	0.84	3.54	15.67
BG <sub>5</sub>	0.75	0.57	.34	1.94	2.11	12.5
BC <sub>1</sub>	0.44	0.42	0.27	0.57	4.6	11.9
BC <sub>2</sub>	0.54	0.57	0.2	1.53	4.46	14.9
BC <sub>3</sub>	0.68	0.75	0.26	1.53	5.07	23.8
BSG <sub>2</sub>	0.64	0.58	0.54	1.08	3.8	13.8
BNP	0.40	1.01	--	1.79	9.48	—
BNP <sub>2</sub>	0.96	0.66	0.27	0.82	3.5	13.8
BNS <sub>2</sub>	0.67	0.86	0.45	0.97	3.58	12.8
BND	0.53	0.76	0.31	3.64	6.75	19.6

contd...

Sample Notation	Decay Constant - 'b'			Life time - $\tau$ (sec)		
	$b_1$	$b_2$	$b_3$	$\tau_1$	$\tau_2$	$\tau_3$
BPG <sub>1</sub>	0.55	0.15	0.33	1.86	5.23	16.12
BPS <sub>2</sub>	0.75	0.75	0.35	1.08	3.46	18.21
BPS <sub>3</sub>	0.78	0.68	0.29	1.03	4.42	12.3
BPS <sub>2</sub>	0.71	0.58	0.3	1.34	4.14	13.47
BPS <sub>3</sub>	0.9	0.55	0.15	1.15	4.96	23.8
BCP <sub>2</sub>	0.32	1	0.46	1.48	5.07	15.3
BCS <sub>2</sub>	0.87	0.62	0.3	1.40	5.7	25.8
BCG <sub>2</sub>	0.84	0.62	0.3	1.40	5.7	25.8
BC (Sm, Gd)	0.54	0.84	0.44	1.0	4.4	20.4
BC (Pr, Sm)	1	0.57	0.33	0.61	5.37	26.31
B (Pr, Sm, Gd)	0.52	0.7	0.32	1.06	1.83	22.7

### 6.5 Evaluation of Decay Constant - b

The values of decay constants calculated from the slopes of  $\log I - \log t$  plots fig.6.3 ((a) to (h)) and are tabulated in Table 6.2(a) and 6.2 (b) given above. The values of 'b' are found to fluctuate between 1.1 to 0.2 and the variation of 'b' with respect to dopants is not systematic. The values of 'b' are also calculated by using the method of least squares using the relation [8]

$$b = \frac{\sum x_i \sum y_i - n \sum x_i y_i}{(\sum x_i)^2 - n \sum x_i^2} \quad 6.(6)$$

and found to be in the range 0.5 to 0.98. These values suggest that the distribution of traps according to this model is neither uniform nor exponential. So the trap distribution may, therefore be taken as quasi-uniform. The variation of decay constants points towards a variation in trap distribution.

Another feature noticed from analysis is that, the method of preparation of the phosphor considerably influence the formation of defects in the host-lattice. It is seen that the trap depth values, electron population ratios and decay constants vary considerably for the phosphor systems prepared by method I and method II (Tables 6.1 and 6.2). The phosphor samples prepared by method I have got higher trap depth values show the formation of deeper traps in these systems. But the low values of electron population ratio in this case is due to the lower de-activation rate(as seen by low values of decay constants) as compared to the phosphor systems prepared by method II. This may be due to the variation in the preparation conditions. This suggests that the preparation condition affect the formation of defects in the host lattice. Also, eventhough the afterglow intensities are low, the decay is found to be more in the case of phosphor samples prepared by method I.

A comparative study of the phosphor systems prepared in these two methods are given in the next chapter.

## REFERENCES

- [1]. Patil M.G., Lawangar R.D., Journal of Lumin. 22 (1981) p.377
- [2]. Rao R.P., Rao D.R. and Banerjee H.D., Mat. Res. Bull. 13 (1978) p.491
- [3]. Chakravarthi K., Mathur V.K., Joanna F. Rhodes and Abbundi, J. Appl. Phys. 64 (1988) p.1363
- [4]. Kulkarni V.W, S.S.Patwardhan and Ghanbahadur, Physica Scripta 25 (1982) p.496
- [5]. Rao R.P., J. of Mater. Science, 21 (1986) p.3357
- [6]. Tomaschek R. Ruchsber, Phys. 1, (1944) p.139
- [7]. Randall J.T. and M.H.F. Wilkins, Proc. R. Soc. A184, (1945) p.336
- [8]. Singha O.P and Sivaraman S, Indian J. of Pure and Appl. Phys. 18 (1972) p.134
- [9]. Chakravarthi A.K., Mor S.L and Ranade J.D, Indian J. of Pure and Appl Phys. 12 (1974) p.603
- [10]. Balakrishna S and Kanari P.S., Indian J. of Pure and Appl. Phys. 13 (1975) p.71
- [11]. Lawangar R.D. and Narlikar A.V. Indian J. of Pure and Appl. Phys. 16 (1972) p.617
- [12]. Booth A.H., Can. J. Chem. 32 (1954) p.214
- [13]. Bube R.H., Phy.Rev. 80 (1950) p. 655

## **CHAPTER VII**

## GENERAL CONCLUSIONS

Luminescence characteristics of Barium Sulphide phosphor doped with  $RE^{3+}$  and  $Cu^+$  have already been described in previous chapters. Discussions and important findings from the present investigations were also included in these chapters. This chapter gives the general conclusions derived from the present studies.

The work presented in the previous chapters can be divided broadly as follows:

- (i) synthesis of phosphors
- ii) fluorescence emission under
  - (a) nitrogen laser (337.1 nm) excitation
  - (b) UV (365 nm) excitation
- iii) phosphorescence decay characteristics
- iv) thermoluminescence emission

The properties of phosphors are found to depend on preparative conditions and nature of dopants. For example as described in chapter VI, phosphorescence decay of BaS depends on the type of impurities incorporated in the lattice. BaS:Cu phosphors have afterglow for short durations (40-50sec), while most of the BaS:RE systems exhibit intense afterglow emission which lasts for longer durations. However it is observed that  $Cu^+$  in presence of RE, (i.e. BaS:Cu:RE systems) enhances the overall emission which lasts upto 350 seconds or more. Colour of the fluorescence emission depends on the nature of dopants as described in chapters IV and V. Also, the overall fluorescence emission efficiency is found to be high for the samples prepared by method II and for excitation under  $N_2$  laser. In addition, the samples prepared by method II are found to be more stable as compared to those prepared by method I

The method of synthesis of phosphors found to modify lattice vacancies considerably. Samples prepared in method II (i.e. refired ones) are found to be more effective in creating the lattice defects. The present studies show that the traps are responsible for the luminescence processes in sulphide phosphors and are associated primarily with the host lattice vacancies such as sulphur ion and barium ion vacancies. Emissions, which are characteristic to the dopants are also observed in certain cases.  $N_2$  laser excitation is more effective in causing band-to-band transitions in BaS and hence helps to obtain characteristic emission of the dopants. From the emission models it is suggested that the possible sites of  $RE^{3+}$  dopants in BaS lattice are mainly due to substitutional  $Ba^{2+}$ . However the possibility of  $RE^{2+}$  ion occupying a  $S^{2-}$  site is also cannot be completely ruled out even though it is not a stable position for a positive ion. Of



all the RE dopants studied (i.e. BaS:RE phosphor systems), there is clear evidence that the chances of  $Dy^{3+}$  goes into BaS lattice as interstitial substitution too. Copper in its monovalent form ( $Cu^+$ ) enters into BaS lattice as interstitial as well as substitutional sites

As indicated elsewhere, during the preparation of II-VI compounds like BaS, no stable interstitial type of defects (similar to Frenkel type) acting like donors or acceptors are observed in significant concentrations. Results could be explained mainly on the basis of substitutional incorporation of impurities. These impurities and related lattice vacancies (due to charge compensation) formed during the preparation of phosphors create localized levels in the forbidden energy region of the host lattice. These localized levels will act (depending upon their nature) as electron and hole centres which depends both on the type of impurities and nature of excitation source and accordingly thermoluminescence yield and related energy storage phenomena are also get modified.

Fig. 7.1 indicates the various types of lattice defects possible on incorporating BaS with  $Cu^+$  and  $RE^{3+}$  impurities due to charge compensation. Note that simultaneous inclusion of  $Cu^+$  and  $RE^{3+}$  impurities can reduce the number of cation vacancies.

The fact that the absorption spectra (fig.4.1) do not show any characteristic feature of dopants implies that electrons are excited directly from the valence band to the conduction band, thereby creating holes in the valence band. Electrons in the conduction band can then be captured by excited levels of dopants so as to exhibit characteristic emission as in the case of  $Sm^{3+}$  (fig. 4.12). From the absorption spectra, it is clear that, the influence of dopants is only to enhance lattice defects and to create trapping and luminescence centres.

One of the important points dealt with in these investigations is the evaluation of stark splitting patterns of  $Sm^{3+}$  and  $Pr^{3+}$  levels in BaS (fig 4.13 and fig 4.16). Crystal field parameters were evaluated and it has been shown that cubic crystal field approximations of BaS lattice agrees well with the experimental observations.

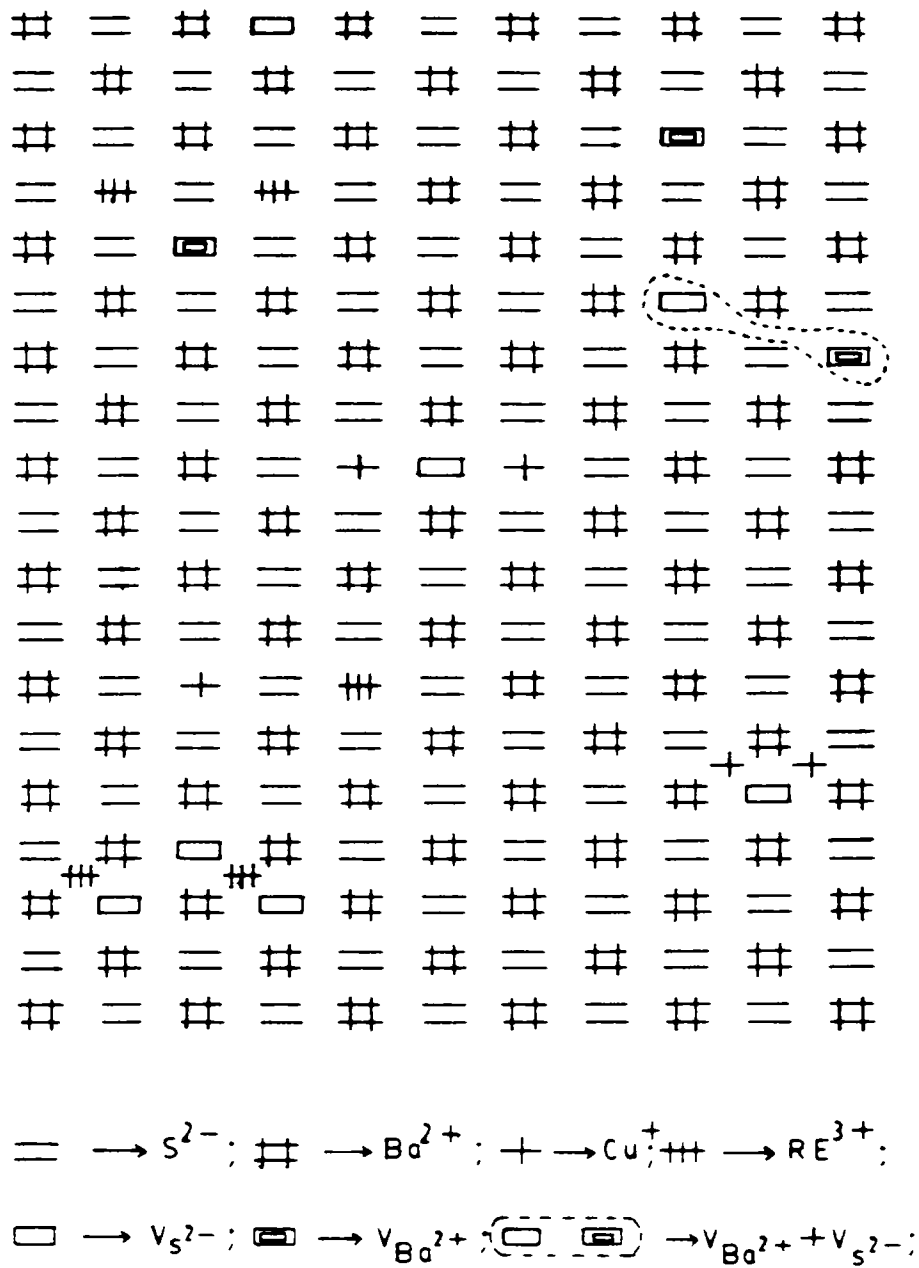


Fig 7.1 Pattern of possible defects formation in BaS lattice (charge compensation type) due to the inclusion of  $Cu^+$  and  $RE^{3+}$  impurities

## **Future Scope of the Work**

The work described in this thesis is based on experiments conducted at room temperature. Various phonon assisted mechanisms will become clear when one carries out the observations at low temperature. Samples in the form of thin films will have applications in various types of devices. Properties of thin film samples may be different from those of bulk samples and hence detailed investigations on thin film samples are necessary. Studies on electroluminescence properties will supplement the observations described in the present thesis.

## APPENDIX

### **PHOTOLUMINESCENCE STUDY OF $YBa_2Cu_3O_x$ SUPERCONDUCTING SAMPLES.**

#### **A.1 Introduction**

Since the discovery of the new class of ceramic oxide high temperature superconductors (HTSC) by Bednorz and Muller [1] large number of papers dealing with the use of different techniques to characterise the HTSC materials have been appeared in the literature. Such investigations have provided some insight into acoustical [2], thermal [3], electrical [4] and optical [5] properties of materials. Due to the variations in the method of synthesis followed by various workers, results reported in the literature are sometimes confusing. Theoretical models which explain all the observed properties of the HTSC materials have not yet been evolved.

Most of the investigations on the optical properties of HTSC materials are centred around Raman spectroscopy and optical reflectivity studies. The present section of the thesis contains the results obtained from photoluminescence studies of  $YBa_2Cu_3O_{7-x}$  (1-2-3 compounds) using Xenon arc lamp as the source of excitation.

The ceramic oxide superconductors which are oxygen deficient perovskites have mixed valence Cu states and experiments indicate the presence of an anisotropic structure with copper atoms lying in planes, separated by trivalent rare-earth ions or divalent ions like  $Ba^{2+}$ ,  $Sr^{2+}$  and  $O^{2-}$  [6]. For example  $YBa_2Cu_3O_{7-x}$  is a semiconductor for  $x=0.5$  with normally bivalent Cu ions. The transition from semiconductor to metallic phase is observed for  $x < 0.5$  and transition temperature ( $T_c$ ) increases with  $x$  in the region  $0 < x < 0.5$  [7]. Different spectroscopic techniques have been used to understand the nature of the electronic states and valency states of Cu ions. Studies like XANES, XPS and Auger spectroscopy of  $YBa_2Cu_3O_7$  reveal the absence of  $Cu^{2+}$  ions [8-9]. This information is very important when one constructs a theoretical model for HTSC phenomenon. Moreover, experimental evidence support the description of HTSC as pairing of holes in the oxygen valence band interacting with localized electrons at the copper sites [10]. It should be possible to excite localized levels and to observe the resulting fluorescence emission.

#### **A.2 Experimental**

$YBa_2Cu_3O_7$  used in the present studies were provided by Dr. Choudhari et. al, ICAS, Calcutta. Samples were prepared following the technique reported in the literature [11]. Yttrium-Barium-Copper oxide was synthesized in air by the high temperature (950°C) solid state reaction of stoichiometric quantities of the Yttrium oxide, Copper oxide and Barium carbonate. The heating schedules of the mixed powder as follows: 950°C; 24 hours in air, two repeat

grindings and heatings; pelletization, heating at 950°C, 24 hours in air and final heating at 900°C for 24 hours in flowing O<sub>2</sub>; followed by slow cooling to room temperature. Samples were grouped (from conductivity studies) into two ; one, containing superconducting (SC) samples and, the other containing non superconducting (NSC) samples. We have selected samples from each group for photoluminescence studies.

Fluorescence spectra were recorded using a 0.25m grating monochromator coupled with PMT and chart recorder. Xenon arc source (450 W) along with a source monochromator was used as the excitation source. Schematic experimental set up is as shown in fig.A.1. The excitation spectra show a prominent band centered at 420nm for both superconducting (SC) and non superconducting (NSC) samples (fig.A.2). Fig.A.3 show the photoluminescence spectra recorded at room temperature (RT) and liquid N<sub>2</sub> temperature (LNT). The low temperature cell used in the experiment is shown in fig.3.3 of chapter III.

### A.3 Results and Discussion

The spectra at RT show remarkable difference for SC and NSC samples, while emission is completely suppressed at LNT in both the cases. At RT, SC samples show emission peaks at 540 nm and 580 nm while NSC samples have emission only at 640 nm. It may be noted that excitation energy is same (3 eV, above the oxygen derived valence band corresponding to 420 nm excitation) for both SC and NSC samples and can be attributed to  $3d^9 \rightarrow 3d^{10} \underline{\uparrow}$  ( $\underline{\uparrow}$  is a hole in oxygen derived valence band). For NSC, 640 nm emission is due to radiative de-excitation from the lower edge of  $3d^{10} \underline{\uparrow}$  to  $3d^9$  state. For SC samples in addition to  $3d^9$ ,  $3d^9 \underline{\uparrow}$  state is also formed [8]. Thus 580nm and 540 nm bands arises for SC samples due to transitions  $3d^{10} \underline{\uparrow} \rightarrow 3d^9 \underline{\uparrow}$  and  $3d^{10} \underline{\uparrow} \rightarrow 3d^9$  with  $3d^9 \underline{\uparrow}$  level at 0.2 eV above the  $3d^9$  level. The quenching of fluorescence emission at LNT suggests that the observed fluorescence emission is probably phonon assisted.

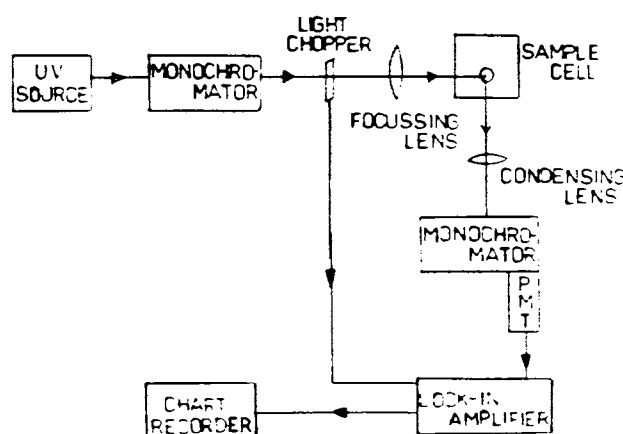


Fig. A-1 Schematic experimental set up

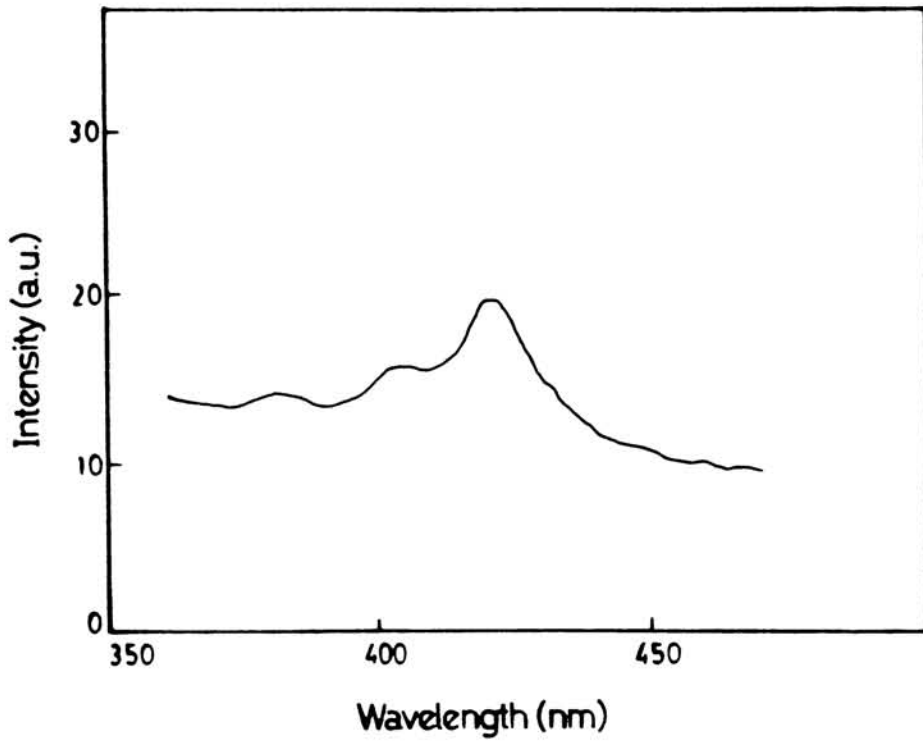


Fig. A-2 Excitation spectrum for 550nm emission

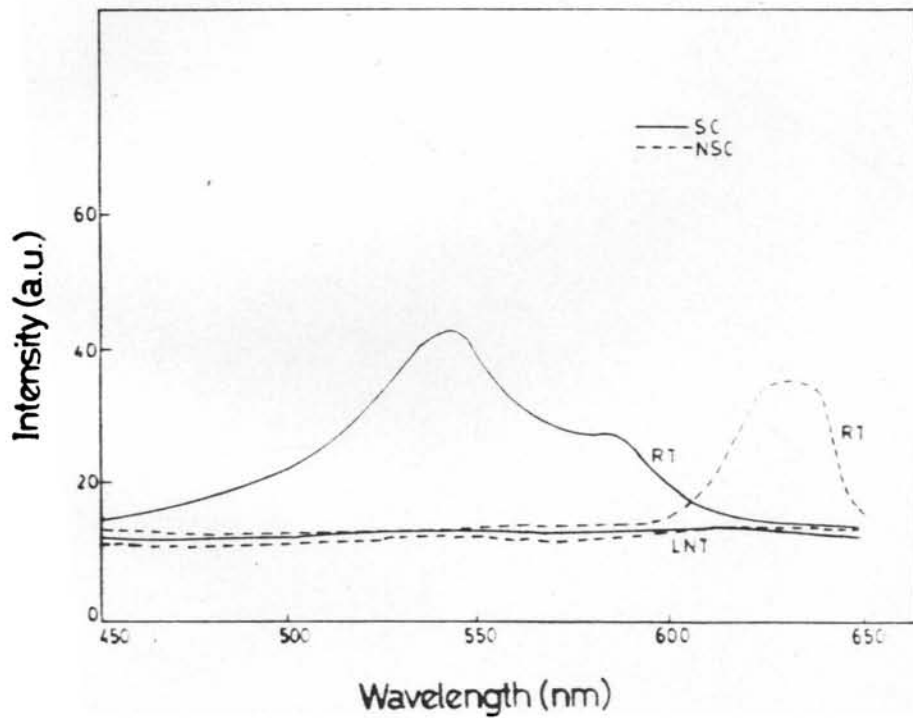


Fig. A-3 Photoluminescence spectra of SC and NSC samples at room temperature (28°C) and liquid nitrogen temperature (-77°C).

## REFERENCES :

- [1]. Bednorz J.G. and Muller K.A., Z. phys. B64, (1986) p. 189.
- [2]. Gopal K. and S.Ramana Murthy, J. Acoustical Society of India, 18 (1990) p. 65.
- [3]. Srinivasan R. - 'Measurement of Resistivity and thermopower of super conducting materials in the normal state'p.86. in the book on "*HIGH TEMPERATURE SUPER CONDUCTORS*" Edited by E.S.R. Gopal and S.V. Subramanyan. Wiley Eastern Ltd. (Delhi)1989
- [4]. Ogale S.B., Dyjklamp D., Venketesan, T., Appl. Phys. Lett. 51, 11 (1987) p.861.
- [5]. Philips J.C. "*PHYSICS OF HIGH  $T_c$  SUPERCONDUCTORS*", AT& T Bell Laboratories, New Jersey. Academic press Inc. (London) Ltd.1989
- [6]. Cava R.J. et. al Phys. Rev. Lett. 58 (1987) p. 1676.
- [7]. Bianconi et. al Solid State Comm. 63 (1987) p.1135.
- [8]. Bianconi et. al Int. J. Mod. Phys. B. 1 (1987) p. 853
- [9]. Sharma D.D. and C.N.R. Rao, Solid State Comm. 65 (1988) p.47.
- [10]. Hirsch J.E., Phys. Rev. Lett.59 (1987). p. 228
- [11]. Subha Rao G.V. - High  $T_c$  oxide superconductors - Synthesis and characterization - p.18 in the book "*HIGH TEMPERATURE SUPER CONDUCTORS*" Edited by S.V. Subramanyan and E.S.R. Gopal, Wiley Eastern Ltd. (Delhi) 1989.